The Involvement of Hyaluronan Matrix in Regulating Peritoneal Infection, Inflammation & Fibrosis

Aled Prys Williams MB ChB MRCP (UK)

Thesis presented for the degree of Philosophiae Doctor

2019

Wales Kidney Research Unit,
Division of Infection and Immunity (I&I)
School of Medicine
Cardiff University
Heath Park
Cardiff
CF14 4XN

CARDIFF UNIVERSITY
PRIFYSGOL CAERDYDD

DECLARATION

This work has not previously been accepted in substance for any degree and is not concurrently submitted in candidature for any degree.

Signed _____ (candidate) Date _____

STATEMENT 1

This thesis is being submitted in partial fulfilment of the requirements for the degree of PhD

Signed _____ (candidate) Date _____

STATEMENT 2

This thesis is the result of my own independent work/investigation, except where otherwise stated.

Other sources are acknowledged by explicit references.

Signed _____ (candidate) Date _____

STATEMENT 3

I hereby give consent for my thesis, if accepted, to be available for photocopying and for inter-library loan, and for the title and summary to be made available to outside organisations.

Signed _____ (candidate) Date _____

STATEMENT 4: PREVIOUSLY APPROVED BAR ON ACCESS

I hereby give consent for my thesis, if accepted, to be available for photocopying and for inter-library loans **after expiry of a bar on access previously approved by the Graduate Development Committee.**

Signed _____ (candidate) Date _____

Dedication

To Leanne, Ollie and Ella - This thesis is dedicated to the love, support and endless joy you give me every day. I love you to the moon and back!

Acknowledgements

First and foremost, I would like to thank my supervisor Dr Soma Meran along with my co-supervisors Prof Donald Fraser and Dr Timothy Bowen for their supervision and support throughout this project. I would especially like to thank Dr Soma Meran for her constant encouragement, guidance and patience throughout this project. I am indebted for her ability to continuously challenge me from the beginning and for having unrelenting confidence in me when experiments didn't go to plan. She has been an inspiration to work with and an exceptional supervisor.

The success of this project has been the result of the Wales Kidney Research Unit and all the researchers and staff who work there. Many thanks to Dr Robert Steadman and Professor Aled Phillips for sharing their wealth of HA knowledge with me, and to everyone based in the WKRU who have provided advice, ideas and help with experiments (especially when the snow came). Thank you to Dr Melissa Lopez-Anton and Dr Chantal Colmont for getting me settled into the lab and teaching me how to handle a pipette! Thank you to Dr Adam Midgley, Dr John Martin and Dr Glyn Morris for their support and ideas during HA group meetings. A special mention for Dr Anne-Catherine Raby, Dr Magdalena Czubala and Dr Robert Jenkins for their help with the animal work – I will be forever grateful for your help with these experiments. To everyone else in the WKRU, thank you for the great memories.

I must thank my parents, John and Bernice, for their tireless devotion to my upbringing and for making me the person I am today. Finally, and most importantly, I would like to thank my wife Leanne for her love, support and incredible patience throughout this project, especially while writing up my thesis.

Thesis Summary

The prevalence of Chronic Kidney Disease (CKD) is rising owing to increased diabetes and obesity in our ageing populations. Hence, end-stage renal disease (ESRD) has become a major global health burden. For many ESRD patients, kidney transplantation is not possible. Hence these patients require dialysis to regulate their salt/fluid levels, and to remove toxins from the body. Peritoneal Dialysis (PD) is a well-established and effective form of treatment for ESRD. However, the longevity of PD is limited because of the constant exposure of the peritoneum to bioincompatible PD solutions. This, alongside unavoidable repeated episodes of PD peritonitis, alters the structural and functional integrity of the peritoneal membrane and plays a pivotal role in the development of peritoneal fibrosis leading to failure of the peritoneal tissue to act as a semi-permeable membrane. This results in failure of PD as a therapy for ESRD, limiting a patient's options for renal-replacement therapy. A key process that drives peritoneal fibrosis during PD is mesothelial-to-mesenchymal transition (MMT). MMT is a process whereby mesothelial cells (known to comprise the majority of cells in the peritoneal membrane) undergo myofibroblast differentiation and lay down increased fibrous matrix. Numerous studies have demonstrated that TGF-β1 plays an established role in driving MMT and in the subsequent development of peritoneal fibrosis. Therefore, delineating the regulators of TGF-β1-driven MMT are important in identifying novel mechanisms to prevent peritoneal fibrosis and PD failure.

In solid organ fibrosis (lungs, kidneys, skin) TGF-β1-driven myofibroblast differentiation is mediated through increased expression and alterations in the matrix polysaccharide, hyaluronan (HA). Previous studies demonstrate that PD therapy is associated with increased HA generation by mesothelial cells. However, the role of this in mediating TGF-β1-driven in the peritoneum has not been established and the role of increased HA generation during PD is not understood. The aim of this study was to determine the role of the increased HA generated during PD in regulating peritoneal infection, inflammation and fibrosis. This work uses primary human peritoneal mesothelial cells to study the involvement of HA in mediating TGF-β1-driven MMT in an in vitro experimental model. The role of HA in prevention and/or reversal of TGF-β1-driven MMT is also investigated in vitro. The role of HA in modulating peritoneal immunity and inflammation following acute bacterial infection is also examined using an in vivo mouse-model of PD peritonitis.

Patients with PD peritonitis had significantly increased HA concentrations in their PD effluent after developing acute bacterial peritonitis compared to non-infected patients. Cell studies established that TGF-β1-driven MMT in primary human mesothelial cells significantly increased HA generation, and this was predominantly driven by Hyaluronan Synthase-1 (HAS1) isoenzyme expression. However, the increased HA was not causally related to TGF-β1-driven MMT; but was simply a consequence of this process. The increased HA also did not mediate prevention and/or reversal of TGF-β1-driven MMT in primary human mesothelial cells. Blocking HA in the peritoneum with PEP1 blocking antibody during bacterial infection lead to a delayed resolution of inflammation, characterized by increased and persistent neutrophil infiltration, dysregulated monocyte recruitment and decreased cytokine and chemokine release. In conclusion, following peritoneal injury, HA generated by mesothelial cells is predominantly HAS1 driven and promotes enhanced peritoneal inflammation and alters leukocyte recruitment following acute bacterial infection.

Publications

Bowen, T., Meran, S., Williams, A. P., Newbury, L. J., Sauter, M., Sitter, T. Regulation of Synthesis and Roles of Hyaluronan in Peritoneal Dialysis. BioMed Research International, 2015; Article ID 427038.

Raby, A. C., Gonzalez-Mateo, G. T., Williams, A. P., Topley, N., Fraser, D., Lopez-Cabrera, M., Labeta, M. O. Targeting Toll-like Receptors with Soluble Toll-like Receptor 2 Prevents Peritoneal Dialysis Solution-Induced Fibrosis. Kidney International, 2018; 94(2):346-362.

Presentations

Williams, A. P., Lopez-Anton, M., Midgley, A. C., Bowen, T., Fraser, D. J., Meran, S. Regulation of HA Matrix Components involved in Peritoneal Infection, Inflammation and Fibrosis. Wales Kidney Research Unit Annual Meeting, Cardiff, 2016 (Poster).

Williams, A. P., Lopez-Anton, M., Midgley, A. C., Phillips, A. O., Bowen, T., Fraser, D. J., Meran, S. The Role of Hyaluronic Acid in the Peritoneal Cavity. Annual Infection & Immunity Meeting, Cardiff, 2017 (Poster).

Williams, A. P., Lopez-Anton, M., Midgley, A. C., Phillips, A. O., Bowen, T., Fraser, D. J., Meran, S. The Role of Hyaluronic Acid in the Peritoneal Cavity. Euro PD Meeting, Dublin, 2017 (Poster).

Williams, A. P., Lopez-Anton, M., Midgley, A. C., Phillips, A. O., Bowen, T., Fraser, D. J., Meran, S. Regulation of HA Matrix Components in Response to Factors that Promote/Prevent Peritoneal Fibrosis. Welsh Association of Renal Physicians and Surgeons, Cardiff, 2017.

Williams, A. P., Midgley, A. C., Brown C. V. M., Roberts, T., Morris, N. G., Phillips, A. O., Bowen, T., Steadman, R., Meran, S. The Hyaluronan Synthase-1 (HAS1) isoenzyme promotes

differentiation to a distinct subset of myofibroblasts that limit fibrosis progression. UK Renal Association, Harrogate, 2018 (Oral). Prize Awarded.

Williams, A. P., Lopez-Anton, M., Midgley, A. C., Raby, A. C., Phillips, A. O., Steadman, R., Bowen, T., Fraser, D. J., Meran, S. Hyaluronan generated during peritoneal dialysis does not drive fibrosis, but regulates inflammatory cell recruitment during peritoneal infection. UK Renal Association, Harrogate, 2018 (Poster).

Williams, A. P., Lopez-Anton, M., Midgley, A. C., Phillips, A. O., Bowen, T., Fraser, D. J., Meran, S. Regulation of HA Matrix Components involved in Peritoneal Infection, Inflammation and Fibrosis. Welsh Association of Renal Physicians and Surgeons, Cardiff, 2018 (Oral).

Williams, A. P., Midgley, A. C., Brown C. V. M., Roberts, T., Morris, N. G., Phillips, A. O., Bowen, T., Steadman, R., Meran, S. The Hyaluronan Synthase-1 (HAS1) isoenzyme promotes differentiation to a distinct subset of myofibroblasts that limit fibrosis progression. American Society of Nephrology, San Diego, 2018 (Oral).

Williams, A. P., Lopez-Anton, M., Midgley, A. C., Raby, A. C., Phillips, A. O., Steadman, R., Bowen, T., Fraser, D. J., Meran, S. Hyaluronan generated during peritoneal dialysis does not drive fibrosis, but regulates inflammatory cell recruitment through differential Hyaluronan Synthase (HAS) Expression. American Society of Nephrology, San Diego, 2018 (Poster).

Williams, A. P., Lopez-Anton, M., Midgley, A. C., Raby, A. C., Czubala, M., Phillips, A. O., Steadman, R., Bowen, T., Fraser, D. J., Meran, S. Hyaluronan generated during peritoneal dialysis does not drive fibrosis, but regulates inflammatory cell recruitment through differential Hyaluronan Synthase (HAS) Expression. International Society for Hyaluronan Sciences, Cardiff, 2019 (Oral).

Table of Contents

Abbreviations

α-SMA	α-Smooth Muscle Actin
AAPD	Assisted Automated Peritoneal Dialysis
AGE	Advanced Glycation End-products
ALKR	Specific Type I Serine-Threonine Kinase Receptor
ANOVA	Analysis of Variance
APC	Antigen Presenting Cells
APD	Automated Peritoneal Dialysis
ARDS	Acute Respiratory Distress Syndrome
ATP	Adenosine Triphosphate
BAL	Bronchoalveolar Lavage
BHABP	Biotinylated Hyaluronan Binding Protein
BM	Basement Membrane
BMI	Body Mass Index
BMP	Bone Morphogenic Protein
BAS	Bovine Serum Albumin
Ca	Calcium
CamKII	Calcium/Calmodulin-dependent Protein Kinase II
CA-125	Cancer Antigen-125
CAPD	Continuous Ambulatory Peritoneal Dialysis
CCAAT	Cytosine-Cytosine-Adenosine-Adenosine-Thymidine
CCL	Chemokine C-C Motif Ligand
CKD	Chronic Kidney Disease
CRP	C-Reactive Protein
C-Src	Proto-oncogene Tyrosine Kinase Src
CT	Threshold Cycle
CTGF	Connective Tissue Growth Factor
CXCL	Chemokine C-X-C Ligand
DAMP	Damage Associated Molecular Pattern
DMSO	Dimethyl Sulfoxide
DNA	Deoxyribonucleic Acid

ECM	Extracellular Matrix
EDTA	Ethylenediaminetetraacetic Acid
EGF	Epidermal Growth Factor
EGFR	Epidermal Growth Factor Receptor
ELISA	Enzyme-Linked Immunosorbent Assay
EMT	Epithelial-to-Mesenchymal Transition
EPS	Encapsulating Peritoneal Sclerosis
ER	Endoplasmic Reticulum
ERK	Extracellular Signal-Regulated Kinase
ESRD	End-Stage Renal Disease
FACS	Fluorescence-Activated Cell Sorting
FAP	Fibroblast Activated Protein
FCS	Fetal Calf Serum
FGF	Fibroblast Growth Factor
FITC	Fluorescein Isothiocyanate
GAG	Glycosaminoglycan
GBM	Glomerular Basement Membrane
GFP	Green Fluorescent Protein
GFR	Glomerular Filtration Rate
GI	Gastrointestinal
GDP	Glucose Degradation Products
GlcUA	Glucuronic Acid
GPI	Glycosylphosphatidylinositol
HA	Hyaluronan
HABP	Hyaluronan Binding Protein
HARE	Hepatic Hyaluronan Clearance Receptor
HAS	Hyaluronan Synthase
HC	Heavy Chain
HD	Haemodialysis
HGF	Hepatocyte Growth Factor
HK-2	Human Kidney 2 Immortalised Proximal Tubular Cell Line
HMW-HA	High Molecular Weight Hyaluronan

HPMC	Human Peritoneal Mesothelial Cells
HRP	Horseradish Peroxidase
HYAL	Hyaluronidase
HYALp1	Hyaluronidase pseudogene
IαI	Inter-α-Inhibitor
IBD	Inflammatory Bowel Disease
ICAM-1	Intercellular Adhesion Molecule-1
ID-1	Inhibitor of DNA Binding-1
IFN-γ	Interferon-γ
IL	Interleukin
IRI	Ischaemia Reperfusion Injury
ISPD	International Society of Peritoneal Dialysis
KCP	Kielin/Chordin-Like Protein
kDa	Kilodalton
KDIGO	Kidney Disease Improving Global Outcomes
LMW-HA	Low Molecular Weight Hyaluronan
LYVE-1	Lymphatic Vessel Endothelial Hyaluronan Receptor-1
MAPK	Mitogen-Activated Protein Kinase
MC	Mesothelial Cells
MCP-1	Monocyte Chemoattractant Protein-1
MET	Mesenchymal-to-Epithelial Transition
MHC	Major Histocompatibility Complex
MIP	Macrophage Inflammatory Protein
MMP	Matrix Metalloproteinase
MMT	Mesothelial-to-Mesenchymal Transition
mRNA	Messenger RNA
NF-κβ	Nuclear Factor kappa beta
NTC	Non-Treatment Control
OA	Osteoarthritis
ORF	Open Reading Frame
PI3K	Phosphatidylinositol 3-Kinase
PAI	Plasminogen Activator Inhibitor

PD	Peritoneal Dialysis
PDGF	Platelet-Derived Growth Factor
PDOPPS	Peritoneal Dialysis Outcomes and Practice Patterns Study
PEP-1	Hyaluronan Binding Peptide
PET	Peritoneal Equilibrium Test
PH20	Hyaluronidase 5
PKC	Protein Kinase C
PMP	Per Million Population
PTC	Proximal Tubular Epithelial Cell
RA	Rheumatoid Arthritis
RAGE	Receptors for Advanced Glycation End-products
RANTES	Regulated on Activation, Normal T cell Expressed and Secreted
rER	Rough Endoplasmic Reticulum
RHAMM	Receptor for HA Mediated Motility
RhoA	RAS Homolog Gene Family Member A
RNA	Ribonucleic Acid
RQ	Relative Quantification
RT	Reverse Transcription
PBS	Phosphate Buffered Saline
PCR	Polymerase Chain Reaction
PDE	Peritoneal Dialysis Effluent
PLCe	Phospholipase Enzyme Epsilon
QPCR	Quantitative Polymerase Chain Reaction
ROS	Reactive Oxygen Species
RRT	Renal Replacement Therapy
SEM	Standard Error of Mean
SiRNA	Small Interfering RNA
SnRNA	Small Nuclear RNA
Sp1	Transcription Factor Specificity Protein 1
STAT	Signal Transducer and Activator of Transcription
TF	Tissue Factor
TGF-β1	Transforming Growth Factor-β1

ThC	T-helper Cells
TLR	Toll-Like Receptor
TNF-α	Tumour Necrosis Factor-α
TPA	Tissue Plasminogen Activator
TSG-6	Tumour Necrosis Factor-inducible Gene-6
UDP	Uridine 5’-diphospho
UF	Ultrafiltration
UPA	Urokinase Plasminogen Activator
UPAR	Urokinase Plasminogen Activator Receptor
USAG-1	Uterine Sensitization Associated Gene-1
VCAM -1	Vascular Cell Adhesion Molecule-1
VEGF	Vascular Endothelial Growth Factor
VEGFR	Vascular Endothelial Growth Factor Receptor
WT	Wild Type
ZO-1	Zonula Occludens-1
4-MU	4-Methylumbelliferone

Chapter 1

General Introduction

1.1 Chronic Kidney Disease

1.1.1 Overview of Chronic Kidney Disease

Chronic diseases present a significant challenge to 21st century health organisations worldwide [1]. Chronic Kidney Disease (CKD) in particular has become a major global health burden due to the rapid rise in conditions such as Diabetes Mellitus, Hypertension and obesity, in both developing and developed countries [2]. Several epidemiological studies have reported that the prevalence of CKD in the general population is increasing, leading some researchers to describe it as a worldwide epidemic [3-9]. CKD is defined as the presence of abnormal kidney function and/or structure that has persisted for more than three months, irrespective of the cause. CKD is conventionally divided into five stages based on the 2012 Kidney Disease: Improving Global Outcomes (KDIGO) guidelines (Table 1) [10].

Prognosis of CKD by GFR and albuminuria category

Prognosis of CKD by GFR and Albuminuria Categories: KDIGO 2012				Persistent albuminuria categories Description and range		
				A1	A2	A3
				Normal to mildly increased	Moderately increased	Severely increased
				<30 mg/g <3 mg/mmol	30-300 mg/g 3-30 mg/mmol	>300 mg/g >30 mg/mmol
GFR categories (ml/min/ 1.73 m²) Description and range	G1	Normal or high	≥90			
	G2	Mildly decreased	60-89			
	G3a	Mildly to moderately decreased	45-59			
	G3b	Moderately to severely decreased	30-44			
	G4	Severely decreased	15-29			
	G5	Kidney failure	<15			

Green: low risk (if no other markers of kidney disease, no CKD); Yellow: moderately increased risk; Orange: high risk; Red, very high risk.

Table 1.1. CKD Classification based on Glomerular Filtration Rate and Albuminuria [10]

As life expectancy increases, the role of age in CKD progression is becoming more apparent. The UK Renal Registry report a clear association between increasing age and higher CKD prevalence; with 1.9% of people aged 64 and under having CKD stage 3-5, 13.5% of people aged 65-74 and 32.7% of people aged 75 and over [11]. This comes at an estimated cost to the NHS in England of £1.4 billion/year, amounting to 1.3% of the total NHS annual budget in 2009-10 [12].

1.1.2 End-Stage Renal Disease (ESRD)

Progression to End-Stage Renal Disease (or CKD Stage 5) occurs in a small but significant percentage of people. In general, a patient is defined as having End-Stage Renal Disease (ESRD) when the GFR drops below 15ml/min and it indicates that renal replacement therapy (RRT) may be required. In the UK, the rates of patients reaching ESRD has increased year on year since 1990 (Figure 1.1), with most recent Renal Registry data indicating that the incidence rate increased from 115 per million population (pmp) in 2014 to 120 pmp in 2015 [11]. Over half of the money spent on CKD in the UK is spent on RRT, emphasizing the disparity of provisions required to treat the 2% of CKD patients who progress to ESRD.

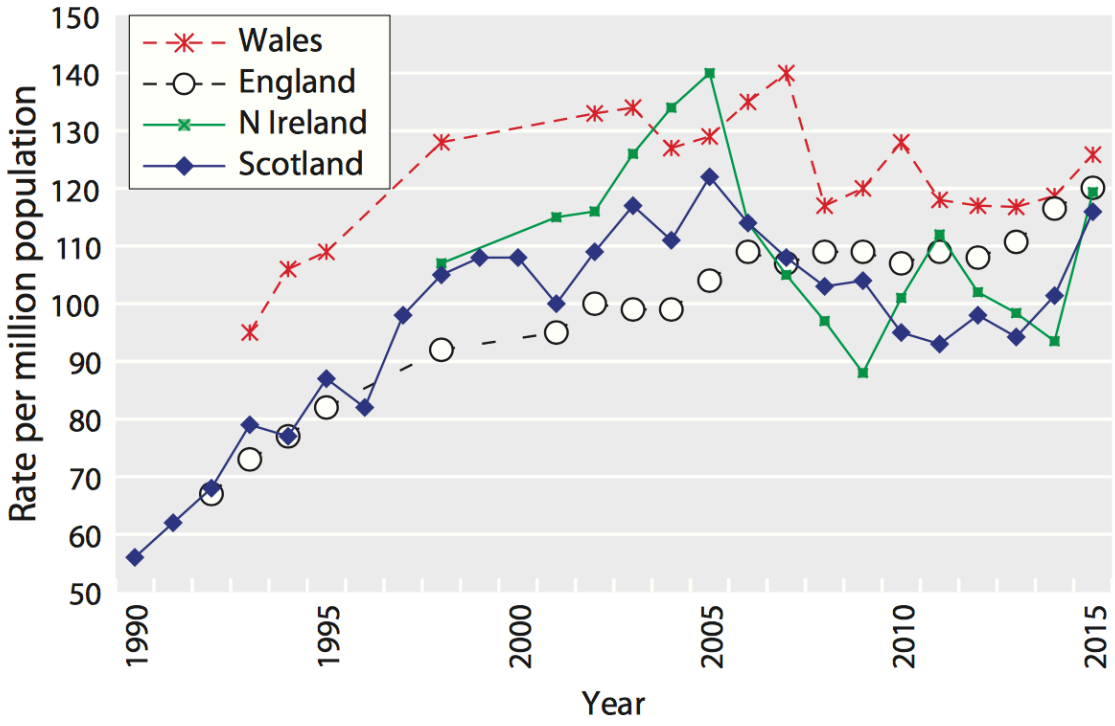

Figure 1.1 RRT Incidence in the countries of the UK 1990-2015 [11]

Kidney transplant remains the most desired and cost-effective outcome for patients with ESRD [13]. But, despite this, there are still several limitations in access to transplantation worldwide mainly due to the supply of healthy kidney donors and suitability of recipients [14]. In 2015, 67.3% of ESRD patients were on Haemodialysis (HD), 18.4% on Peritoneal Dialysis (PD), 8.6% had a functioning transplant and 5.7% had died or stopped treatment by 90 days [11]. Dialysis remains the mainstay of treatment for most patients requiring RRT, and patients are encouraged to make an informed decision about the type of life sustaining dialysis treatment they wish to receive [15]. In the UK, all RRT centres should be able to offer either PD or HD in a variety of programmes (Continuous Ambulatory PD (CAPD), Automated PD (APD), assisted APD (aAPD), Home HD, Nocturnal HD and Unit HD) thus enabling patients to select the most autonomous modality.

1.1.3 Peritoneal Dialysis (PD)

PD is a well-established and effective form of RRT for ESRD patients, that is currently used by around 6% of patients needing RRT in the UK [11]. Studies comparing both HD and PD modalities have shown that overall patient survival is similar but PD remains underused compared to HD in the UK [16]. Self-care modalities, such as PD, are associated with improved quality of life, are cost efficient to use and better preserve residual renal function. Nonetheless, there are many medical and socio-economic factors as well as individual preconceptions that influence what dialysis modality people choose. In terms of medical indications for dialysis modality, patients more suited to PD often have poor cardiac function and have issues with vascular access, whereas, patients with a higher Body Mass Index (BMI) or are obese tend to be offered HD. The contraindications to PD include previous intra-abdominal surgery, recurrent hernias or inability to learn the technique of administering PD therapy unless a carer is available. In general, caucasian race, younger age and fewer comorbidities correlate with selection of PD as do flexibility of schedule, convenience of performing dialysis anywhere, preservation of lifestyle and separation from dialysis units [17]. Socio-economic factors, such as being married, employed, cohabitating and patients of a higher educational background are more likely to choose PD [18].

Peritoneal Dialysis (PD) uses the thin membrane that surrounds the outside of the abdominal organs, called the peritoneum, as the membrane through which fluid and by-products are exchanged with the blood. A permanent in-dwelling catheter allows sterile dialysis fluid to be instilled into the peritoneal cavity and this fluid removes water, solutes and other by-products previously filtered by the kidneys. To maximise the removal of waste from the blood, the fresh

dialysis fluid is kept in the peritoneum for a certain amount of time, termed dwell time, and eventually drained and replaced by fresh dialysis fluid. Each time fluid is drained from the peritoneum and replaced is called “an exchange” and the effectiveness of the therapy depends on the (i) gradient concentration, (ii) membrane surface, and (iii) membrane permeability. PD can be safely delivered at home or at other locations outside of clinical environments. There are several different ways of performing PD in a continuous or intermittent fashion that patients can administer themselves; either by having continuous dialysis throughout the day (CAPD) or overnight whilst they are asleep (APD). Several studies have shown that the relative risk of mortality comparing patients on HD vs PD changes over time, with a lower risk on PD reported for the first 2 years followed by equivocal or slightly higher mortality risk thereafter, depending on country and centre experience [16, 19-24]. However, despite the lower costs associated with PD and higher patient satisfaction, the number of patients on PD are declining in most economically developed countries with the UK no exception to this trend (Figure 1.2).

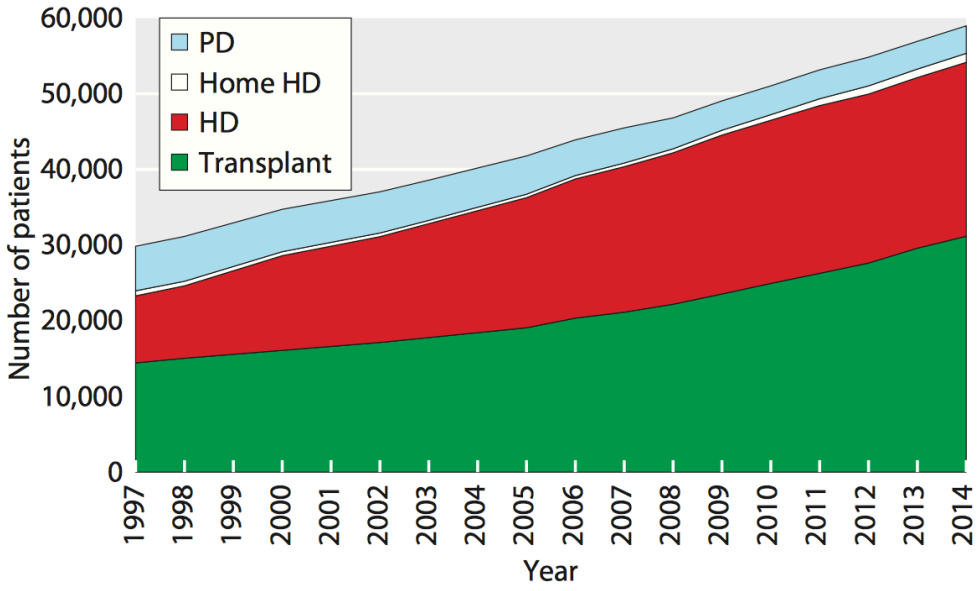

Figure 1.2 Growth in prevalent patient numbers by treatment modality at the end of each year 1997-2014 [11].

1.1.4 Limitations of PD

Many people can be successfully treated with PD for over 10 years but the general assumption in current practice is that a patient can expect to stay on PD for 2-3 years before having to transition onto haemodialysis. PD needs to provide patients with both solute clearance and fluid removal through ultrafiltration. Many studies have previously described the medium and long-term outcomes of patients on PD [25-27] and subsequently shown that a significant proportion of technique failure occurs in the first 2 years of treatment necessitating a permanent transition onto HD [28]. This loss of dialysis capacity and transition to HD is responsible for increased morbidity and mortality amongst PD patients [29]. However, it is important to recognise a small number of 'positive reasons' for stopping PD, such as transplantation or recovery of renal function. PD technique failure, is often multifactorial and recent guidance from the Peritoneal Dialysis Outcomes and Practice Patterns Study (PDOPPS), in collaboration with the International Society for Peritoneal Dialysis (ISPD), have recently provided standardised causes and definitions of technique failure (Table 1.2).

Primary Cause		**Sub Causes**
Dialysis Related	Peritonitis	Acute severe
		Refractory
		Relapsing
		Recurrent
	Exit-site infection	Exit-site infection only
		Tunnel infection
Catheter Malfunction	Catheter blockage	Fibrin
		Omental wrap
		Adhesions
		Catheter misplaced

	Catheter displacement	Cuff extrusion
		Catheter fell out
Ultrafiltration Failure and Volume Overload	Solute	Inadequate clearance – defined by Kt/V or creatinine clearance
		Inadequate clearance – phosphate clearance
		Uremic symptoms/poor nutrition
		Loss of RRF
		Patient size
	Fluid/UF	UF failure - PET defined
		Unable to remove excess body water
		Unwillingness to prescribe more dialysate glucose to achieve sufficient UF
Anatomical	Peritoneal leaks	Scrotal Oedema
		Pleuro-peritoneal leak
		Abdominal wall
		Elsewhere
	Hernia	Inguinal
		Peri-umbilical
		Elsewhere
Psychosocial /medical	Psychosocial	Patient choice/"burn out"
		Career choice/"burn out"
		Change in circumstance (e.g. death of caregiver, change in job, etc.)
	Medical	Severe depression
		Physical incapacity
		Cognitive impairment
Long-term Issues	Diagnosed EPS	Diagnosed EPS
	Risk of EPS	Time on PD
		GI symptoms but not formally diagnosed with EPS
Other		Haemo-peritoneum
		Intra-abdominal pathology
		Other reason not included elsewhere

Table 1.2 Standardised Causes of Peritoneal Dialysis Technique Failure: A Multi-Level Approach (adapted from [28]). RRF = residual renal function; UF = ultrafiltration; PET = peritoneal equilibration test; EPS = encapsulating peritoneal sclerosis; PD = peritoneal dialysis; GI = gastrointestinal.

Peritoneal fibrosis is one of the most serious complications of PD, characterised by activation of resident cells (mesothelial cells, fibroblasts and macrophages), inflammation, accumulation of excess matrix proteins and neoangiogenesis within the peritoneal membrane [30]. The use of bioincompatible PD solutions, containing elevated concentrations of glucose, alter the structural and functional integrity of the peritoneum and play a pivotal role in the initiation of peritoneal fibrosis [31].

1.2 Peritoneal Fibrosis

1.2.1 The Peritoneum

The peritoneal cavity is the largest cavity in the body and contains several crucial organs including the lower part of the oesophagus, stomach, small intestine, colon, liver, gallbladder, pancreas, spleen, kidneys and bladder [32]. The cavity is created by the continuation of two distinct layers of peritoneum lining each surface; the *parietal* layer lines the abdominal wall and the *visceral* layer lines the viscera and internal organs [33]. Both layers are similar in structure, differing slightly in terms of vascular and nerve supply. The *parietal* peritoneum receives somatic nerve supply, which renders it highly sensitive to pain, stretch and irritation. The *visceral* peritoneum on the other hand shares its nerve supply with the other internal organs, bestowing upon it a low sensitivity and inability to localise a stimulus [34]. As each layer or membrane is continuous with the other, it creates a 'sealed' space in-between known as the peritoneal cavity. Under physiological conditions, cells lining the peritoneal membrane produce a small amount of peritoneal fluid (PF) into the cavity, typically around 50-100ml. This PF resembles an ultrafiltrate of plasma containing various proteins, sugars, resident inflammatory cells and various enzymes [35]. Its main function is to facilitate the frictionless

movement of the abdominal organs, but it also contains resident cells that are important in the response to tissue injury [33].

1.2.2 The Peritoneal Membrane

The peritoneal membrane is most extensive serous membrane in the body, with a large surface area of up to $2m^2$ in adults due to the arrangement of peritoneal folds within the cavity [36]. The peritoneal membrane has a uniform structural composition, consisting of 3 distinctive layers; mesothelium, basement membrane and sub-mesothelial zone (Figure 1.3) [37]. The luminal surface of the peritoneal membrane is lined by a monolayer of mesothelial cells, often referred to as the mesothelium. Bio-structurally, the mesothelium is a semi-permeable laminar interface that separates the fluid-filled peritoneal cavity from blood vessels and lymphatics running within the sub-mesothelial zone of loose connective tissue and sub-mesothelial cells [38]. These two layers are separated by a discontinuous thin basement membrane (BM), which supports the mesothelium [39]. The BM is composed of thin layers of specialised extracellular matrix that form the supporting structure for MCs to adhere to. BMs are mainly composed of type IV collagen, which provide a scaffolding for a network of Laminins, proteoglycans and other structural macromolecules to form [40, 41]. The sub-mesothelial zone lies beneath the mesothelium and BM. It is a highly vascularised area containing plexuses of blood and lymphatic vessels [34]. Structurally, it is composed of a complex network of extracellular matrix (ECM) macromolecules (such as collagen, elastin and fibronectin), glycosaminoglycans (such as hyaluronan, heparan sulphate and chondroitin sulphate) and various resident and invasive cells (fibroblasts and macrophages). The sub-mesothelial zone has important role in regulating peritoneal homeostasis, allowing the exchange of solutes and water across the peritoneal membrane as well as having a key role

in host response to injury through regulation of fibroblast and macrophage infiltration to sites of injury. Patients on PD develop irreversible changes in this sub-mesothelial zone, characterised by thickening, neoangiogenesis and fibrosis [42].

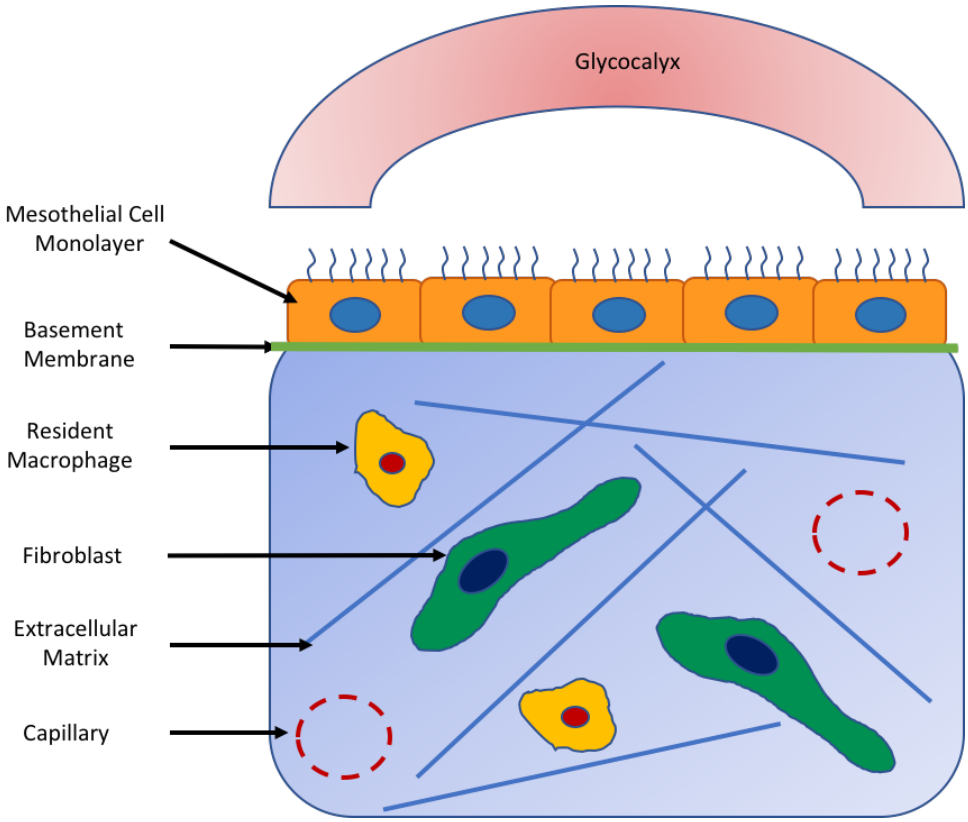

Figure 1.3 Illustration of the laminar structure and cellular components of the peritoneal membrane (Adapted from [43]). Mesothelial cells form a monolayer that line the peritoneal membrane. Their apical surface is endowed with a glycocalyx that provides a protective barrier. Mesothelial cells adhere to a discontinuous basement membrane composed of specialized extracellular matrix. The sub-mesothelial zone is composed of a complex network of extracellular matrix containing various resident and invasive cells (fibroblasts and resident macrophages) supporting a plexuses of blood and lymphatic vessels.

1.2.3 Mesothelial Cells

In 1827, *Bichat* first described a single layer of flattened cells that covers the three serosal cavities in the human body (pleural, pericardial and peritoneal). It was later identified as the mesothelium by *Minot* in 1880, in reference to the proposed mesodermal origins of these cells [44]. Mesothelial cells are a specialised type of epithelial cell derived from mesodermal tissue that form the mesothelium. They are a homogenous population of cells, numbering up to $1x10^9$, that adopt a predominantly elongated, flattened and squamous appearance on most parietal surfaces [36]. A small subset of cuboidal mesothelial cells have been identified, that adopt a different morphological appearance and have heightened biochemical activity. These cuboidal cells tend to be found on visceral surfaces near organs such as the liver and spleen [45]. Mesothelial cells morphologically resemble epithelial cells in many ways: (i) Firstly, they have surface microvilli lining the luminal surfaces, which increase the surface area for exchange between mesothelial cells and the peritoneal cavity. Microvilli also entrap water and serous exudates, which protect the delicate surface of mesothelial cells from frictional damage [46]. They also allow mesothelial cells to sense their microenvironment and function to entrap bacteria thereby preventing infection [47]. (ii) Secondly, mesothelial cells display an apical/basal polarity (present in epithelial cells) and adhere to each other through tight junctions, adherens junctions and desmosomes. They also express E-Cadherin, which is a cardinal feature of epithelial monolayers [48]. A loss of E-Cadherin from the intercellular junctions of epithelial cells is strongly associated with epithelial de-differentiation and Epithelial-to-Mesenchymal Transition (EMT) [49, 50]. During inflammation, there is a reduction in the levels of adherens junctions proteins associated with a breakdown of cell-cell communication and cell-matrix interactions resulting in cell death and disruption of the

mesothelial monolayer [43]. (iii) Thirdly, mesothelial cells are able to undergo a conformational change in their phenotype comparable to changes seen in EMT, which will be discussed later in this section [44]. However, mesothelial cells aren't entirely epithelial in character as they also demonstrate mesenchymal intermediate filaments vimentin and desmin [51] and share properties with vascular endothelium, including various adhesion molecules [52]. For this reason, mesothelial cells are not considered to be true epithelium. Instead, they have a number of specific benefits in terms of structure, function, plasticity and anti-inflammatory properties to protect and regenerate the peritoneum.

1.2.4 Functions of Mesothelial Cells in the Peritoneum

1.2.4.1 Physical Barrier and Lubrication

A monolayer of mesothelial cells across the surface of the peritoneal membrane provides protection of the inner basement membrane and sub-mesothelial zone from injury. Historically, this was originally thought to be the main role of mesothelial cells in forming a physical barrier against damage and invading organisms [44]. However, mesothelial cells also secrete lubricants onto their apical surface that stay electrochemically entrapped within the numerous microvilli [38]. This thin outer coat of fluid is called the glycocalyx and is mainly composed of glycosaminoglycans, especially Hyaluronan, as well as other lipoproteins and phospholipids. The glycocalyx not only protects mesothelial cells from abrasions and adhesions, but it also plays an important role in cell-cell contact, tissue hydration, regulation of inflammation, tissue repair and remodelling, and flow of nutrients across the peritoneal membrane [43].

1.2.4.2 Extracellular Matrix Production

Mesothelial cells produce and secrete numerous extracellular matrix (ECM) molecules, which provide a substratum onto which mesothelial cells adhere [47]. The ECM molecules produced by mesothelial cells are collagen types I, III and IV, elastin, fibronectin, laminin, proteoglycans and glycosaminoglycans [53]. They play an essential role in maintaining the structural architecture of mesothelial cells and matrix homeostasis is achieved through the balance between synthesis and degradation. Previous work from our laboratory has also shown that mesothelial cells are able to control ECM accumulation through selective secretion of specific matrix metalloproteinases (MMPs); namely MMP-2, MMP-3 and MMP-9 which are known to be influenced by numerous cytokines produced by mesothelial cells during PD [53].

1.2.4.3 Transport of Solutes and Fluids

The peritoneum is a semi-permeable membrane, which allows the transport of fluid, solutes and small molecules across it. The mesothelium allows passive transport through a network of hydrostatic and osmotic pressure gradients created via intercellular junctions and stomata (cavities at the junctions of two or more mesothelial cells and active formation of (micro)pinocytic vesicles on the surface of mesothelial cells [37]. Once across the mesothelium, the basement membrane creates no resistance to fluid, solutes and small molecules allowing direct access to the underlying sub-mesothelial capillary and lymphatic system [44]. The capacity of the peritoneum to transport fluids provides the basis for PD exchanges and in response to peritoneal dialysis solutions, ultrafiltration and diffusion of water, salt and uraemic toxins across the peritoneum occurs [37].

1.2.4.4 Inflammation & Tissue Repair

Mesothelial cells play a crucial role in the modulation of inflammation within the peritoneum through their ability to synthesize cytokines, chemokines, growth factors, ECM proteins and intercellular adhesion molecules [35]. Following initial injury and denudation, mesothelial cells respond quickly to restore the uninterrupted monolayer and replenish lost or damaged cells using various mechanisms; including centripetal migration from wound edges, exfoliation of healthy cells from opposing surfaces or distant sites, and free-floating reserve cells attaching to denuded or exposed areas [33, 54, 55]. Resident macrophages within the peritoneal cavity and the sub-mesothelial zone, play a key role in the recognition and induction of an inflammatory response. Activated macrophages, secrete inflammatory mediators such as TNF-α, IL-1β and Interferon γ (IFN-γ) which in turn stimulate mesothelial cells to produce cytokines such as transforming growth factor-β1 (TGF-β1), monocyte chemoattractant protein-1 (MCP-1; or chemokine C-C motif ligand 2, CCL2), RANTES (or chemokine C-C motif ligand 5, CCL5), IL-8 (or chemokine C-X-C motif ligand 8, CXCL8) and adhesion molecules including intercellular adhesion molecule-1 (ICAM-1), vascular cellular adhesion molecule-1 (VCAM-1), E-cadherin, N-cadherin, CD49a, CD49b, CD44 and CD29 [35, 52, 56, 57]. The main effect of these is to elicit the recruitment of leukocytes that are normally restricted to the blood vessels to the site of injury and facilitate leukocyte adherence and directed transmigration across the mesothelium [35]. This is critical to resolve any inflammatory episode and signals transition from innate to acquired immunity [56, 58, 59].

1.2.4.5 Recognition of Foreign Pathogens

Antigen presentation and T-cell activation are the first steps in the generation of a specific immune response to microorganisms and foreign antigens [44, 60]. This response is mainly controlled by T-helper (Th) cells, which recognise foreign material presented by major histocompatibility complex (MHC) - class 2 molecules on antigen-presenting cells (APCs) [37]. In addition to the resident and migratory immune cells able to present antigens (namely dendritic cells, macrophages, monocytes and B-cells), mesothelial cells have also been shown to be APCs and effectively contribute to antigen presentation to T-cells [60-62]. To do this, mesothelial cells produce ICAM-1, and effective accessory molecule (T-cells require contact accessory molecules alongside presenting cells to mount effective T-cell activation) which allow mesothelial cells to present antigens.

1.2.4.6 Fibrogenesis and Fibrinolysis

Fibrin deposition and adhesion formation occurs early during an inflammatory response, typically within 72 h [33]. Mesothelial cells are important regulators of both the local fibrin deposition and clearance within the peritoneum through pro-coagulant generation or secretion of fibrinolytic enzymes [35]. Mesothelial cells exert their procoagulant activity through production and regulation of tissue factor (TF), a transmembrane receptor for factor VII/VIIa, which is a potent activator of the extrinsic coagulation cascade [63]. Fibrin deposition is enhanced by the secretion of plasminogen activator inhibitors 1 and 2 (PAI-1/2) which inhibit urokinase plasminogen activator (uPA), an enzyme responsible for the cleavage of plasminogen to plasmin, therefore preventing the breakdown of fibrin to fibrin degradation products [44]. Fibrinolysis counteracts this phenomenon and is also regulated by mesothelial

cells, mainly through generation of tissue plasminogen activator (tPA), uPA and its receptor (uPAR). Determination of whether fibrogenesis or fibrinolysis predominates in the peritoneum depends on inflammatory mediators such as lipopolysaccharides, TNF-α, IL-1 and fibrogenic mediators such as TGF-β1 and thrombin. During normal repair, fibrinous adhesions are removed under the activity of fibrinolytic factors secreted by regenerating mesothelial cells [44]. During a persistent insult or injury, fibrin continues to be produced and sub-mesothelial fibroblasts migrate into the fibrin matrix and deposit ECM proteins (mainly collagen) to form permanent adhesions within the peritoneal cavity [64].

1.2.5 Changes to the Peritoneal Membrane during PD and Peritonitis

1.2.5.1 Causes of Peritoneal Membrane Changes with PD

The efficacy of PD as a treatment modality largely depends upon the maintenance of peritoneal integrity over time [65]. It is well recognised that chronic low-grade inflammation plays a crucial role in peritoneal membrane dysfunction, with the estimated prevalence of systemic inflammation in PD patients ranging between 12-65% [66, 67]. The causes of inflammation in PD can broadly be categorised into factors related to a decrease in renal function and factors related to PD therapy. There is a strong causal relationship between exposure to bioincompatible PD solutions and/or episodes of peritonitis leading to the long-term loss of peritoneal membrane function. These are generally considered to be the most important causes of technique failure and subsequent transfer to haemodialysis [43]. However, residual renal function and uraemic toxins are likely to exacerbate the inflammatory burden in PD patients, and are therefore important to mention first.

Residual renal function plays an important role in regulating inflammatory activity in patients with ESRD, with several studies reporting a correlation between elevated levels of acute inflammatory markers (such as C-reactive protein (CRP), IL-6 and tumour necrosis factor (TNF)-α) and a reduced glomerular filtration rate (GFR) [68-76]. This is not universally supported, with some studies reporting no major differences in serum cytokine levels between PD patients and ESRD patients [77-79]. Instead they hypothesize that comorbidity, traditional lifestyle factors, genetic predisposition and uraemia may promote an ongoing chronic low-grade inflammatory state which starts in advancing CKD and is exacerbated by PD. Uraemia is common in all ESRD patients and contributes to low-grade persistent inflammation through production of advanced glycation end-products (AGEs) and their receptors (RAGEs) alongside increased oxidative stress. A normal kidney plays an important role in the metabolism of AGEs and with declining renal function, the clearance of these becomes impaired, further contributing to their accumulation in the peritoneum. PD therapy does reduce the impact of uraemia to a degree, but it does not remove it completely [80].

The effects of residual renal function and uraemia on pro-inflammatory cytokine production in PD are somewhat unclear. One small study of incident PD patients found those with a higher CRP level starting PD had a greater loss of RRF after 1-year when compared to patients with a normal CRP [72]. Another single centre study of 95 prevalent PD patients found higher CRP levels in anuric patients on PD compared to those with residual renal function [81]. However, the largest cohort study to date, comprising 959 incident and prevalent PD patients followed up for 8 years, could not corroborate these findings and showed no link between a reduction in urine volume and increasing cytokine concentrations of IL-6, TNF-α and IFN-γ [73]. Preservation of residual renal function during PD isn't always in the forefront of causes

of peritoneal membrane changes, but is associated with lower mortality, less morbidity (better nutrition, less degree of anaemia) and ultimately better quality of life on PD [82-85].

Initiation of PD therapy, using various PD solutions, introduces a persistent inflammatory factor that accelerates peritoneal membrane changes. PD therapy involves the constant exposure of the peritoneal membrane to bio-incompatible PD solutions, that contain elevated concentrations of glucose to provide the osmotic drive across the peritoneal membrane. High glucose-containing PD solutions typically have 15-40X the physiological concentrations of glucose normally found in peritoneal fluid and is one of the factors leading to peritoneal membrane alterations [86, 87]. Chronic exposure to high glucose load in conventional PD solutions induce the synthesis and release of proinflammatory and profibrotic factors, including vascular endothelial growth factor (VEGF), TGF-β and AGEs [67]. Conventional PD solutions also contain glucose degradation products (GDPs), as a direct result of heat sterilisation at a low pH to prevent glucose caramelisation. This process results in the breakdown of some glucose products, termed glucose degradation products (GDPs), which accumulate in PD solutions during storage. GDPs have been implicated as responsible for some of the glucose mediated peritoneal damage associated with PD solutions, with the use of filter-sterilised fluids (rather than heat-sterilised) detecting much lower concentrations with less biological effects on the peritoneal membrane [87-92]. Newer generations of PD solutions have been produced over the last 25 years that are more 'biocompatible' and are associated with fewer membrane changes [80]. The divergence from high glucose loading in PD fluid to using either lower glucose concentrations or glucose alternatives, such as icodextrin and amino acids, not only lessens the generation of GDPs but also avoids the metabolic and nutritional consequences of absorbing 100-200g of glucose per day.

Furthermore, newer solutions utilise lactate and bicarbonate as buffers, giving a lower pH and/or a reduced content of GDPs without compromising on the ultrafiltration rates [93, 94]. Despite the enhanced biocompatibility of using newer solutions and the associated risk to both membrane and patient of glucose-based solutions, glucose is still used as the main osmotic agent and will therefore continue to promote inflammation within the peritoneum.

Peritonitis is a potentially life-threatening condition associated with PD and remains the leading cause of technique failure. Peritonitis is diagnosed when a patient presents with 2 or more of the following criteria; (1) Clinical features consistent with peritonitis (abdominal pain and/or cloudy PD effluent bag) (2) Dialysis effluent white cell count >100/μL or >0.1 x 10^9/L (after a dwell time of at least 2 hours) with >50% polymorphonuclear cells (3) Positive PD effluent culture [95]. The morbidity and mortality risk with PD peritonitis is high with patients often requiring prolonged hospital admissions for treatment and mortality reported at around 16% in the UK [96-98]. The most common micro-organisms responsible for peritonitis are *Staphylococcus aureus, staphylococcus epidermidis* and *Pseudomonas aeruginosa*, which are all normal commensals of the skin in healthy individuals, but have direct access to the peritoneal cavity due to the presence of an in-dwelling PD catheter. They account for up to 60% of cases of peritonitis, with the remainder being due to gram negative bacteria and fungi [80]. Importantly, culture negative peritonitis accounts for 10-20% of all peritonitis episodes and can be difficult to treat [95, 99]. The inflammatory response to peritonitis is well documented and is an important source of inflammation during PD. Studies have reported elevated dialysate cytokine levels of Il-1β, IL-6 and TNF-α up to 24 hours prior to onset of clinical features, which drives the mesothelial cell response to infection [66, 100]. These levels can remain significantly elevated for up to 6 weeks post infection, despite the resolution of

clinical features. There is a strong causal relationship between the frequency and severity of peritonitis episodes and long-term loss of peritoneal membrane function, which lead to functional and morphological changes in the peritoneal membrane, especially mesothelial cells [42]. Hence understanding the factors that influence peritoneal infection and inflammation are important research areas in trying to prevent PD failure and promote longevity of PD therapy.

1.2.5.2 Morphological and Functional Changes to the Peritoneal Membrane during PD

Peritoneal inflammation generated by PD causes significant morphological alterations to the peritoneal membrane, and over time contribute to the functional deterioration of the peritoneum's dialysis capacity. Approximately 50% of all PD patients develop alterations in their peritoneal membrane, such as progressive fibrosis, angiogenesis and vascular degeneration, which eventually leads to increased solute transport and loss of ultrafiltration [29, 42, 101]. Specifically, the characteristic changes seen in the membrane include denudation of the mesothelial layer, reduplication of basement membranes, increasing thickness of the sub-mesothelial compact zone through matrix deposition, myofibroblast presence, progressive sub-endothelial hyalinisation, neoangiogenesis and vasculopathy [42, 43, 102] (Figure 1.4). These alterations are considered to be the main cause of accelerated small solute transport across the membrane, dissipating the osmotic gradient necessary for fluid exchange, resulting in UF failure [103]. There is particular interest in the role of mesothelial cells in driving the fibrotic response during PD, as changes below the monolayer correlate with loss of the mesothelial cells above [29]. Mesothelial cells arguably undergo the greatest structural and functional alterations during PD; both *In vitro* and *ex vivo* studies of

human peritoneal mesothelial cells show significant changes upon exposure to PD solutions and local inflammation [42, 47, 53, 55, 56, 59, 102, 104-108]. These include (1) Reduction in glycocalyx volume and a concomitant loss of anionic charge in the glycocalyx (2) Reduction in the length and density of microvilli and cilia on the surface of mesothelial cells (3) Detachment of mesothelial cells from the basement membrane resulting in complete or partial denudation of the mesothelial monolayer (4) Reduplication of the basement membrane (5) Mesothelial cell activation and production of profibrotic cytokines and matrix proteins, which in turn activate other resident cells including fibroblasts (6) hyalinisation of blood vessels and vasculopathy (7) Induction of a phenotypic change from mesothelial cells to mesenchymal cells, termed epithelial-to-mesenchymal transition (EMT) [43].

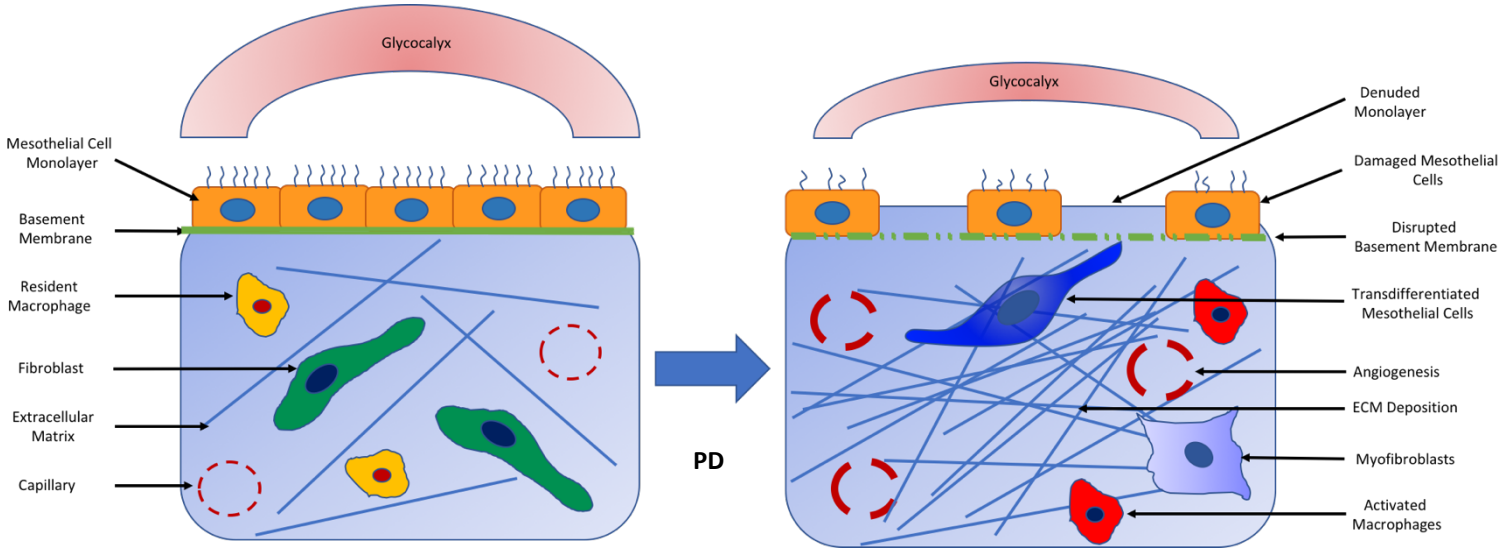

Figure 1.4 Schematic representation of the structural and functional alterations seen in the peritoneal membrane of patients on PD (Adapted from [43]). Constant exposure of the peritoneal membrane to bioincompatible PD fluid, together with repeated episodes of PD peritonitis causes: Reduction of glycocalyx volume and charge, reduction in length and density of microvilli on surface of mesothelial cells, denudation of the mesothelium monolayer and basement membrane, activation of infiltrating and resident peritoneal cells, increased synthesis of proinflammatory cytokines and matrix proteins, induction of EMT in mesothelial cells and activation of peritoneal fibroblasts to myofibroblasts, hyalinization of blood vessels and vasculopathy.

1.2.5.3 Epithelial-to-Mesenchymal Transition (EMT) of Mesothelial Cells

EMT is a biological process essential for embryological development, beneficial in normal wound healing, and pathogenic in malignancy and fibrosis. Epithelial cells have the ability to transition from an epithelial phenotype into a mesenchymal phenotype and back, termed EMT [109]. During EMT, epithelial cells undergo several changes to assume a mesenchymal cell phenotype (Figure 1.5). This process in cultured HPMCs typically occurs within 48 hours with return of epithelial phenotype occurring within 96 hours [110].

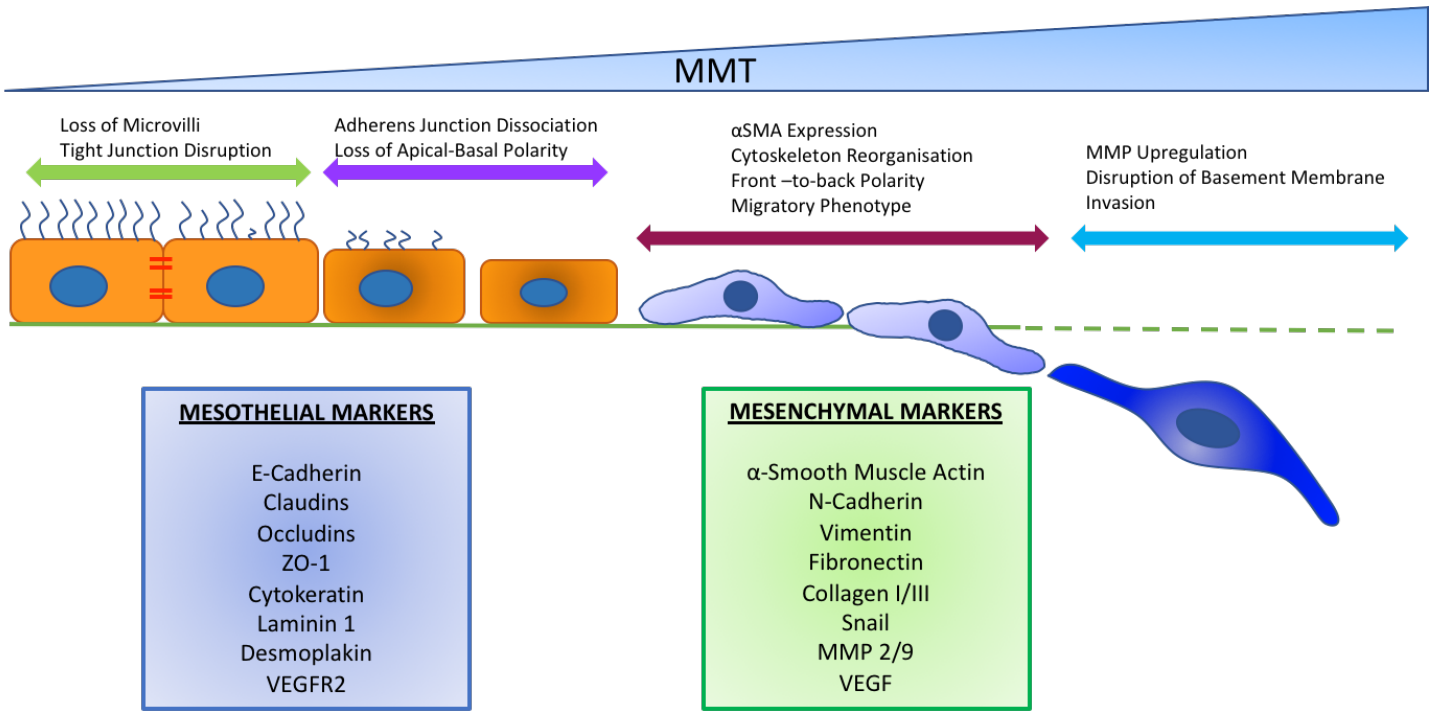

Figure 1.5 Schematic illustration of key events during MMT (Adapted from [111]). MMT starts with the dissociation of intercellular junctions, as a result of downregulation of adhesion molecules such as E-Cadherin, Occludins, Claudins, Zona Occludens-1 (ZO-1) and Desmoplakin. This is associated with a loss of microvilli and apical-basal polarity. Mesothelial cells then adopt a front-back polarity as a result of cytoskeleton reorganization, acquire α-SMA expression and increased migratory capacity. In the later stages of MMT, mesothelial cells acquire the capacity to degrade basement membrane by upregulating the expression of matrix metalloproteinases (MMP). During the end-stages of MMT, mesothelial cells are able to produce a large amount of extracellular matrix components and synthesize a variety of inflammatory, profibrotic and angiogenic factors that may contribute to the structural and functional alterations of the peritoneal membrane.

This conversion into mesenchymal cells allows these former epithelial cells to develop a migratory and invasive phenotype, with similar characteristics to activated fibroblasts, termed myofibroblasts. These myofibroblasts are are involved in ECM production and remodeling, and are essential for fibrous scar formation [112, 113]. There is a progressive accumulation of myofibroblasts in the peritoneum of patients on long-term PD, which is not a feature in a normal peritoneum. The origin of myofibroblasts in the peritoneum remains a matter of intense debate, but there is consensus that they constitute a heterogeneous population derived from multiple sources (Figure 1.6) [110, 111, 114-117].

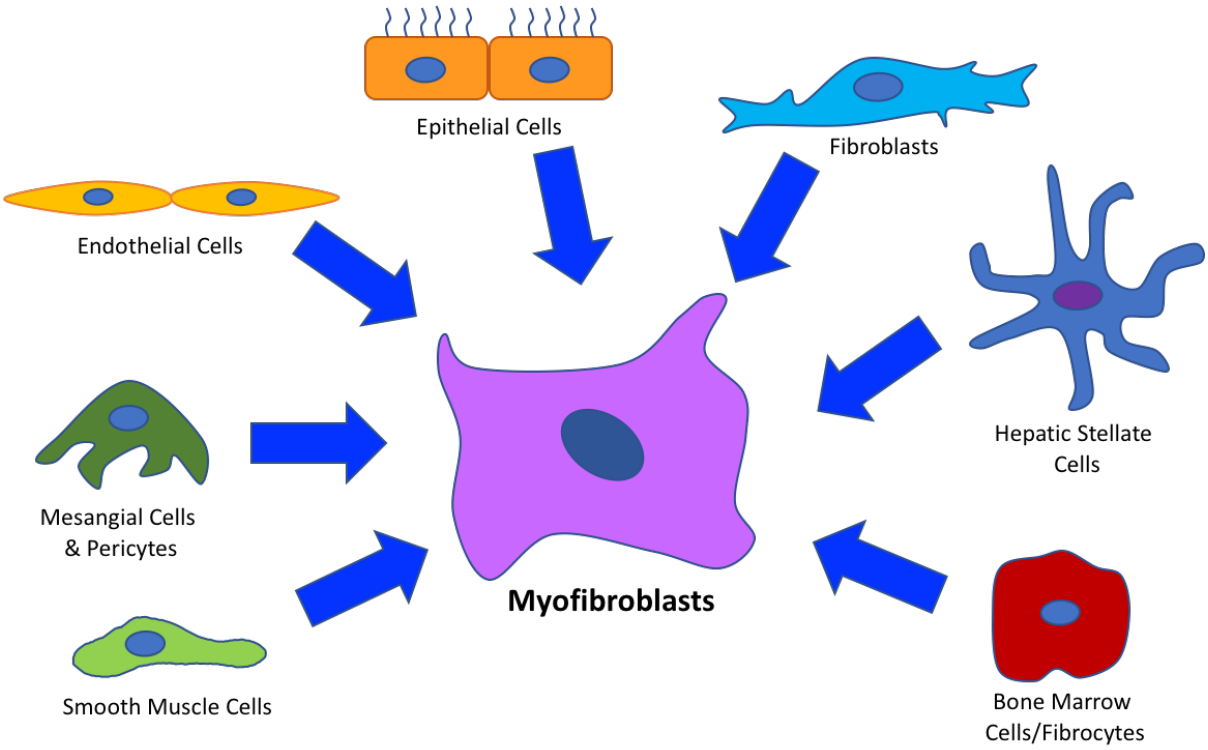

Figure 1.6 Multiple Sources of Myofibroblasts (Adapted from [118])

A landmark paper by Yanez Mo et al [110] first reported the mesenchymal transition of mesothelial cells, found in the effluent of dialysis fluid, soon after induction of PD therapy. These mesothelial cells showed a progressive loss of epithelial phenotype and acquired a myofibroblast phenotype. Since then, other studies have furthered the knowledge on the

main characteristics of mesothelial cells undergoing EMT [119-122]. Consequently, the term mesothelial-to-mesenchymal transition (MMT) has superseded EMT in this context, owing to the mesodermal origin of mesothelial cells. Subsequent studies by Margetts et al [49, 123] have found this process to be largely driven by the pro-fibrotic cytokine transforming growth factor-(TGF)-β1. They induced peritoneal fibrosis using adenovirus-mediated gene transfer of active TGF-β1 to the rat peritoneum. They observed early up-regulation of EMT markers (αSMA, MMP-2 and type-1 collagen) following injection (days 1 to 4) coupled with increased staining for cytokeratin and αSMA in the mesothelium. This was followed by migration and accumulation of these cells into the sub-mesothelial compact zone through a disrupted basement membrane, neoangiogenesis and increased peritoneal membrane solute transport. Similarly, TGF-β1 has been shown to promote myofibroblast persistence in other tissues and organ fibrosis through promoting fibroblast to myofibroblast differentiation [124-126]. Hence the study of factors that regulate TGF-β1 driven pro-fibrotic cell differentiation has been the focus of much study.

Despite the breadth of knowledge that TGF-β1 plays an important role in the development of fibrosis, much less is known about factors that prevent or reverse myofibroblast differentiation. Bone morphogenic protein-7 (BMP-7) is an anti-fibrotic cytokine that has been shown to prevent and reverse renal fibrosis in numerous *in-vivo* models [127-136], possibly through anti-TGF-β1 effects [131, 133, 137]. Our group has previously studied the in vitro mechanisms of BMP7 action and identified that it antagonizes the effects of TGF-β by preventing and reversing TGF-β driven myofibroblast differentiation [138].

1.3 Hyaluronan

1.3.1 Structure and Function

Hyaluronan (HA) is a linear glycosaminoglycan (GAG) produced by animal cells and bacteria and is most commonly associated with the extracellular environment [139]. It is one of four classes of GAGs, otherwise known as mucopolysaccharides, with Heparan Sulphate, Chondroitin Sulphate and Keratan Sulphate making up the others. The properties of HA were first determined by the work of Karl Meyer and John Palmer in the 1930s, who purified a *"polysaccharide acid of high molecular weight*" from bovine vitreous humour that they later termed *"Hyaluronic Acid"* [140, 141]. Its structure has since been identified as a repeating disaccharide unit, consisting of alternating *N*-acetyl-D-glucosamine and D-glucuronic acid residues linked by β (1-4) and β (1-3) bonds (Figure 1.7) [142]. It differs from the other GAGs in its core disaccharide structure, which is not influenced by post-synthetic molecular modification, for example through sulfation or epimerisation of the glucuronic acid isomers. Therefore, the structure can be reliably reproduced by any cell that synthesizes HA [143]. The simplicity and versatility of HA suggests that it has early evolutionary origins relative to the other complex GAGs. However, *Drosophila melanogaster* and *Caenorhabditis elegans* (two simple organisms with fully mapped and sequenced DNA) do not possess the necessary synthases for its assembly suggesting HA first arose much later in evolutionary terms [141]. The number of repeat disaccharide units varies considerably between tissues and in theory, an infinite number of disaccharide units can be added to a HA polymer. This can number 30,000 in some tissues with an end-to-end length of 2-25μm [144]. Detailed analyses of the three-dimensional structure of HA suggest that it forms a rigid, helical configuration in physiological solution creating an overall coiled structure irrespective of size [145, 146].

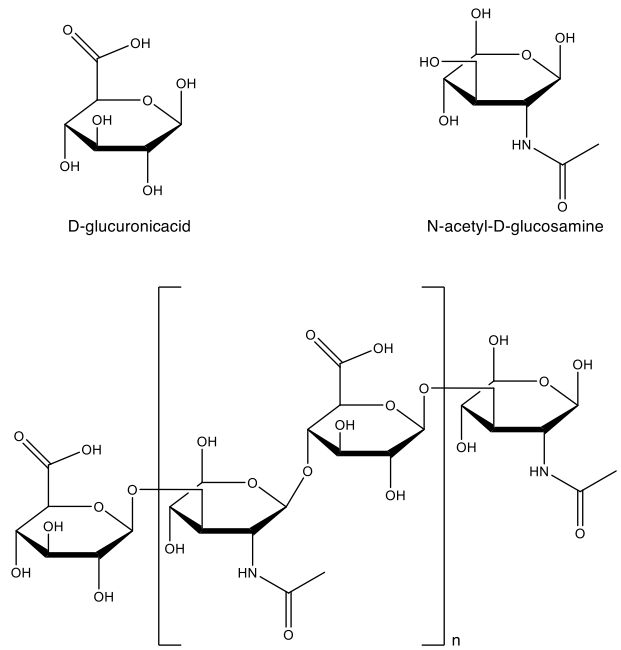

Figure 1.7 Chemical Structure of Hyaluronan. HA consists of repeating disaccharides composed of *N*-acetyl-D-glucosamine (GlcNAc) and D-glucuronic acid (GlcA) residues linked by β (1-4) and β (1-3) bonds. Each disaccharide unit is around 1 nm in length with a molecular mass of around 200 Da and can form large HA chains of indefinite length, typically in the range of 10^4 disaccharides.

One of the main biological functions of HA is its ability to occupy tertiary structures in aqueous solutions by binding to other HA polymers in a repeated anti-parallel array [146]. This creates large hydrodynamic volumes when in contact with water, forming solutions of high viscosity with viscoelastic properties [141]. The synovial fluid of articular joints and the vitreous humour of the human eye display these functions, where HA provides lubrication, protection and structural support to those tissues. Another important function of HA is to assemble a pericellular matrix or "coat" around a cell when its retained at the cell surface. This hyaluronan-dependent coat has multiple complex roles; ranging from structural and mechanochemical support, to the regulation of cell division and motility and even influencing tumour growth and metastasis [147]. Finally, HA is able to influence and regulate cell

behaviour by interacting with various cell surface receptors to initiate intracellular signaling pathways and to regulate cell-cell adhesion, migration and differentiation [148]. It is therefore unsurprising that elevated HA levels have been described in both health and disease contexts, from embryonic development and wound healing to inflammation, fibrosis, tumourigenesis and vessel thickening [149].

1.3.2 HA Synthesis

Conventionally, GAGs are made in the Golgi and attach covalently to protein cores made in the rough endoplasmic reticulum (rER) through post-translational modification to form proteoglycans [150]. HA, on the other hand, is not made in the Golgi but is synthesized by three related membrane-bound synthases on the inner surface of the plasma membrane in eukaryotic cells [141]. There are three mammalian HA synthase (HAS) isoforms termed HAS 1, 2 and 3. These proteins are encoded by the corresponding genes (*HAS1-3*) which are located on different chromosomes [143]. Much of our knowledge about the HAS gene comes from bacterial characterisation and cloning work in the 1990's [151-154]. Since then all 3 HAS genes have been identified in mammals [155-158]. Work from our laboratory defined the genomic structures for the 3 HAS genes and a detailed analysis of HAS1 and HAS2 was carried out using nested sets of luciferase promoter constructs [159-161]. Similar methods have recently been employed to identify the HAS3 promoter region [162, 163]. Despite their location on different genes, HAS isoforms share a significant degree of similarity in their amino acid sequences of about 55-70% [164, 165]. Structurally, all the HAS isoenzymes have molecular masses ranging between 42-64 kDa and consist of multiple membrane-spanning regions, that may be trans-membrane or membrane-associated domains, connected to large cytosolic loops [166]. Over 60% of the whole HAS structure resides within the cell and only

about 5% is exposed to the extracellular environment [167, 168]. Knocking out the activity of *HAS* genes has been instrumental in understanding their normal function. Knockout of *HAS2* in mice is lethal as the mouse embryos develop severe cardiac and yolk sac defects that are almost entirely deficient of HA [164]. Knockout of *HAS1* and *HAS3* on the other hand produces viable and fertile mice, but double knockout of *HAS1* and *HAS3* does lead to an enhanced inflammatory state, accelerated wound closure and fibrosis [169]. This is thought to be related to the temporal expression of *HAS1* and *HAS3* later in embryonic development as opposed to *HAS2* which is required throughout all stages of embryogenesis [170, 171].

The physiological roles of each HAS isoenzyme are not fully understood, but each HAS differs in enzymatic activity, sub-cellular localisation and regulation suggesting they have distinct biological and physiological roles [172]. Furthermore, each synthase is thought to produce different molecular weight HA, which some researchers believe is critical to many pathological conditions [149, 173]. In general, HAS3 is thought to synthesize the smallest HA polymers (between 1 x 10^5 and 1 x 10^6 Da), termed low-molecular weight HA (LMW-HA) whereas HAS1 and HAS2 synthesize larger HA chains (greater than 1 x 10^6 Da), termed high-molecular weight (HMW-HA) [143]. Synthesis of the HA chain begins on the inner cytoplasmic surface of the plasma membrane in mammalian cells, where the synthases utilise both of the HA precursors to transfer the growing HA polymer through the HAS protein complexes (Figure 1.8) [158, 166]. The HASs are structurally adept for this purpose as they possess two distinct binding regions for the two disaccharide substrates of HA (UDP-glucuronic acid and UDP-N-acetyl-glucosamine), whereas most glycosyltransferases possess only one [172]. It is therefore most likely that elongation of the HA chain then occurs from the cytoplasmic side

of the plasma membrane within the cell through addition of new intracellular sugar-UDPs, rather than other ATP-dependent transport mechanisms [174]. Numerous studies have shown that HAS proteins are transported to the plasma membrane via the normal secretory pathways, using green fluorescent protein (GFP)-labelled *HAS* constructs in live cells. *Rilla et al* [175] found that HAS2 and HAS3 isoenzymes travelled to the plasma membrane through the endoplasmic reticulum (E.R.) and Golgi respectively, and formed endocytic vesicles in normal keratinocytes. A similar mechanism of transport through the E.R. and Golgi to the plasma membrane is seen with GFP-HAS1 from the *Xenopus sp* [176]. Interestingly their observations suggest that GFP-HAS2 and GFP-HAS3 do not reside in their functionally active site on the plasma membrane. Recent studies have shown that all HAS isoenzymes can form homo- and hetero-dimeric complexes with each other, and were found in abundance in the Golgi rather than plasma membrane, suggesting they may have functional consequences on HA synthesis, but little is known about this phenomenon at present [177].

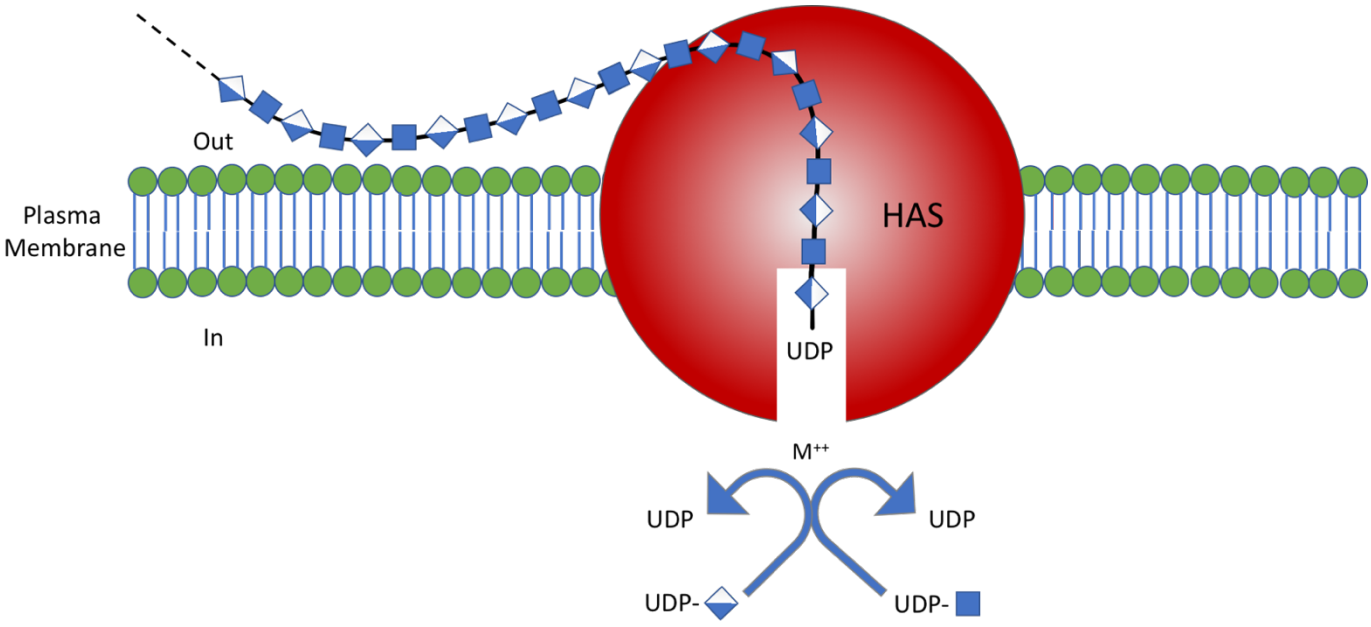

Figure 1.8 Hyaluronan biosynthesis (Adapted from [141]) HA biosynthesis by HAS enzymes occurs by addition of UDP-sugars (UDP-*N*-acetyl-glucosamine and UDP-glucuronic acid) to the reducing end of the polymer with release of the anchoring UDP. M^{++} refers to a metal ion cofactor.

Given that all the HAS' probably generate HA the same way, a hallmark of HAS activity is therefore their ability to generate peri- and extra-cellular matrices. HAS1 is thought to be the least active of the HAS isoenzymes and generates a smaller pericellular matrix than HAS2 and HAS3. This is thought to be related to the differing half-life of the HAS isoenzymes and their binding affinity to HA, with HAS1 having a lower binding affinity and shorter half-life [148, 156]. Even when HAS1 is overexpressed, the HA-coat generated tends to be small when compared to HAS2 and HAS3. However, overexpression of HAS1 does lead to a reduction in HA synthesized by HAS2 and HAS3 suggesting a functional co-operation or negative feedback mechanisms between the isoenzymes [166, 177]. The coat generated by HAS1 is indistinct and is often described as 'cloudy' in appearance rather than the distinct HA coats produced by HAS2 and HAS3 [178]. HAS2 readily assembles tight and concentrated HA coats with a radius equivalent to cell diameter in some cell types [179, 180]. Overexpression of HAS2 also leads to enhancement of HA across the cell surface, that can form cable-like protrusions spanning several cell lengths [181]. Inhibition of HAS2-dependent HA synthesis by various techniques (gene silencing of HAS2/cell surface receptors or removal of HA coat with hyaluronidase treatment) inhibits phenotypic activation of dermal fibroblasts *in-vitro* [124, 182-184]. HAS3 has the highest activity of the 3 enzymes.

Regulation of the HAS proteins can occur at any stage to co-ordinate HA production and all 3 HAS' are often differentially regulated [185, 186]. The regulation of HAS expression can be influenced by numerous pro-inflammatory cytokines and growth factors, that increase synthesis of HA. TGF-β1, IL-1β, TNFα and epidermal growth factor (EGF), have all been implicated in the transcriptional regulation of HAS expression in various cell types [168, 173,

180, 187-189]. Table 1.3 gives a summary of the main growth factors and cytokines that have been shown to regulate HAS/*HAS* expression in human studies.

Growth Factor/ Cytokine/Agent	Organism	Isoenzyme Investigated	Change Seen	Reference
TGF-β1	Human Pleural Mesothelial Cells	HAS1 HAS2 HAS3	↔ ↑ ↔	[187]
TGF-β1	Human Lung Fibroblast	HAS2	↑	[182, 190, 191]
TGF-β1	Human Epidermal Keratinocytes	HAS1 HAS3	↑ ↓	[192, 193]
TGF-β1	Human Dermal Fibroblasts	HAS1 HAS2	↑ ↑	[183, 184, 192, 194]
TGF-β1	Human Oral Mucosal Fibroblasts	HAS1 HAS2	↔ ↓	[183]
TGF-β1	Human Fibroblast-like Synoviocytes	HAS1 HAS3	↑ ↓	[195, 196]
TGF-β1	Human Vascular Endothelial Cells	HAS2	↑	[197]
TGF-β1	Human Lung Adenocarcinoma Cell lines	HAS2 HAS3	↑ ↔	[198]
TGF-β1	Human Articular Chondrocytes	HAS1 HAS2 HAS3	↑ ↑ ↑	[199]
IL-1β	Human Dermal Fibroblasts	HAS1	↑	[194]
IL-1β	Human Orbital Fibroblasts	HAS1 HAS2 HAS3	↑ ↑ ↑	[200, 201]

IL-1β	Human Synovial Fibroblastic Cells	HAS1	↑	[196]
IL-1β	Human Lung Adenocarcinoma Cell lines	HAS2 HAS3	↑ ↑	[198]
IL-1β	Human Articular Chondrocytes	HAS1 HAS2 HAS3	↑ ↓ ↓	[199]
IL-1β EGF	Human Oral Mucosal Epithelial Cells	HAS1 HAS2 HAS3	↑ ↑ ↑	[202]
IL-1β, TNFα	Human Lung Fibroblasts	HAS2	↑	[189]
TNF-α	Human Synovial Fibroblastic Cells	HAS3	↑	[196]
IFN-ɣ	Human Epidermal Keratinocytes	HAS3	↑	[193]
PDGF	Human Pleural Mesothelial Cells	All HAS'	↑	[188]
PDGF	Human Dermal Fibroblasts	HAS1 HAS2 HAS3	↑ ↑ ↑	[203]
PDGF	Arterial Smooth Muscle Cells	HAS2 HAS1	↑ ↑	[204, 205]
FGF, IGF-1	Human Skin Fibroblasts	HAS1 HAS2 HAS3	↑ ↑ ↑	[206]
FGF	Human Articular Chondrocytes	HAS1 HAS2 HAS3	↑ ↑ ↑	[199]
EGF	Human Lung Adenocarcinoma Cell lines	HAS2 HAS3	↑ ↑	[198]

Table 1.3. Transcriptional Regulation of HA Synthase Enzymes in response to different Growth Factors, Cytokines and Agents. ↑ = Increased; ↓ = Decreased; ↔ = No Change

Other regulatory mechanisms for HAS expression have also been described. The transcription factor signal transducer and activator of transcription 3 (STAT3) has been implicated in mediation of *HAS2* upregulation in response to EGF [172]. Detailed analysis of the *HAS2* promoter region in our previous laboratory work also identified several upstream transcription factor binding sites that may regulate HAS2 transcription, namely Sp1, CCAAT (including NF-Y subunit) and nuclear factor kappa B (NFκB) [159, 160]. Furthermore, a natural antisense transcript of HAS2 can be generated from the genomic locus of *HAS2*, called HAS2-AS1, that has been shown to both induce and downregulate HAS2 mRNA expression [161, 207-209]. HAS activity is also regulated post-transcriptionally by post-translational modification to modulate enzymatic activity and possibly alter the trafficking of HAS proteins to the plasma membrane [172]. These regulatory mechanisms account for the discrepancies in findings from numerous studies that the mRNA level of the HAS' don't necessarily correlate with the amount of HA generated. HA generation also requires large quantities of N-acetyl-D-glucosamine and D-glucuronic acid and the concentrations of these substrates can therefore regulate *HAS2* transcription.

1.3.3 HA Degradation

Hyaluronidases (HYALs) are a class of enzyme that predominantly degrade HA. All the HYALSs belong to the glycoside hydrolase (or glycosidase) family that degrade HA by cleaving the β (1,4) glycosidic bonds between N-acetyl-D-glucosamine and D-glucuronic acid residues [210]. In humans, there are six hyaluronidase-like sequences identified to date, called *hyaluronidase 1-4 (HYAL1-4), PH20* and *HYALp1* [211]. *HYAL1, HYAL2* and *HYAL3* have the same genomic location, clustered together on chromosome 3p21.3, whereas *HYAL4, PH20 and HYALp1* are located in a separate cluster on chromosome 7q31.3 [212]. Of the 6 HYAL genes, only *HYAL1,*

HYAL2 and *HYAL3* encode proteins that are expressed in humans; *HYAL4* encodes a protein that appears to have chondroitinase activity, but not hyaluronidase activity, *PH20* is restricted to the testes and *HYALp1* is an expressed pseudogene [141, 211]. Yet the exact mechanism of HYAL mediated HA breakdown is not yet fully understood.

HYAL1 was the first hyaluronidase to be purified from human plasma and is expressed widely in both plasma and urine [210]. HYAL1 expression has been demonstrated in major parenchymal organs such as the liver, kidneys, spleen and heart and genetic mutation in HYAL1 results in an autosomal recessive disease called Mucopolysaccharidosis IX, where circulating HA levels are 40 times higher than normal [168, 213, 214]. HYAL2 is also expressed in somatic tissues, but its enzymatic activity is much lower compared to HYAL1. *Hyal2*$^{-/-}$ mice have extremely high plasma levels of HA, develop chronic haemolytic anaemia, skeletal abnormalities and severe cardiopulmonary dysfunction [214, 215]. Mutations in the *HYAL2* gene have been described in both humans and mice, associated with syndromic orofacial clefting and severe heart defects [216].

HYAL1 is found predominantly intracellularly, whereas HYAL2 can be found both intracellularly and at the cell surface [217, 218]. Both HYAL1 and HYAL2 need an acidic environment with an optimum pH of around 4 for activity and cleavage of HA [219]. On the cell surface, HYAL2 is anchored to the plasma membrane via a glycosylphosphatidylinositol (GPI)-link. Previous researchers have postulated that optimized pH for its cell-surface activity is achieved through the creation of acidic microenvironments by close proximity with NHE1,

a membrane-bound Sodium-Hydrogen exchange enzyme [220]. The bulk of HA cleavage by cell-membrane bound HYAL2 is therefore thought to occur in acidic pockets generated by NHE1 [138, 220]. Activated HYAL2 at the cell surface degrades HMW-HA into intermediate HA fragments of about 20 kDa in size (50 disaccharides) [217]. It has been speculated that HYAL1 and HYAL2 work in succession to degrade HA, with the hypothesis that HYAL2 generates HA fragments of about 20 kDa, which is then internalized and further degraded to tetrasaccharides by lysosomal HYAL1/HYAL2 [143, 211, 217, 221]. Little is known of the role of HYAL3 in HA degradation currently, but there is some evidence that HYAL3 may support and augment the activity of HYAL1 [222]. Knockout of HYAL3 alone in mice however leads to subtle differences in ECM architecture with little change in phenotype, fertility and viability of the mice suggesting limited sole function [222, 223].

Cell-surface HYAL2 has also been reported to have a number of non-enzymatic functions, including formation of complexes with other membrane proteins and regulation of Smad-driven promoters [138, 224]. HYAL2 and NHE1 have been shown to form a complex with the standard CD44 isoform, CD44s, to promote breast cancer invasiveness [220]. Recent work from our laboratory has shown that HYAL2 can also act as a regulator of alternative splicing. Under the influence of BMP-7, HYAL2 was found to translocate from the cell-surface to the nucleus and displace splice regulators from snRNA's and intronic regions on pre-mRNA to influence alternative splicing of CD44 [138].

1.3.4 Hyaladherins

Hyaluronan-binding proteins, also known as hyaladherins, are a large group of heterogeneous proteins. All Hyaladherins share a common ability to bind HA, but differ in their tissue expression, cellular location, specificity, affinity and regulation [225]. As previously mentioned, many of the biological functions of HA depend upon binding to these hyaladherins present either on the cell surface or in the extracellular matrix (Figure 1.9) [141]. Most hyaladherins belong to the link-module superfamily, including; CD44, hyalectans (Aggrecan, Versican, Brevican, Neurocan), lymphatic vessel endothelial receptor-1 (LYVE-1) and the protein product of tumour necrosis factor-stimulated gene-6 (TSG-6) [225]. This link module is a protein domain specific for binding HA, consisting of two α-helices and two antiparallel β-sheets arranged around a large hydrophobic core. Hyaladherins that bind to HA in this way usually have one or two link modules [226]. Notable hyaladherins that lack a link-module include the receptor for HA mediated motility (RHAMM), HA-Binding Protein-1 (HABP1) and HABP-2. [141]

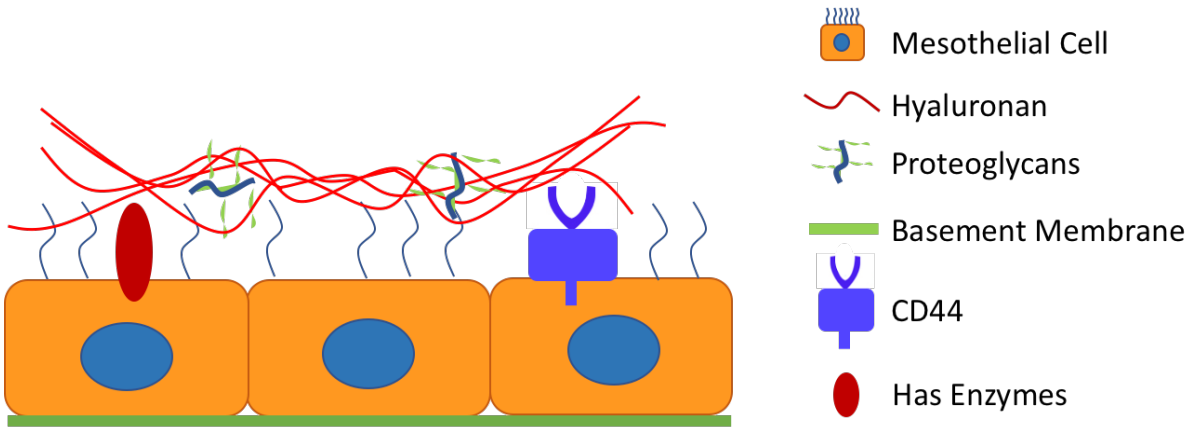

Figure 1.9 Illustration of Pericellular/Glycocalyx-Associated HA anchoring to receptors and HA binding partners. The HA-rich pericellular matrix (glycocalyx) must be anchored to the cell surface in order to form. Several hyaladherins that can bind to HA have been described, with CD44 mediating this function in most instances. HA can also remain attached to the Has enzymes to contribute to HA matrix formation.

1.3.4.1 CD44

CD44 is a polymorphic type I transmembrane glycoprotein that serves as the primary cell-surface HA receptor [227]. It has four functional domains and governs a wide variety of cellular functions from the cell surface through its HA-CD44 interaction. CD44 is transcribed from a single gene on chromosome 11p13 but can undergo complex posttranslational modification to create multiple splice variants, also known as isoforms, of the protein. However, all CD44 isoforms retain the same HA-binding link module, located at the N-terminus, and share a common transmembrane region and C-terminal cytoplasmic domain [228]. Numerous variant isoforms of CD44 have been described, including CD44 standard isoform (CD44s) and CD44 variant isoforms 1-10 (CD44v1-10) [229]. CD44s is the smallest isoform and is encoded by exons 1-5 and 16-20, which translates into a polypeptide with a molecular mass ranging between 80-85 kDa. CD44v isoforms have a longer extracellular domain by addition of up to 10 exons (Figure 1.10). It is important to note that the functional significance of many of these isoforms have yet to be determined.

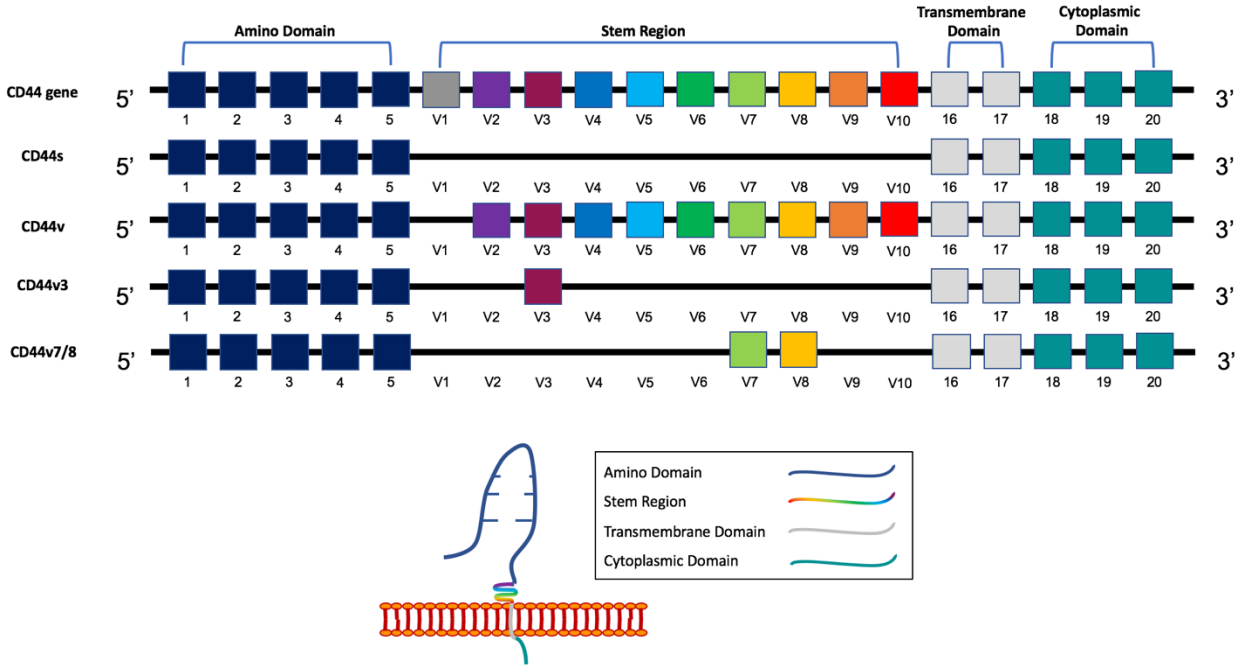

Figure 1.10 Schematic representation of key CD44 domains and alternative CD44 splicing

Many of the cellular functions of HA are modulated by their specific binding to CD44. HA-CD44 interactions can activate numerous intracellular signaling pathways to influence gene expression. HA signaling pathways influencing gene expression will be discussed separately, but, numerous cytokines and growth factors have been shown to influence CD44 expression, including IL-1, TGF-β, TNF-α, EGF and BMP-7 [230-235]. For example, chondrocyte CD44 is upregulated by the cytokine IL-1, which induces a pro-catabolic phenotype leading to intracellular HA accumulation [179]. CD44 can also provide a platform for other cell-surface receptors to bind to that can then influence its own activity as well as the signaling pathways for those receptors. Examples of this include CD44 and ICAM-1, that interact to enhance IL-1β-dependent fibroblast-monocyte binding [236], or the co-localisation of CD44 with TGF-β type I and II receptors to augment TGF-β signaling [237, 238], and coupling of CD44 to epidermal growth factor receptor (EGFR) to promote TGF-β-dependent fibroblast proliferation [182]. In some cancers, CD44v6 isoforms have been shown to bind to receptor tyrosine kinases (RTKs) and effectively act as a signaling hub controlling the activation of those cell surface receptors [239]. CD44:HA interactions are involved in a wide variety of functions and have been demonstrated to play important roles in physiological contexts including cellular adhesion, proliferation, differentiation, signal transduction, maintenance of the pericellular matrix and linking of the extracellular matrix with the cytoskeleton. They also play an important role in embryonic development, inflammation, T-cell recruitment and activation, fibrosis, tumorigenesis and metastasis [227, 240, 241].

1.3.4.2 Other Hyaladherins

There are several other hyaladherins that belong to the link-module superfamily and can be differentiated according to their cellular location. Three cell-surface receptors have been

identified; lymphatic vessel endothelial hyaluronan receptor (LYVE-1), hepatic hyaluronan clearance receptor (HARE/STABILIN-2) and STABILIN-1, that participate in endocytic uptake of HA in endothelial cells. The remaining link-module hyaladherins are extracellular and either form components of the ECM or exist as soluble proteins. The hyalectans are a family of proteoglycans that are components of the ECM. Each hyalectan has HA-binding capacity but differs in tissue distribution; Aggrecan is a major component of articular cartilage; Versican is present in various tissues like blood vessels and skin; Neurocan and Brevican are brain-specific proteoglycans [168]. Anchoring of HA to the cell surface of articular chondrocytes occurs through its binding to Aggrecan and is therefore essential for maintenance of stable pericellular coats. Without Aggrecan, the load bearing function of cartilage becomes compromised [179]. Interestingly the HA-Aggrecan complex must also be tethered to CD44 or HAS proteins themselves to form stable pericellular matrices [242-244]. Versican has been shown to have roles in cell adhesion, migration and proliferation, reviewed in [245]. The secreted product of TSG-6 is another hyaladherin that's critical in the formation and remodeling of HA pericellular coats. TGF-β1-driven fibroblast differentiation is associated with an induction in TSG-6 [190], which binds directly to HA and is involved in tissue remodeling of the kidney through its ability to covalently transfer heavy chains (HC) of the inter-α-inhibitor (IαI) family onto HA, thereby stabilizing the HA matrix [181, 246].

The receptor for HA-mediated motility (RHAMM) is the main hyaladherin that doesn't bind to HA via a link module. RHAMM is an acidic, coiled-coil protein, that was first identified in the early 1990's, along with CD44, as one of the main HA receptors [247, 248]. In contrast to CD44 and other cell surface receptors, RHAMM proteins lack transmembrane domains and don't

express signal peptides at the N-terminus to prompt its translocation from within the cell. RHAMM proteins should therefore be strictly 'cytoplasmic' receptors but are often found on the cell surface where they interact with HA and CD44 to influence cell motility [249]. It is unclear how newly formed RHAMM proteins are transported to the cell surface, as the primary structure of RHAMM lacks sequences that predict classical secretion or integration into the plasma membrane [249]. There has been some suggestion that RHAMM interacts with transmembrane HA Synthases to prompt translocation but probably utilises many possible routes for non-conventional protein export. Nevertheless, once at the cell surface, RHAMM remains bound via GPI-anchoring and binds to HA through clusters of basic amino acids, termed BX7B motifs, on its COOH terminus [240]. It is Important to note that RHAMM mRNA and protein expression is low in normal human tissues and is found intracellularly, where it associates with microtubules to regulate mitosis and maintenance of mitotic spindle integrity to modulate a normal cell cycle [147, 249-251].

1.3.5 HA Signaling

In its native state, HA exists as a HMW polymer (>10^6 Da) and plays an important role in the interplay between cells and other components of the ECM in the maintenance of normal physiological processes. HMW-HA functions as an extracellular signaling molecule and regulates a variety of cell behaviours that are cell specific by binding to its many receptors (Figure 1.11)[240]. Numerous studies have shown that both high molecular weight HA and HA fragments can bind these receptors and activate intracellular signaling pathways [168, 252]. Disruption of ECM homeostasis, for example during inflammation and tumorigenesis, leads to breakdown in cell-cell communication and extensive remodeling of the ECM microenvironment [240]. This causes fragmentation of HMW-HA into LMW-HA (<10^6 Da)

driven by dysregulation of HAS:HYAL activity and rising levels of reactive oxygen species (ROS) as a direct result of tissue injury [168]. However, the size of HA can have a significant influence on receptor activation and downstream signaling, irrespective of receptor expression, signaling pathway or HA location [143]. HA is able to promote clustering of receptors at the cell surface, with HMW-HA having stronger avidity for clustering than LMW-HA and HA fragments. For example, increased levels of peri-cellular HMW-HA promote EGFR and CD44 coupling, and promotes myofibroblast differentiation through MAPK/ERK signaling in response to TGF-β1 [253]. Long chains of HA are also able to bind to several receptors to induce stronger signal transduction [143]. LMW-HA on the other hand has the ability to signal through toll-like receptors (TLRs), either independently or alongside CD44 and RHAMM to trigger pro-inflammatory and pro-fibrotic responses [149, 254]. The effects of receptor co-operation and/or clustering on HA signaling remains an area of much interest mechanistically, to elucidate how different HA sizes engage receptors and modulate signaling pathways.

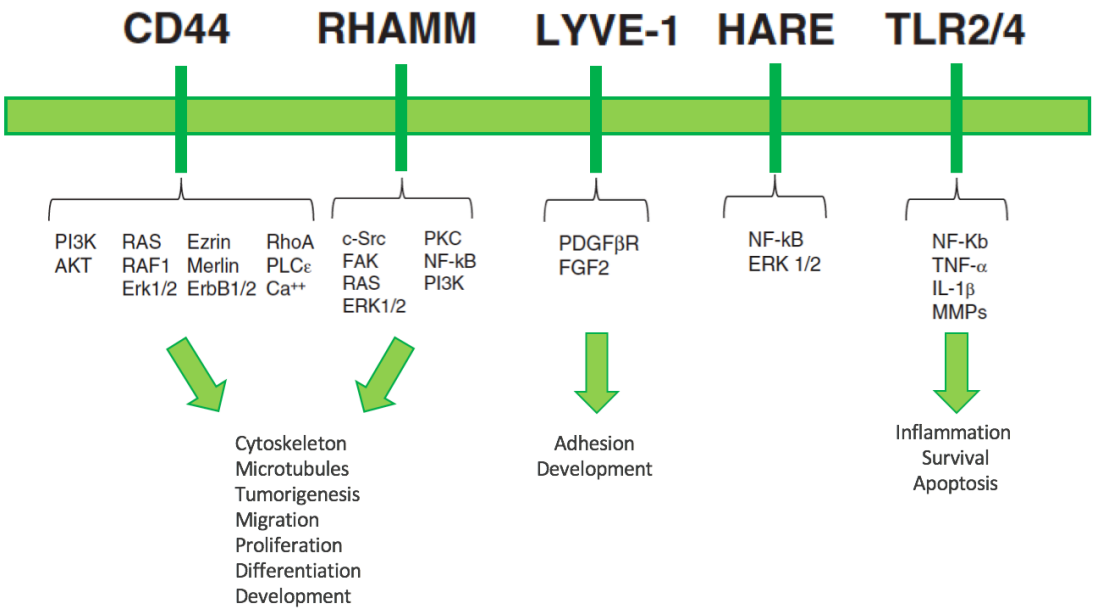

Figure 1.11 Schematic Illustration of HA receptor signaling cascade and biological function (Adapted from Vigetti et al [149]). HA binds to a variety of proteins to influence cell behaviour.

Membrane bound HA binding proteins include receptors such as CD44, RHAMM, LYVE-1, HARE and toll-like receptors (TLR2 and TLR4). HA interactions with these cell receptors triggers several cell signaling responses that are specific for the cell type allowing HA to regulate a variety of cell behaviours including proliferation, migration and inflammation.

1.3.6 HA and Inflammation

It is widely recognised that increased HA deposition in the ECM is associated with numerous inflammatory diseases. Increased accumulation of HA has been demonstrated; in joint tissue of Rheumatoid Arthritis (RA) patients; lung diseases such as Sarcoidosis and Acute Respiratory Distress Syndrome (ARDS); Inflammatory Liver Diseases, Cardiovascular Disease, Rejected Kidney Transplants, Diabetic Nephropathy and Inflammatory Bowel Disease (IBD) [255-268]. A number of human studies, animal and in-vitro models have enhanced our knowledge of how HA modulates inflammation in these disease states.

During inflammation, HA is degraded into fragments that are capable of signaling through specific receptors to initiate an inflammatory response, as described in section 1.3.5 [269]. The synovial membrane of patients with RA is characterized by extensive infiltration of mononuclear cells and deposition of HA [257, 270, 271]. The molecular weight of HA in these synovial joints is significantly more polydisperse and contains a variety of HA polymers with overlapping lengths and different biological functions [269]. Numerous *in-vivo* models have shown that differing molecular weight HA can have distinct and sometimes opposing functions; HMW-HA binding to CD44 has been shown to protect lung epithelial cells from injury and death [272] and prevent liver injury by reducing proinflammatory cytokines in a T-

cell mediated lung injury model [273]. *Teder et al* also showed that $CD44^{-/-}$ mice succumb to unremitting inflammation following non-infectious lung injury associated with accumulation of HA fragments [274]. They found that $CD44^{+}$ macrophages are required to clear the HA fragments, which are found in wild-type mice exposed to the same level of tissue injury. However, several other *in-vivo* studies have demonstrated that HA fragments can stimulate inflammation in the absence of CD44 ($CD44^{-/-}$ mice) suggesting that, although CD44 is the most important cell-surface HA receptor, it is not essential for HA fragment signaling in certain inflammatory settings [272, 275-277]. HA fragments are also recognized as an early biological marker and perpetuator of inflammation in animal models of Rheumatoid Arthritis (RA) [278-280].

Toll-like Receptors (TLRs) are increasingly recognised as the missing link between innate and adaptive immunity, with several studies demonstrating that HA fragments activate innate immune responses through their interaction with TLRs [272, 275, 281, 282]. TLRs are a single pass, transmembrane receptor expressed in innate immune cells such as dendritic cells and macrophages, but are also found on non-immune cells such as fibroblasts and epithelial cells [254]. TLRs recognise and respond to a wide range of damage-associated molecular patterns (DAMPs) that are released following cellular stress, by invading pathogens or generated from ECM remodelling [272, 283]. HA fragments and LMW-HA are major DAMPs that serve as endogenous ligands for TLRs. TLR2 and TLR4 are the major DAMP receptors associated with HA and are expressed in dendritic cells and epithelial cells and are associated with inflammatory pathologies of the serosal cavities [272, 275, 284-286]. Binding of HA fragments to TLRs activate different signaling pathways often triggering the release of pro-inflammatory

and pro-fibrotic mediators like TGF-β, IL-6, TNF-α and IL-8 [254, 287]. In $TLR2^{-/-}TLR4^{-/-}$ mice, induction of chemokine and cytokine release by HA fragments was completely abolished, indicating that TLR2 and TLR4 are required for inflammatory macrophages to express inflammatory genes in response to HA fragments necessary to resolve inflammation [173].

HA can form pericellular coats around cells, and can interact with cell-surface receptors to prevent immune cell recognition and block phagocytosis by macrophages [269]. In inflammatory settings, HA has been shown to form cable-like structures that differ from HA pericellular coats, as they serve as attachment-ligands for receptors on inflammatory cells and are partly responsible for leukocyte recruitment and retention [282, 288]. HA cables have been described in numerous inflammatory conditions such as Inflammatory Bowel Disease (IBD), Atherosclerosis, Diabetic Nephropathy and CKD [269, 288-292]. In these inflammatory conditions, there is a correlation between HA synthesis, leukocyte accumulation and ER stress, suggesting that HA cables act as distress signals that perpetuate the inflammation [293-295]. The presence of HA cables is not exclusive to inflammatory settings. Organisation of HA into cables has been shown to have anti-inflammatory roles as well. For example, monocytes have been shown to adhere tightly to HA cables in clusters whilst inactive, mainly through CD44 expression on their cell surface. Stimulation of kidney proximal tubular epithelial cells (PTC) with BMP7 lead to increased HA cable formation and a dose-dependent increase in leukocyte binding, but a reduction in leukocyte interaction with ICAM-1 thereby preventing their activation. Therefore, cables in this context prevented monocyte interactions with resident cells, and abrogated monocyte dependent inflammatory cytokine production [181, 289, 293, 296].

HA is also able to recruit leukocytes through other mechanisms. The transmigration of leukocytes from the bloodstream is mediated by endothelial cells within blood vessels that engage with adhesion molecules on circulating leukocytes [297]. Leukocytes begin translocation by rolling on the vessel endothelium, which signals the first stage in the trafficking of lymphocytes from the bloodstream to sites if injury [298]. Lymphocytes have been demonstrated to roll on HA coated plates and on cultured endothelial cells *in-vitro*. In these models, blocking the HA-CD44 interaction inhibited this rolling phenomenon [299]. HA expressed on endothelial cells can also bind to chemokines, such as RANTES (CCL5), MCP-1 (CCL2), IL-8 (CXCL8) and MIP-1α (CCL3), to initiate extravasation of lymphocytes within blood vessels to the site of injury [300-303]. The next stage of migration involves adhesion of the rolling lymphocytes to the vascular endothelium. Numerous *in-vitro* and *in-vivo* studies have demonstrated that disruption of HA-CD44 interactions (either through CD44 gene silencing/editing, blocking antibodies to CD44 or removal of HA) limits the adhesion of activated lymphocytes to endothelial cells [297].

1.3.7 HA and Fibrosis

Chronic inflammation is one of the main contributors to progressive organ fibrosis, and it is now increasingly recognised that HA plays a critical role in driving this process. Increased tissue expression of HA has been described in numerous fibrotic conditions and this not only associates with chronic diseases, but often correlates with the degree of fibrosis [173]. Asthma, emphysema and pulmonary fibrosis are three chronic lung diseases associated with abnormal ECM remodeling, where there is evidence for HA accumulation and deposition in human tissues [304-306]. Enhanced levels of HA have been described in the tissues and bronchoalveolar lavage (BAL) fluid of patients with these conditions that correlate with serum

biomarkers of inflammation and fibrosis, such as CRP and surfactant protein-D [307]. HA levels have also been shown to be elevated in other chronic conditions associated with tissue fibrosis, such as liver disease, inflammatory bowel disease (IBD), arthritis and pulmonary arterial hypertension [280, 308, 309]. In liver cirrhosis, there is a strong association between abnormal ECM deposition and high levels of HA in tissues and serum. Degradation of HA normally occurs in liver endothelial cells, thus any condition affecting liver cells can affect serum levels of HA. Furthermore, serum HA levels correlate with severity of liver fibrosis, giving scope for HA use as a clinical biomarker for the diagnosis, evaluation and monitoring of certain liver conditions associated with fibrosis [310, 311].

Our group previously reported that the patterns of HA deposition in progressive renal disease followed a similar pattern to above, wherein the severity of CKD and fibrosis correlated with the degree of HA deposition [54, 312-317]. Increased HA levels are seen in the interstitium of patients with biopsy-proven diabetic nephropathy at all stages, and progressive HA accumulation was observed as patients progressed towards advanced nephropathy [318]. Increased deposition of HA have also been described in other renal diseases associated with fibrosis, including IgA Nephropathy, Lupus Nephritis, anti-GBM glomerulonephritis, Ischaemia-reperfusion injury (IRI) and chronic allograft nephropathy [54, 312-317]. A common pathway in all of these conditions involved the recruitment and increased presence of myofibroblasts in the kidney. Hence, our research group has previously extensively studied the role of HA in the modulation of fibroblast-myofibroblast differentiation in the context of solid organ fibrosis.

1.3.7.1 Cellular Mechanisms of HA-Induced Fibrosis

The association between HA and fibrosis in experimental models has been reported since the early 1990's, with numerous models showing increased expression of HA in chronic inflammation and fibrosis [319]. Experimental models of pulmonary fibrosis demonstrated transiently elevated levels of HA in the interstitium of alveoli, that corresponded to increased HA levels in BAL and lung tissue extracts [168, 320, 321]. An *in-vivo* murine model of bleomycin-induced lung fibrosis showed that targeted overexpression of HAS2 by myofibroblasts induced a more aggressive phenotype, leading to severe lung fibrosis and early death [322]. Primary fibroblasts isolated from the lungs of transgenic mice overexpressing HAS2, also showed a greater capacity to invade matrix. Conditional deletion of HAS2 or CD44 abrogated the invasive fibroblast phenotype, reduced myofibroblast accumulation and inhibited development of lung fibrosis. These findings highlighted the dependency of pulmonary fibrosis progression on HAS2 and CD44 expression [322]. The addition of exogenous HA has shown a beneficial effect in mouse models of smoke-induced pulmonary emphysema, where aerosolized HA led to a reduction in degree of alveolar injury and emphysema [323]. In this context, the exogenous HA protected the endogenous lung tissue HA against degradation from reactive oxygen species generated by cigarette smoke. HA may also protect the airways in emphysema via interactions with the airway epithelium. Epithelial derived HA protected primary lung epithelial cells against apoptosis through its interaction with TLR2 and TLR4 [272]. Addition of exogenous HMW-HA to primary lung epithelial cells prevented bleomycin-induced alveolar fibrosis through TLR-dependent basal activation of NF-κB signaling. The protective effect of HA was lost in *Tlr2*$^{-/-}$*Tlr4*$^{-/-}$ mice. These

finding suggest that HA-TLR2 and HA-TLR4 interactions provide signals that maintained epithelial cell integrity and promoted recovery from acute lung injury.

Myofibroblasts are the principal effector cells that drive fibrosis. They are specialised cells within the human body, that are important in the context of normal wound healing and tissue repair. They exert large contractile forces on their immediate environment and participate in tissue remodelling following injury, through upregulated α-smooth muscle actin (αSMA) expression, and production of ECM components such as collagens/fibronectins and HA [319]. Myofibroblasts are typically derived from activated resident fibroblasts (the most abundant cell type in connective tissue) but can also differentiate from other cell types including: epithelial cells, endothelial cells, and bone marrow derived progenitor cells [118, 324]. Despite the heterogeneity of myofibroblast origin, the differentiation to myofibroblasts follows similar cascades of events, ultimately resulting in the upregulation of pro-fibrotic genes, proteins and molecules. The cytokine, TGF-β1 is the most influential driver of myofibroblast differentiation and therefore important in the context of dysregulated tissue repair and fibrosis [325-330]. Thus persistence of TGF-β-driven myofibroblast activation leads to excessive contraction and aberrant ECM secretion, and is therefore considered to be the main driver of progressive tissue fibrosis [331].

Studies from our laboratories have shown that HA plays a critical role in regulation of TGF-β1 signaling [237] and TGF-β1-driven responses in fibroblasts [253]. Collectively, the studies from this laboratory have proposed a model of the mechanism through which HA mediates TGF-

β1 driven myofibroblast differentiation in solid organ fibrosis (Figure 1.12). [125, 182, 183, 246, 332].

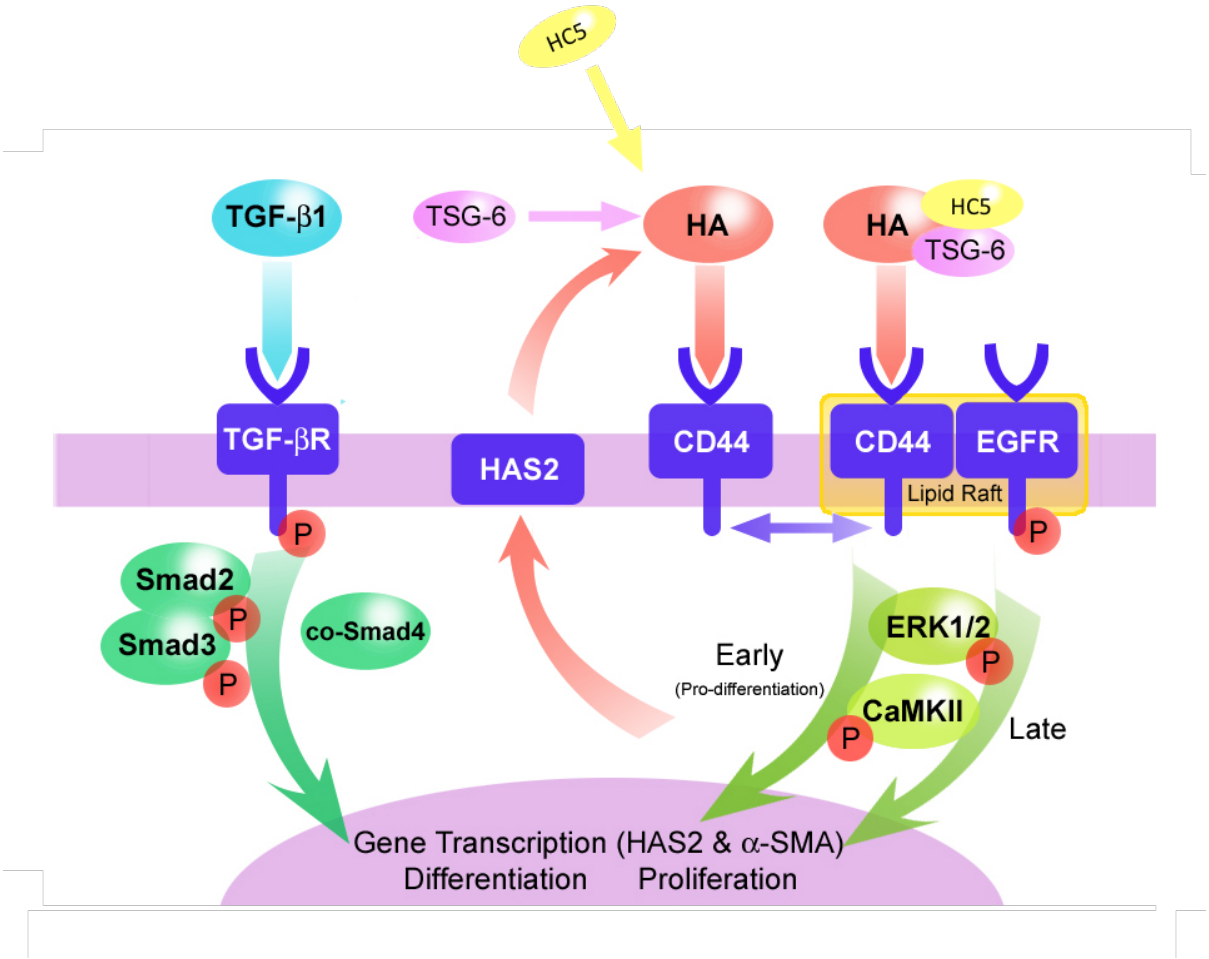

Figure 1.12 Mechanism of TGF-β1-HA-mediated fibroblast to myofibroblast differentiation (Adapted from Meran et al [182] and Simpson et [190]). When fibroblasts are stimulated by TGF-β1, TGF-βR is phosphorylated (P), signalling through Smad2/3 and co-Smad4. HA-mediates CD44-EGFR co-localisation in lipid rafts (yellow), CaMKII activation downstream of ERK1/2 (light-green pathway), indication of the bi-phasic ERK1/2-CaMKII signalling with early phase association to pro-differentiation; and HAS2 gene upregulation (red arrow) dependent on the EGFR branch of the differentiation response CD44/EGFR signalling is through ERK1/2. When both pathways signal in parallel the cell undergoes differentiation into a myofibroblast.

Meran et al demonstrated that HA was required for TGF-β1-driven myofibroblast differentiation, and TGF-β1-dependent fibroblast proliferation [253]. Webber et al and Simpson et al subsequently established that TGF-β1-driven fibroblast-to-myofibroblast differentiation is mediated by the generation of a HAS2 dependent HA pericellular coat [125, 126, 183, 184]. This HA pericellular coat is imperative for the maintenance of terminally differentiated myofibroblasts, as its enzymatic removal *in-vitro* results in loss of phenotype [125, 332]. Importantly, the assembly of the HA coat and response to TGF-β1 was controlled by regulation of HAS2 expression, suggesting that fibroblast expression of HAS2 is critical for maintaining myofibroblast phenotype [183]. This is consistent with what other groups have published in organ systems such as the skin [169] and lungs [322], demonstrating that HAS2 driven HA synthesis promotes fibrosis. Martin et al and Bommaya et al have also identified other hyaladherins that are required to maintain pericellular structure and organisation of the HA coat; namely TSG-6 and the protein subunit of IαI complex, Heavy Chain 5 (HC5) [246, 333]. Midgley et al studied the cellular downstream mechanisms of HA-coat dependent myofibroblast differentiation and demonstrated that the HA pericellular coat promotes CD44 and Epidermal Growth Factor Receptor (EGFR) interactions within cell membrane lipid rafts. This interaction is essential for subsequent intracellular MAPK/ERK and CamKII signaling, which is critical to increased α-SMA expression. Thus, in solid organs such as the kidneys and lungs, TGF-β1-driven fibroblast to myofibroblast differentiation and EMT are not only dependent on changes in HA synthesis but also its pericellular organization.

However, HA can also have opposing actions depending on its manner of synthesis, its organisation and assembly and its interaction with a wide variety of proteins and cell-surface

receptors. Isolated studies have demonstrated that HA can also mediate and modulate BMP-7 responses [231, 296, 334]. More recently, our group have delineated the mechanism of BMP7 prevention and reversal of myofibroblast differentiation in the lungs and kidneys, and shown that this is also dependent on alterations in HA synthesis, assembly and cellular organisation [138]. Midgley et al studied the cellular mechanisms of BMP7 action and demonstrated that BMP7 promotes increased cell-surface expression of the CD44 splice variant, CD44v7/8. CD44v7/8 cell-surface expression leads to internalization and subsequent degradation of cell-surface associated HA, which results in prevention and/or reversal of TGF-beta driven myofibroblast differentiation (Figure 1.13) [138].

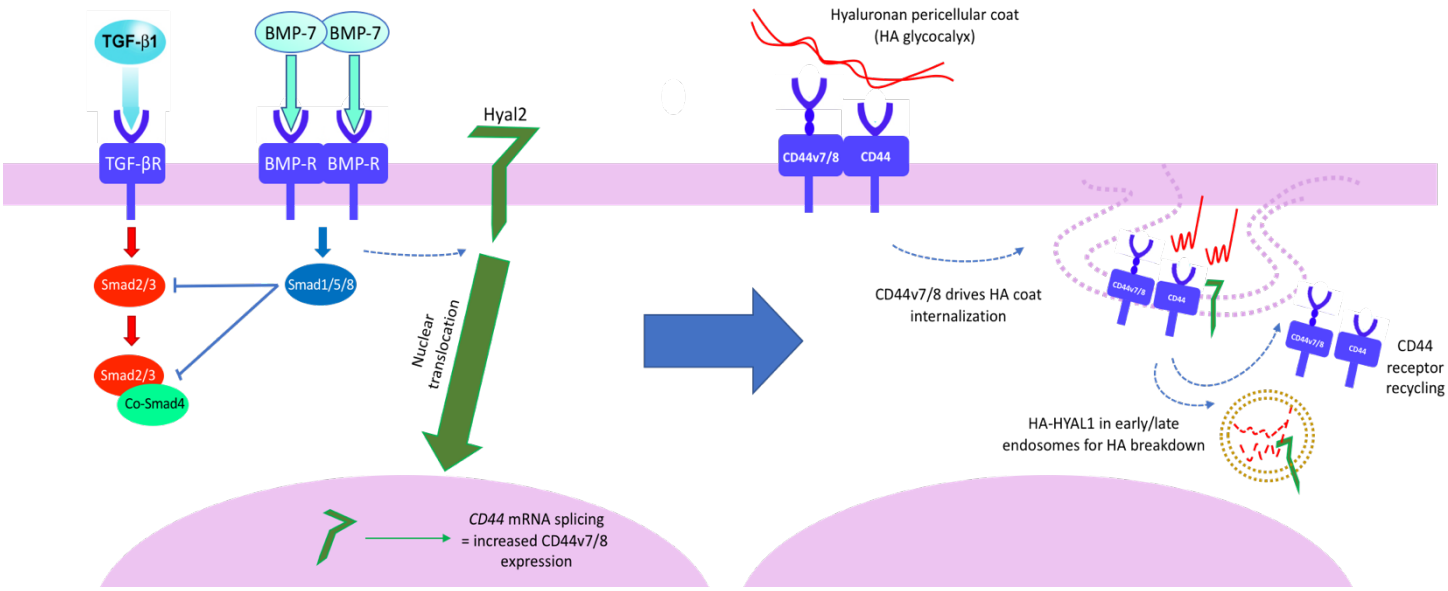

Figure 1.13 Mechanism of BMP-7 internalisation of HA in prevention and reversal of myofibroblast phenotype. BMP7 antagonizes the pro-fibrotic effects of TGF-β1 in fibroblasts and myofibroblasts through dissolution and internalization of the TSG-6 and CD44-EGFR-dependent pericellular HA coat into hyaluronidase-containing endosomes. These events are dependent on increased expression of CD44v7/8 at the cell surface, along with the action of cell-surface Hyal2, which translocate to the nucleus to regulate CD44 alternative splicing.

In conclusion, work from our laboratory has shown that HA is a critical mediator of progressive organ fibrosis, rather than a consequence of it. Importantly, alterations in HA synthesis, degradation, localization and binding can result in distinct and sometimes opposing effects on pro-fibrotic cellular function. Characterisation of HA in the normal peritoneum, and alterations in HA associated with peritoneal dialysis are not yet fully elucidated. Moreover, the role of HA in either promotion or prevention of MMT and peritoneal fibrosis in the context of PD has never been examined. Thus, understanding the role of HA in contributing towards peritoneal infection, inflammation and membrane fibrosis is important in trying to understand the determinants that drive PD failure.

1.3.8 HA in PD

HA is detected in the peritoneal effluent of patients on PD and the concentration of this HA increases during episodes of peritonitis and with increasing duration of dialysis treatment [335]. Peritoneal effluent HA is therefore believed to reflect the intensity of intraperitoneal inflammation, and is often used as a surrogate biomarker of inflammation [336]. The Euro-balance trial highlighted the effect of bioincompatible PD solutions containing high glucose degradation products (GDPs) on HA generation, with higher levels seen in the overnight effluent of patients on these conventional PD solutions [337]. The balANZ trial was the most significant trial to date undertaken to evaluate the clinical benefits of biocompatible PD solutions [338]. Whilst it didn't measure the levels of HA in PD effluent, it reaffirmed the benefit of biocompatible PD solutions on inflammation. The use of low-glucose PD regimens has also been shown to increase levels of anti-fibrotic markers in the peritoneum alongside a reduction in inflammatory markers such as CA-125, vascular endothelial growth factor (VEGF), IL-6 and HA [87]. A reduction in these biomarkers was associated with better preservation of

peritoneal membrane integrity, suggesting a link between HA and peritoneal membrane fibrosis associated with PD.

Some animal studies have been performed to determine the role of HA on peritoneal function during PD. The addition of HA to PD solutions administered to rats resulted in improved membrane function and ultrafiltration [339]. *Rosengren et al* [340] on the other hand, showed that both small solute transfer and net ultrafiltration was not influenced by HA supplementation of PD solutions. The content of HA in peritoneal tissue was increased in chronic PD rats which prevented back-filtration of fluid from peritoneum to plasma by forming a 'filter-cake'. The effect of HA on peritoneal inflammation has also been analysed in animal studies. IP administration of HA in rats reduced the percentage of neutrophils in PD effluent, and was associated with lower levels of TNFα, MCP-1 and IL-10 after 4 weeks exposure in comparison to rats treated with PD solutions alone [339].

PD therapy has been shown to increase HA synthesis by mesothelial cells [313]. Yung *et al* demonstrated that 90% of HA synthesized by HPMCs was secreted into the culture medium and its molecular weight is the same as that found in PD fluid, implying that HPMCs are the predominant generators of HA in peritoneal fluid [47]. During episodes of PD peritonitis, levels of HA are increased and are 10-fold higher than corresponding serum levels, implying that local production accounts for the HA detected in peritoneal fluid [341, 342]. Broborowicz *et al* demonstrated that exposure to dialysate fluids containing high glucose concentrations initiates HA synthesis in HPMCs [343] but also showed that chronic exposure to dialysis fluids

changes the synthetic activity of HPMCs, and actually downregulates HA synthesis [344]. Some of these effects were prevented by a glutathione-precursor L-2-oxothiazolidine-4-carboxylic acid, suggesting that glucose-induced free radicals are responsible for changing mesothelial cell phenotype and HA synthesis in PD conditions. GDPs also have a toxic effect on mesothelial cells upon prolonged exposure [88] and produce AGEs that cause injury and inflammation to mesothelial cells lining the peritoneal membrane. However, little is known about the functional role of HA generated by HPMCs in the peritoneum.

A reliable and reproducible method to study HPMCs in vitro [55, 345] has provided some mechanistic evidence that HA is relevant in the context of PD therapy. Yung *et al* showed that HA was induced after mechanical denudation of a mesothelial monolayer, as seen in PD therapy, driven by upregulated HAS2 expression and downregulated HAS3 expression [346]. Horiuchi *et al* confirmed the relationship between re-mesothelialisation and HA in a similar HPMC wound healing system [347]. In their model, HA was predominantly found in and around migrating mesothelial cells, thought to promote cell mobility at the wound edge. However, as previously mentioned, there are numerous factors that influence the effect that HA has, which is relevant when considering the effects of exogenous versus endogenous HA. Yung *et al*, in their study [346], added exogenous HA preparations to HPMC monolayers damaged by mechanical denudation, which accelerated in vitro healing in a dose-dependent manner between 50 and 3300 ng/ml. Exogenous HA therefore appears to be protective in vitro, similar to its effects in other organ systems. Ito et al demonstrated mechanistic evidence that exogenous HA limits renal injury in PTCs by attenuating TGF-β1 signaling and

TGF-β1 receptor compartmentalization [237, 348], which may be relevant in the context of mesothelial cells.

1.3.8.1 HA as a Potential driver of MMT during PD

Accumulating evidence implicates MMT as a potential mechanism contributing to the development and progression of peritoneal fibrosis during long-term PD [349]. Whilst the role of HA in myofibroblast differentiation in solid organs has been established, the role of HA in MMT in the peritoneum is unclear and relatively few studies have provided insight into its role in development of peritoneal fibrosis. Yung et al demonstrated a 15-fold upregulation in HAS2 expression associated with MMT following mechanical injury to cultured monolayers of mesothelial cells [346]. Once the monolayer was replenished, HAS expression and HA levels returned to constitutive levels. They also showed that MMT was enhanced in the presence of exogenous HA at doses in the range detected in the peritoneum of infected and non-infected PE effluent, mainly through enhanced migration at the leading wound edge rather than proliferation. In the peritoneum, cells with an activated fibroblastic phenotype arise from the local conversion of mesothelial cells by MMT. Some of these myofibroblasts survive independently in the effluent whilst others migrate into the sub-mesothelial zone, where they participate in the fibrotic and angiogenic processes that ultimately lead to PD failure [114]. HA therefore has the potential to be a regulator of MMT, and thus a possible regulator of peritoneal fibrosis.

This thesis aims to investigate whether HA generated by mesothelial cells in response to TGF-β1-driven MMT has the same critical role as in other solid organs such as the lungs and

kidneys. As shown in figure 1.11, TGF-β1-driven fibroblast to myofibroblast differentiation and EMT of proximal tubular cells of the kidney are dependent on changes in the synthesis and organisation of HA, but it is unclear if HA generated during MMT influences the differentiation of mesothelial cells in the same way. Furthermore, in other studies, researchers have shown that treatment with BMP-7 can prevent or reverse scarring in numerous animal models of solid organ fibrosis [131, 133, 135, 137, 350-352]. In the peritoneum, BMP-7 has been shown to ameliorate high glucose induced MMT in an animal model of PD fibrosis and promote mesenchymal-to-epithelial transition (MET) of effluent derived mesothelial cells [120, 353-355]. Our group have delineated the mechanism of BMP7 prevention and reversal of myofibroblast differentiation in the lungs and kidneys, and shown that this is also dependent on HA synthesis, assembly and cellular organisation (Figure 1.12) [138]. This thesis aims to investigate whether BMP-7 can prevent TGF-β1-driven MMT through alternative splicing of CD44 and HA internalisation.

1.3.8.2 HA as a Potential Regulator of Infection and Inflammation During Episodes of PD Peritonitis

Mesothelial cells are involved in the peritoneal response during episodes of PD peritonitis and, alongside resident inflammatory cells, coordinate leukocyte recruitment into the peritoneal cavity to induce an inflammatory response. As previously discussed in 1.2.4.4, mesothelial cells are activated by macrophages that secrete various inflammatory mediators such as TNF-α, IL-1β and IFN-γ. The net effect of mesothelial cell activation is the production of other cytokines and chemokines to elicit the recruitment of leukocytes across the peritoneal membrane to remove the invading pathogen and resolve the inflammatory episode. In doing so, they generate significant amounts of HA. Most of the HA generated by

mesothelial cells exist as HMW polymers in their immediate microenvironment, interacting with various receptors to influence cell behaviour during normal tissue homeostasis. It is clear that HA plays a complex role in inflammation as a regulator of innate and acquired immunity. Whether HA promotes or attenuates inflammatory processes again appears to depend on how it is synthesized, degraded and organised within the peri-cellular matrix. All the research to date indicates that alterations in the synthesis, assembly and interaction of HA with various receptors and signaling molecules in response to inflammation provides cues to ECM remodeling to drive tissue repair and renewal. This thesis aims to investigate whether HA generated by mesothelial cells in response to infection is involved in regulating the induction and resolution of peritoneal inflammation during an episode of PD peritonitis.

1.4 Research Aims and Objectives

HA is a unique glycosaminoglycan, which demonstrates increased expression in numerous fibrotic diseases. Its increased synthesis, assembly and manner of interaction with cell-surface receptors (CD44) and HA binding proteins (hyaladherins) have been shown to influence many cellular processes and disease states. We have previously shown that HA in various contexts can both promote and prevent pro-fibrotic phenotypes. The overall aim of this work is to establish the role of HA in regulating peritoneal infection, inflammation and/or fibrosis by investigating its role in regulating MMT in the mesothelium. Specifically, this thesis aims to determine whether HA alterations identified as relevant in regulating myofibroblast phenotype and solid organ fibrosis can be applied in the peritoneum to promote and/or prevent PD failure.

The aims of the project were:

1. To characterise the profile of HA matrix components in the mesothelium and determine the role of HA in promoting TGF-β1-driven MMT.
2. To investigate the role of HA in the peritoneum in the prevention and/or reversal of TGF-β1-driven MMT.
3. To investigate the role of HA in the peritoneum in regulating peritoneal infection and inflammation.

Chapter 2

Materials and Methods

2.1 Materials

All general and tissue culture reagents were purchased from Sigma-Aldrich (Poole, UK), Thermo Fisher Scientific (Waltham, Massachusetts, USA), BD Biosciences (San Jose, USA) and GIBCO/Life Technologies (Paisley, UK) unless otherwise stated. PCR and QPCR reagents and primers were purchased from Thermo Fisher Scientific (Applied Biosystems, Life Technologies, Invitrogen). The source of any other reagents used is described in the following sections.

2.2 Patient Samples

Fresh frozen PDE samples were utilised from different PD patients recruited to the PERIT-PD study (Time on peritoneal dialysis and peritonitis modulate the phenotype of peritoneal mononuclear leukocytes). Use of these samples was approved by the South East Wales Local Ethics Committee under reference number 02/MRE09/14. It was conducted according to the ethics principles set out in the declaration of Helsinki regarding human experimentation. All individuals provided written informed consent prior to recruitment for the study.

The PERIT-PD study is a prospective, multicenter observational study of 400 patients from 22 centres across the UK. The aim of this study is to establish a multicenter network for collection and analysis of peritoneal effluent samples and accompanying clinical information from PD patients with acute peritonitis. All prevalent PD patients with any episode of suspected peritonitis (based on presence of cloudy peritoneal effluent with >100 WCC/mm^3 with symptoms that might also include abdominal pain, fever or vomiting) were eligible for inclusion in the study provided they could provide informed consent. The study opened in

September 2008 and recruitment is ongoing. PD samples were collected from patients on day 1 of peritonitis episode and simultaneous clinical data collected and stored in a purpose built Peritoneal Dialysis Access database. In total, 18 PD patients recruited as part of the PERIT-PD study were obtained; 9 patients with acute peritonitis and 9 prevalent PD patients without peritonitis appropriately matched for age, sex, length of time on PD and number of previous episodes of PD peritonitis.

2.3 Human Peritoneal Mesothelial Cells

2.3.1 Cell Isolation and Culture

Human peritoneal mesothelial cells (HPMCs) were obtained from healthy omental donors undergoing abdominal surgery. Appropriate ethical approval was in place for all experiments involving specimens derived from patients, and all patients gave informed consent for use of their specimens for research purposes, as previously described [345]. Omentum samples were transported in a sterile plastic container containing PBS at 4°C upon retrieval from the donor.

Isolation of HPMCs were obtained from these omentum samples through a series of enzymatic digestion cycles with 0.05% trypsin-EDTA solution (Invitrogen, T4174). Omentum samples were initially manipulated gently in PBS to remove red blood cells and any other unwanted surface material, then cut into approximately 2 cm x 2 cm x 1 cm pieces using a sterile scalpel. Each of the pieces were placed in a sterile container filled with 10 – 15 ml trypsin-EDTA solution (0.05% (w/v) trypsin and 0.53 mM EDTA in phosphate buffered saline (PBS)) and digested for 15 minutes at 37°C on a rotating wheel. Extracted cells were pelleted

by centrifugation at 1,600 rpm for 6 minutes at 20°C. The tissue was removed for further digestion and supernatant carefully removed without disturbing the cell pellet. Each cell-pellet was resuspended in 20 ml Earle's M-199 medium (Life Technologies) supplemented with 10 % fetal calf serum (Biologic Industries Ltd., Cumbernauld, UK), 2 mM L-Glutamine (Invitrogen), 100 U/ml Penicillin, 100 μg/ml Streptomycin, 5 μg/ml Transferrin (Sigma-Aldrich), 5 μg/ml Insulin (Sigma-Aldrich, Poole, UK) and 0.4 μg/ml Hydrocortisone (Sigma-Aldrich) and re-pelleted by centrifugation at 1,600 rpm for 6 minutes at 20°C. Washed cells were then resuspended in 5 ml of supplemented Earle's M-199, transferred into T_{25} flask (Nunc, Thermo Scientific) and maintained at 37 °C in a humidified incubator with an atmosphere of 5% CO2. Fresh growth medium was added to the cells every 3 to 4 days until the cells were ≥ 90% confluent and ready for sub-culture by regular trypsinisation. All experiments were performed on HPMCs after the second passage and all experiments were performed under serum-free conditions unless otherwise stated. All experiments were undertaken using cells at passage 2.

2.3.2 Sub-Culture

Confluent HPMCs were sub-cultured once at ≥ 90% confluence in T_{25} and T_{75} flasks. Cells were harvested by treatment with 2 ml trypsin-EDTA solution in PBS, activated by incubation at 37°C for 3-5 minutes until cells became detached. Once detached, 5 ml of supplemented medium was added to the suspension to neutralize the protease activity. Cells were then pelleted by centrifugation at 1,600 rpm for 6 minutes at 20°C and supernatant carefully removed. Cells were then resuspended in fresh supplemented medium and seeded into fresh tissue culture flasks or experimentation plates.

2.3.3 Cryostorage and Revival

HPMCs isolated from omentum samples were also amenable to cryogenic preservation for future use. HPMCs grown to ≥ 90% confluence in T_{25} flasks were harvested by treatment with 2 ml trypsin-EDTA solution in PBS, activated by incubation at 37°C for 3-5 minutes until cells became detached. Once detached, 5 ml of supplemented Earle's M-199 medium was added to the suspension to neutralize the protease activity. Cells were then pelleted by centrifugation at 1,600 rpm for 6 minutes at 20°C and supernatant carefully removed. Cells were then resuspended in a 1 ml solution containing 600 µl supplemented M-199, 300 µl 10% fetal calf serum and 100 µl 100% dimethyl sulphoxide (DMSO). Resuspended cells were then transferred into a cryogenic vial (Thermo-Fisher Scientific) and placed in a -80°C freezer for 24 hours and subsequently transferred to liquid Nitrogen (-196°C) for long-term storage.

Cryopreserved HPMCs were revived by rapid thawing at 37°C, using a water bath. Upon complete thaw, the suspension was transferred directly into 20 ml pre-warmed supplemented M-199 and centrifuged at 1,600 rpm for 6 minutes at 20°C. Resuspended cell pellets were then subject to standard cell culture conditions until experimentation. Cryopreserved HK-2 cells were subject to the same rapid thaw procedure as HPMCs but were resuspended in supplemented D-MEM/Ham's F12 medium.

2.4 Cell Counting

HPMCs were sub-cultured, as above, using regular trypsinisation. Upon cell re-suspension in 10% FCS medium and prior to cell seeding, three 20µL volumes of cell-suspension were taken and each added to 20mL of sterile isotonic water in Coulter Counter compatible sample cups. The average cell counts of three readings were taken for each sample using a Coulter Z2 Series

cell counter (Beckman Coulter Inc., Indianapolis, USA). The formulae shown below were used to calculate the total number of cells in the re-suspension solution:

$$\textbf{Total cell count} = \left(\frac{\textbf{Cells}}{\textbf{mL}}\right)\textbf{x}(\textbf{Volume resuspension solution})$$

Cells/mL = (Average cell number) x 2000

2.5 Cell Viability Assay

AlamarBlue™ assay was used for examination of relative cell number and/or viability. The assay incorporates an oxidation-reduction indicator (REDOX) that both fluoresces and changes colour in response to chemical reduction of the growth medium resulting from cell growth. The fluorescent and colorimetric signal is proportional to the number of living cells in the sample. To perform the assay, cells were incubated for 1 hour at 37°C in supplemented serum-free medium containing 10% (v/v) AlamarBlue® reagent (Bio-Rad). After 1 hour of incubation, 100 µl aliquots of medium was transferred onto black 96 well plates (Thermo Labsystems, MA, USA) and fluorescence measured at 544 nm excitation wavelength and 590 nm emission wavelength using a Fluostar Optima Meter (BMG Labtechnologies Ltd., Aylesbury, UK). Medium with 10% (v/v) AlamarBlue reagent were used as reagent blank and were subject to the standardised incubation conditions.

2.6 Cell Stimulations

Phenotypic differentiation of HPMCs were induced by stimulation with 10ng/ml human recombinant TGF-β1 (R&D Systems, Abingdon, UK) for 48 h unless otherwise stated, according to time course and dose response experiments. Time course and dose response experiments were also initially done to determine optimum concentration of human recombinant BMP-7 (PeproTech EC Ltd., London, UK). A dose of 400ng/ml was subsequently

used in all experiments. HPMCs were grown to 90% confluence before undergoing growth arrest in serum-free medium for 24 h. Medium was then replaced with serum-free medium containing 10ng/ml TGF-β1 and the incubations continued for 48 h. The experimental cell system used to determine effects of BMP7 and related alterations in HA on TGF-β1 responsiveness was a prevention model of fibrosis. For the prevention model, cells were treated with 10ng/ml TGF- β1 and 400ng/ml BMP-7 at the same time.

2.7 Chemical Treatments

4-Methylumbelliferone (4-MU) (Sigma-Aldrich) was used to inhibit HA synthesis in HPMCs. 4-MU is a coumarin derivative that is known to inhibit HA synthesis in numerous cell culture models [356-360]. This agent inhibits HA synthesis by depletion of cellular UDP-GlcUA by enzymatic conjugation to glucuronic acid. 4-MU has also been shown to have a direct effect on HAS enzymatic activity through disruption of phospholipids (specifically cardiolipin) associated with the HAS enzymes in the cell membrane. Interference with these phospholipids can potentially results in disruption of the cell membrane resulting in cell death. Therefore, the cytotoxicity of 4MU was assessed. Cytotoxicity of 4MU was assessed by light microscopy and the commercial alamarBlue assay. For this assay, confluent monolayers of HPMCs were incubated for 48 hours in serum-free medium alone or serum-free medium containing 0.1% (v/v) Dimethyl Sulphoxide (DMSO), 0.2mM, 0.5mM, 1mM or 2mM of 4MU. Following 48 hours, alamarBlue was added and analysed as previously described.

Hyaluronidase from *Streptomyces hyalurolyticus* (Sigma-Aldrich) was used to provide a HA depleted state around cells for an extended period of time. Hyaluronate lyase cleaves HA at the β-D-GalNAc-(1→4)-β-D-GlcA bond yielding 3-(4-deoxy-β-D-gluc-4-enuronosyl)-N-acetyl-

D-glucosamine tetra- and hexasaccharides. Unlike other hyaluronidases, this enzyme is specific for HA and is inactive with chondroitin and chondroitin sulphate. Cells were treated with 1iU *Streptomyces* Hyaluronidase for 1 hour prior to stimulation with TGF-β1 unless otherwise stated.

2.8 Visualisation of Pericellular HA by Particle Exclusion Assay

The exclusion of horse erythrocytes was used to visualise the HA pericellular coat around cells. HPMCs were grown to 80% confluence, growth arrested for 24 hours, and then experimented under serum-free conditions for 48 hours. Medium was removed and cells gently washed with PBS. Formalised horse erythrocytes were washed in PBS and centrifuged 1600 rpm for 6min at 20˚C. The pellet was resuspended in serum-free medium at an approximate density of 1 x 10^8 erythrocytes/ml. 100-200µL of this suspension was added per well on a 6-well plate (Corning®, Sigma-Aldrich) and swirled gently to distribute evenly. The dishes were incubated at 37˚C for 15 minutes to allow erythrocytes to settle around the cells. Upon settling, erythrocytes were excluded from zones around the cells with HA pericellular coats. Control cells were incubated with 200 µg/mL bovine testicular hyaluronidase in serum-free medium for 30 min prior to the addition of formalized horse erythrocytes. This was viewed under a microscope as an area of erythrocyte exclusion. Zones of exclusion were visualised on a Zeiss Axiovert 135 inverted microscope.

2.9 Plasmid Generation

2.9.1 CD44v7/8 Overexpression Vector

A CD44v7/8 open reading frame was inserted into the Vector pCR 3.1, using a standard ligation reaction with T4 DNA ligase (New England Biolabs). Amplification of the cloned vector

was achieved via bacterial transformation into one-shot competent *Escherichia coli* (New England Biolabs) and subsequently grown overnight on ampicillin containing agar. Single colonies were extracted, cloned and DNA purified, according to the Miniprep Kit protocol (Sigma-Aldrich). Negative RT experiments were performed alongside CD44v7/8 mRNA QPCR, to ensure pCR 3.1-CD44v7/8 vectors weren't conveying false positive overexpression. Test digestions were carried out to determine whether the vector DNA contained open reading frames using 1% agarose gel electrophoresis to check for ORF presence. All samples were RQ1 DNAse treated (Promega) prior to RT to prevent amplification of open reading frame DNA.

2.10 Transient Transfections

2.10.1 Overexpression Vector Transfection

Transient transfection was performed with the aid of the Lipofectamine LTX Transfection Kit according to manufacturer's protocol (Life Technologies). Briefly, for one 22mm well in a 12-well cell culture plate; 375ng plasmid DNA, 0.5μL PLUS reagent and 1μL Lipofectamine LTX were added to 200μL OPTIMEM transfection medium, mixed well and incubated at room temperature for 25-30 minutes. Following incubation, 200μL of transfection solution was then added the well containing 800μL supplemented M-199 medium with 10% FCS. Cells were incubated for 24h before the medium was replaced with serum-free medium for further experimentation or analysis. As a negative control, an empty pCR 3.1 plasmid (containing no open reading frame sequence) was also transfected into cells. HPMCs were grown to 70% confluence prior to transfection.

2.10.2 Small Interfering (siRNA) Transfection

Transient transfection of HPMCs was performed with specific siRNA nucleotides targeting HAS2 (I.D.: s6457, s6458, s6459, Applied Biosystems), HAS1 (I.D.: s6454, Applied Biosystems) and CD44 (I.D.: s2681, Applied Biosystems).

HPMC transfection was performed in either 35mm diameter wells on 6-well cell culture plates or 22mm diameter wells on 12-well cell culture plates using Lipofectamine RNAiMAX transfection reagent (Life Technologies, 13778075) in accordance with the manufacturer's protocol. HPMCs were grown to 80% confluence prior to transfection and 700μL supplemented M-199 (excluding Penicillin/Streptomycin) containing 10% FCS added to each well. For transfection of a single 22mm well; 3μL Lipofectamine RNAiMAX was diluted in 100μL OPTIMEM Reduced Serum Medium and mixed gently. 3μL of target siRNA (with a final transfection concentration of 30nM unless otherwise stated) was diluted in separate Eppendorf containing 100μL OPTIMEM Reduced Serum Medium. The diluted siRNA was then added to diluted Lipofectamine RNAiMAX reagent (1:1 ratio) and incubated for 5 minutes at room temperature. Following incubation, the siRNA-lipid complexes were added to the well in dropwise fashion, mixed gently and incubated for 5-7 hours after which the medium was replaced with fresh supplemented M-199 containing 10% FCS for further 24 hours. The medium was then removed and replaced with serum-free media, in preparation for further cell treatments or analysis. As a negative control, cells were transfected with negative siRNA (I.D.: AM4611, Applied Biosystems), a scrambled sequence that bore no homology to the human genome.

2.11 RNA Analysis

2.11.1 RNA Isolation

2.11.1.1 HPMCs

HPMCs grown and experimented on culture plates were lysed in TRIzol™ reagent (Thermo Fisher Scientific; Cat. No. 15596-026), and RNA was extracted as per the manufacturers recommended protocol. For a single well on 6-well plates, cells were lysed with 1000µL TRIzol™ reagent solution and incubated at room temperature for 5 minutes to favour total dissociation of nucleoprotein complexes. 200 µl of chloroform (Sigma) were added to the homogenate solution and agitated by inversion for 15 seconds. The sample was incubated for 5 minutes at room temperature and then centrifuged at 12,000 *x g* for 15 min at 4°C to separate aqueous and organic phases. The transparent aqueous phase was isolated and RNA precipitated by adding 500 µl of isopropanol (Sigma). The mixture was vortexed briefly, then incubated for 10 minutes at room temperature before centrifuging at 12,000 *x g* for 10 min at 4°C. RNA precipitates were washed 3 times with 1 ml of 75% (v/v) ethanol (Sigma) and centrifuged 12,000 *x g* for 5 min at 4°C. Clean RNA pellet was air-dried for 15 min and rehydrated in 16µL of RNase-free distilled H_2O (MilliQ; Merck Millipore). Sample purity and RNA concentration was measured using 1 µl of sample by NanoDrop 2000 spectrophotometer (Thermo Scientific). The ratio of 260:280 gave an indication of protein contamination (>1.8 was considered to indicate sufficiently pure RNA for further analysis). The concentration of RNA was calculated from the absorbance at 260nm

$$\frac{ABS_{260} \text{ x dilution factor (50) x RNA coefficient (40)}}{1000} = \text{RNA IN } \mu g/\mu L$$

RNA was stored in all cases at -80°C prior experiment.

2.11.1.2 Mouse Peritoneal Membranes

RNA was extracted from snap frozen mouse peritoneal membranes using RNeasy kit (Qiagen), which is specifically designed to enable recovery of mRNAs from animal cells/homogenized tissue within the range of 10-10^6 cells. Approximately 25mg mouse peritoneal membranes were homogenized in 2ml TRI reagent and incubated at room temperature for 5 minutes to promote dissociation of nucleoprotein complexes. 140 µl of chloroform (Sigma) was added to the homogenised solution and agitated by inversion for 15 seconds. The sample was incubated for 2-3 minutes at room temperature and then centrifuged at 12,000 *x g* for 15 min at 4°C to separate aqueous and organic phases. The transparent aqueous phase was isolated and 1.5X volume (usually 525 µl) of 100% ethanol mixed thoroughly by pipetting up and down several times. 700 µl of the mixture was pipetted into an RNeasy Mini spin column (including any precipitate that may have formed) and placed in a 2ml collection tube, then centrifuged at 10,000 x *g* for 15 seconds at room temperature. The flow through was discarded and 700 µl Buffer RWT was added to the spin column and centrifuged at 10,000 x *g* for 15 seconds at room temperature. The flow through was discarded and 500 µl of 80% ethanol added into the column then centrifuged at 10,000 x *g* for 2 minutes at room temperature. The spin column was placed into a new 2ml collection tube and centrifuged at 10,000 x *g* for 5 minutes at room temperature to dry the membrane. The column was then air dried for 5 minutes and 10-14 µl RNAse free water added to the centre of the column then centrifuged at 10,000 x *g* for 1 minute at room temperature to elute RNA. Sample purity and RNA concentration was measured using the Agilent 2100 bioanalyzer (Agilent). RNA was stored at -80°C until use. Before performing RT-PCR reactions, the RNA was treated with RNAse-free DNAse I following the manufacturer's instructions.

2.11.2 RNA Detection

mRNA was measured in whole samples by a two-step quantitative reverse transcription – polymerase chain reaction (RT-qPCR).

2.11.2.1 Reverse Transcription

mRNA reverse transcription (RT) and resultant cDNA generation was performed using High-capacity cDNA Reverse Transcription Kit with RNase Inhibitor (Thermo Fisher Scientific; Cat. No. 4374966). The RT was conducted using a final volume of 20µL per reaction, containing; 1µg RNA (diluted in 10µL RNase-free distilled H_2O), 2µL of 10x RT random primers, 2µL of 10x RT buffer, 0.8µL of 25x 100 mM dNTPs (deoxynucleotide triphosphates; mixed nucleotides: dATP, dCTP, dGTP and dTTP), 1µL of 50 U/µL Multiscribe Reverse Transcriptase, 0.5µL of 20 U/µL RNase Inhibitor and 3.7µL RNase-free distilled H_2O. RT non-template control (RT-NTC) or negative control reaction contained an equal volume of water instead of diluted RNA. Thermal cycling conditions used were: 10 minutes at 25°C, 2 hours at 37°C and 5 minutes at 85°C, followed by a cooling step at 4°C. Generated cDNA was diluted by adding 60 µl of water and stored at -20°C until further use. RNA isolated from mouse peritoneal membranes were treated with RNAse-free DNAse I (Promega) following the manufacturers protocol prior to RT as above.

2.11.2.2 Quantitative Polymerase Chain Reaction

mRNA quantitative polymerase chain reaction (qPCR) was performed by combining 0.6 µl of mRNA specific PCR primers (300 nM, forward and reverse, Table 2.1), with 10 µl of Power SYBR® Green PCR Master Mix (Thermo Fisher Scientific, Cat. No. 4367659) and 4.8 µl of

RNase-free distilled H_2O. 16 µl of mRNA specific master mix and 4 µl of diluted cDNA, diluted (RT-NTC) and RNase-free distilled H_2O water alone (qPCR-NTC) were added into wells on an Optical 96-Well Fast Plate (Thermo Fisher Scientific, Cat. No. 4346906). A MicroAmp Optical Adhesive Film (Thermo Fisher Scientific, Cat. No. 4311971) was used to seal the plate. qPCR was then performed using the ViiA-7 Real-Time PCR System (Thermo Fisher Scientific, Cat. No. 4453534) according to manufacturer's cycling parameter recommendations: 10 min at 95°C, 40 cycles of 15 secs at 95°C and 1 min at 60°C. Single PCR product amplification was confirmed by melting curve analysis. Specific mRNA primers (Tables 2.1 and 2.2) were designed using Primer-BLAST and NCBI sequence database, to amplify all known splice-variants. To elude genomic DNA amplification, primers were in different exons or bound to exon-exon junctions for design. PCR product length was, ideally, between 75 – 150 bp.

2.11.3 RT-qPCR Data Analysis

Following completion of qPCR, relative expression was calculated using the $2^{-\Delta\Delta CT}$ method for relative quantification of gene expression. The threshold cycle (C_T) indicates the number of PCR cycles required to detect fluorescence during specific PCR product amplification. A standard reference gene (GAPDH unless otherwise stated) was subtracted from the target gene C_T to obtain the delta C_T (dC_T).The mean dC_T for the experimental control group was calculated then expression of the target gene was calculated relative to this control. The $2^{-\Delta\Delta CT}$ method therefore provides quantity expression of target gene relative to the experimental control in a way that experimental control = 1 and all other quantities are expressed as a n-fold difference, termed relative expression (RQ). Alternatively $40\text{-}C_T$ was used where appropriate.

Relative Expression (RQ) = 2,-(dC_T (Experimental Sample) - dC_T (Mean Control Group))

Target Gene	Custom Primer Sequence
E-CADHERIN	FORWARD: TCCCAATACATCTCCCTTCACA REVERSE: ACCCACCTCTAAGGCCATCTTT
ZO-1	FORWARD: GGAGAGGTGTTCCGTGTTGT REVERSE: GGCTAGCTGCTCAGCTCTGT
OCCLUDIN	FORWARD: TAAATCCACGCCGGTTCCTGAAGT REVERSE: AGGTGTCTCAAAGTTACCACCGCT
CLAUDIN-1	FORWARD: CGGGTTGCTTGCAATGTGC REVERSE: CCGGCGACAACATCGTGAC
α-SMA	FORWARD: AACTGGGACGACATGGAAA REVERSE: AGGGTGGGATGCTCTTCAG
FIBRONECTIN-1	FORWARD: CCGAGGTTTTAACTGCGAGA REVERSE: TCACCCACTCGGTAAGTGTTC
EDA-FIBRONECTIN	FORWARD: GCTCAGAATCCAAGCGGAGA REVERSE: CCAGTCCTTTAGGGCGATCA
COLLAGEN 1α1	FORWARD: CATGTTCAGCTTTGTGGACCTC REVERSE: TTGGTGGGATGTCTTCGTCT
GAPDH	FORWARD: CCTCTGACTTCAACAGCGACAC REVERSE: TGTCATACCAGGAAATGAGCTTGA
ID1	FORWARD: GTGGCCATCTCGCGCT REVERSE: TGTCGTAGAGCAGCACGTTT
HAS1	FORWARD: ACCCACTGTACTTTTGGGGA

	REVERSE: ACCTGGAGGTGTACTTGGTAG
HAS2	FORWARD: AATTTTGGAAACTGCCCGCC REVERSE: TCACAATGCATCTTGTTCAGCTC
HAS3	FORWARD: TACATCCAGGTGTGCGACTCT REVERSE: GATCCTCCTCCAGGACTCGAA
HAS2AS1	FORWARD: CACAAGGAGCTGTTTGGATCAG REVERSE: TCAAAACCTGAAAGGGATGCG
HYAL1	FORWARD: GAACCAAGGAATCATGTCAGGC REVERSE: TCACGTTCAGGATGAAGGGC
HYAL2	FORWARD: CGGACTCGAACACAGTTCCT REVERSE: CCAGGGCCAATGTAACGT
TOTAL CD44 (CD44p)	FORWARD: CTTCAATGCTTCAGCTCCACC REVERSE: TCCATCAAAGGCATTGGGCA
STANDARD CD44 ISOFORM (CD44s)	FORWARD: GCTACCAGAGACCAAGAC REVERSE: GCTCCACCTTCTTGACTCCC
CD44 VARIANT ISOFORM 7/8 (CD44v7/8)	FORWARD: AGGAAGAAGGATGGATATGGACT REVERSE: GTCTTGGTCTCGCGTTGTCA
RHAMM	FORWARD: CAATGACCCTTCTGGTTGTGC REVERSE: TCCTTCTTTGATTCCGAAGACT
TGF-B1	FORWARD: CCTTTCCTGCTTCTCATGGC REVERSE: ACTTCCAGCCGAGGTCCTTG

Table 2.1. Human qPCR SYBR Green primers

Target Gene	Custom Primer Sequence
HAS1	FORWARD: GAAGAGAGAATCCAGGAGGACC REVERSE: GCAGGGCAAGATGATCGTG
HAS2	FORWARD: AGGAGCTGAACAAGATGCATTG REVERSE: TGGATGATGAGATGCGAGGC
HAS3	FORWARD: ACCTTCTTTGACCAGCCTCC REVERSE: CACCGGCATCCTGCAACG
HYAL1	FORWARD: TGCCCGTAATGCCCTACGT REVERSE: GCTGTGCTCCAGTTCCTCCA
HYAL2	FORWARD: CGAGGAACTACGGGATGA REVERSE: GGCACTCTCACCGATGGTAGA
CD44s	FORWARD: CTTGGCCACCAGAGATCGAG REVERSE: GTGGTCACTCCACTGTCCTG
YWHAZ	FORWARD: TTGAGCAGAAGACGGAAGGT REVERSE: GAAGCATTGGGGATCAAGAA

Table 2.2 Mouse qPCR SYBR Green primers

2.12 Protein Analysis

2.12.1 HA ELISA

An ELISA-like assay (HA ELISA) was commercially purchased (Corgenix, Broomfield, CO) and used to assess the concentrations of HA in conditioned HPMC cell cultures, and PD effluent (PDE) of patients on PD. Cells were grown to 90% confluence, growth arrested for 24 hours,

and then experimented under serum-free conditions for 48 hours. Conditioned cell culture medium was removed and transferred into eppendorf microcentrifuge tubes and kept on ice. Cells were then washed with PBS before adding 500 µl trypsin-EDTA solution for 5 min at room temperature, to detach pericellular HA. The supernatant was transferred to Eppendorf microcentrifuge tubes, and trypsin was deactivated by heating to 90 °C for 5 min then kept on ice. The remaining cell layer was scraped and re-suspended in 500 µl 10% (v/v) passive lysis buffer (Promega, Wisconsin) and kept on ice for 10 min. PDE samples were thawed overnight at 4°C on ice and centrifuged at 1000 x *g* for 10 mins at room temperature.

HA was then quantified by ELISA, according to the manufacturer's protocol. The assay used micro wells coated with a highly specific HA binding protein (HABP) from bovine cartilage to capture HA and an enzyme-conjugated version of HABP to detect and measure HA in samples. Diluted samples and HA reference solutions were incubated in the micro wells allowing HA to bind to immobilized HABP. The wells were then washed and HABP conjugated with Horseradish Peroxidase (HRP) was added to the wells. Following a second wash, a chromogenic substrate (TMB/H_2O_2) was added to develop a coloured reaction. Stopping solution was added to the wells and the intensity of colorimetric signal was measured using a Fluostar Optima Meter spectrometer at 450 nm wavelength. HA concentrations were analysed by comparing the absorbance of the samples against a reference curve prepared from five reference solutions (50, 100, 200, 500 and 800 ng/mL) and reagent blank (0 ng/ml) included in the kit. The assay was sensitive to 10 ng/ml, with no cross-reactivity reported with other GAG components.

2.12.2 Mouse Cytokine Array

Cell-free peritoneal lavages from inbred 7-8 week-old WT C57/BL6 (Charles River Ltd, Margate, UK) were collected (described in section 2.17) and relative expression levels of 40 mouse cytokines determined using a Proteome Profiler Array (Mouse cytokine array panel A; R&D Systems, Abingdon, UK) according to the manufacturer's instructions. Membranes were exposed to X-ray film for 1, 5, 10, 30 and 50 minutes prior to analysis. Average pixel density was determined using ImageJ software (USA).

2.13 Immunohistochemistry

All immunocytochemistry was performed on cells grown to 70% confluence in either 8-well Permanox chamber slides (Nunc; Scientific Laboratory Supplies (SLS), 177445K) or 8-well glass chamber slides (Millicell EZ SLIDE; Merck Millipore, PEZGS0816). Cells were subject to the same experimental conditions as previously described and each incubation step was followed by a 3-stage wash in appropriate solution. Culture medium was removed from each chamber, and the cells washed with sterile PBS before fixation in cold 4% paraformaldehyde for 15 minutes at room temperature. Cells were then washed thoroughly in PBS after fixation, and permeabilised with 0.1% (v/v) Triton X-100 in PBS for 5 minutes at room temperature (when required) followed by additional thorough washes. Non-specific binding was blocked with 1% (w/v) bovine serum albumin (BSA) in PBS for 1h at room temperature and the cells were washed thoroughly with 0.1% (w/v) BSA in PBS. Subsequently the cells were incubated overnight at 4°C with the appropriate primary antibody (diluted with 0.1% (w/v) BSA in PBS) (Table 2.3). When visualising HA, biotinylated HA-binding protein (bHABP) was used in place of primary antibody. Cells were washed three times with 0.1% (w/v) BSA in PBS, and then

incubated with the appropriate secondary antibody for 1h at room temperature (Table 2.4), again diluted with 0.1% (w/v) BSA in PBS. Avidin-FITC was used in place of secondary antibody when visualising HA. Incubation of secondary and nuclear staining was performed whilst covered to avoid photobleaching. After removing the secondary antibody, the cells were washed with 0.1% (w/v) BSA in PBS, and cell nuclei were stained with Hoechst solution for 30 minutes at room temperature (Sigma-Aldrich; dilution 1:2000 in 0.1% (w/v) BSA in PBS). Following further washes with 0.1% (w/v) BSA in PBS, the slides were mounted with FluorSave mountant (Merck Millipore) and analysed by confocal and fluorescent microscopy (Leica Dialux 20 Fluorescent Microscope (Leica Microsystems UK Ltd, Milton Keynes, UK)).

Indirect immuno-fluorescent identification of Phalloidin was used as confirmation of myofibroblastic differentiation using different staining protocol. After incubation in 1% (w/v) bovine serum albumin (BSA) and washes, cells were incubated with Phalloidin toxin conjugated to FITC (Sigma) diluted in 0.1% BSA and PBS for 2 h at room temperature. After a further washing step, cell nuclei were stained with Hoechst solution (Sigma). Cells were then mounted and analysed by fluorescent microscopy as before.

Antibody	**Type**	**Host**	**Dilution**
HAS1 (AbCam; Ab198846)	POLYCLONAL	RABBIT	1:200
anti-HAS2 (AbCam; Ab140671)	MONOCLONAL	MOUSE	1:200
anti-CD44 (AbCam; Ab6124)	MONOCLONAL	MOUSE	1:250
anti-CD44v7/8 (Thermofisher; MA5-16964)	MONOCLONAL	MOUSE	1:200
PHALLOIDIN	-	-	1:50
bHABP (Merck Millipore; 385911)	-	-	1:100

Table 2.3 Primary Antibodies/MARKERS for Immunocytochemistry

Antibody	Type	Host	Dilution
Alexa Fluor Plus 488 (FITC) (Thermofisher; A32723)	POLYCLONAL ANTI-MOUSE-IgG	GOAT	1:1000
Anti-Mouse Alexa Fluor 594 (Thermofisher; A-11032)	POLYCLONAL ANTI-MOUSE-IgG	GOAT	1:1000
Alexa Fluor 488 (AVIDIN) (Thermofisher; A21370)	-	-	1:500

Table 2.4 Secondary Antibodies for Immunocytochemistry

2.14 Flow Cytometry

Flow cytometry was used to determine leukocyte populations in peritoneal lavage samples. Cells were washed twice and resuspended in FACS buffer (PBS, 0.5% BSA, 0.05% NaN^3), at a density of 5 x 10^6cells/ml, and 100 µl aliquots were distributed in wells of round bottom 96-well plates. Fc receptors on cells were blocked by incubating the samples with a 20% normal rabbit serum solution (in FACS buffer; 100 µl/5 x 10^5 cells) for 15 minutes at room temperature. Samples were then incubated with the specific fluorochrome-labelled antibodies or corresponding isotype controls (Table 2.5). After 1 hour at 4°C, cells were washed twice and resuspended in 200µL fresh FACS buffer and transferred into FACS tube. The stained cells were then analysed using Attune (Thermofisher) or BD FACSCanto II (BD Biosciences) flow cytometer. 20,000 events were acquired for each sample. All analysis was performed using FlowJo (v10.4; TreeStar Inc.)

Antigen	Fluorochrome	Clone	Isotype	Company
Ly6C	Alexa Fluor 488	HK1.4	Rat IgG2c	Biolegend
Ly6G	Alexa Fluor 647	1A8	Rat IgG2a	Biolegend

Table 2.5 Fluorochrome-conjugated anti-mouse monoclonal antibodies used

2.15 In-vivo Experiments

All experimental procedures were conducted following Home Office approval under project license number PPL PA4A9D766. Inbred 7-8 week-old WT C57/BL6 (Charles River Ltd, Margate, UK) were injected i.p. with 500 µl PBS in 50% DMSO (v/v) or heat-killed *Staphylococcus Epidermidis* (HKSE) at 5 x 10^8 cfu/mouse (InvivoGen) in the presence of a custom made HA blocking peptide PEP1 in 50% DMSO (v/v) at 500 µg/mouse (GAHWQFNALTVR, Thermofisher Scientific). At the indicated time points, the mice were sacrificed and the peritoneal cavity was lavaged with 2 ml of ice cold PBS. Leukocyte numbers in the lavages were determined by Coulter counting (Coulter Z2, Beckman-Coulter) and differential double staining performed (anti-Ly6C; anti-Ly6G, Biolegend) as described in section 2.16 followed by flow cytometric analysis. Levels of selected mouse cytokines and chemokines in cell-free peritoneal lavage samples were quantified by cytokine array (described in section 2.14.1.2) and sections of peritoneal membrane were collected and snap-frozen in liquid nitrogen and stored at -80°C until processing for analysis of RNA expression by RT-qPCR (described in section 2.13).

2.16 Statistical Analysis

Statistical analyses were performed using Microsoft® Excel 2016 or GraphPad Prism 7. Graphical data were expressed as averages ± standard error mean (S.E.M) and statistical analyses were performed using a two-tailed Student's *t* test. For experiments with multiple experimental conditions, one-way or two-way analysis of variance (ANOVA) was used to identify statistical differences across groups, followed by Tukey's post-test to identify statistical significance unless otherwise stated. A *p* value of less than 0.05 was considered statistically significant (ns = $p>0.05$, * = $p\leq0.05$, ** = $p\leq0.01$, *** = $p\leq0.001$, **** = $p\leq0.0001$).

Chapter 3

The Role of Hyaluronan Matrix and related HA-binding proteins in driving MMT during Peritoneal Dialysis

3.1 Introduction

One of the most important goals in PD therapy is preservation of the integrity of the peritoneal membrane. Approximately 50% of all PD patients develop alterations in their peritoneal membrane whilst on PD, and chronic PD evokes both a morphological and functional adaptation of the peritoneum [29]. A characteristic alteration seen in the peritoneal membrane during PD is disruption of the mesothelial monolayer and progressive accumulation of myofibroblasts. Myofibroblasts are the principal effectors cells that lay down fibrous matrix, and they are the principal drivers of peritoneal fibrosis leading to peritoneal membrane failure. They are derived from a heterogenous population, as already discussed in section 1.3.7.1, however, mesenchymal transition of mesothelial cells (MMT) is considered to be a prominent source of myofibroblasts during peritoneal fibrosis. Numerous studies have demonstrated that TGF-β1 plays a central role in driving MMT and in the subsequent development of peritoneal fibrosis [49, 101, 120, 123, 361]. Indeed, TGF-β1 is one of the main EMT- and MMT-inducing cytokines in many physiological and pathological states. Hence delineating the regulators of TGF-β1-driven MMT is important in identifying novel mechanisms to prevent peritoneal fibrosis and failure.

HA is known to play an important role in regulating TGF-β1-driven cellular processes [125, 126, 182-184, 190, 236, 237, 253, 332, 348, 362, 363]. It is enriched in many types of human cancers and there is considerable experimental evidence implicating HA in tumour progression through TGF-β1-driven EMT [166, 364-372]. Moreover, TGF-β1 found within cancer exosomes can cause differentiation of fibroblasts to myofibroblasts associated with an increase in HA pericellular coat generation through upregulated HAS2 expression [166, 373].

HA has also been shown to mediate TGF-β1-driven EMT in proximal tubular epithelial cells in kidney fibrosis [333]. Numerous studies on mesothelial cells during PD have indicated that there are alterations with HA in PD [341, 343, 346, 374, 375]. PD therapy has been shown to increase HA synthesis by mesothelial cells, which is associated with increased cell migration, proliferation and phenotypic changes [365]. Yung et al previously demonstrated that mesothelial cells develop a migratory phenotype following disruption of the mesothelial monolayer associated with induction of HA synthesis [55]. Since HA-rich matrix is known to have a profound effect on cellular movement, it was not surprising to see an increase in HAS expression in response to interruption of the mesothelial monolayer in their *in-vitro* model. Notably, HA levels and HAS genes expression returned to constitutive levels after the monolayer was replenished.

During PD HA levels are persistently elevated. They are increased further during episodes of PD peritonitis and with increasing time on PD [335]. However, the role of HA in driving TGF-β1-driven MMT in the context of peritoneal fibrosis has not been studied. The work in this chapter aims to identify the role of HA in driving MMT in the peritoneum.

3.2 Results

3.2.1 TGF-β1 Induces Phenotypic Changes in hPMCs.

Initial experiments were performed on primary cultures of mesothelial cells to confirm that TGF-β1 promoted mesothelial-to-mesenchymal transition (MMT). Mesothelial cells treated with 1, 5 and 10 ng/ml TGF-β1 for 48 hours under serum-free conditions underwent myofibroblast differentiation, and the effects were concentration dependent (Figure 3.1). TGF-β1 down-regulated mRNA expression of epithelial markers E-Cadherin, ZO-1 and Claudin-1 (Figures 3.1A-C) and up-regulated mRNA expression of mesenchymal markers α-SMA, Fibronectin and Collagen IαI (Figures 3.1D-F). The threshold for statistical significance for these effects was reached at all doses, but was greatest at 10 ng/ml. A concentration of 10 ng/ml TGF-β1 was comparable to levels of TGF-β1 seen in the peritoneal effluent of patients on PD and mesothelial cells exposed to high-glucose loading to reproduce PD environments [376-378]. As a result, a TGF-β1 concentration of 10 ng/ml was chosen for subsequent experiments.

Time course experiments were then performed to characterise temporal variation of downstream TGF-β1 regulation. Two time points of 24 and 48 hours were chosen based on previous experience from our laboratory. Down regulation of epithelial markers and upregulation of mesenchymal markers was observed at both 24 and 48 hours (Figure 3.2). 10ng/ml of TGF-β1 down-regulated mRNA expression of epithelial markers E-Cadherin, ZO-1 and Claudin-1 (Figures 3.2A-C) and up-regulated mRNA expression of mesenchymal markers α-SMA, Fibronectin and Collagen IαI (Figures 3.2D-F) at both 24 and 48 hours, but with more pronounced changes and increased statistical significance at 48 hours. Cell morphological

changes related to MMT were subsequently confirmed by visualising filamentous actin (F-Actin) reorganisation in hPMCs stimulated with 10 ng/ml TGF-β1 for 24 and 48 hours (Figure 3.3). F-Actin was distributed at the cell periphery in unstimulated hPMCs at both time points, characteristic of mesothelial and epithelial cells. HPMCs stimulated with 10 ng/ml TGF-β1 demonstrated a larger "poached egg" appearance and this was associated with cytoskeletal reorganization with F-actin filaments coalescing to form thick parallel bundles that extend from end to end of the cells, characteristic of myofibroblast cells.

3.2.2 TGF-β1 Induces HAS Expression in hPMCs.

Initial experiments were performed to assess HA generation during MMT (Figure 3.4). This was initially assessed by mRNA expression of HA synthase enzymes: HAS1, HAS2, HAS3, (including the natural antisense to HAS2; HAS2AS1)**,** Hyaluronidase enzymes: HYAL1 and HYAL 2 and HA receptor, CD44. Treatment of mesothelial cells with 1, 5 and 10 ng/ml TGF-β1 for 48 hours under serum-free conditions demonstrated that myofibroblast differentiation of mesothelial cells was associated with upregulation of HAS1, HAS2 and HAS2AS expression, which was most apparent at a concentration of 10 ng/ml (Figures 3.4A-C). Conversely there was significant downregulation of HAS3 and HYAL1 expression (Figure 3.4D and 3.4E), which was most apparent with 10 ng/ml TGF-β1. No significant change was seen in HYAL2 and CD44 mRNA expression (Figure 3.4F and 3.4G), irrespective of TGF-β1 dose. Using 10ng/ml TGF-β1 as the preferred dose to stimulate myofibroblast differentiation, HAS enzyme expression was then analysed in hPMCs at 24 and 48-hour timepoints (Figure 3.5). Basal expression of HAS1 was significantly higher in undifferentiated hPMCs compared to HAS2, with average HAS1 CT values of 25.5 and 25 at 24 and 48 hours respectively (Appendix A, Figure 1). The average HAS2 CT values in undifferentiated hPMCs was 27.5 and 27 respectively over the same time

points. Following TGF-β1-driven MMT, there was upregulation of HAS1 and HAS2 expression at 24 and 48 hours (Figure 3.5A and 3.5B). The average HAS2 CT values in TGF-β1 treated hPMCs was 25 at 24 and 48 hours, whilst HAS1 expression was much higher with average CT values of 23.5 over the same time points.

There was low constitutive expression of HAS2AS1 in undifferentiated hPMCs, but TGF-β1 induced a significant upregulation of HAS2AS1 expression (Figure 3.5C). There was significant downregulation of HAS3, HYAL1 and HYAL2 expression at 24 and 48-hours following Induction of MMT (Figures 3.5D-F). There was also a significant downregulation of HA receptor proteins, RHAMM and CD44, in response to 10ng/ml TGF-β1 at 24 and 48 hours (Figure 3.5G and 3.5H). HA and CD44 cell localisation and within hPMCs were subsequently assessed using immunocytochemical staining for FITC-labelled HABP and AlexaFluor 594-labelled anti-CD44 antibody (Figure 3.6). In undifferentiated hPMCs, cell surface and intracellular HA were observed, with intracellular HA distributed diffusely within the cytoplasm (Figure 3.6A). In TGF-β1 stimulated myofibroblasts, there was increased HA present both at the cell surface and within the cytoplasm. Furthermore, HA distributed within the cytoplasm was organised around the actin cytoskeleton. CD44 also demonstrated diffuse distribution within the cytoplasm and on the cell surface of undifferentiated hPMCs. Following TGF-β1 stimulation CD44 was identified at the cell surface and demonstrated punctate staining in distinct areas on the plasma membrane (Figure 3.6B).

3.2.3 TGF-β1 Induces Increased Extracellular and Cell-Surface Hyaluronan in hPMCs.

Previous studies in fibroblasts demonstrated increased extracellular and pericellular HA in response to TGF-β1 [183, 253]. We investigated cell-associated HA changes in mesothelial cells in response to TGF-β1. An ELISA-like assay was performed to assess HA levels and cellular distribution in hPMCs (Figure 3.7). There was HA present in undifferentiated hPMCs and was predominantly extracellular in its location with a smaller amount of cell-surface HA also present. TGF-β1 significantly increased extracellular HA levels, with concentrations in excess of 3000 ng/ml quantified from 3 individual donor experiments. There was also an increased trend in cell-surface HA deposition following myofibroblast differentiation, although this did not reach statistical significance ($p=0.0529$). The presence of cell-surface HA pericellular coats was subsequently visualized using a particle exclusion assay (Figure 3.8). In this assay erythrocytes are excluded from the cell membranes of hPMCs by the large size and negative charge of any pericellular HA present. This is observed under microscopy as a zone of erythrocyte exclusion surrounding the cells. The results demonstrate that normal hPMCs in culture did not assemble a discernible pericellular coat (Figure 3.8A). Stimulation of hPMCs with 10ng/ml TGF-β1 for 48 hours was associated with the assembly of a notable HA coat (Figure 3.8B). To confirm that the pericellular coats were HA derived, hPMCs were treated with a specific exogenous hyaluronidase. This demonstrated a loss of the area of red-cell exclusion, confirming the coats to be formed from HA (Figure 3.8C and 3.8D).

3.2.4 Effect of cellular HA alterations on TGF-β1 driven MMT

The results presented in this chapter have so far demonstrated that MMT is associated with increased HA generation, up-regulation of HAS1 and HAS2 expression and assembly of HA pericellular matrices (coats) around myofibroblasts. In light of these results, a causal link between HA and myofibroblast differentiation was investigated.

Initially, HA synthesis was blocked by depletion of the UDP-glucuronic acid pool using the chemical inhibitor 4-methylumbelliferone (4MU). Initial experiments were conducted in hPMCs to establish the optimum concentration of 4MU to inhibit HA synthesis, with minimal cytotoxicity. The cytotoxicity of 4MU on hPMCs was analysed using the alamarBlue™ assay. The measurement of fluorescence intensity was representative of the cell number and viability. 4MU was dissolved in DMSO, at a final concentration of 0.1% v/v in the culture medium. Thus, the effect of 0.1% DMSO alone on cells was also determined as a control. Incubation of hPMCs with increasing concentrations of 4MU (0.2 mM to 2mM) resulted in a dose-dependent reduction in fluorescence (Figure 3.9). 0.5 mM was determined to be the optimum dose of 4MU, with over 80% survival of cells at this dose. The effect of DMSO 0.1% alone had a comparable effect to 0.5 mM 4MU on cell viability. This effect was confirmed by direct visualisation of hPMC after incubation with 4MU and the solvent DMSO for 48 hours (Figure 3.10). Confluent monolayers of hPMCs incubated with serum-free medium alone maintained their polygonal shape and had the typical “cobblestone” appearance (Figure 3.10A), whereas there was progressive loss of this shape and appearance with increasing dosage of 4MU (Figure 3.10C-F). Again, 0.1% v/v DMSO had no toxic effect on hPMCs (Figure 3.10B).

An optimum concentration of 0.5 mM 4MU was subsequently used to investigate the role of HA in MMT. *Streptomyces* hyaluronidase was also used to breakdown any cell-surface HA, thus specifically assessing the effect of the HA pericellular coat on TGF-β1-driven MMT. In this experiment, the comparative effect of *Streptomyces* hyaluronidase and 4MU on TGF-β1 stimulated hPMCs was determined by incubating confluent monolayers of hPMCs with TGF-β1 in the continual presence of 4MU or *Streptomyces* hyaluronidase (Figure 3.11). Expression of epithelial markers (E-Cadherin, ZO-1 and Occludin), mesenchymal markers (α-SMA, Fibronectin and Collagen 1α1) was assessed by RT-qPCR. Incubation with 4MU did not influence TGF-β1-driven downregulation of E-Cadherin, ZO-1 and Occludin expression (Figure 3.11A-C). Furthermore, 4MU did not influence the TGF-β1-driven increase in α-SMA, Fibronectin and Collagen 1α1 expression (Figure 3.11D-F). FITC-phalloidin staining of hPMCs in the presence of 4MU did not prevent TGF-β1-driven F-actin reorganisation (Figure 3.12). Previous studies in myofibroblasts and epithelial cells indicate that the presence of the HA pericellular coat is essential for fibroblast to MF differentiation. However, degradation of the HA coat using *Streptomyces* hyaluronidase did not influence TGF-β1 driven downregulation in the expression of E-Cadherin, ZO-1 and Occludin (Figure 3.11A-C). In addition, it did not prevent the upregulation of α-SMA, Fibronectin and Collagen 1α1 expression in response to TGF-β1 (Figure 3.11A-F). Similarly, *Streptomyces* hyaluronidase treatment did not influence TGF-β1-driven F-actin reorganisation in hPMCs. Given previous reports indicating additional effects of 4MU on HAS2 transcription [186], the effect of 4MU and *Streptomyces* hyaluronidase on HAS isoform expression was also assessed. 4MU treatment led to a significant induction of HAS1 expression following TGF-β1 stimulation, and no effect on HAS2 expression (Figure 3.11 G-H). *Streptomyces* hyaluronidase treatment also increased HAS1 expression, whilst not affecting HAS2 expression (Figure 3.11 G-H).

3.2.5 Relationship between HAS Isoenzymes and MMT

Previous results in this chapter have shown that HAS1 was upregulated by TGF-β1 and inhibition of HA synthesis by 4MU and *Streptomyces* hyaluronidase induced HAS1 expression following induction of MMT by TGF-β1. Therefore, the significance of HAS1 expression in relation to MMT was specifically investigated. To assess the significance of HAS1 in influencing MMT, siRNA targeting HAS1 were used to downregulate HAS1 transcription. Initial experiments were performed to assess transfection efficiency and cytotoxicity in hPMCs using Lipofectamine RNAiMAX transfection reagent (Figure 3.13). Transfection was performed as described in section 2.12.2, and HAS1 knockdown was confirmed by RT-qPCR (Figure 3.13A). Knockdown of HAS1 was observed in control hPMCs transfected with HAS1 siRNA at all concentrations. However, siRNA mediated HAS1 knockdown was lost following stimulation with TGF-β1 10 ng/ml, and this was irrespective of the concentration of HAS1 siRNA used. A 50% HAS1 knockdown was achieved following use of 100 nM concentration of HAS1 siRNA. No cytotoxic effects were seen following transfection at the higher concentration of 100 nM HAS1 siRNA (Figure 3.13B). Subsequently, the concentration of 100 nM HAS1 siRNA was used to assess effect of HAS1 knockdown on MMT from different omentum donors. A 50% reduction in HAS1 expression was again achieved following TGF-β1 stimulation when compared to scramble siRNA (Figure 3.14A). However, this had no effect of TGF-β1 mediated MMT with no change in E-Cadherin, ZO-1, Occludin, α-SMA, Fibronectin and Collagen 1α1 expression with TGF-β1 stimulation compared to untransfected hPMCs (Figure 3.14B-G).

HAS2 has been demonstrated to drive the assembly of HA pericellular coats and promote myofibroblast differentiation in fibroblasts and epithelial cells in type 1 and type 2 EMT [125,

126, 183, 184]. Earlier experiments demonstrated that mesothelial cells generated a HA pericellular coat in response to TGF-β1, and that both HAS1 and HAS2 expression was induced. We have demonstrated that HAS1 knockdown and the HA coat do not appear to mediate TGF-β1-driven MMT. The link between HAS2 and MMT was subsequently investigated. Initial experiments were performed on hPMCs to assess transfection efficiency using different siRNA sequences and Lipofectamine RNAiMAX transfection reagent (Figure 3.16). Transfection was performed as described in section 2.12.2, and HAS2 downregulation was confirmed by RT-qPCR (Figure 3.15). All three siRNA sequences significantly downregulated HAS2 expression in control cells, but TGF-β1 stimulation resulted in HAS2 induction to varying degrees in all siRNA's used. SiRNA 1 and siRNA 2 attenuated HAS2 induction with TGF-β1 and were statistically significant ($p<0.05$), but siRNA1 showed most successful HAS2 knockdown, so this was used in subsequent experiments (Figure 3.15B). Statistically significant knockdown of HAS2 expression was seen in control cells transfected with HAS2 siRNA with the threshold for significance reached at 30nM siRNA concentration. TGF-β1-driven MMT was associated with an induction of HAS2 expression, compared with corresponding scrambled treated hPMCs. However, a concentration of 100nM provided the most knockdown and was subsequently used to assess effect of HAS2 downregulation on MMT from 3 different omentum donors (Figure 3.16A). HAS2 knockdown had no effect on TGF-β1 driven MMT, as assessed by effects on epithelial markers (E-Cadherin, ZO-1 and Occludin expression) and myofibroblast markers (α-SMA, Fibronectin and Collagen 1α1) (Figures 3.16B-G).

3.2.6 Relationship between CD44 and MMT

TGF-β1 stimulation of fibroblasts has been demonstrated to promote the membrane redistribution of CD44 following the assembly of HA into pericellular coats[138, 190, 332]. This resulted in the colocalization of CD44 with EGFR and subsequent activation of MAPK/ERK signalling necessary for myofibroblast differentiation. In view of these results in fibroblasts, the involvement of CD44 in mediating MMT in hPMCs was investigated. CD44 siRNA was used to knockdown total CD44 expression as described in section 2.12.2, and CD44 knockdown was confirmed by RT-qPCR (Figure 3.17). Statistically significant knockdown of total CD44 expression was seen in both control and TGF-β1 stimulated hPMCs transfected with CD44 siRNA when compared to scramble siRNA (Figure 3.17A). However, CD44 knockdown did not influence TGF-β1-driven MMT in hPMCs (Figure 3.17B-G).

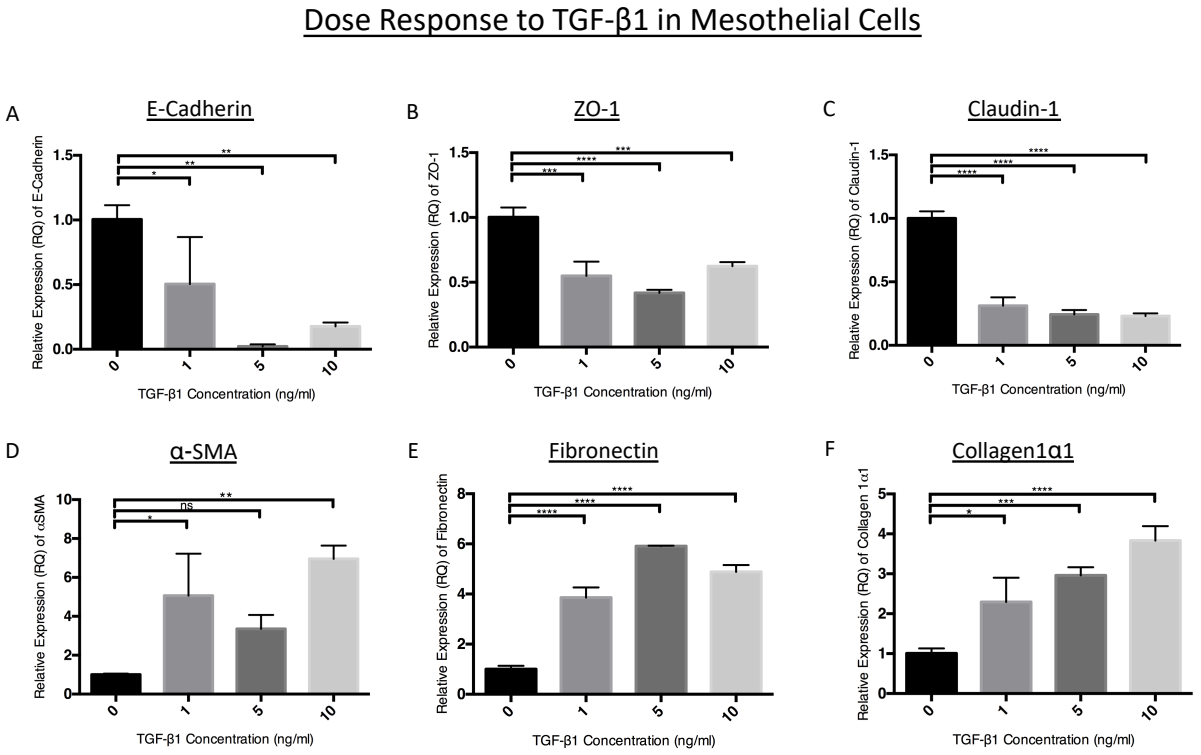

Figure 3.1 TGF-β1 represses epithelial and induces mesenchymal markers in mesothelial cells in a concentration dependent fashion. HPMCs treated with TGF-β1 1, 5 and 10ng/ml concentrations for 48hours after 24hours growth arrest in serum free medium. Expression of epithelial Markers: E-Cadherin, ZO-1 and Claudin-1 **(A-C)** and Mesenchymal Markers: α-SMA, Fibronectin and Collagen1**α**1 (**D-F)**. mRNA expression of all markers analysed by RT-qPCR and normalised to GAPDH mRNA expression. Data represents the mean ± S.E.M from triplicate single donor experiment. Data was analysed by a one-way ANOVA followed by Tukeys post hoc analysis (ns = p>0.05, * = p≤0.05, ** = p≤0.01, *** = p≤0.001, **** = p≤0.0001).

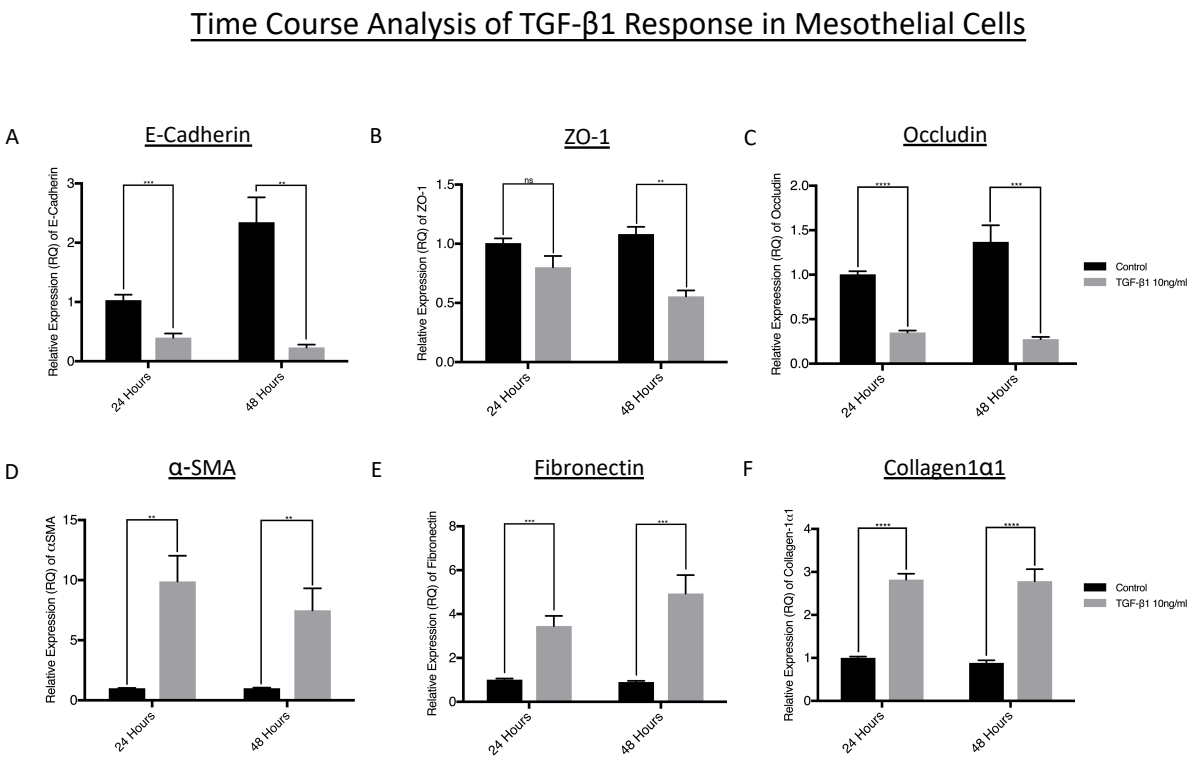

Figure 3.2 TGF-β1 represses epithelial and induces mesenchymal markers in a time dependent fashion. HPMCs treated with 10ng/ml TGF-β1 for 24 hours and 48 hours after 24 hours growth arrest in serum free medium. Expression of epithelial Markers: E-Cadherin, ZO-1 and Claudin-1 **(A-C)** and Mesenchymal Markers: αSMA, Fibronectin and Collagen-1α1 (**D-F)**. mRNA expression of all markers analysed by RT-qPCR and normalised to GAPDH mRNA expression. Data represents the mean ± S.E.M from 3 different donor experiments. Data was analysed by a paired Student's t-test with $p<0.05$ considered as statistically significant (ns = $p>0.05$, * = $p\leq0.05$, ** = $p\leq0.01$, *** = $p\leq0.001$, **** = $p\leq0.0001$).

Phalloidin Staining of TGF-β1 Stimulated Mesothelial Cells

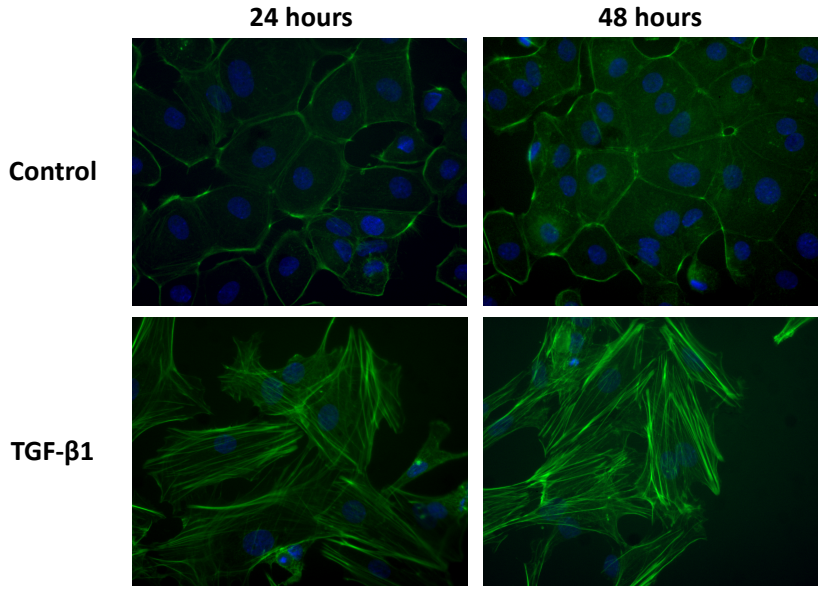

Figure 3.3 Characterisation of mesothelial phenotype in sub-confluent layers of mesothelial cells grown on chamber slides. Confluent monolayers of omentum derived mesothelial cells grown to 80% confluence on 8-well Permanox® chamber slides and treated with TGF-β1 10ng/ml for 24 and 48 hours. The cells were then fixed and antibodies for F-Actin (Phalloidin FITC) were added. Chamber slides were then mounted and imaged under UV-light. Images shown above representative of separate wells from 2 omentum donors. Original magnification X40.

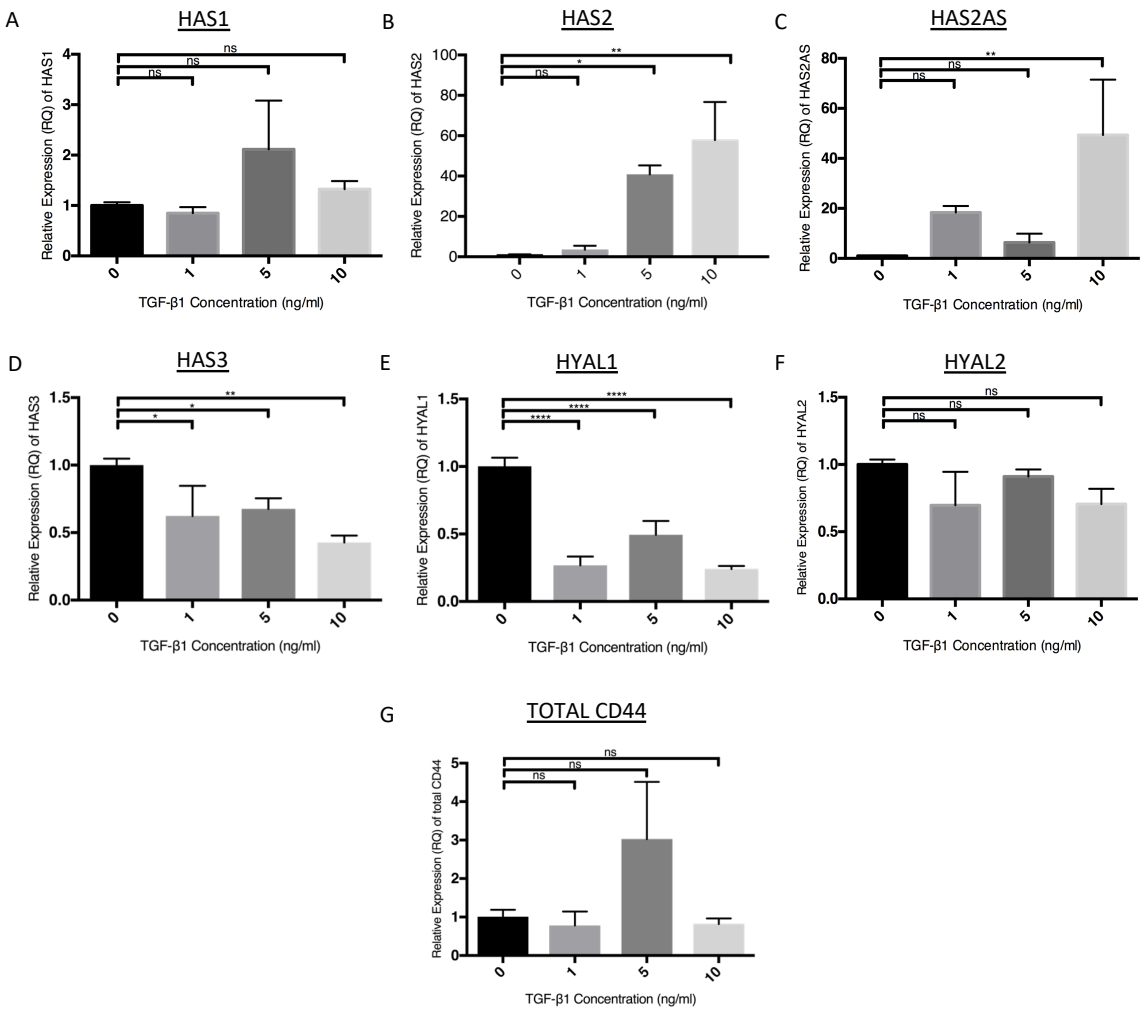

Figure 3.4 TGF-β1 stimulation of mesothelial cells generates HA in a concentration dependent fashion. Confluent monolayers of omentum derived mesothelial cells treated with TGF-β1 1, 5 and 10ng/ml concentrations for 48hours. Expression of HA synthase enzymes: HAS1, HAS2, HAS3 and HAS2AS **(A-D)** Hyaluronidase enzymes: HYAL1 and HYAL 2 (**E-F)** HA receptor proteins: total CD44 **(G).** mRNA expression of all markers analysed by RT-qPCR and normalised to GAPDH mRNA expression. Data was analysed by a one-way ANOVA followed by Tukeys post hoc analysis (ns = p>0.05, * = p≤0.05, ** = p≤0.01, *** = p≤0.001, **** = p≤0.0001). Data represents the mean ± S.E.M from triplicate single donor experiment.

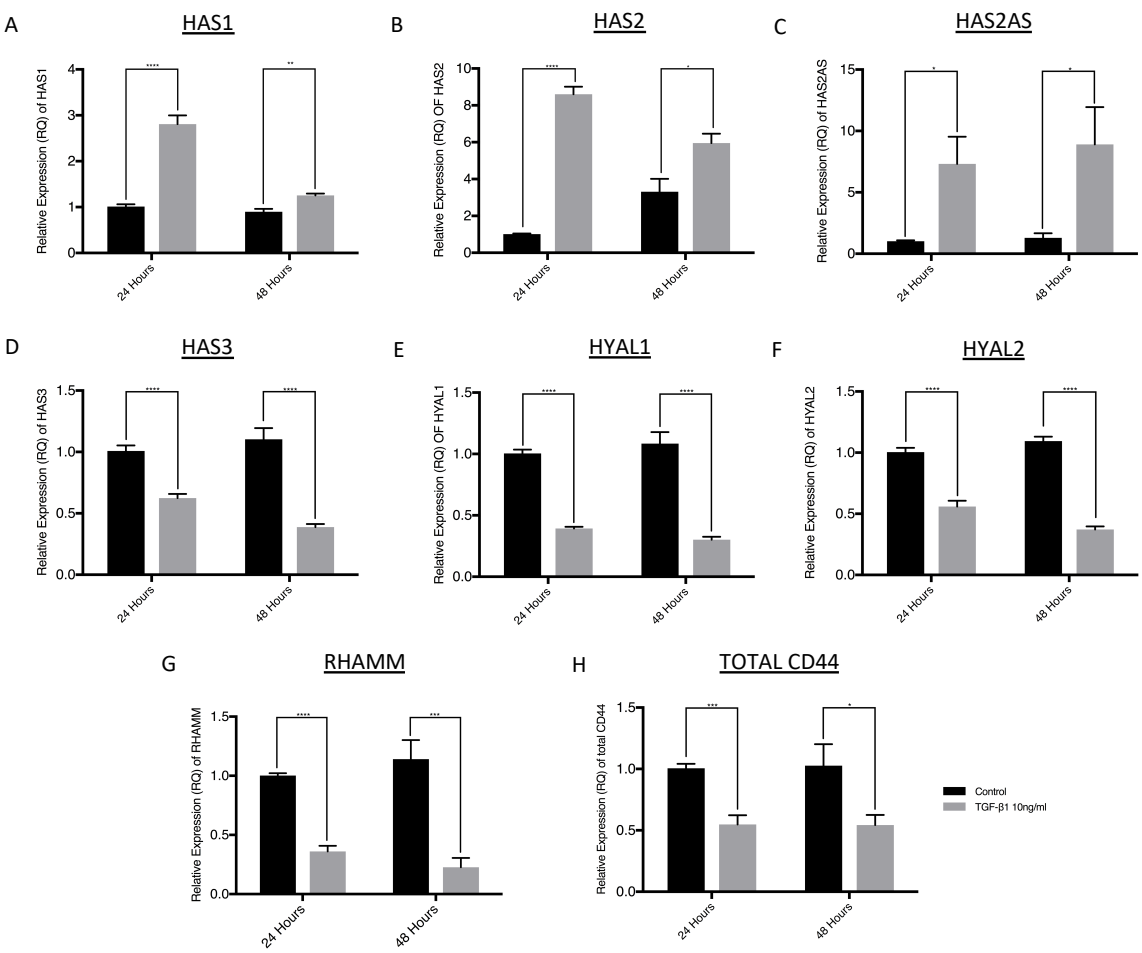

Figure 3.5 TGF-β1 stimulation of mesothelial cells generates HA in a time dependent fashion. Confluent monolayers of omentum derived mesothelial cells treated with 10ng/ml TGF-β1 for 48hours. Expression of HA synthase enzymes: HAS1, HAS2, HAS3 and HAS2AS **(A-D)** Hyaluronidase enzymes: HYAL1 and HYAL 2 (**E-F)** HA receptor proteins: RHAMM and total CD44 **(G-H).** mRNA expression analysed by RT-qPCR and normalised to GAPDH mRNA expression. Data represents the mean ± S.E.M from 3 different donor experiments. Data was analysed by a paired Student's t-test with $p<0.05$ considered as statistically significant (ns = $p>0.05$, * = $p\leq0.05$, ** = $p\leq0.01$, *** = $p\leq0.001$, **** = $p\leq0.0001$).

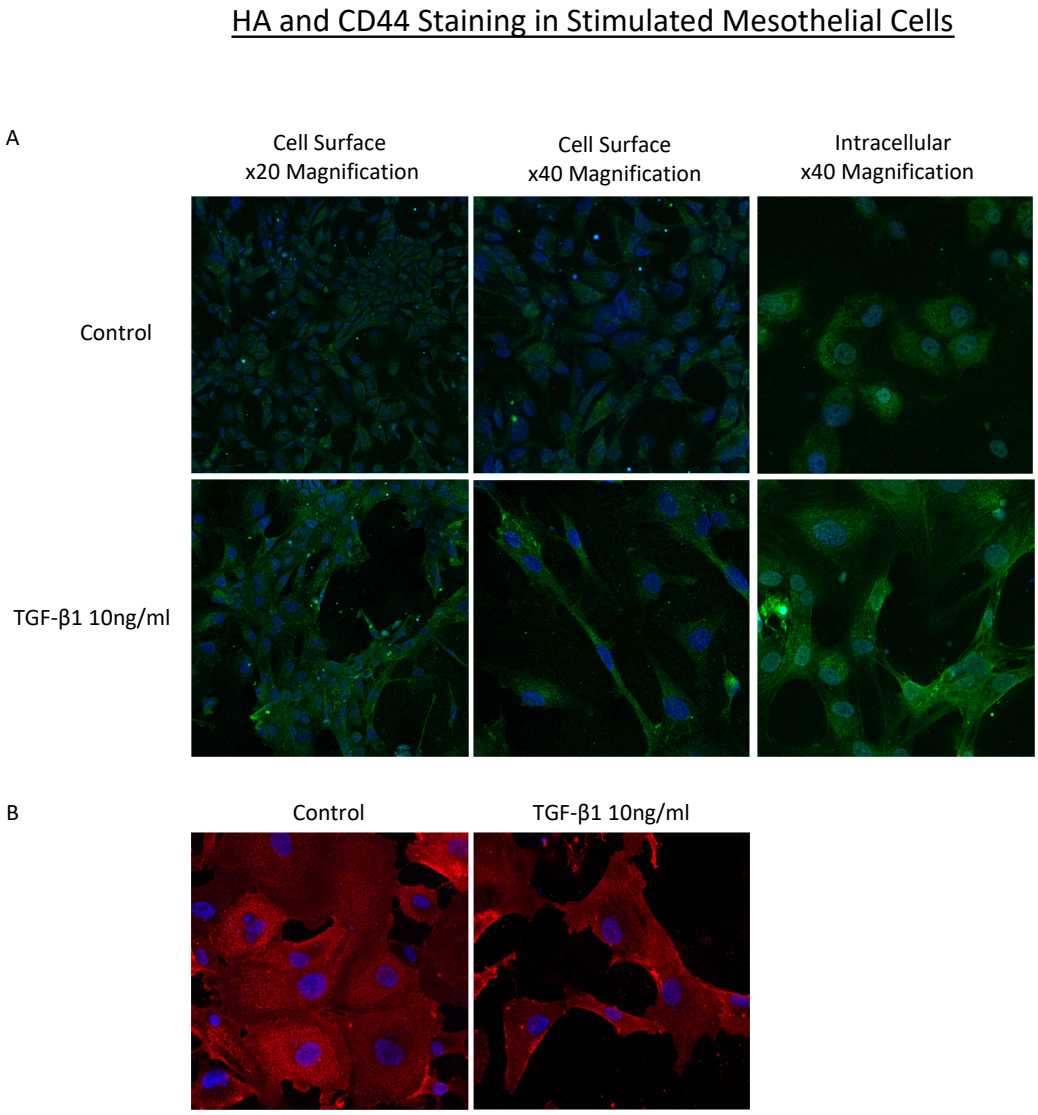

Figure 3.6. Characterisation of HA and CD44 deposition in sub-confluent layers of mesothelial cells grown on chamber slides. Sub-confluent monolayers of omentum derived mesothelial cells grown on 8-well Permanox® chamber slides and treated with 10ng/ml TGF-β1 for 48hours. Cells were then fixed and stained for biotinylated HA-binding protein (bHABP) (Green) **(A**) and CD44 (Red) **(B)**. Chamber slides were then mounted and analysed by confocal microscopy. Images shown above representative of 3 different donor experiments. Original magnification as described for bHABP, x40 magnification for CD44.

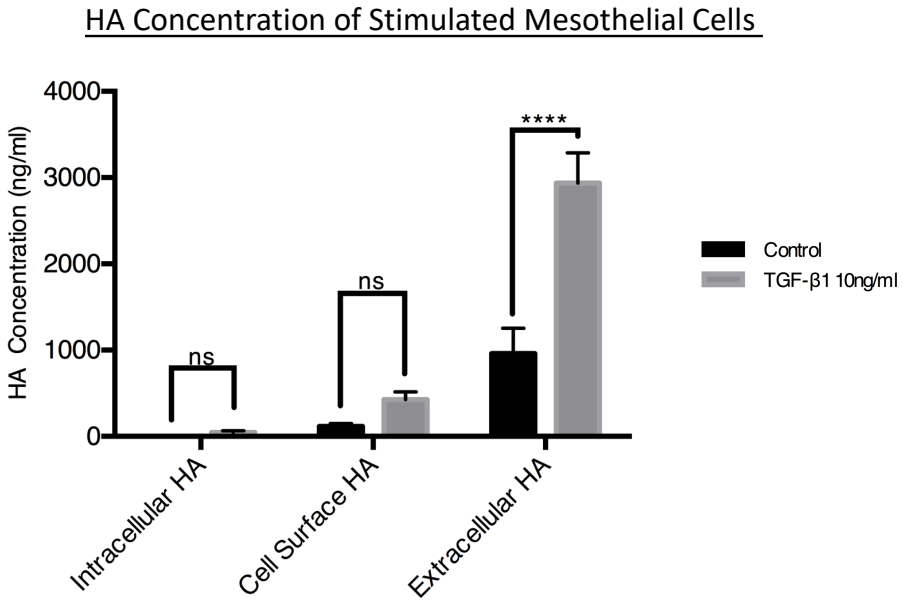

Figure 3.7 TGF-β1 stimulation of mesothelial cells generates extracellular HA. Confluent monolayers of omentum derived mesothelial cells treated with 10ng/ml TGF-β1 for 48hours. Quantification of intracellular, cell surface and extracellular HA by ELISA. Data was analysed by a one-way ANOVA followed by Tukeys post hoc analysis (ns = $p>0.05$, * = $p\leq0.05$, ** = $p\leq0.01$, *** = $p\leq0.001$, **** = $p\leq0.0001$). Data represents the mean ± S.E.M from 3 different donor experiments.

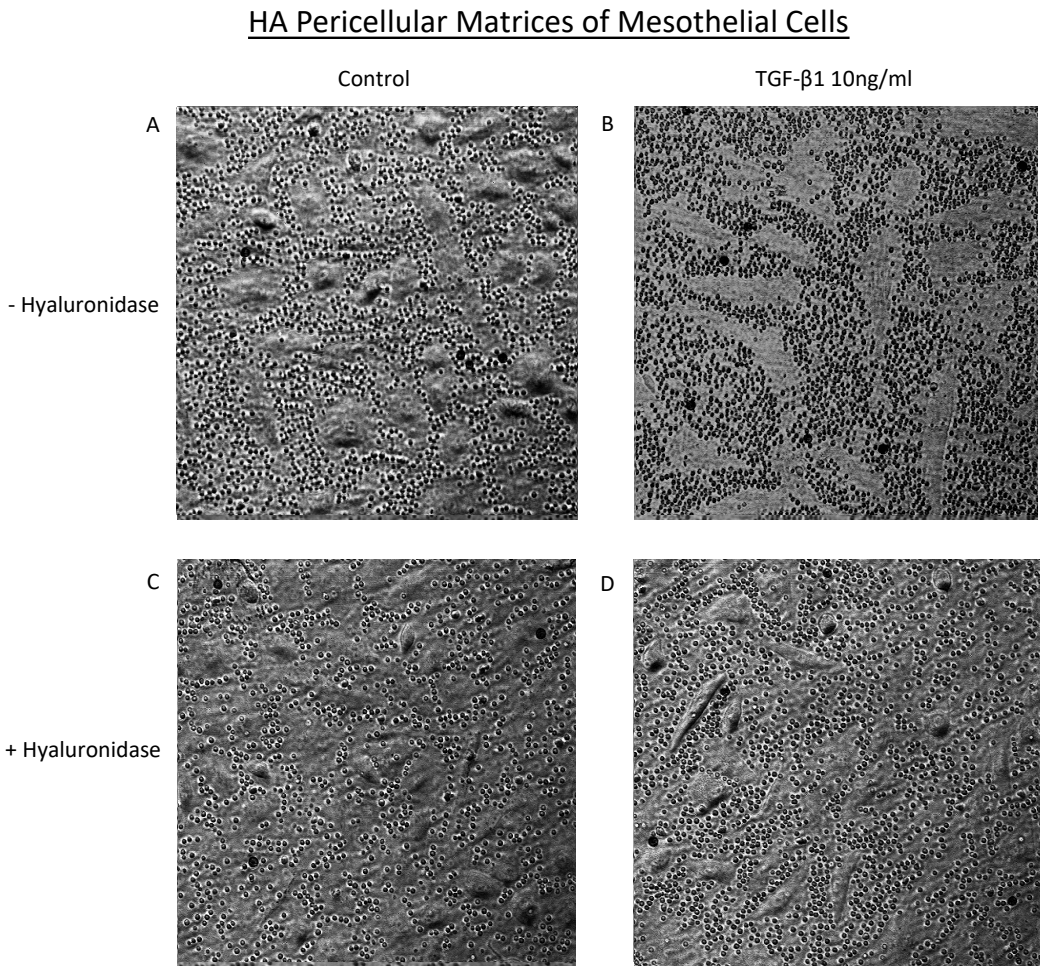

Figure 3.8 TGF-β1 stimulates mesothelial cells to form HA dependent pericellular matrices. Sub-confluent monolayers of omentum derived mesothelial cells treated with 10ng/ml TGF-β1 for 48 hours. Formalised horse erythrocytes were then added to visualise the HA pericellular HA coat (**A-B)**. 200μg/ml of Bovine Testicular Hyaluronidase was added **(C-D)** after 10 minutes incubation with of horse erythrocytes. Zones of exclusion were visualised using Zeiss Axiovert 135 inverted microscope. The results are representative on triplicate single donor experiment. Original magnification x40.

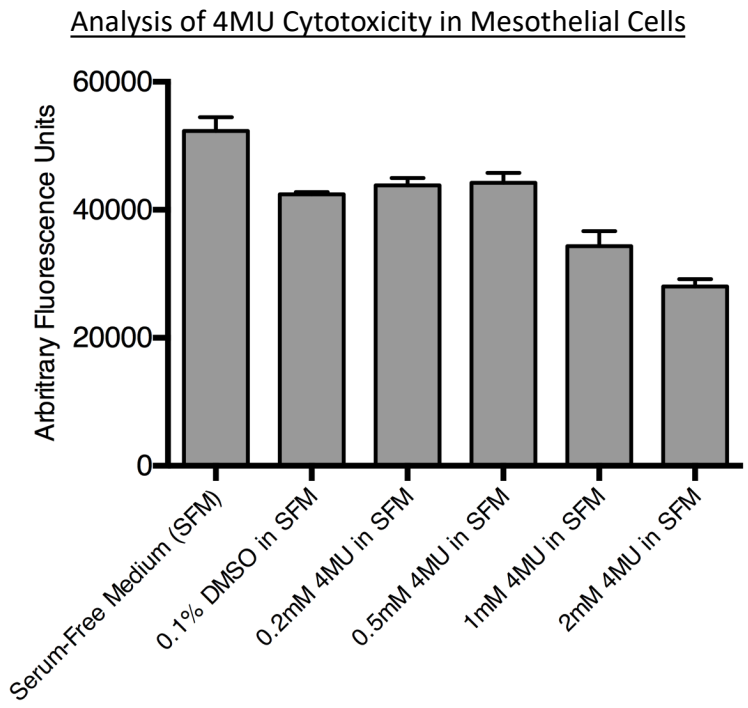

Figure 3.9 Alamar Blue Assay for analysis of 4MU cytotoxicity in Mesothelial Cells. Confluent monolayers of omentum derived mesothelial cells treated with 0.1% DMSO or 0.2, 0.5, 1, 2mM of 4-Methylumbelliferone (4MU) for 48 hours. Subsequently the medium was replaced with serum-free medium containing 10% Alamar Blue and incubated for 1 hour. Fluorescence was measured as described in section 2.7. The results are represented as mean ± standard error measurements derived from triplicate single donor experiment.

Light Microscopy of 4MU Cytotoxicity in Mesothelial Cells

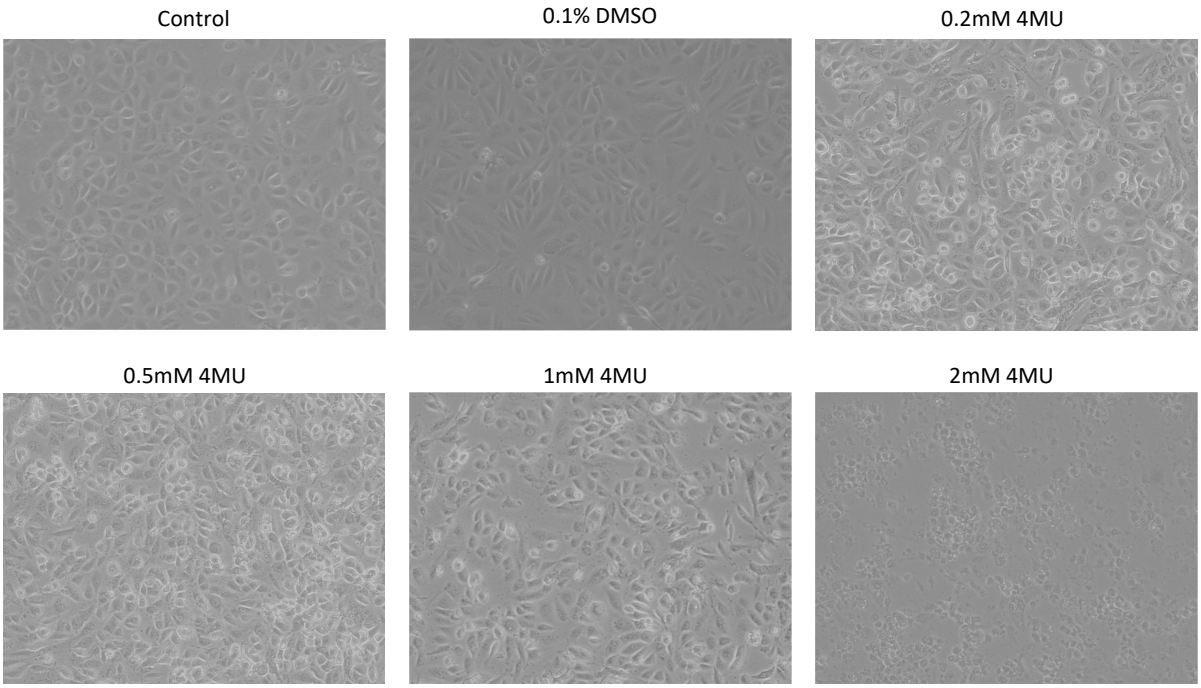

Figure 3.10 4MU cytotoxicity in Mesothelial Cells. Confluent monolayers of omentum derived mesothelial cells treated with 0.1% DMSO or 0.2, 0.5, 1, 2mM of 4-Methylumbelliferone (4MU) for 48 hours. Cells were then visualised using Zeiss Axiovert 135 inverted microscope. The results are representative on triplicate single donor experiment. Original magnification x40.

Effect of 4MU and *Streptomyces* Hyaluronidase on Myofibroblast Phenotype

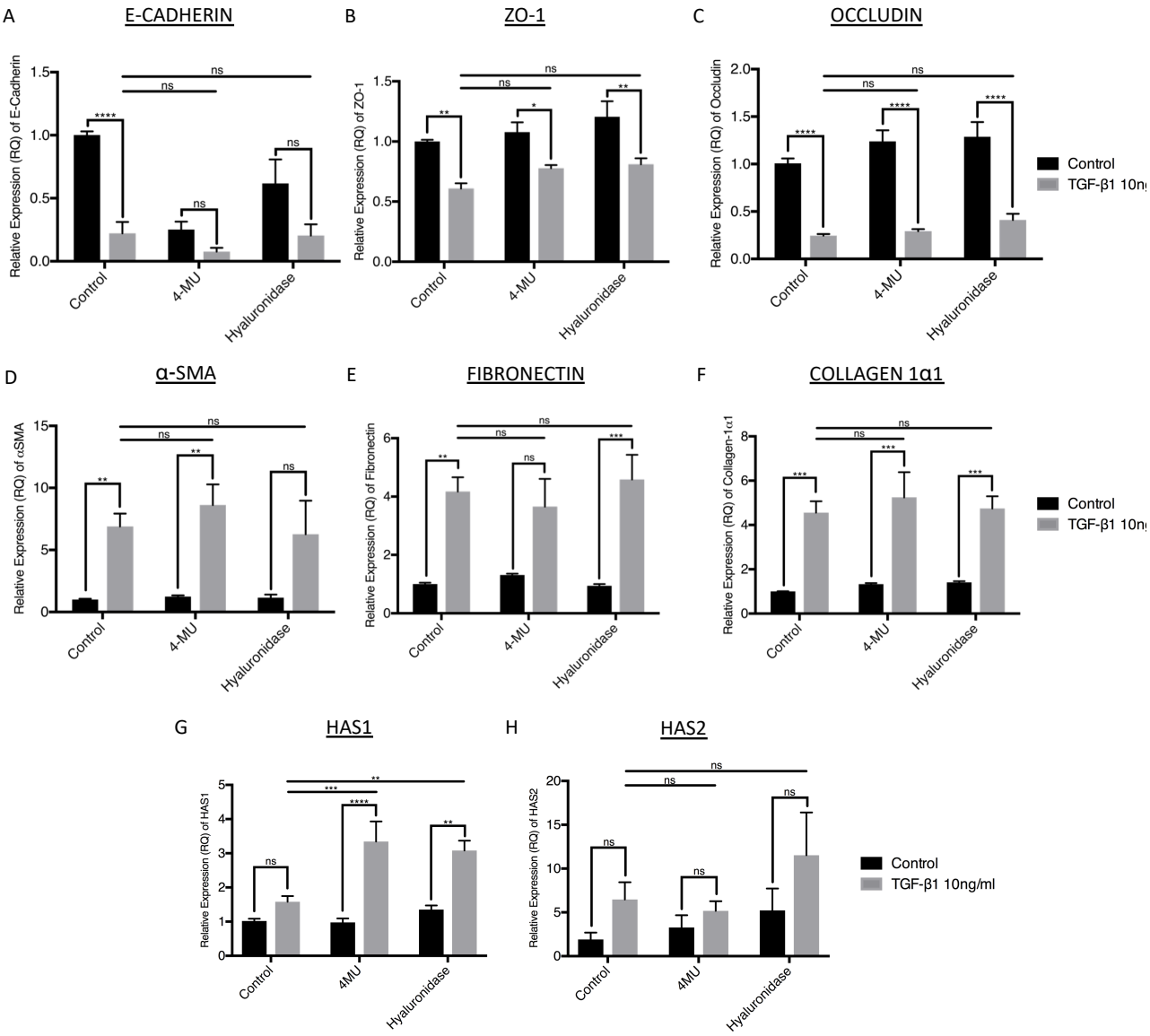

Figure 3.11 4MU and *Streptomyces* hyaluronidase have no effect on MMT but upregulate HAS1 expression. Confluent monolayers of omentum derived mesothelial cells treated with 0.5mM 4MU or 1iU *Streptomyces h*yaluronidase for 1 hour. Subsequently, the medium was removed and cells washes with PBS. Fresh 4MU and *Streptomyces h*yaluronidase were added to cells with 10ng/ml TGF-β1 and incubations continued for 48 hours. Expression of epithelial Markers: E-Cadherin, ZO-1, Claudin-1 **(A-C)** Mesenchymal Markers: α-SMA, Fibronectin, Collagen 1 (**D-F)** and HA Synthases; HAS1 and HAS2 **(G-H)** determined by RT-qPCR and normalised to GAPDH mRNA expression. Data represents the mean ± S.E.M from 3 different donor experiments. Data was analysed by a two-way ANOVA followed by Tukeys post hoc analysis (ns = p>0.05, * = p≤0.05, ** = p≤0.01, *** = p≤0.001, **** = p≤0.0001).

Effect of 4MU and *Streptomyces* Hyaluronidase on HPMC Phenotype

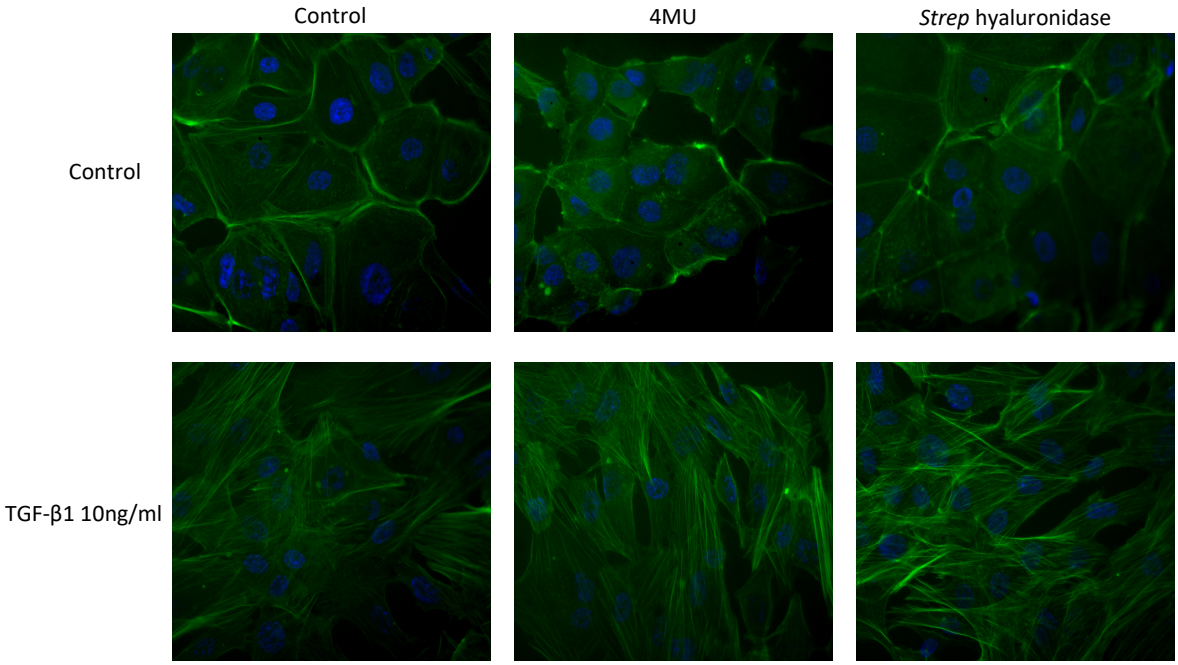

Figure 3.12 4MU and *Streptomyces* hyaluronidase have no effect on on phenotype. Sub-confluent monolayers of omentum derived mesothelial cells grown on 8-well Permanox® chamber slides and treated with 0.5mM 4MU or 1iU *Streptomyces* Hyaluronidase for 1 hour. Subsequently, 10ng/ml TGF-β1 was added to 4MU and *Streptomyces* Hyaluronidase pre-treated cells and incubations continued for 48 hours. The cells were then fixed and antibodies for F-Actin (Phalloidin FITC) added. Chamber slides were then mounted and imaged using fluorescent microscopy. Images shown above representative of separate wells from 2 different donor experiments. Original magnification X40

Optimisation of HAS1 Knockdown in Mesothelial Cells

A

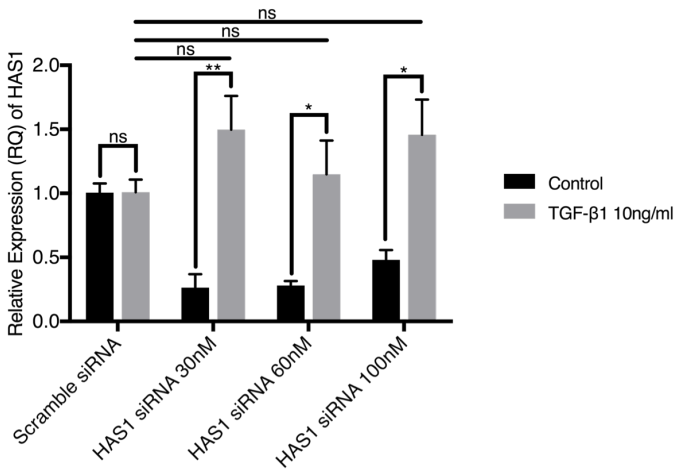

B

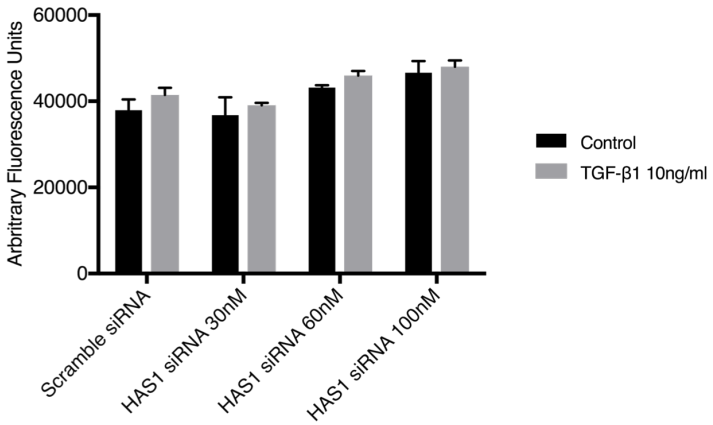

Figure 3.13 Optimisation of HAS1 knockdown in TGF-β1 Stimulated Mesothelial Cells. Omentum derived mesothelial cells grown to 60% confluence and transfected overnight with a scrambled siRNA sequence or siRNA targeting HAS1 at different concentrations then treated with TGF-β1 10ng/ml for 48 hours. mRNA expression of HAS1 was then determined (**A)**. Alamar Blue cytotoxicity assay for analysis of HAS1 siRNA cytotoxicity in hPMCs at different concentrations (**B**)**.** mRNA expression by RT-qPCR and normalised to GAPDH mRNA expression. Data represents the mean ± S.E.M from triplicate single donor experiment. Data was analysed by a two-way ANOVA followed by Tukeys post hoc analysis (ns = p>0.05, * = p≤0.05, ** = p≤0.01, *** = p≤0.001, **** = p≤0.0001).

HAS1 Knockdown in Mesothelial Cells

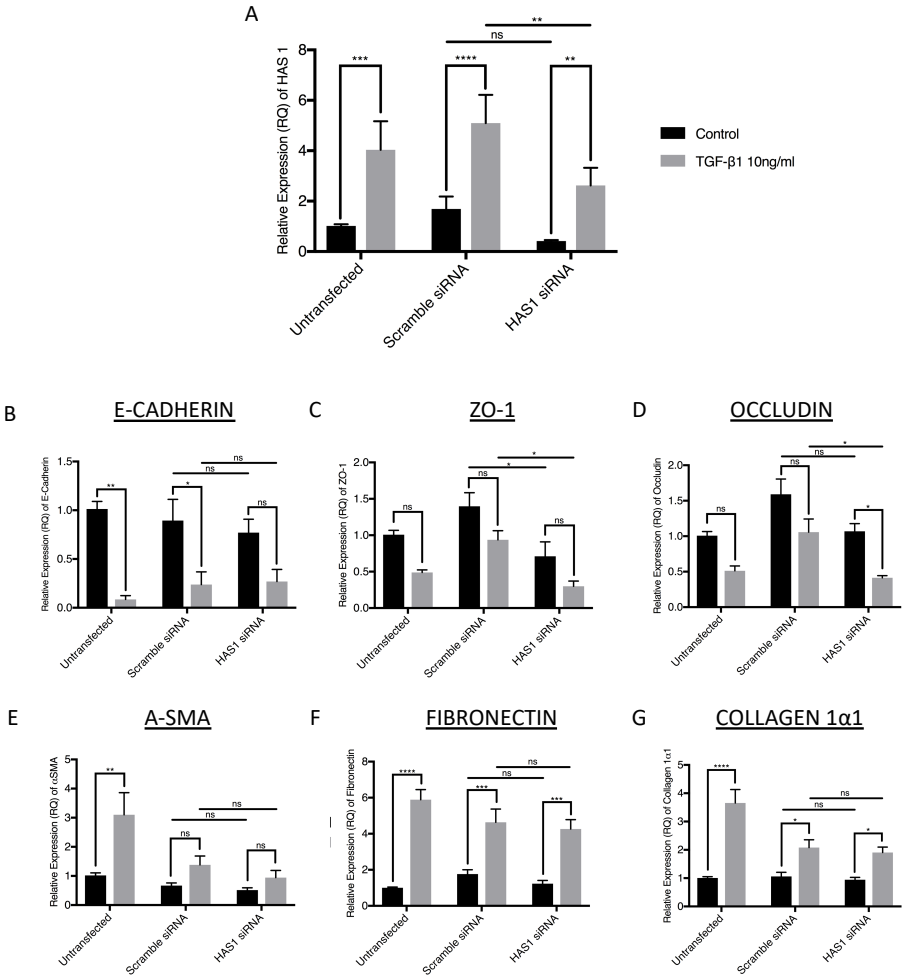

Figure 3.14 HAS1 knockdown has no effect on MMT. Omentum derived mesothelial cells grown to 60% confluence and transfected overnight with a scrambled siRNA sequence or siRNA targeting HAS1 then treated with TGF-β1 10ng/ml for 48 hours.. mRNA expression HAS1 using siRNA targeting HAS1 **(A)**. Expression of Epithelial Markers: E-Cadherin, ZO-1 and Occludin **(B-D)** and Mesenchymal Markers: αSMA, Fibronectin and Collagen-1 (**E-G)**. mRNA expression by RT-qPCR and normalised to GAPDH mRNA expression. Data represents the mean ± S.E.M from 3 different donor experiments. Data was analysed by a two-way ANOVA followed by Tukeys post hoc analysis (ns = p>0.05, * = p≤0.05, ** = p≤0.01, *** = p≤0.001, **** = p≤0.0001).

Optimisation of HAS2 Knockdown in Mesothelial Cells

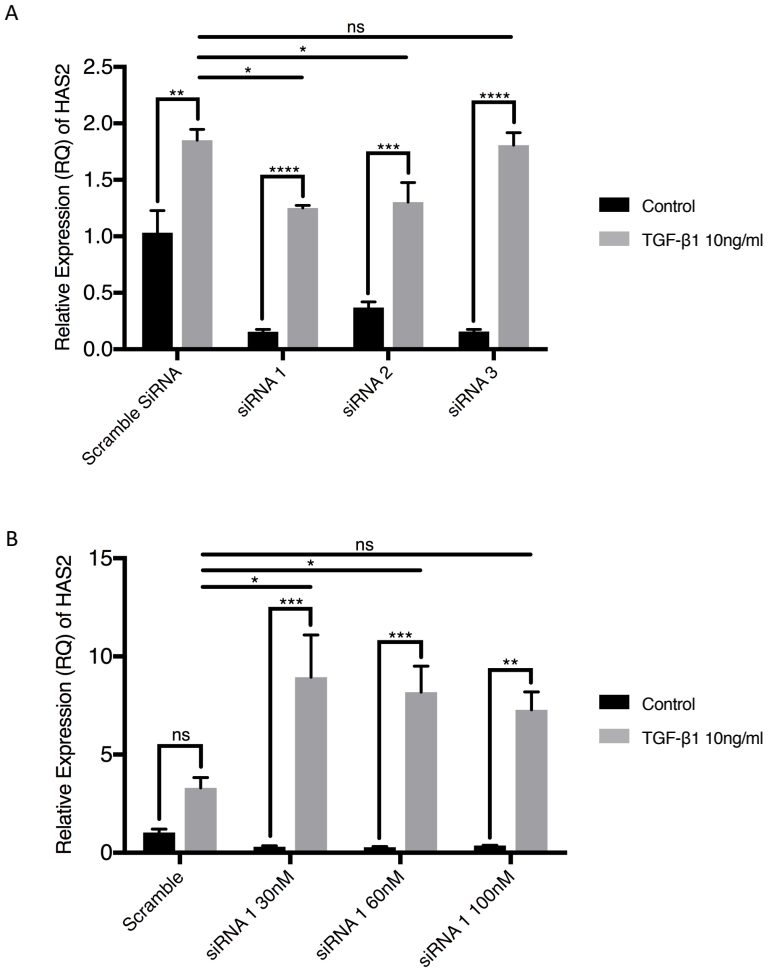

Figure 3.15 Optimisation of HAS2 knockdown in TGF-β1 Stimulated Mesothelial Cells. Omentum derived mesothelial cells grown to 60% confluence and transfected overnight with a scrambled siRNA sequence or siRNA targeting HAS2 then treated with TGF-β1 10ng/ml for 48 hours. Expression HAS2 analysed using different siRNA targeting HAS2 (**A)** and siRNA 1 targeting HAS2 at different concentrations (**B**). mRNA expression by RT-qPCR and normalised to GAPDH mRNA expression. Data represents the mean ± S.E.M from triplicate single donor experiment. Data was analysed by a two-way ANOVA followed by Tukeys post hoc analysis (ns = p>0.05, * = p≤0.05, ** = p≤0.01, *** = p≤0.001, **** = p≤0.0001).

HAS2 Knockdown in Mesothelial Cells

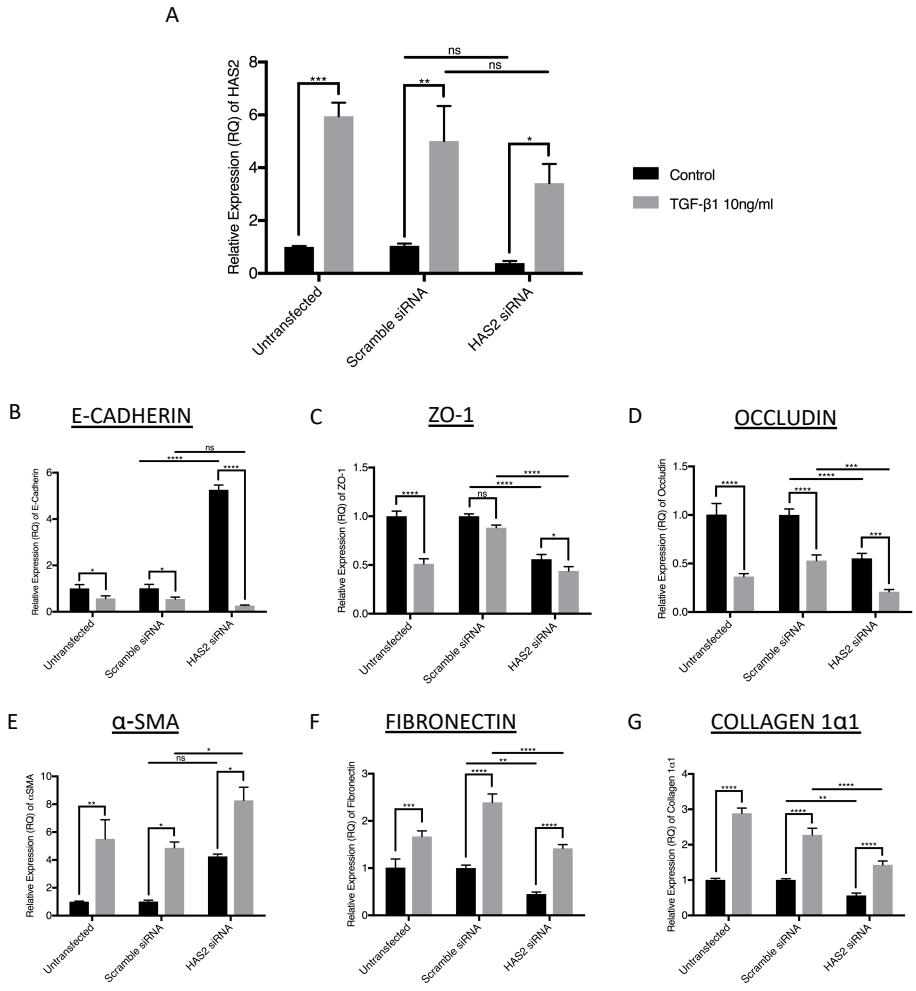

Figure 3.16 HAS2 knockdown has no effect on MMT. Omentum derived mesothelial cells grown to 60% confluence and transfected overnight with a scrambled siRNA sequence or siRNA targeting HAS2 then treated with TGF-β1 10ng/ml for 48 hours. mRNA expression HAS2 using siRNA targeting HAS2 **(A)**. Expression of Epithelial Markers: E-Cadherin, ZO-1 and Occludin **(B-D)** and Mesenchymal Markers: αSMA, Fibronectin and Collagen-1 (**E-G)**. mRNA expression by RT-qPCR and normalised to GAPDH mRNA expression. Data represents the mean ± S.E.M from 3 different donor experiments. Data was analysed by a two-way ANOVA followed by Tukeys post hoc analysis (ns = p>0.05, * = p≤0.05, ** = p≤0.01, *** = p≤0.001, **** = p≤0.0001).

CD44 Knockdown in Mesothelial Cells

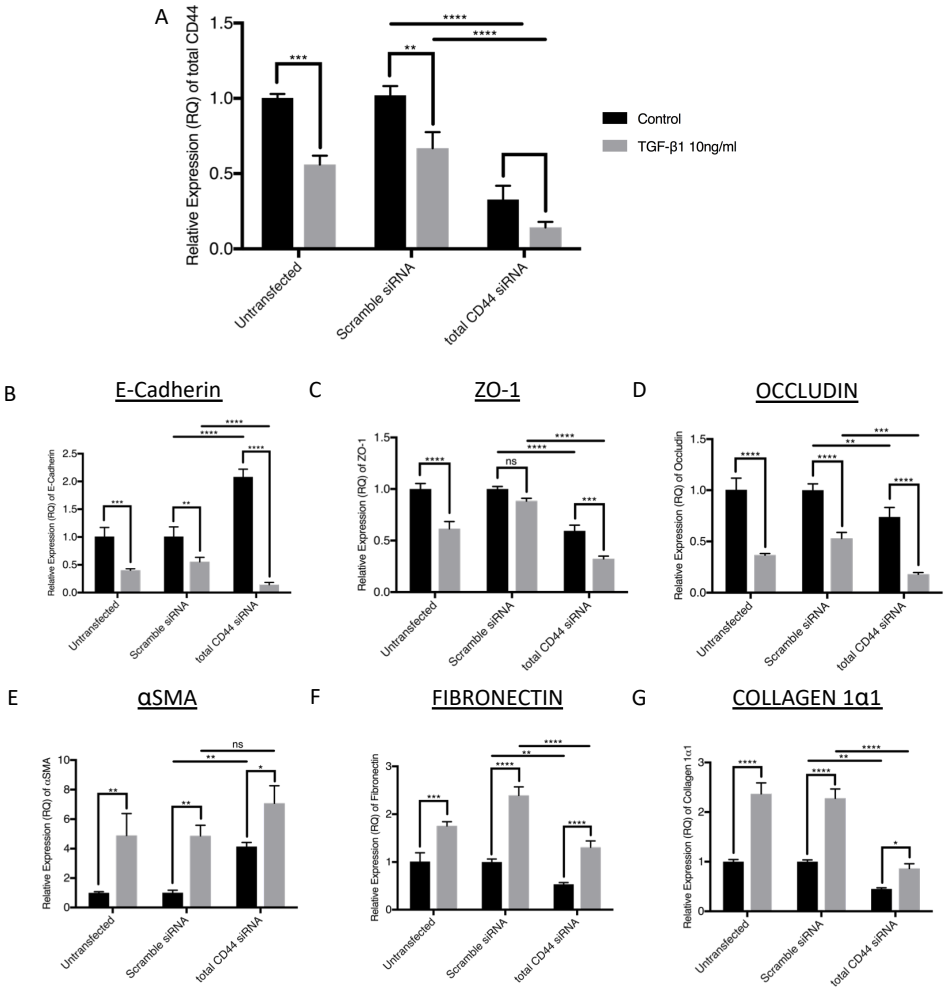

Figure 3.17. Total CD44 knockdown has no effect on MMT. Omentum derived mesothelial cells grown to 60% confluence and transfected overnight with a scrambled siRNA sequence or siRNA targeting total CD44 then treated with TGF-β1 10ng/ml for 48 hours.. mRNA expression total CD44 using siRNA targeting total CD44 **(A)**. Expression of epithelial Markers: E-Cadherin, ZO-1 and Occludin **(B-D)** and Mesenchymal Markers: αSMA, Fibronectin and Collagen-1 (**E-G)**. mRNA expression by RT-qPCR and normalised to GAPDH mRNA expression. Data represents the mean ± S.E.M from 4 different donor experiments. Data was analysed by a two-way ANOVA followed by Tukeys post hoc analysis (ns = p>0.05, * = p≤0.05, ** = p≤0.01, *** = p≤0.001, **** = p≤0.0001).

3.3 Discussion

PD causes characteristic changes in the peritoneal membrane over time. As a result of the constant exposure to bioincompatible PD solutions and recurrent episodes of peritonitis, the peritoneal membrane undergoes progressive fibrosis, angiogenesis and hyalinizing vasculopathy [42, 43, 102]. These changes eventually culminate in increased small-solute transport and loss of ultrafiltration leading to failure of PD as a means of renal replacement therapy [29, 42, 101]. It has been clear for some time that the pro-fibrotic cytokine TGF-β1 is a master molecule in the development of peritoneal membrane fibrosis, and its overexpression has been correlated with worse PD outcomes [100, 114, 379, 380]. TGF-β1-driven MMT is a key mechanism through which TGF-β1 promotes peritoneal membrane fibrosis. The work in this chapter investigates the role of HA in mediating TGF-β1-driven MMT.

Previous studies from our laboratory have shown that HA is a mediator of fibroblast-to-myofibroblast differentiation in response to TGF-β1 [237, 348]. Subsequent studies revealed a complex inter-relationship between the HA pericellular matrix and interactions between CD44-EGFR and the TGF receptor [124-126, 182-184, 253, 332]. HA is enriched in numerous types of human cancer and is essential for mesenchymal transformation of certain epithelial cell-lines required for tumour growth and progression [365, 381]. The majority of malignant tumours contain elevated levels of both HA and CD44, and it has been demonstrated that HA-activated CD44 promotes proliferation, invasion, metastases and stemness of cancer cells [166, 240, 365, 369-371, 382-386]. Li *et al* demonstrated that TGF-β1 induced EMT through the transactivation of EGF signalling through HA/CD44 in lung and breast cancer cells during cancer progression [387]. However, it is not known whether this occurs in mesothelial cells

during PD. In PD mesothelial cells have been shown to constitutively synthesise HA, and this synthesis is upregulated during episodes of PD peritonitis [341]. During MMT, mesothelial cells acquire greater capacity to synthesize HA that is secreted into the immediate microenvironment [341, 343, 346, 374, 375]. Mechanical disruption to the mesothelial monolayer has provided useful insight into the changes in HA synthesis by mesothelial cells. In an *in vitro* model of peritoneal wound healing [55], increased HA synthesis in mesothelial cells was associated with increased cell migration, proliferation and phenotypic changes to repopulate the monolayer [346]. Yung *et al* demonstrated that mesothelial cells migrated from the leading edge of the wound into the denuded area, as a result of myofibroblastic differentiation of mesothelial cells. Furthermore, this increase in HA synthesis by mesothelial cells during re-mesothelialisation was predominantly mediated through an increase in HAS2 mRNA expression. Once the monolayer was restored, HA synthesis returned to constitutive levels along with resumption of normal mesothelial architecture. Martin *et al* also demonstrated that mesothelial cells have the ability to control the accumulation of ECM by secreting the matrix degrading molecules MMP-2, MMP-3 and MMP-9 [53]. The authors elucidated that TGF-β1 regulated secretion of these enzymes, and their inhibitors (TIMPs), highlighting the potential importance of TGF-β1 in the development of peritoneal fibrosis. Given these studies and the evidence that HA mediates TGF-β1 driven EMT in fibrosis and cancer, it was important to establish whether HA generated by mesothelial cells was a mediator for TGF-β1 driven MMT.

In this chapter, the conversion of mesothelial cells to myofibroblasts was initially assessed in the presence or absence of TGF-β1. TGF-β1 induced reproducible mesenchymal changes at a dose of 10 ng/ml for 48 hours. Whilst expression patterns of mesenchymal conversion began

to change at lower concentrations and shorter time-courses, gross phenotypical changes were only apparent with higher concentrations over 48 hours. Following characterisation of TGF-β1-driven MMT, the HA profile of mesothelial cells and myofibroblasts derived from them was assessed. The majority of HA generated by mesothelial cells with TGF-β1 stimulation was located extracellularly; either in the form of pericellular coats or as soluble HA. MMT was also associated with increased HAS1 and HAS2 mRNA expression, attenuated HAS3 and HYAL1 mRNA expression and cellular re-distribution of CD44. However, unlike in fibroblasts and cancer cells, degradation of pericellular HA, inhibition of HA synthesis and knockdown of the principal HA receptor (CD44) did not appear to influence TGF-β1-driven MMT. This suggests that HA generation by mesothelial cells, may not be causally linked to TGF-β1-driven MMT, but rather the increased HA generation is simply a consequence of mesothelial cells having undergone MMT.

Removal of HA from the cell surface by hyaluronidase and inhibition of HA synthesis by 4MU led to significant upregulation of HAS1 expression but not HAS2. Numerous studies have reported that 4MU causes a significant reduction in HAS2 transcription by an unknown mechanism [185, 186, 388, 389] which may explain the compensatory HAS1 upregulation. However, HAS1 expression was also induced by removal of HA pericellular matrices surrounding hPMCs with *Streptomyces* hyaluronidase and had no significant effect of HAS2 expression. This suggests that HAS1 may be the main contributor to the development and maintenance of HA pericellular coats in mesothelial cells as opposed to HAS2. Overexpression of HAS1 has been demonstrated to downregulate HAS2 and HAS3 expression in fibroblast-like cells suggesting a functional co-operation or negative feedback mechanisms between these isoenzymes [177]. Recent reports also suggest that HAS1 may regulate HAS2 levels

during wound healing in experimental models of OA [390], and may synthesize a different HA pericellular coat that differentially regulates cell behaviour. Interestingly HAS3, which is thought to generate LMW-HA, was downregulated following mechanical denudation as well as following TGF-β1 stimulation and may therefore be a counter-regulatory enzyme to HAS1 and HAS2.

The distribution of HA within myofibroblasts was an interesting finding, as HA appeared to form distinct lines within the cytoplasm of cells treated with TGF-β1. These could be in-keeping with the F-Actin filaments distributed within the cytoplasm of myofibroblasts seen previously. Whilst the reason for this is unclear, Assmann *et al* have previously demonstrated that the HA receptor, RHAMM, was exclusively found in the cytoplasm of human breast cancer cells [391]. Furthermore, they demonstrated that RHAMM was a filamentous protein capable of interacting with microtubules and microfilaments whilst bound to HA [392]. It is therefore possible that the intracellular HA may be binding to filamentous RHAMM proteins colocalising with various cytoplasmic scaffolding fibres.

Much of the research undertaken in this field has shown that HA can have distinct and even opposing biological functions depending on its manner of synthesis and degradation, its assembly and organisation within the cell-associated connective tissue and its interaction with different HA-binding proteins. In contrast to the established role of HA in TGF-β1-driven fibroblast-to-myofibroblast differentiation, in types I and II EMT and in cancer-associated type II EMT, HA does not appear to promote TGF-β1-dependent MMT in the peritoneum. This is different to the role of HA in other solid organ fibroses, as HA does not appear to be critical to myofibroblast phenotype.

The data from this chapter also indicate differences in HAS isoenzyme expression in mesothelial cells. In fibroblasts and epithelial cells HAS1 is poorly expressed and only shows little (if any) induction following TGF-β1 stimulation. Instead, TGF-β1 drives a HAS2 mediated increase in HA synthesis. This leads to synthesis of large HA pericellular coats that promote CD44/EGFR coupling and subsequent MAPK/ERK signalling. In contrast, in mesothelial cells HAS1 expression was significantly higher than in other cell types we have previously investigated, and was upregulated following TGF-β1 stimulation. HAS2 expression on the other hand is low in comparison. HAS2 is known to be the isoenzyme that drives fibrosis in lungs, kidneys, joints, heart etc. The role of HAS1 and HAS1-driven HA generation has been poorly understood so far. However, TGF-β1 upregulates HAS1 more than HAS2 in mesothelial cells to generate HA. This could account for the difference in HA function seen in the peritoneum versus other solid organs. Each HAS enzyme has different enzymatic activity, sub-cellular localisation and regulation suggesting they have distinct biological and physiological roles [172]. Each HAS isoform is thought to produce different molecular weight HA, which some researchers believe is critical to many pathological conditions [149, 173].

Many of the biological functions of HA depend upon binding to HA-binding proteins, such as CD44. CD44 is widely expressed in mammalian tissues and has been shown to have important roles in inflammation, tumour progression, embryogenesis, immune cell activation and fibrosis [138, 269, 288, 393-395]. The specific binding of HA to CD44 influences numerous intracellular signalling pathways, which can be altered by various cytokines and growth factors including TGF-β1 [230-235]. However, knockdown of the standard CD44 isoform did not appear to influence TGF-β1-driven MMT. Recent work from our laboratory and elsewhere have demonstrated that alternative splicing of exons encoding the extracellular domain of

CD44 lead to the formation of variant isoforms, which can have distinct modes of action and a range of functions [138, 396-401]. These CD44 splice variants may be relevant to the functions of HA in the peritoneum and warrants further investigation.

In summary, the findings from this chapter demonstrate that HA is generated in mesothelial cells as they undergo TGF-β1-driven MMT. However, this appears to be a consequence of MMT and does not appear to mediate MMT. The role of the increased HA generated during MMT is not known. Our previous work indicates that HA, in certain contexts, can also mediate in BMP7-driven prevention/reversal of TGF-β1 actions. Hence it is possible that HA generated in this context is an attempt by the body to prevent/reverse TGF-β1-driven fibrotic damage. Moreover, HA has long been established in playing a role in inflammation and immune regulation in other biological tissues. Hence, we will investigate a possible pro-inflammatory role for mesothelial cell HA generation during MMT. We will investigate these putative functions for peritoneal HA in the next two chapters.

Chapter 4

Does BMP-7 Promote the Prevention of TGF-β1-Driven MMT by Altering Hyaluronan Matrix and related HA-binding proteins

4.1 Introduction

EMT is an essential process in many physiological and pathological conditions, such as embryonic development, tumour progression and solid organ fibrosis. The reverse process, termed mesenchymal-to-epithelial transition (MET), is also important and generates epithelial cells. During MET, mesenchymal cells progressively re-establish apical-basal polarity, reform tight junctions between cells and reorganise cytoskeletal structures to restore epithelial phenotypes [402]. In the context of PD, MMT has been demonstrated to be a key event in the development of peritoneal membrane failure, that can be targeted by numerous endogenous factors and pharmaceutical agents [354]. The endogenous factor Bone Morphogenic Protein-7 (BMP-7), has been demonstrated to negatively regulate EMT and promote MET in different types of epithelial and endothelial cells by interfering with the canonical TGF-β1 Smad 2/3 signalling pathways [354, 403-405]. BMP-7 has also been shown to prevent and reverse TGF-β1-induced EMT and subsequent fibrosis of the kidneys, liver and lungs [129, 131, 133, 135-137, 406-409]. However, BMP-7 is essential to normal development and more recently has been implicated in cancer cell invasion, migration and metastases [410, 411]. Thus, understanding the mechanisms by which BMP-7 modulates cell behaviour may elucidate novel therapeutic therapies without affecting normal cellular processes.

BMP-7 is a member of the TGF-β superfamily, and binds to distinct type II receptors, which then form complexes with specific type I serine-threonine kinase receptors (ALK receptors). In epithelial cells, BMP-7 binds specifically to ALK3 and ALK6 receptors to convey intracellular signals through Smad1/5/8 phosphorylation, whilst TGF-β1 binds to ALK5 receptors to signal through Smad2/3 phosphorylation to mediate EMT [133]. Aside from the Smad-dependent

pathways, BMP-7 has also been shown to signal through non-canonical pathways to influence the biological activity of cells [128, 412, 413]. Mesothelial cells constitutively express BMP-7 and display basal activation of Smad1/5/8 contributing to the maintenance on the epithelial-like phenotype [354]. Furthermore, induction of MMT by TGF-β1 results in downregulation of BMP-7 and inactivation of its intracellular signalling pathways [354]. Previous work from our laboratory has shown that BMP-7 can both prevent and reverse TGF-β1 dependent fibroblast-to-myofibroblast differentiation and type II EMT. In the mesothelium, some studies have demonstrated that BMP-7 negatively regulates MMT and promotes reversal of phenotype in both effluent- and omentum-derived mesothelial cells [354, 355]. However, the role of BMP-7 in prevention of TGF-β1-driven MMT has not been investigated. Therefore, the first aim of this chapter is to elucidate whether BMP-7 is able to prevent TGF-β1-driven MMT.

It is widely recognised that the way in which HA is assembled, its interaction with a wide variety of HA-binding proteins and its manner of organisation within the pericellular matrix, are crucial in determining its subsequent biological actions [138, 218]. In the previous chapter, it was demonstrated that changes in HA synthesis and macromolecular organisation did not appear to be involved in directing TGF-β1-driven MMT. Previous studies indicate that depending on these interactions, HA can both mediate as well as prevent TGF-β1-dependent myofibroblast differentiation. In fibroblasts, pericellular HA is organised by TSG-6 and Heavy Chain-5 interactions bound to cell-surface standard CD44. This promoted CD44s/EGF-Receptor coupling, which promoted MAPK/ERK signalling necessary for TGF-β1-driven myofibroblast differentiation. In contrast, cell-surface expression of the CD44 splice-variant CD44v7/8 led to internalisation of pericellular HA and prevention/reversal of TGF-β1-driven fibroblast to myofibroblast differentiation. The second aim of this chapter was to investigate

whether HA generated by mesothelial cells was (like in fibroblasts) able to mediate prevention of TGF-β1-driven MMT during PD.

4.2 Results

4.2.1 BMP-7 Does Not Prevent TGF-β1-Driven MMT in hPMCs

Initial experiments were performed on primary cultures of hPMCs to assess the effect of increasing doses of BMP-7 on TGF-β1 induced MMT. HPMCs were treated with 100, 200 and 400 ng/ml recombinant human BMP-7 (BMP-7) alongside 10 ng/ml TGF-β1 for 48 hours under serum-free conditions (Figure 4.1). Following TGF-β1 and BMP-7 stimulation, hPMCs demonstrated downregulation of epithelial markers E-Cadherin, ZO-1 and Claudin-1 (Figure 4.1A-C) and upregulation of mesenchymal markers α-SMA, Fibronectin and Collagen1α1 (Figure 4.1D-F) irrespective of the BMP-7 dose. Furthermore, there was no difference seen with increasing BMP-7 dose as the mRNA expression of all markers were unchanged when compared to control cells. The highest dose of 400 ng/ml BMP-7 was utilised for subsequent experiments. This concentration of BMP-7 was similar to that employed by others in our laboratory and elsewhere [133, 138, 354]. Time course experiments were then performed to investigate whether 400 ng/ml of BMP-7 prevented TGF-β1-driven myofibroblast differentiation at 24 and 48 hours (Figure 4.2). Treatment of hPMCs with 10 ng/ml TGF-β1 alone induced MMT as previously described in section 3.2.1. HPMCs treated with 400 ng/ml BMP-7 alone maintained an epithelial phenotype, with comparative expression of all markers to control (Figure 4.2A-F). Whilst there was a trend towards downregulated E-Cadherin and Occludin expression at 48 hours after BMP-7 treatment, this did not reach statistical significance (data not shown) nor were reciprocal changes seen in the mRNA expression of the mesenchymal markers to suggest any phenotypic change had occurred. Combined treatment of hPMCs with TGF-β1 and BMP-7 was associated with downregulated E-Cadherin, ZO-1 and Occludin mRNA expression (Figure 4.2A-C) and upregulated α-SMA, Fibronectin and

Collagen1α1 mRNA expression (Figure 4.2D-F). There were no statistically significant differences in the mRNA expression of all these markers when compared with the effects of TGF-β1 stimulation alone, other than with E-Cadherin at 24 hours, demonstrating that BMP-7 had no effect on preventing TGF-β1-driven MMT at an mRNA level.

Morphological changes were then assessed by visualising filamentous actin (F-Actin) reorganisation in hPMCs at 48 hours following the different cytokine treatments (Figure 4.3). As previously demonstrated, F-Actin was distributed on the plasma membrane of control hPMCs but reorganised to form thick bundles extending the length of the cells following TGF-β1 treatment alone, indicative of myofibroblast differentiation. Treatment of hPMCs with BMP-7 alone induced some morphological changes in hPMCs, however the phenotype was indeterminate. Mesothelial cells lost their cobblestone appearance, but did not develop a larger surface area and F-Actin appeared to be present both on the plasma membrane and in occasional bundles extending the length of the cell. Combined TGF-β1 and BMP-7 treatment of hPMCs induced similar phenotypic changes to TGF-β1 treatment alone, as hPMCs demonstrated a larger polygonal shape and reorganised F-Actin into thick bundles within the cells that extended from one end to the other, indicative of myofibroblast differentiation. Hence, according to these results, BMP7 does not influence TGF-β1-driven MMT in mesothelial cells.

Given these findings, the downstream signalling of BMP-7 were confirmed to ensure that BMP7 signaling was intact in these cells. mRNA expression of TGF-β1 was also assessed. The results for TGF-β1 and ID-1 (Inhibitor of DNA Binding-1) respectively were shown in Figure 4.4. Treatment of hPMCs with TGF-β1, either alone or in combination with BMP-7,

upregulated TGF-β1 mRNA expression (Figure 4.4A). This effect was greatest at 24 hours, and no statistically significant difference was demonstrated with BMP-7 and TGF-β1 co-treatment. The mRNA expression of TGF-β1 was low following BMP-7 treatment alone, and comparable to TGF-β1 expression in control cells. In contrast, treatment of hPMCs with BMP-7 alone induced mRNA expression of ID-1, whereas TGF-β1 downregulated ID-1 expression (Figure 4.4B). Co-treatment with TGF-β1 and BMP-7 had some effect on ID-1 mRNA expression; relative expression was comparable to control hPMC expression, but significantly higher than TGF-β1 alone. These experiments confirm that BMP7 was able to upregulate ID-1 expression and that TGF auto-induction was also intact in these cells.

4.2.2 Concurrent TGF-β1 and BMP-7 Stimulation of hPMCs Does Not Alter Cellular HA Generation and Distribution.

Initial experiments were performed to assess HA synthase, hyaluronidase and HA receptor protein mRNA expression in hPMCs concurrently treated with TGF-β1 and increasing doses of BMP-7 (Figure 4.5). Compared to control hPMCs, BMP-7 at low doses (100 and 200 ng/ml) had no effect on HAS1, HAS2 and HAS2AS mRNA expression in the presence of TGF-β1 10 ng/ml (Figure 4.5A-C). However, Co-treatment of hPMCs with 400 ng/ml BMP-7 and 10 ng/ml TGF-β1 led to significant upregulation of HAS1, HAS2 and HAS2AS mRNA expression compared to control. There was significant downregulation of HAS3 expression at 48 hours with all doses of BMP-7, but 400 ng/ml BMP-7 attenuated HAS3 downregulation in response to TGF-β1 (Figure 4.5D). HYAL1 and HYAL2 were equally downregulated at 48 hours, irrespective of BMP-7 dose given with 10 ng/ml TGF-β1 (Figure 4.5E-F) and there was also no BMP-7 dose effect on the downregulation of HA receptor proteins RHAMM and CD44 with TGF-β1 (Figure 4.5G-H).

HA generation was then analysed at 24- and 48-hour time points using the highest dose of BMP-7 available (400 ng/ml) and 10 ng/ml TGF-β1 (Figure 4.6). As previously described, treatment of hPMCs with 10 ng/ml TGF-β1 alone upregulated HAS1, HAS2 and HAS2AS mRNA expression and downregulated HAS3, HYAL1, HYAL2, RHAMM and total CD44. Compared to control, BMP-7 treatment alone had no effect on the expression of all HA-associated genes. HPMCs treated with both TGF-β1 and BMP-7 had upregulated HAS1 and HAS2 mRNA expression compared to TGF-β1 alone, which was most apparent at 24 hours with HAS1 and 48 hours with HAS2 (Figure 4.6A-B). However, no significant difference was seen when comparing the combined effects of TGF-β1 and BMP-7 to TGF-β1 alone with regards to the mRNA expression of all the other markers; HAS2AS, HAS3, HYAL1, HYAL 2, RHAMM and total CD44, at either time point (Figures 4.6C-H)

Immunochemical staining for FITC-labelled HABP was used to assess whether this increased HAS1 and HAS2 mRNA expression translated into increased HA generation following BMP-7 treatment (Figure 4.7). As previously described, undifferentiated hPMCs demonstrated cell-surface expression of HA and diffuse cytoplasmic distribution of intracellular HA. Treatment of hPMCs with BMP-7 alone had some effect on HA localisation as intracellular HA was less apparent when compared to control hPMCs, however no discernible difference was seen in the localisation of HA on the cell surface as HA was distributed evenly across the plasma membrane. Following TGF-β1 treatment, more cell surface and intracellular HA was present and intracellular HA appeared to be assembled around the actin cytoskeleton, as previously described. Co-treatment with TGF-β1 and BMP-7 induced similar effects to TGF-β1 alone in the distribution of HA on the cell surface, with increased HA present. However, the pattern of localisation of HA within the cells was different as HA did not readily assemble along the

actin cytoskeleton and was distributed in the cytoplasm and peri-nuclear region of the cell instead.

An ELISA-like assay was then performed to quantify HA levels and distribution in BMP-7/TGF-β1-stimulated hPMCs (Figure 4.8). As previously described, TGF-β1 increased HA levels above control in the extracellular and pericellular areas. BMP-7 alone did not change the HA levels in hPMCs above control in any areas. However, when comparing the effects of combined BMP-7 and TGF-β1 treatment to TGF-β1 alone, significantly increased levels of intracellular HA (above control and TGF-β1 alone) were demonstrated (Figure 4.8A). Whilst HA levels were significantly increased in pericellular (Figure 4.8B) and extracellular (Figure 4.8C) distribution in hPMCs co-treated with TGF-β1 and BMP-7, no difference was demonstrated when compared to the effects of TGF-β1 alone.

4.2.3 BMP7 Does Not Influence CD44v7/8 Splice-Variant Expression, and Forced CD44v7/8 Over-Expression in hPMCs Does Not Reset Either The TGF-β or BMP7 Response.

CD44 can exist as multiple isoforms due to alternative splicing of exons, and the expression of specific CD44 splice-variants can dictate distinct cell functions. Recent work from our laboratory demonstrated that BMP-7 increased standard CD44 mRNA expression and CD44v7/8 splice variant expression in fibroblasts [138]. Our group have shown that CD44v7/8 mediates the effects of BMP7 in prevention and reversal of TGF-β1-driven MMT in fibroblasts [138]. In hPMC's, however, BMP-7 had no effect on CD44 expression (Figure 4.9A). The influence of TGF-β1 and BMP-7 on CD44v7/8 isoform expression in hPMCs was also

investigated. BMP-7 treatment alone did not upregulate CD44v7/8 expression in hPMCs after 24- and 48 hour-treatments (Figure 4.9B). Furthermore, BMP-7 did not attenuate TGF-β1-driven down-regulation of CD44v7/8 mRNA expression at 24- and 48-hour time points. Of note, CD44v7/8 had low-level expression in hPMCs with threshold cycles of amplification ranging between 36 and 38 depending on the cytokine treatments.

The lack of a BMP-7 induction of CD44v7/8 in hPMC's compared to epithelial cells and fibroblasts was apparent. Hence, we used previously designed CD44v7/8 plasmid over-expression vectors to determine if restoring CD44v7/8 expression restored the TGF-β1 and BMP-7 response to make it similar to the response seen in fibroblasts/epithelial cells. Transient overexpression of the vector was confirmed by mRNA expression of CD44v7/8 (Figure 4.10A). The overexpression induced moderate CD44v7/8 expression in hPMCs with threshold cycles of amplification now ranging between 30 and 33 depending on the cytokine treatments. However, the mRNA expression patterns of E-Cadherin and α-SMA remained unchanged when compared to control and scramble hPMCs (Figure 4.10B-C). In hPMCs over-expressing CD44v7/8, the effects of combined and single BMP7 treatments were also unchanged compared to untransfected/scrambled samples. Overexpression of CD44v7/8 in hPMCs did not alter HAS1 expression in response to different cytokine treatments (Figure 4.10D). However, over-expression of CD44v7/8 was associated with attenuated HAS2 mRNA expression with combined BMP-7 and TGF-β1 stimulation when compared to TGF-β1 effects alone (Figure 4.10E). This was not seen in hPMCs overexpressing a scrambled sequence. No difference was demonstrated in HYAL1, HYAL2 and total CD44 mRNA expression between hPMCs overexpressing CD44v7/8 or scrambled sequences, irrespective of the cytokine treatments (Figure 4.10F-H).

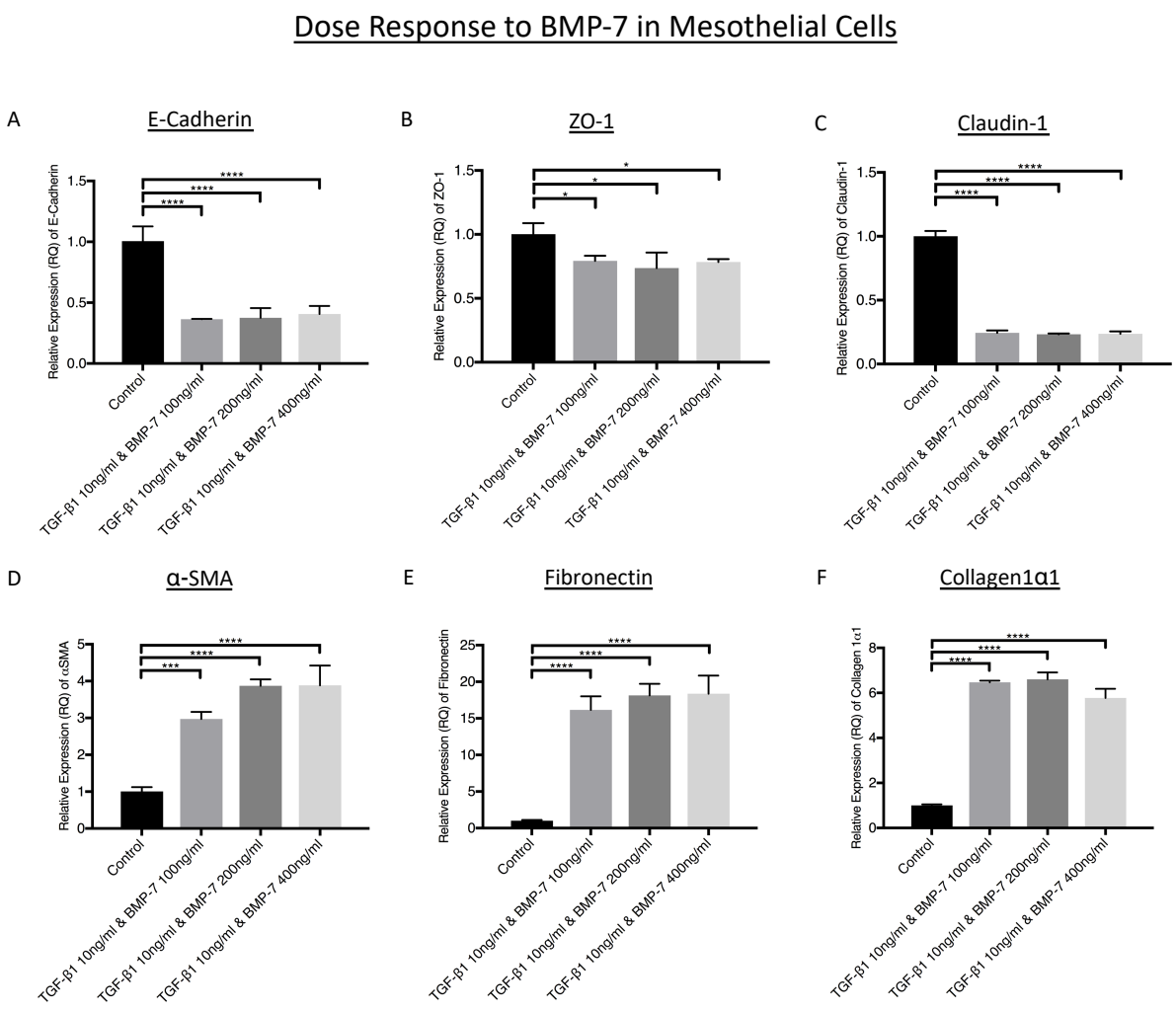

Figure 4.1 TGF-β1 and BMP-7 in combination represses epithelial and induces mesenchymal markers in mesothelial cells in a concentration dependent fashion. Confluent monolayers of omentum derived mesothelial cells treated with TGF-β1 10ng/ml and either 100, 200 or 400ng/ml BMP-7 concentrations for 48hours after 24hours growth arrest in serum free medium. Expression of epithelial markers: E-Cadherin, ZO-1 and Claudin-1 **(A-C)** and mesenchymal markers: αSMA, Fibronectin and Collagen1α1 (**D-F)**. mRNA expression of all markers analysed by RT-qPCR and normalised to GAPDH mRNA expression. Data represents the mean ± S.E.M from triplicate single donor experiment. Data was analysed by a one-way ANOVA followed by Tukeys post hoc analysis (ns = p>0.05, * = p≤0.05, ** = p≤0.01, *** = p≤0.001, **** = p≤0.0001).

Time-Course Analysis of BMP-7 Prevention of TGF-β1-Driven MMT in Mesothelial Cells

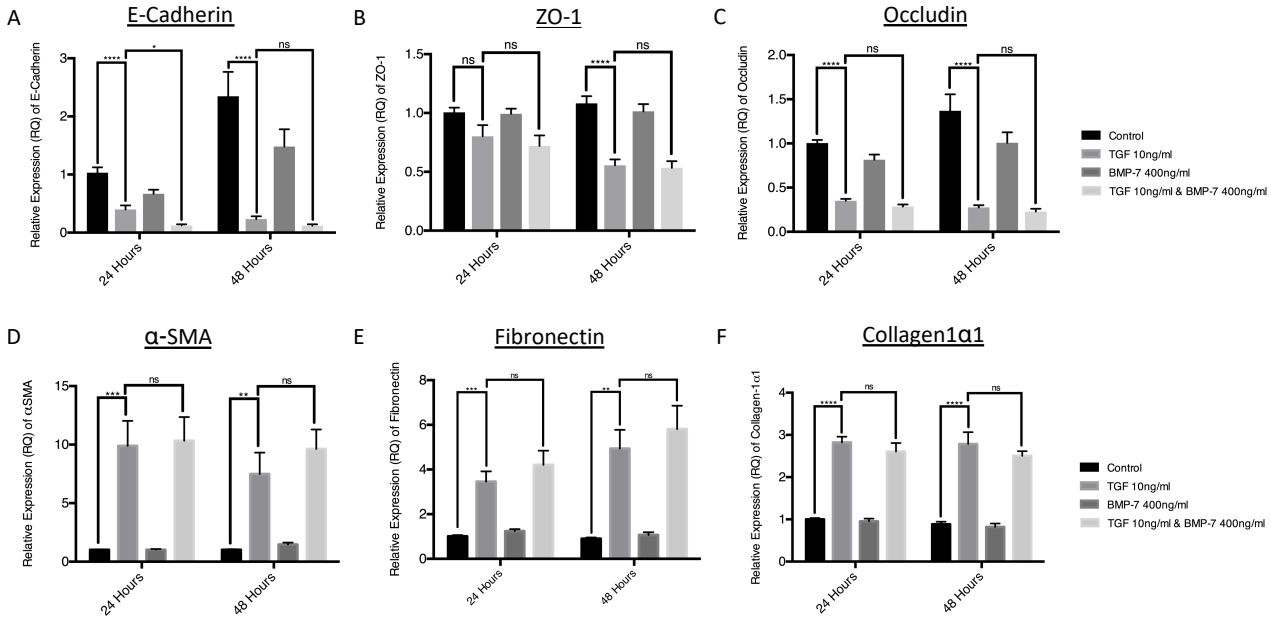

Figure 4.2 BMP-7 has no effect on mesothelial cells but does not prevent MMT following treatment with TGF-β1. Confluent monolayers of omentum derived mesothelial cells treated with BMP-7 400ng/ml, TGF-β1 10ng/ml, or both for 24 hours and 48 hours after 24 hours growth arrest in serum free medium. Expression of epithelial markers: E-Cadherin, ZO-1 and Occludin **(A-C)** and mesenchymal markers: αSMA, Fibronectin and Collagen-1α1 (**D-F)**. mRNA expression of all markers analysed by RT-qPCR and normalised to GAPDH mRNA expression. Data represents the mean ± S.E.M from 3 different donor experiments. Data was analysed by an ordinary one-way ANOVA followed by Tukeys post hoc analysis with $p<0.05$ considered as statistically significant (ns = $p>0.05$, * = $p\leq0.05$, ** = $p\leq0.01$, *** = $p\leq0.001$, **** = $p\leq0.0001$).

Phalloidin Staining of BMP-7 Prevention of Myofibroblast Phenotype

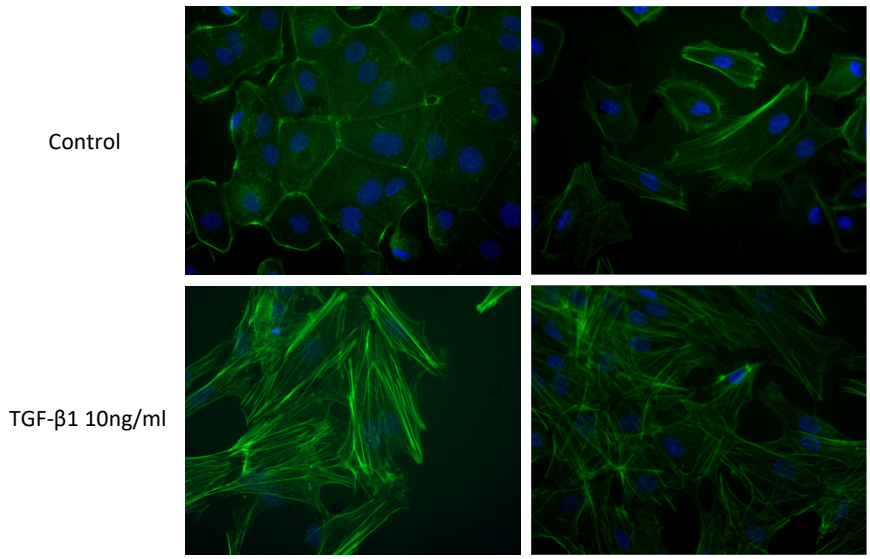

Figure 4.3 Characterisation of mesothelial phenotype in sub-confluent layers of mesothelial cells grown on chamber slides. Confluent monolayers of omentum derived mesothelial cells grown to 80% confluence on 8-well Permanox® chamber slides and treated with the stated cytokine treatments for 48hours. The cells were then fixed and antibodies for F-Actin (Phalloidin FITC) were added. Chamber slides were then mounted and imaged under UV-light. Images shown above representative of separate wells from 2 different omentum donors. Original magnification X40.

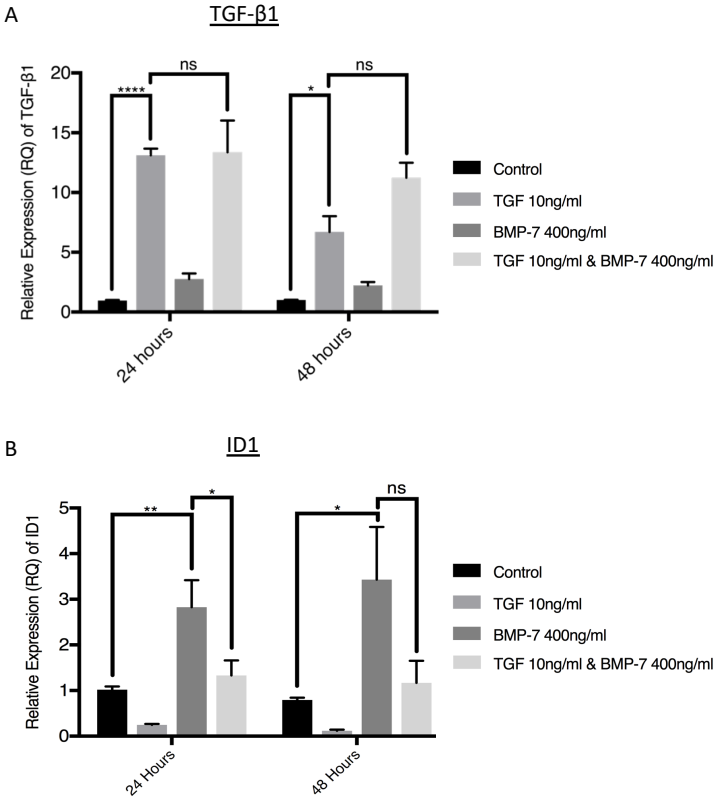

Figure 4.4 BMP-7 and TGF-β1 signal effectively in mesothelial cells. Confluent monolayers of omentum derived mesothelial cells treated with BMP-7 400ng/ml, TGF-β1 10ng/ml, or both for 24 hours and 48 hours after 24 hours growth arrest in serum free medium. Expression of TGF-β1 **(A)** and ID1 **(B)**. mRNA expression of all markers analysed by RT-qPCR and normalised to GAPDH mRNA expression. Data represents the mean ± S.E.M from 3 different donor experiments. Data was analysed by an ordinary one-way ANOVA followed by Tukeys post hoc analysis with $p<0.05$ considered as statistically significant (ns = $p>0.05$, * = $p\leq0.05$, ** = $p\leq0.01$, *** = $p\leq0.001$, **** = $p\leq0.0001$).

Effects of BMP-7 Treatment on the HA Profile in TGF-β1 driven MMT (Dose Response)

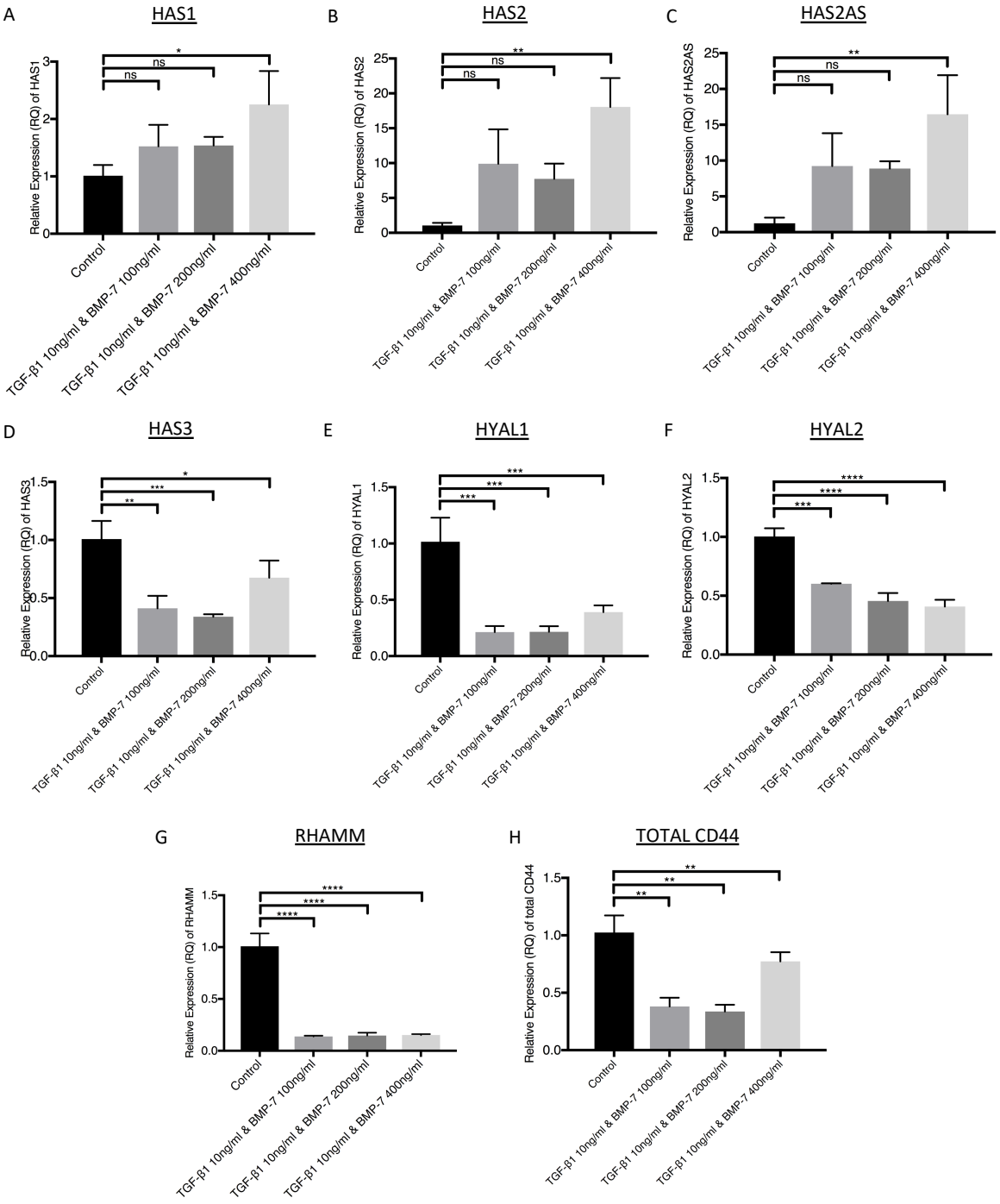

Figure 4.5 Concurrent BMP-7 and TGF-β1 stimulation of mesothelial cells generates HA in a concentration dependent fashion. Omentum derived mesothelial cells treated with TGF-β1 10ng/ml and either 100, 200 or 400ng/ml BMP-7 concentrations for 48hours. Expression of HA synthase enzymes: HAS1, HAS2, HAS3 and HAS2AS **(A-D)** Hyaluronidase enzymes: HYAL1 and HYAL2 (**E-F)** HA receptor proteins: RHAMM and total CD44 **(G-H)**. mRNA expression of all markers analysed by RT-qPCR and normalised to GAPDH mRNA expression. Data was analysed by a one-way ANOVA followed by Tukeys post hoc analysis (ns = p>0.05, * = p≤0.05, ** = p≤0.01, *** = p≤0.001, **** = p≤0.0001). Data represents the mean ± S.E.M from triplicate single donor experiment.

HA Profile in BMP-7 Prevention of Myofibroblast Phenotype Over 24/48h

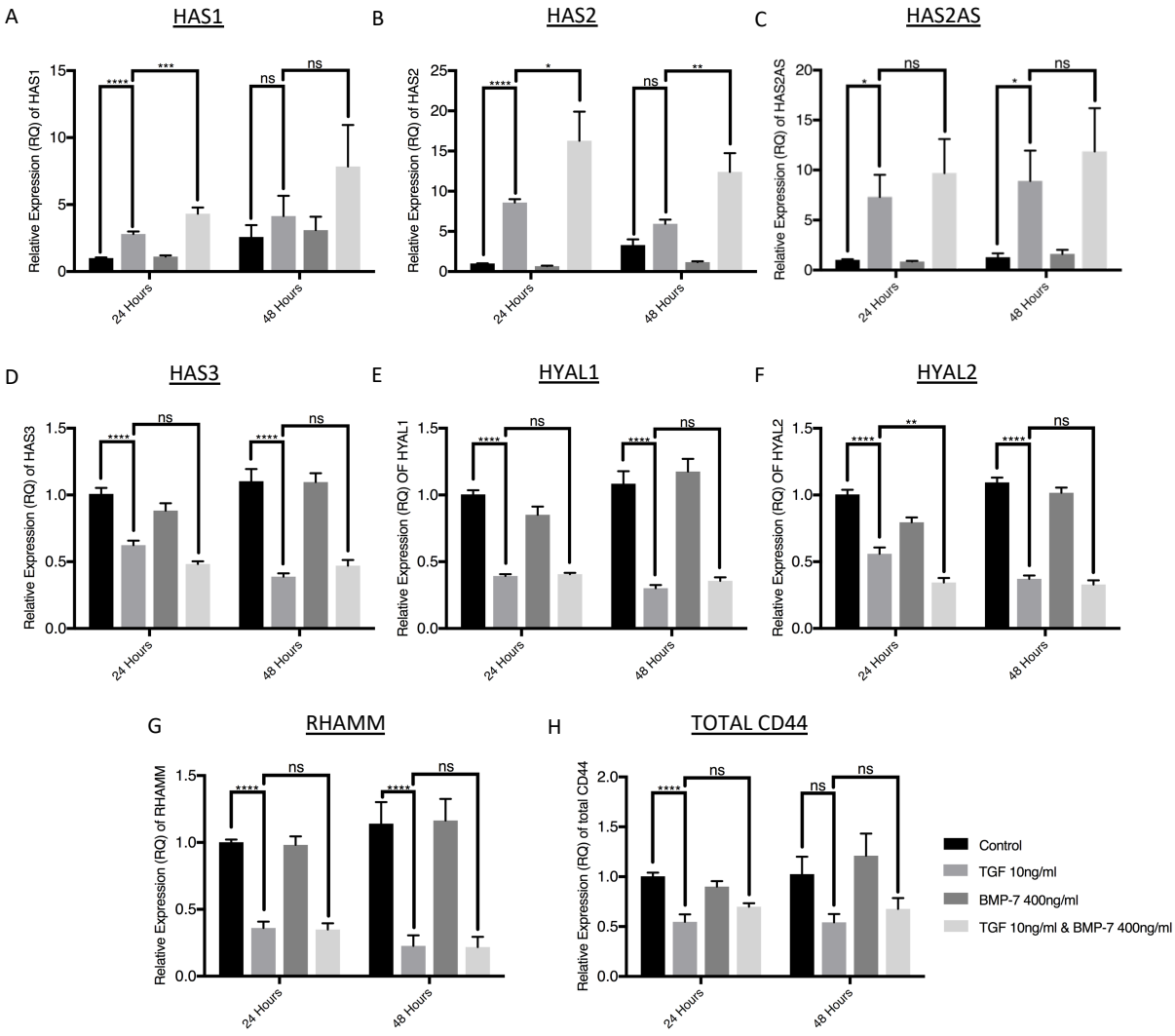

Figure 4.6 Cotreatment with TGF-β1 and BMP-7 does not alter HA-associated gene expression. Confluent monolayers of omentum derived mesothelial cells treated with 10ng/ml TGF-β1, 400ng/ml BMP-7 or both for 48hours. Expression of HA synthase enzymes: HAS1, HAS2, HAS2AS and HAS3 **(A-D)** Hyaluronidase enzymes: HYAL1 and HYAL 2 (**E-F)** HA receptor proteins: RHAMM and total CD44 **(G-H)**. mRNA expression analysed by RT-qPCR and normalised to GAPDH mRNA expression. Data represents the mean ± S.E.M from 3 different donor experiments. Data was analysed by a one-way ANOVA followed by Tukeys post hoc analysis (ns = p>0.05, * = p≤0.05, ** = p≤0.01, *** = p≤0.001, **** = p≤0.0001).

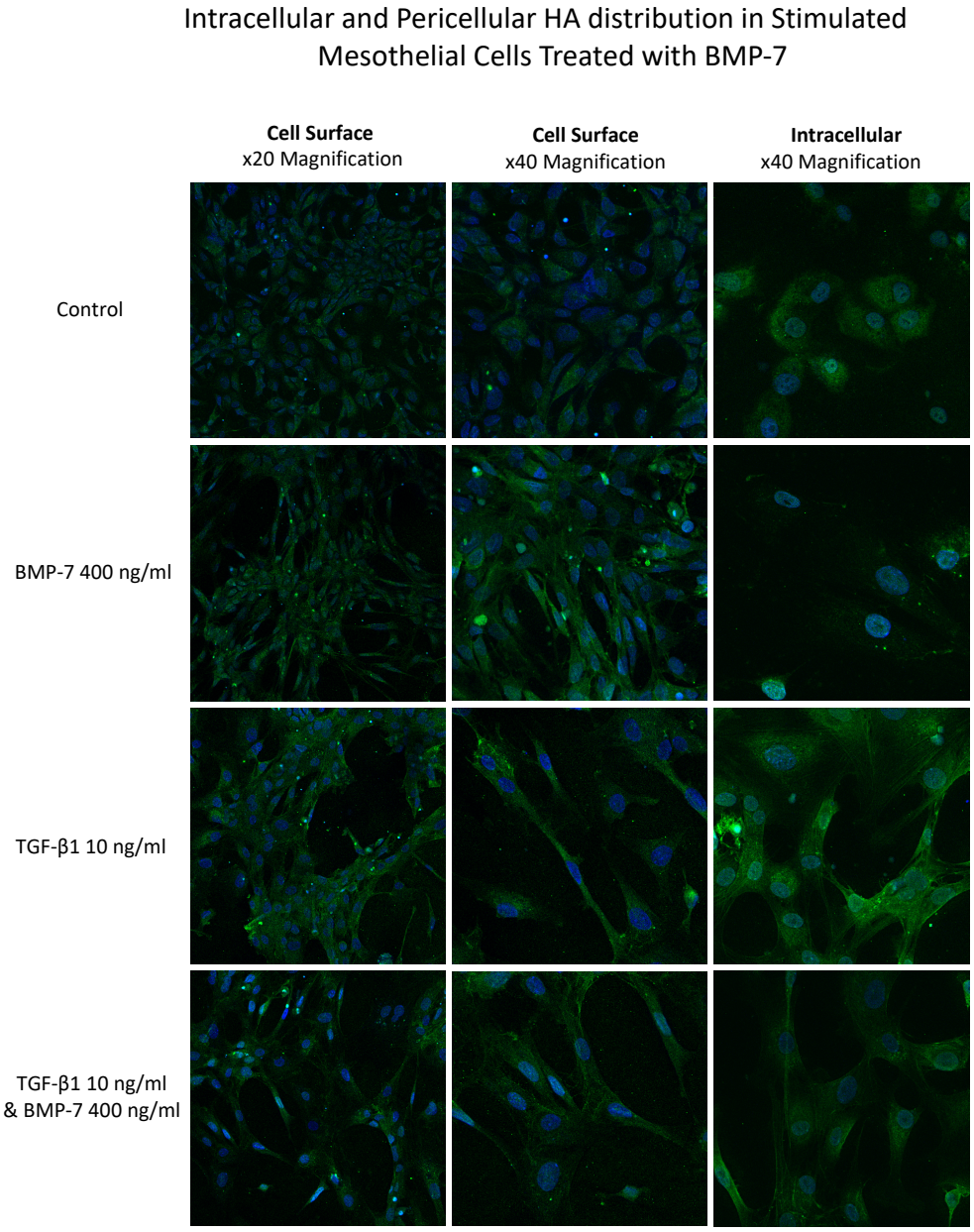

Figure 4.7 Cotreatment with TGF-β1 and BMP-7 doesn't alter pericellular and intracellular HA distribution in mesothelial cells. Confluent monolayers of omentum derived mesothelial cells grown to 80% confluence on 8-well Permanox® chamber slides and treated with the stated cytokine treatments for 48hours. Cells were then fixed and stained for biotinylated HA-binding protein (bHABP). For visualisation of intracellular HA, cells underwent additional treatment with *Streptomyces Hyaluronidase* 1 iU/ml prior to fixation. Chamber slides were then mounted and analysed by confocal microscopy. Images shown above representative of separate wells from 3 omentum donors. Original magnification as described. Images for Control and TGF-β1 treated cells reproduced from figure 3.6

Concentration and Distribution of HA in Stimulated Mesothelial Cells Treated with BMP-7

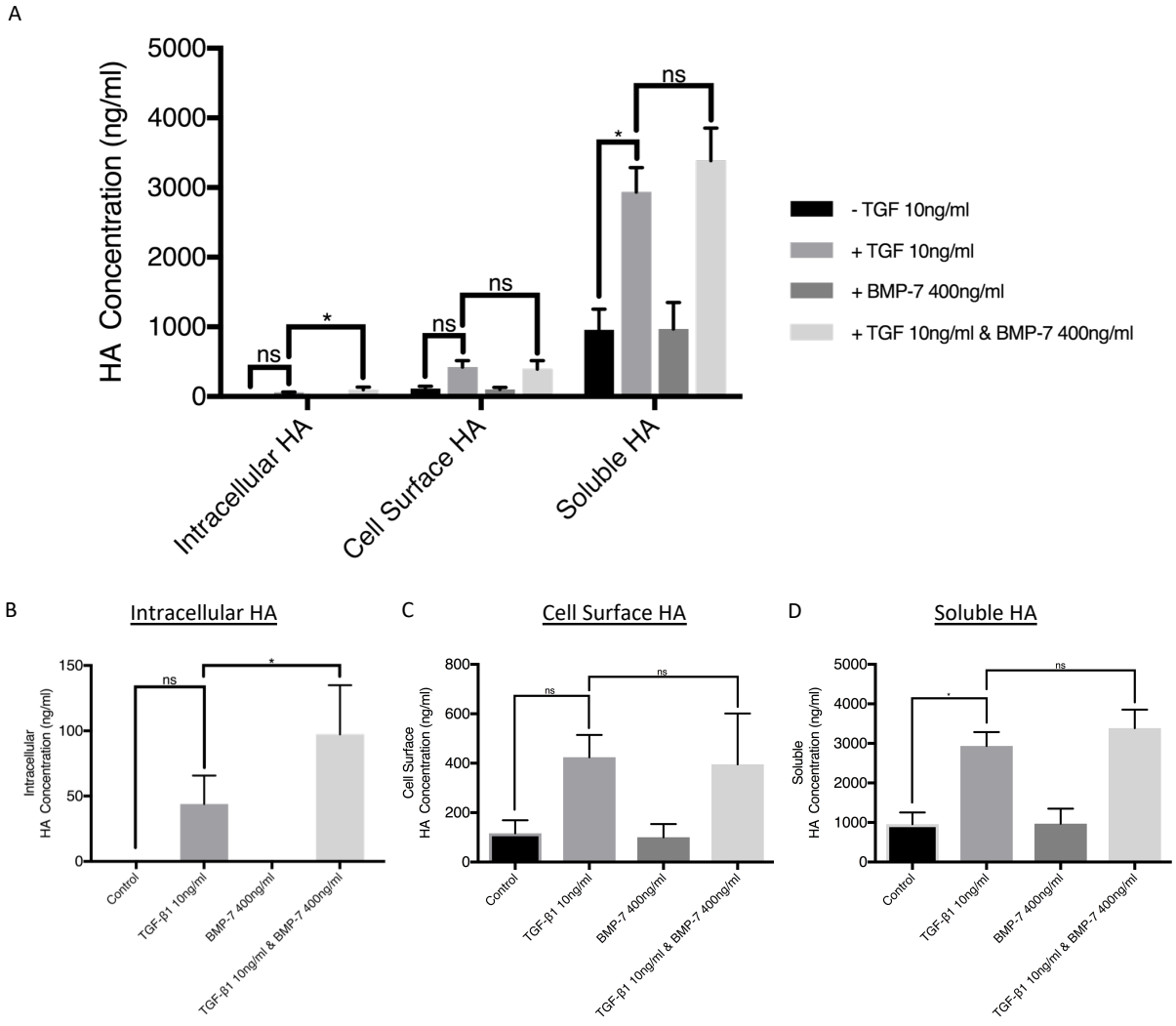

Figure 4.8 Cotreatment with TGF-β1 and BMP-7 doesn't alter HA generation and distribution in stimulated mesothelial cells. Confluent monolayers of omentum derived mesothelial cells treated with 10ng/ml TGF-β1, 400ng/ml BMP-7 or both for 48hours. Quantification of intracellular, cell surface and extracellular HA by ELISA as described in 2.14.1.1 **(A)**. Individual concentrations of HA in intracellular lysate **(B) c**ell surface trypsinates **(C)** and conditioned cell culture media **(D)**. Data represents the mean ± S.E.M from 3 different donor experiments. Data was analysed by a one-way ANOVA followed by Tukeys post hoc analysis (ns = p>0.05, * = p≤0.05, ** = p≤0.01, *** = p≤0.001, **** = p≤0.0001).

CD44v7/8 Expression in Mesothelial Cells

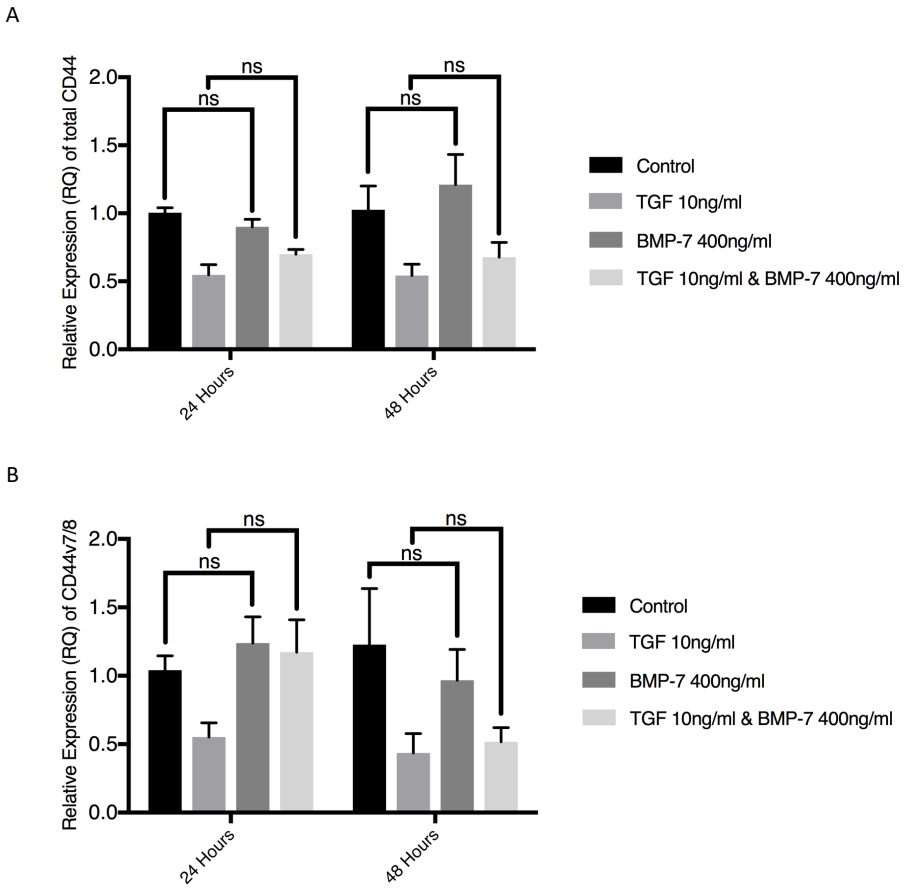

Figure 4.9 BMP-7 does not induce CD44v7/8 expression in Mesothelial Cells. Confluent monolayers of omentum derived mesothelial cells treated with 10ng/ml TGF-β1, 400ng/ml BMP-7 or both for 48hours. Comparison of mRNA Expression of Total CD44 **(A)** and alternatively spliced variant CD44 receptor isoform (CD44v7/8) **(b)**. mRNA expression of all markers analysed by RT-qPCR and normalised to GAPDH mRNA expression. Data represents the mean ± S.E.M from 3 different donor experiments. Data was analysed by a one-way ANOVA followed by Tukeys post hoc analysis (ns = $p>0.05$, * = $p\leq0.05$, ** = $p\leq0.01$, *** = $p\leq0.001$, **** = $p\leq0.0001$).

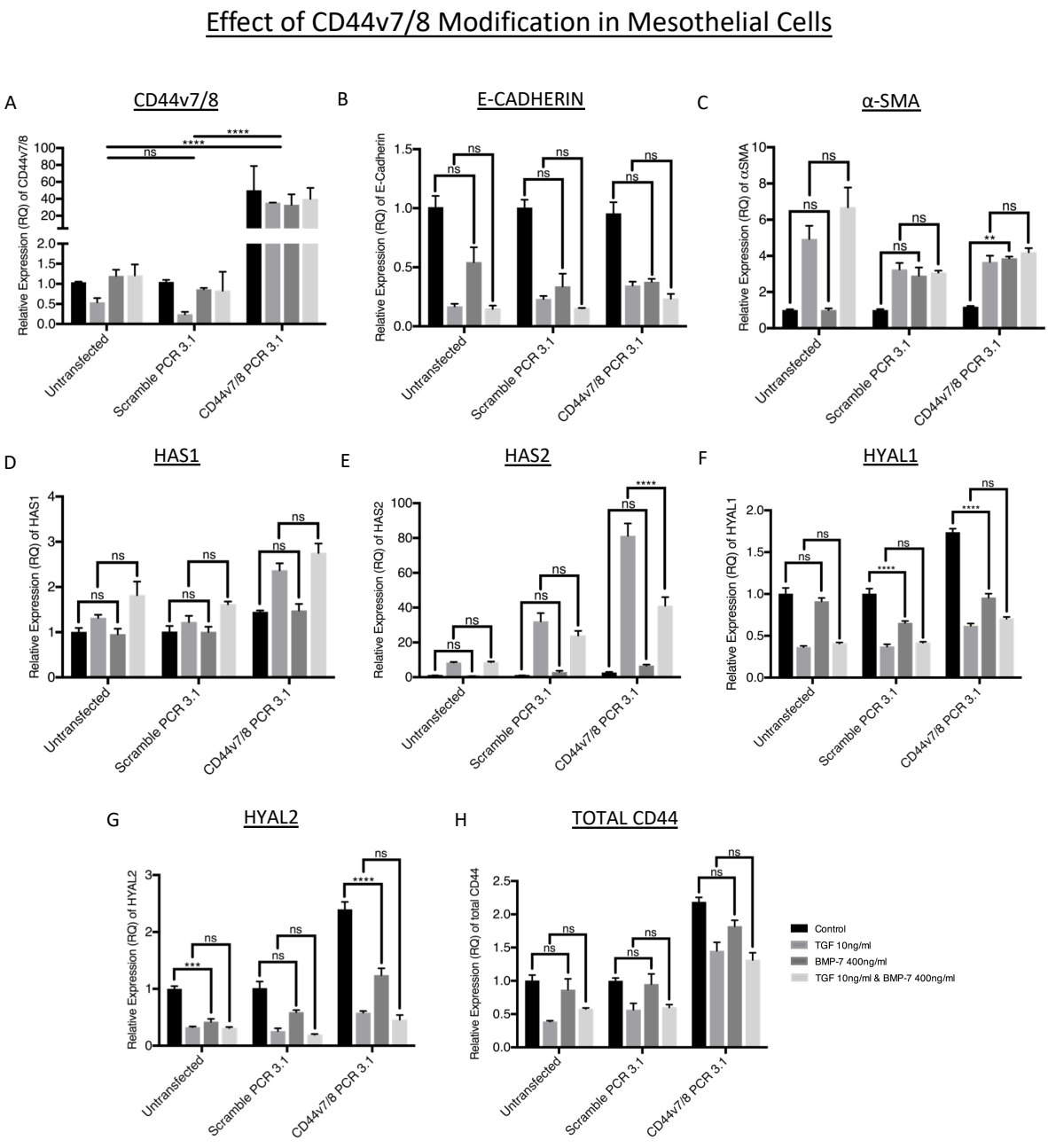

Figure 4.10 Forced over-expression of CD44v7/8 in mesothelial cells and treatment with BMP-7 doesn't alter HA-associated gene expression. Confluent monolayers of omentum derived mesothelial cells treated with 10ng/ml TGF-β1, 400ng/ml BMP-7 or both for 48hours following forced over-expression of CD44v7/8. Expression of CD44v7/8 **(A)** E-Cadherin **(B)** α-SMA **(C)** HAS1 **(D)** HAS2 **(E)** HYAL1 **(F)** HYAL2 **(G)** Total CD44 **(H).** mRNA expression of all markers analysed by RT-qPCR and normalised to GAPDH mRNA expression. Data represents the mean ± S.E.M from triplicate single donor experiment. Data was analysed by a one-way ANOVA followed by Tukeys post hoc analysis (ns = p>0.05, * = p≤0.05, ** = p≤0.01, *** = p≤0.001, **** = p≤0.0001).

4.3 Discussion

The concept that BMP-7 counteracts and reverses TGF-β1 activity in fibrosis has been confirmed in many organ systems. However, only a couple of isolated studies have identified that BMP-7 reverses TGF-β1-driven MMT to date. Vargha *et al* demonstrated that BMP-7 is able to promote MET in effluent-derived mesothelial cells cultured from paediatric PD patients [355]. Incubation of *ex vivo*-derived 'fibroblastoid' cells from PD effluent with 100 ng/ml rhBMP-7 for 24 hours reverted these fibroblast-like cells to an epithelial-like phenotype with downregulated α-SMA expression. Loureiro *et al* demonstrated that that mesothelial cells constitutively express BMP-7 and exhibit activation of BMP-7-dependent Smads 1, 5 and 8 *in vitro* under normal conditions [354]. Whilst exposure to PD fluid downregulated this signalling pathway, interestingly, exposure of these same cells to low glucose degradation products (GDP) containing PD fluid did not elicit the same responses. The findings from these studies suggested that BMP-7 is antagonistic to TGF-β1 in mesothelial cells, as in other solid organs.

Loureiro *et al* suggested that there is a loss of balance between TGF-β and BMP signalling in mesothelial cells during PD leading to the alterations in cellular phenotype and subsequent morphological changes in the peritoneal membrane [354]. The data in this chapter, however, suggests that restoring this imbalance in mesothelial cells does not appear to prevent MMT, and the TGF-β1 effect predominates. This is demonstrated by data indicating strong induction of TGF-β1 target gene expression with combined treatment with TGF-β1 and BMP-7 after 24 and 48 hours, to the same effect as TGF-β1 alone. ID-1 expression was attenuated following co-treatment with BMP-7 and TGF-β1 compared to treatment with BMP-7 alone. This is

possibly an effect of the TGF-β1 alone, as this is known to attenuate ID-1 expression, but is does indicate that in this setting TGF-β1 appears to override BMP-7 signalling effects.

One reason why in our studies BMP-7 does not prevent TGF-β1-driven MMT as compared to other studies is the dose of TGF-β1 that is utilised in our studies. Compared to the authors, Loureiro *et al*, 10X the dose of TGF-β1 was used in this thesis for reasons previously mentioned, whilst the final concentration of BMP-7 was similar (500 ng/ml vs 400 ng/ml). Therefore, a disparity in signalling could be explained by higher TGF-β1 doses used, however, it is difficult to justify using lower doses of TGF-β1 as the aim was to reflect levels seen in the peritoneum of patients on PD. However, the cellular mechanisms of TGF-β and BMP signalling are probably more complex than this. For example, TGF-β1-driven inhibition of BMP-7 is likely a result of multiple direct and indirect actions, as some studies have suggested that certain modulators of BMP-7 and TGF-β1 pathways are upregulated in response to certain cytokines. The cytokine connective tissue growth factor (CTGF) is induced in mesothelial cells following TGF-β1 stimulation, and exerts this effect by binding and inactivating the BMP-7 receptor whilst binding and activating the TGF-β receptor thereby modulating both pathways [114, 414-417]. Mesothelial BMP signalling might also be influenced by other BMP-7 modulators such as gremlin-1, kielin/chordin-like protein (KCP) or uterine sensitization-associated gene 1 (USAG-1) [114, 351, 418].

In solid organ fibrosis, work from our lab and elsewhere have elucidated that TGF-β1 promotes HAS2-driven HA pericellular coat formation and this HA coat is essential in maintaining myofibroblast phenotype [125, 126, 169, 182-184, 246, 253, 322, 332]. However, alternative forms of HA pericellular matrix formations have been identified, which have

distinct and sometimes opposing functions depending on cytokine treatments [236]. Work from our laboratory have previously identified that fibroblasts stimulated with IL-1β were not able to differentiate into myofibroblasts and formed 'spiculated' HA pericellular coats which enhanced fibroblast-monocyte interactions through CD44 and ICAM-1 co-localisation [236]. BMP-7 has likewise been demonstrated to modulate HA-matrix-driven cell function. For example, reduction of pericellular HA matrices in articular chondrocytes diminishes the cellular response to BMP-7, but not to TGF-β1, which was restored by renewal the HA pericellular matrix [231, 419]. In the kidney, BMP-7 modulates inflammation by generation of HA cable-like structures that facilitate HA-monocyte interactions through CD44 [296]. The authors demonstrated that BMP-7 induced HAS2 and downregulated HYAL1 and HYAL2 expression leading to generation of these HA cables. In this chapter, BMP-7/ TGF-β1 co-treated hPMCs induced HAS1 and HAS2 expression more than the TGF-β1 effect alone. However, this did not translate into an increase in pericellular HA generation nor a change in assembly, for example, into cables or 'spiculated' coats.

Work from our laboratory has shown that BMP-7-driven prevention of TGF-β1-mediated fibroblast-to-myofibroblast differentiation was also not associated with a distinct pericellular HA matrix, but instead BMP-7 promoted internalisation of HA into intracellular endosomes for breakdown [138]. In comparison, BMP-7 did not promote intracellular HA accumulation in mesothelial cells. In fibroblasts the CD44v7/8 splice variant was responsible for mediating the BMP-7 effects of cytoplasmic internalisation of pericellular HA. However, in mesothelial cells CD44v7/8 splice-variant expression is low and not inducible following BMP-7 treatment, which could explain why the BMP-7 effects on HA are different in these two settings.

CD44 acts as a co-receptor for a number of cell-surface growth factors and cytokine receptors [420]. CD44 has four domains and governs a wide variety of cellular functions from the cell surface through its HA-CD44 in development, tumorigenesis, metastasis, inflammation and fibrosis [138, 269, 288, 393-395]. CD44 can undergo complex post-translational modification to create multiple splice variants or isoforms (Figure 1.9) but all share a common HA-binding link module. Numerous studies have highlighted that these CD44 variant isoforms can have distinct modes of action leading to differential functions, especially in cancer contexts [385]. Our group have previously demonstrated that TGF-β1 and BMP-7 differentially regulate total CD44 and expression of the variant isoform CD44v7/8, translated from mRNA containing the CD44s exons plus the addition of exons 11 and 12 to the stem region. In mesothelial cells, this was not the case as BMP-7 did not upregulate total CD44 and CD44v7/8. Furthermore, there was a deficiency in CD44v7/8 expression in mesothelial cells [138]. Since CD44v7/8 was minimally expressed in mesothelial cells and was not induced by BMP-7, it was overexpressed to investigate whether its re-expression altered the TGF-β1 or BMP-7 response to a response that is more in keeping with the response seen in fibroblasts and epithelial cells. However, it was clear that CD44v7/8 over-expression did not alter the responses of these growth factors warranting no further investigation in these cells.

In conclusion, the work in the last two chapters have indicated that in peritoneal cells HA does not appear to mediate either promotion or prevention of TGF-β1-dependent MMT. In the final chapter, the role of mesothelial generated HA in influencing peritoneal infection and inflammation is investigated.

Chapter 5

Investigating the Role of HA in the Peritoneum During Peritoneal Infection and Inflammation

5.1 Introduction

Inflammation is one of the most important factors causing structural and functional alterations to the peritoneal membrane during PD, and this process is driven by the constant exposure to bioincompatible PD solutions and repeated episodes of PD peritonitis. It is clear that long-term PD promotes a state of chronic inflammation, which is normally followed by peritoneal fibrosis and neoangiogenesis within the peritoneal membrane. This inflammation is characterised by the enhanced production of acute phase proteins and other inflammatory mediators such as TNF-α and various interleukins (ILs). Numerous studies have demonstrated elevated levels of these inflammatory mediators prior to and during episodes of PD peritonitis as well as long-term PD therapy itself [59, 107, 340, 421-432].

Mesothelial cells are involved in the peritoneal response to injury or infection, and coordinate the recruitment of other inflammatory cells into the peritoneal cavity including mononuclear phagocytes, lymphocytes and neutrophils [114]. Upon challenge by infection or exposure to dialysis fluid, there is a massive influx of leukocytes from the circulation [43, 433]. Under normal circumstances, this infiltration occurs within minutes, followed by a swift return to constitutive levels within days following resolution. Mesothelial cells, along with other immune cells, mediate leukocyte infiltration in a number of ways. Mesothelial cells are activated by proinflammatory cytokines released by resident macrophages, such as TNF-α, IL-1β and IFN-γ, which in turn induce cytokine production by mesothelial cells including monocyte chemoattractant protein-1 (MCP-1), RANTES, IL-8 and various adhesion molecules [35, 52, 56, 434, 435]. The net effect of these cytokines is to further recruit leukocytes and facilitate leukocyte adherence and migration across the mesothelium [56]. The recruitment

of leukocytes is critical to resolve any inflammatory episode and signals transition from innate to acquired immunity [58]. This inflammatory response is characterised by enhanced vascular permeability, an initial influx of neutrophils followed by their clearance and replacement by a more sustained population of mononuclear cells.

HA has been shown to be associated with inflammation during PD through the local production of HA by mesothelial cells. There is a correlation between PD and increased HA levels in the peritoneal cavity, which are augmented during episodes of peritonitis. Mesothelial cells are responsible for most of the local HA generated, which exists as HMW polymers in the PD effluent [341, 342, 346]. In experimental models of PD, Yung *et al* [342] demonstrated that mesothelial cells synthesize HA in response to stimulation with IL-1β, IL-6, TNF-α, TGF-β1 and platelet-derived growth factor (PDGF). Furthermore, experimentally generated exogenous HA fragments added to mesothelial cells in-vitro can activate the inflammatory cascade through activation of the NF-κβ signalling pathway leading to induction of IL-8 and MCP-1 production [35, 436]. Thus, chronic induction of these inflammatory cytokines and HA during PD may therefore perpetuate the inflammatory process in the peritoneum and lead to long-term peritoneal membrane changes and the development of fibrosis. However, the role of the increased endogenous HA generated by mesothelial cells in regulating inflammation has yet to be established. The aim of this chapter is to investigate whether endogenous HA generated in the peritoneum plays a role in regulating the immune or inflammatory response during PD peritonitis.

5.2 Results

5.2.1 HA Levels in Non-Infected and Infected PD Effluent

Initial experiments were performed on the PD effluent of non-infected and infected patients currently receiving CAPD to corroborate previous findings that PD peritonitis increases HA levels in the PD effluent (Figure 5.1). The median HA level in PDE from 9 non-infected patients was 59.31 ng/ml (range, 43.19 to 635.3 ng/ml; mean, 155.6 ± 67.92 S.E.M). The median HA levels in PDE from 9 infected patients was 561.3 ng/ml (range, 443 to 1136 ng/ml; mean, 708.1 ± 92.42 S.E.M) and demonstrated a statistically significant difference (p=0.0002) in the levels of HA during episodes of PD peritonitis.

5.2.2 PEP-1 Binding to HA Alters Leukocyte Recruitment During Peritoneal Infection

In order to evaluate the biological activity of HA and assess its role as a modulator of inflammation *in vivo*, the effect of HA blockade using a HA blocking peptide (PEP1) on a well-established model of acute peritoneal infection was tested. This model is based on the intraperitoneal (i.p.) administration of a defined dose of heat-killed *S. epidermidis*, termed HKSE, described in section 2.15. This model mimics the progression of a *S.epidermidis*-induced peritonitis episode, which is one of the most common organisms isolated from patients on PD with episodes of peritonitis. PEP-1 has previously been demonstrated to bind specifically to HA in other experimental models of inflammation [278, 279, 298, 437-439] and was therefore chosen to block and antagonise peritoneal HA in these experiments.

The effects of HA blockade on HKSE-induced acute peritoneal inflammation was observed at two time points, 4 and 16 hours, by determining the leukocyte populations and chemokine levels in the peritoneal lavages. Figure 5.2 shows an example of the flow cytometry gating strategy used in all *in vivo* experiments to characterise leukocyte populations in mouse peritoneal effluent. A step-wise flow-cytometric strategy beginning with exclusion of cellular debris and doublets, followed by characterisation of neutrophils and monocyte populations using Ly6C and Ly6G staining was used. Firstly, cells were gated on size based on the forward scatter height (FSC-A) and side scatter height (SSC-A) (Figure 5.2A). Doublets were then excluded by correlating the forward scatter height (FSC-H) with the forward scatter area (FSC-A), giving the graph a diagonal display and then gating out the cells that did not correlate (Figure 5.2B). Leukocyte populations were then identified based on staining for $Ly6C^{+}$ and $Ly6G^{+}$ populations (Figure 5.2C). Within these cells, neutrophils could be readily identified as $Ly6C^{+}Ly6G^{+}$ and monocytes were $Ly6C^{+}Ly6G^{Low}$. Further gating of neutrophils and monocytes was based on cell size using FSC-A and SSC-A to exclude and potential contaminations (Figure 5.2D-E).

Initial *in-vivo* experiments were performed on mice inoculated with PBS, HKSE alone or HKSE + PEP-1 for 4 and 16 hours (Figure 5.3). Intraperitoneal administration of PBS to mice resulted in low levels of neutrophils and monocytes at both time points (Figure 5.3A). Intraperitoneal administration of HKSE resulted in a significant increase in the peritoneal levels of neutrophils at 4 and 16 hours compared to PBS, but no difference was observed in the levels comparing the two time points. Monocyte levels were not increased 4 hours after HKSE administration but were significantly elevated after 16 hours. Intraperitoneal administration of HKSE + PEP-1 significantly increased levels of neutrophils at 4 and 16 hours. The was no difference in the

levels of neutrophils present at 4 hours compared to HKSE alone but levels of neutrophils were significantly increased at 16 hours compared to HKSE infection at 16 hours. There was no difference in the levels of monocytes seen with HKSE + PEP-1 after 4 hours compared to PBS or HKSE alone, with low levels detected. However, monocyte levels were significantly attenuated compared with levels seen with HKSE alone. Monocyte levels were significantly higher than PBS alone at 16 hours.

This initial experiment demonstrated that binding of PEP-1 to HA resulted in increased neutrophil levels and reduced monocyte levels at 16 hours following HKSE infection. However, the effects of PEP-1 alone were not known and subsequent experiments were performed to confirm PEP-1 effects on leukocyte recruitment patterns and compare to patterns already observed following HKSE infection after 16 hours (Figure 5.4). Intraperitoneal administration of PBS resulted in low detectable levels of neutrophils and monocytes at 16 hours (Figure 5.4A). The combination of PBS + PEP-1 did not show a significant effect on neutrophil and monocyte levels at 16 hours compared to PBS alone. In keeping with the previous experiment, HKSE administration again led to significantly increased levels of neutrophils and monocytes in the peritoneal lavages 16 hours post infection. A further increase in neutrophils was observed in mice inoculated with HKSE + PEP-1, but this was not significant. However, monocyte levels were reduced in HKSE + PEP-1 compared to HKSE alone.

PEP-1 was not fully soluble in aqueous solutions and this may be accountable for the non-significant increase in peritoneal inflammation seen. Therefore, preparation of PEP-1 was optimised, by preparing the peptide/DMSO solution immediately prior to administration and

the experiment was repeated to analyse effect on leukocyte numbers (Figure 5.4B). Preparation of PEP-1 solution immediately prior to administration resulted in negligible neutrophil and monocyte levels in the peritoneal lavages and the levels were no different to those observed with PBS alone. Thus, this optimised method of PEP-1 preparation and administration was used for subsequent experiments.

A further *in-vivo* experiment was performed on mice inoculated with PBS, PBS + PEP-1, HKSE or HKSE + PEP-1 for 4 and 16 hours and the leukocyte populations determined from resulting flow cytometric analysis (Figure 5.5). Intraperitoneal administration of PBS alone or PBS + PEP-1 to mice resulted in low and comparable levels of neutrophils and monocytes at both time points, as seen in previous optimisation experiments (Figure 5.3A). Intraperitoneal administration of HKSE resulted in a significant increase in the peritoneal levels of neutrophils at 4 and 16 hours compared to PBS. There was a modest but significant increase in monocyte levels at 4 hours following HKSE infection, which increased further at 16 hours. Intraperitoneal administration of HKSE + PEP-1 significantly increased levels of neutrophils at 4 and 16 hours. Intraperitoneal administration of HKSE + PEP-1 had no additional effect on monocyte levels after 4 hours and 16 hours compared to PBS or HKSE alone. However, the flow cytometric analysis of the monocyte populations were different compared to the initial experiment comparing HKSE + PEP-1 to HKSE alone (Figure 5.5B).

5.2.3 PEP-1 Binding to HA Alters Cytokine Profile During Peritoneal Infection

The results presented in this chapter have so far demonstrated that HKSE infection is associated with increased neutrophil and monocyte levels in the peritoneal lavages. The addition of PEP-1 to HKSE resulted in a further increase in neutrophil levels without corresponding increases in monocyte levels at 16 hours. In light of these results, the effects of HA blockade on expression of different cytokines, chemokines and acute phase proteins was investigated.

A semi-quantitative proteome profiler array was used to detect 40 different cytokines, chemokines and acute phase proteins in the peritoneal lavages from mice inoculated with PBS, PBS + PEP-1, HKSE or HKSE + PEP-1 at 4 hours (Figure 5.6) and 16 hours (Figure 5.7). Several cytokines were constitutively expressed in the lavages of all samples including B lymphocyte chemoattractant (BLC), complement component C5 and its protein fragment C5a, soluble ICAM-1 (sICAM-1), and stromal cell-derived factor-1 (SDF-1) at 4 hours (Figure 5.6). Intraperitoneal administration of PBS or PBS + PEP-1 was not associated with strong cytokine expression at 4 hours. Intraperitoneal administration of HKSE was associated with induction of several cytokines including macrophage colony-stimulating factor (M-CSF), granulocyte colony-stimulating factor (G-CSF), tissue inhibitor of metalloproteinases-1 (TIMP-1), IL-1β, IL-1 receptor antagonist (IL-1ra), macrophage inflammatory protein-2 (MIP-2), MIP-1α, MIP-1β, monokine induced by γ-interferon (MIG), MCP-1, IL-6, keratinocyte chemoattractant (KC) and interferon γ-induced protein 10 (IP-10). Intraperitoneal administration of HKSE + PEP-1 altered the cytokine profile, with loss of MIP2, MIP-1α, MIP-1β, MIG, IL-6, KC and attenuation of TIMP-1, MCP-1, G-CSF and IP-10 expression. HKSE + PEP-1 administration was also

associated with induction of IL-1β, IL-1α and IL-1ra expression at 4 hours. After 16 hours incubation, most of the cytokines detected had disappeared in all samples, but BLC, C5/C5a and sICAM-1 were again constitutively expressed (Figure 5.7). HKSE infection was associated with increased TIMP-1, IL-1α, IL-1ra, MCP-1, IP-10 and IL-16 after 16 hours. HKSE + PEP-1 was also associated with equivocal increases in these cytokines at 16 hours, except for MCP-1 and IL-1α which were not detected.

5.2.4 PEP-1 Binding to HA Induces HA-Associated Gene Expression During Peritoneal Infection

The effects of PEP-1 on the HA profile in the peritoneum was then investigated. Initial experiments revealed increased HA levels early in infected PD effluent samples and blockade of HA by PEP-1 *in vivo* lead to different leukocyte presence in the peritoneum during HKSE infection. An ELISA-like assay was therefore performed to assess HA levels in peritoneal lavages following HKSE infection and investigate the effects of PEP-1 of HA synthesis (Figure 5.8). Intraperitoneal administration of PBS or PBS + PEP-1 resulted in low HA levels detectable at 4 hours and negligible levels of HA detected at 16 hours. Intraperitoneal administration of HKSE resulted in a significant increase in the peritoneal levels of HA at 4 and 16 hours compared to PBS, but no difference was observed in the levels when compared to HKSE + PEP-1.

The mRNA expression of HA-associated genes was then investigated in peritoneal membranes of mice inoculated with PBS, PBS + PEP-1, HKSE or HKSE + PEP-1 (Figure 5.9). This was assessed by mRNA expression of HA synthase enzymes: HAS1, HAS2, HAS3, (including the natural antisense to HAS2; HAS2AS1)**,** Hyaluronidase enzymes: HYAL1 and HYAL 2 and HA receptor,

CD44. HAS1 mRNA expression was unchanged with intraperitoneal administration of PBS + PEP-1 at both time points (Figure 5.9A). HKSE infection increased HAS1 expression at 16 hours, whilst HKSE + PEP-1 attenuated HAS1 expression at the same time point. HAS2 expression was significantly downregulated with PBS + PEP1, HKSE and HKSE + PEP-1 at both time points (Figure 5.9B). HAS3 expression was unchanged at 4 hours following PBS + PEP-1, HKSE or HKSE + PEP-1 administration, but HKSE and HKSE + PEP-1 downregulated HAS3 expression at 16 hours (Figure 5.9C). Intraperitoneal administration of PBS + PEP-1 has no effect on HYAL1 (Figure 5.9D) and HYAL2 (Figure 5.9E) expression at both time points. Intraperitoneal administration of HKSE downregulated HYAL1 expression at 16 hours but not HYAL2. The addition of PEP-1 to HKSE had no effect on HYAL1 and HYAL2 expression at either time point when compared to HKSE alone. No differences in the mRNA expression of CD44 standard isoform were demonstrated with either treatment at both time points (Figure 5.9F).

5.2.5 PEP-1 Binding to HA Attenuates HAS2 Gene Expression in Mesothelial Cells During MMT

The results presented in this chapter have demonstrated that HA is generated in response to peritoneal infection, predominantly through HAS1 gene expression. Binding of PEP-1 to HA resulted in increased neutrophil recruitment into the peritoneum in response to HKSE, but not a corresponding monocyte influx, which associated with reduced expression of numerous pro-inflammatory cytokines.

Experiments were then conducted in hPMCs to investigate the cytotoxicity of PEP-1 *in-vitro* and establish the optimum concentration of PEP-1 to bind and inhibit HA (Figure 5.10). The cytotoxicity of PEP-1 on hPMCs was analysed using the alamarBlue™ assay (Figure 5.10A) The

measurement of fluorescence intensity was representative of the cell number and viability. PEP-1 was dissolved in DMSO, at a final concentration of 0.1% v/v in the culture medium. Thus, the effect of 0.1% DMSO alone on cells was also determined as a control. Incubation of hPMCs with increasing concentrations of PEP-1 (25 μg/ml to 500 μg/ml) had no effect on fluorescence irrespective of TGF-β1 administration. An ELISA-like assay was then performed to assess HA levels in the supernatant of hPMCs incubated with increasing concentrations of PEP-1 in the presence or absence of TGF-β1 (Figure 5.10B). A dose of 250 μg/ml attenuated HA levels in the supernatant, which did not then increase with TGF-β1 treatment. Therefore, a dose of 250 μg/ml PEP-1 was used to investigate the effects of HA blockade on HA-associated gene expression in hPMCs in response to TGF-β1-driven MMT (Figure 5.11). In this experiment, the effect of PEP-1 was determined by incubating confluent monolayers of hPMCs with TGF-β1 in the continual presence of PEP-1 for 16 hours. Expression of HAS enzymes (HAS1, HAS2 and HAS3), Hyaluronidase enzymes (Hyal1 and Hyal2) and total CD44 (CD44p) was assessed by RT-qPCR. Following TGF-β1 treatment, hPMCs incubated with PEP-1 did not exhibit differences in HAS1 expression compared to control and scramble cells (Figure 5.11A). A significant attenuation of HAS2 expression was seen with PEP-1 compared to control and scramble cells, as TGF-β1 treatment did not significantly upregulate HAS2 expression at 16 hours (Figure 5.11B). PEP-1 also induced a significant downregulation of HAS3 expression after 16 hours, which was not seen in control and scramble hPMCs following TGF-β1 treatment (Figure 5.11C). No change was seen in the expression patterns of HYAL1, HYAL2 and CD44 in response to TGF-β1 with addition of PEP-1 (Figures 5.11D-F).

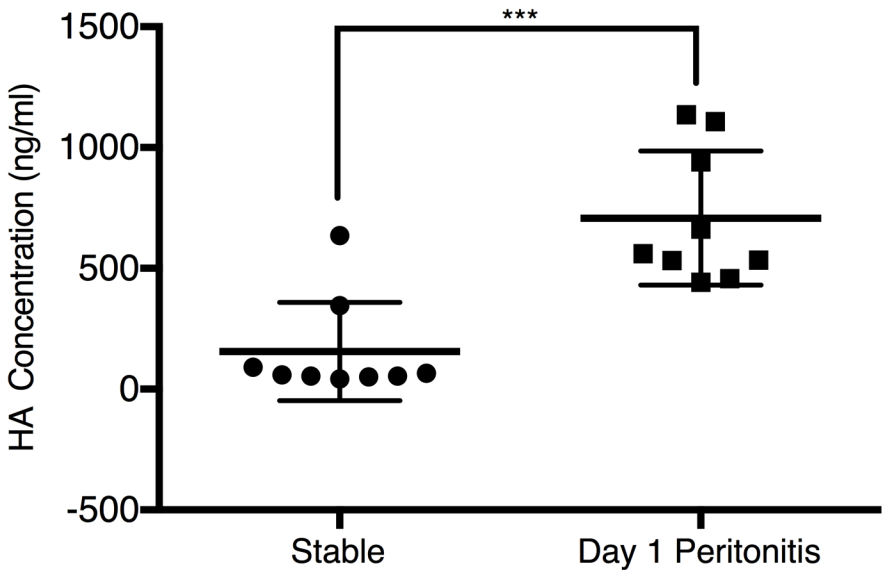

Figure 5.1 PD peritonitis increases HA generation in the peritoneum. Fresh overnight PDE samples from 9 patients day 1 after developing acute bacterial peritonitis were compared to unrelated PDE samples from 9 patients with stable PD (matched for Age, Gender, Length of time on PD and number of previous episodes of PD peritonitis). Aliquots were thawed overnight on ice and then centrifuged at 1600rpm for 10 minutes at room temperature. Cell free supernatant was the analysed for HA concentration by HA ELISA using optimised sample dilutions. Data was analysed by a paired Student's t-test with $p<0.05$ considered as statistically significant (ns = $p>0.05$, * = $p\leq0.05$, ** = $p\leq0.01$, *** = $p\leq0.001$, **** = $p\leq0.0001$).

Gating Strategy for *In-Vivo* Experiments

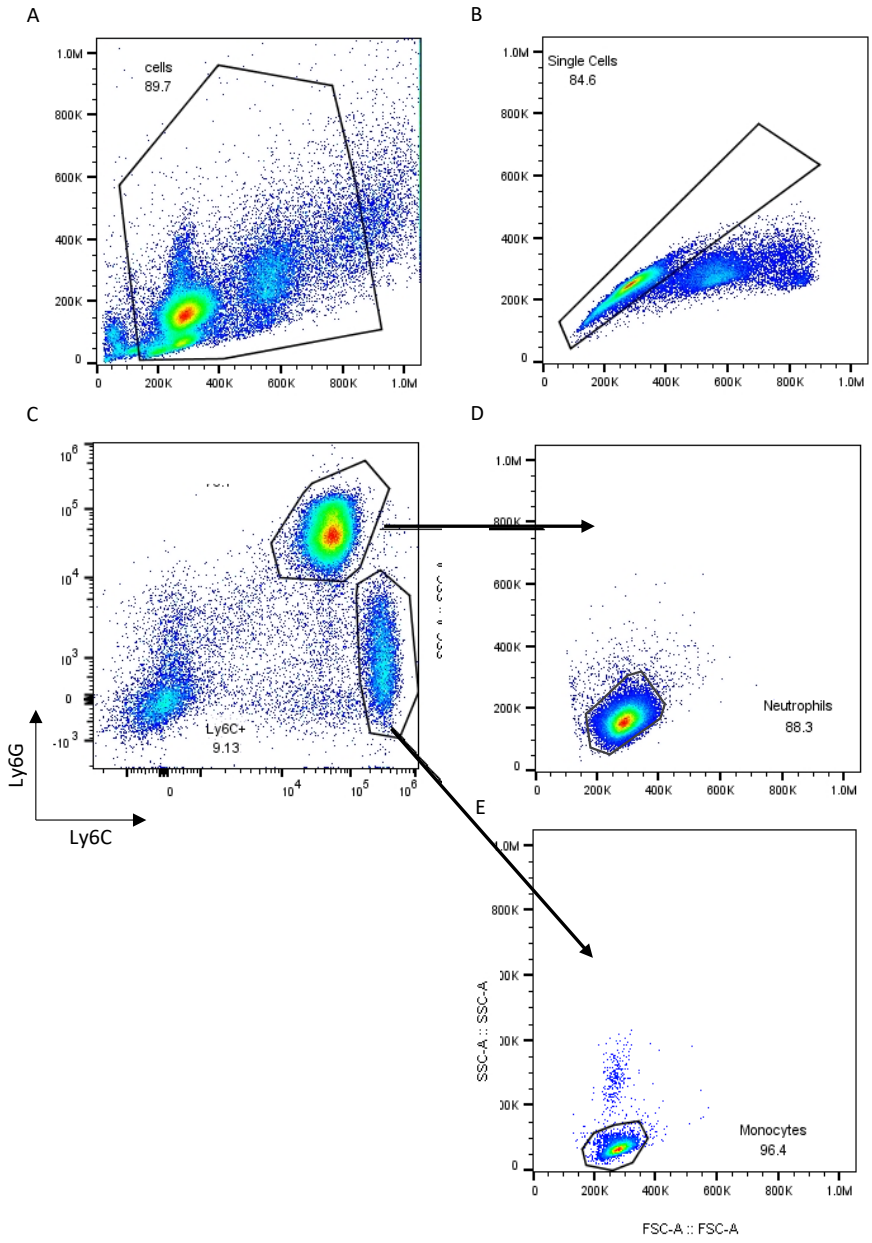

Figure 5.2 Flow cytometry gating strategy to characterise leukocyte populations in mouse peritoneal effluent. Example analysis of mouse peritoneal lavage fluid. Peritoneal lavage fluid was collected from mice with HKSE infection by lavaging peritoneal cavity with 2 ml of PBS. After appropriate preparation, cells were incubated for hour on ice with antibodies using FACS buffer (PBS, 0.5% BSA, 0.05% NaN^3). The antibody combinations for this experiments were Ly6G Alexa Fluor 647 and Ly6C Alexa Fluor 488 (Table 2.5 in methods). Acquisition was performed on Attune (Thermofisher) or BD FACSCanto II (BD Biosciences) flow cytometer. Analysis was performed using FlowJo (v10.4; TreeStar Inc.) software. The gating tree was set as follows; **A –** FSC-A/SSC-A (represents the distribution of cells in the light scatter based on size and intracellular composition, respectively) to **B –** FSC-A/FSC-H (excludes events that could represent more than 1 cell) to **C –** Ly6G/Ly6C subsets to **D/E –** FSC-A/SSC-A (Further gating of Ly6G/Ly6C subsets based on size and intracellular compositions)**.**

Effect of HA Blockade on Leukocyte Recruitment During Peritoneal Infection

A

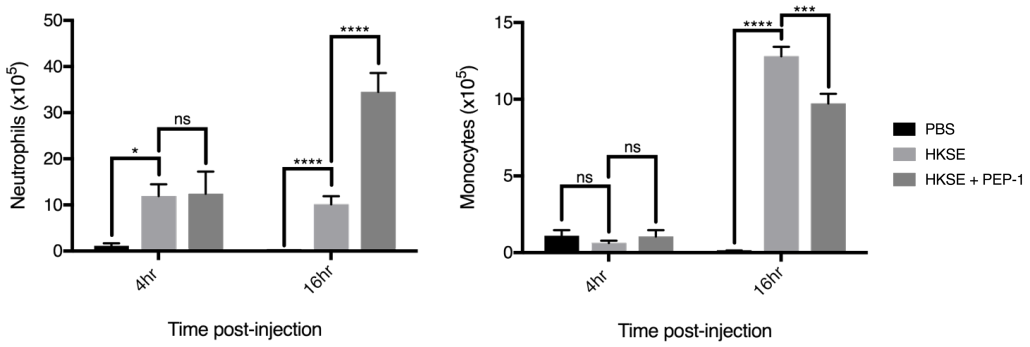

B

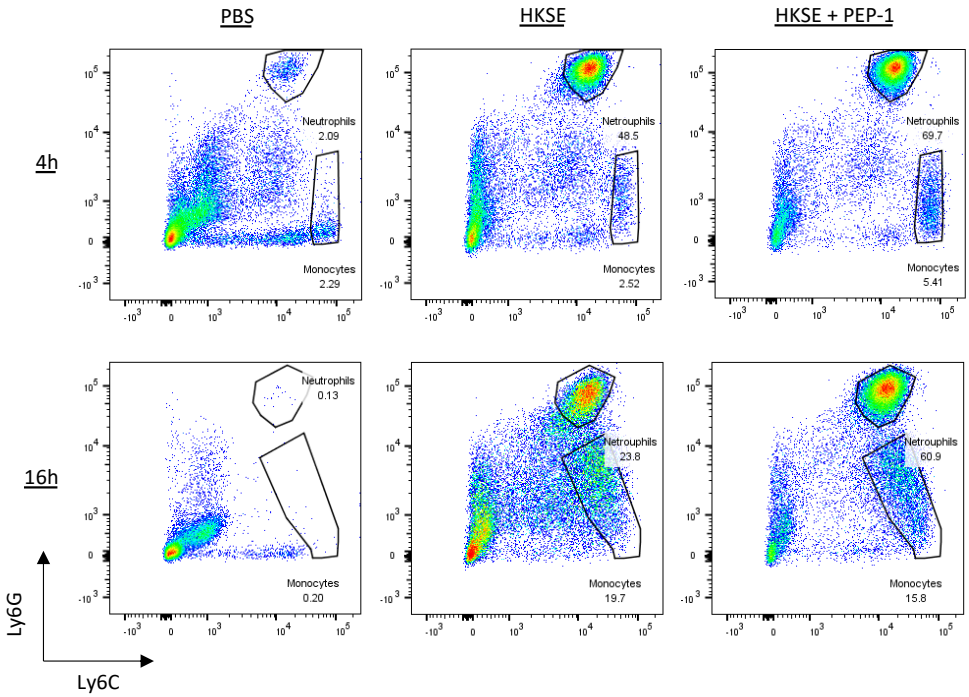

Figure 5.3 Binding of PEP-1 to HA leads to different leukocyte recruitment patterns following *S. epi* infection. Graphs showing absolute numbers of neutrophils ($Ly6C^+Ly6G^+$) and monocytes ($Ly6C^+Ly6G^{Low}$) from mice inoculated with PBS, HKSE alone or HKSE + PEP-1 **(A)**. Mice were innoculated with HKSE (5 x 10^8 cfu/mouse) in the presence/abscence of PEP-1 (500 µg/mouse) and sacrificed at the indicated time points. Control mice were inoculated with equivocal volume sterile PBS. The peritoneal cavity was lavaged and leukocyte populations were determined by $Ly6C^+Ly6G^+$, $Ly6C^+Ly6G^{Low}$ staining patterns. Representative flow cytometric analysis showing the percentages of $Ly6C^+$ or $Ly6G^+$ peritoneal cells **(B)**. Data represents the mean ± SEM and are derived from one experiment with 7- to 8-week old C57BL/6 mice (n=5 per group and time point). Data was analysed by two-way ANOVA followed by Tukeys post hoc analysis with $p<0.05$ considered as statistically significant (ns = $p>0.05$, * = $p\leq0.05$, ** = $p\leq0.01$, *** = $p\leq0.001$, **** = $p\leq0.0001$).

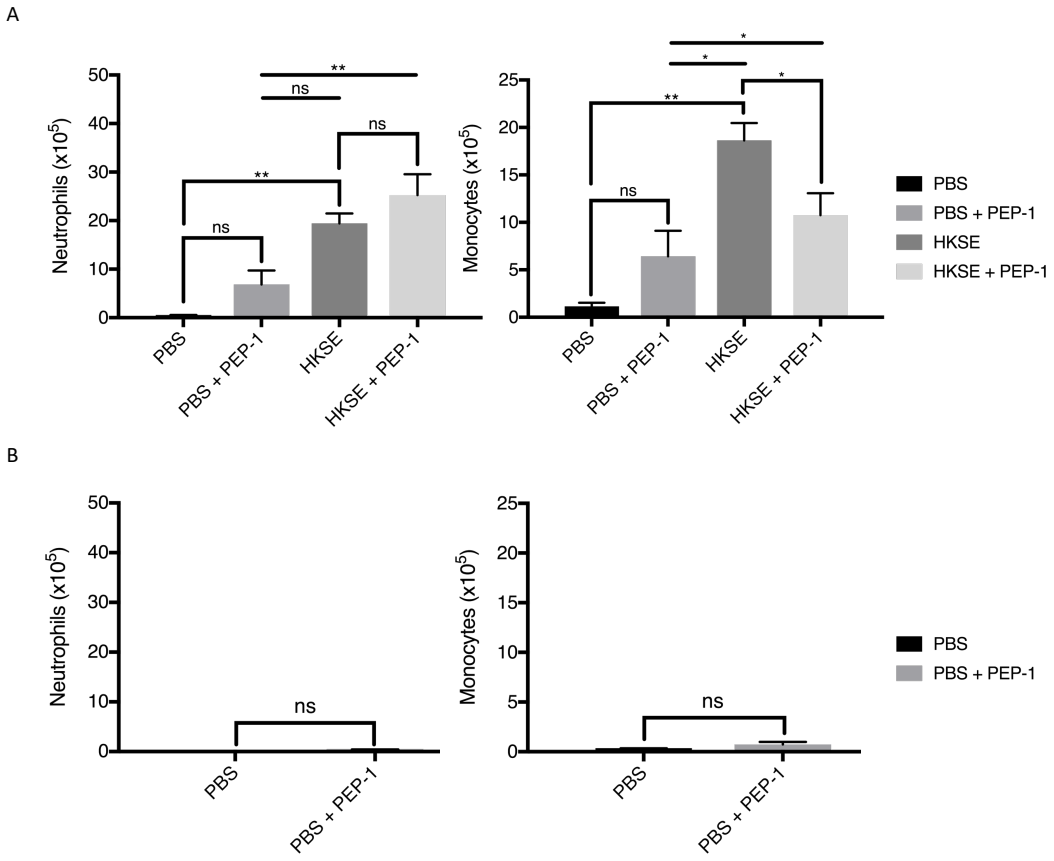

Figure 5.4 Optimisation of PEP-1 innoculation leads to reduced leukocyte response. (**A)** Graphs showing absolute numbers of neutrophils ($Ly6C^{+}Ly6G^{+}$) and monocytes ($Ly6C^{+}Ly6G^{Low}$) from mice inoculated with PBS, PBS + PEP-1, HKSE or HKSE + PEP-1 for 16 hours. Mice were innoculated with HKSE (5 x 10^{8} cfu/mouse) in the presence/abscence of PEP-1 (500 µg/mouse) and sacrificed after 16 hours. Control mice were inoculated with equivocal volume sterile PBS or PBS + PEP-1. The peritoneal cavity was lavaged and leukocyte populations were determined by $Ly6C^{+}Ly6G^{+}$, $Ly6C^{+}Ly6G^{Low}$ staining patterns. **(B)** Graphs showing absolute numbers of neutrophils ($Ly6C^{+}Ly6G^{+}$) and monocytes ($Ly6C^{+}Ly6G^{Low}$) from mice inoculated with PBS alone or PBS + PEP-1 for 16 hours, following optimisation of PEP-1 preparation and inoculation. Data represents the mean ± SEM and are derived from two separate experiments with 7- to 8-week old C57BL/6 mice (n=3 per group). Data was analysed by one-way ANOVA followed by Tukeys post hoc analysis with $p<0.05$ considered as statistically significant (ns = $p>0.05$, * = $p\leq0.05$, ** = $p\leq0.01$, *** = $p\leq0.001$, **** = $p\leq0.0001$).

Full Effect of HA Blockade on Leukocyte Recruitment During Peritoneal Infection

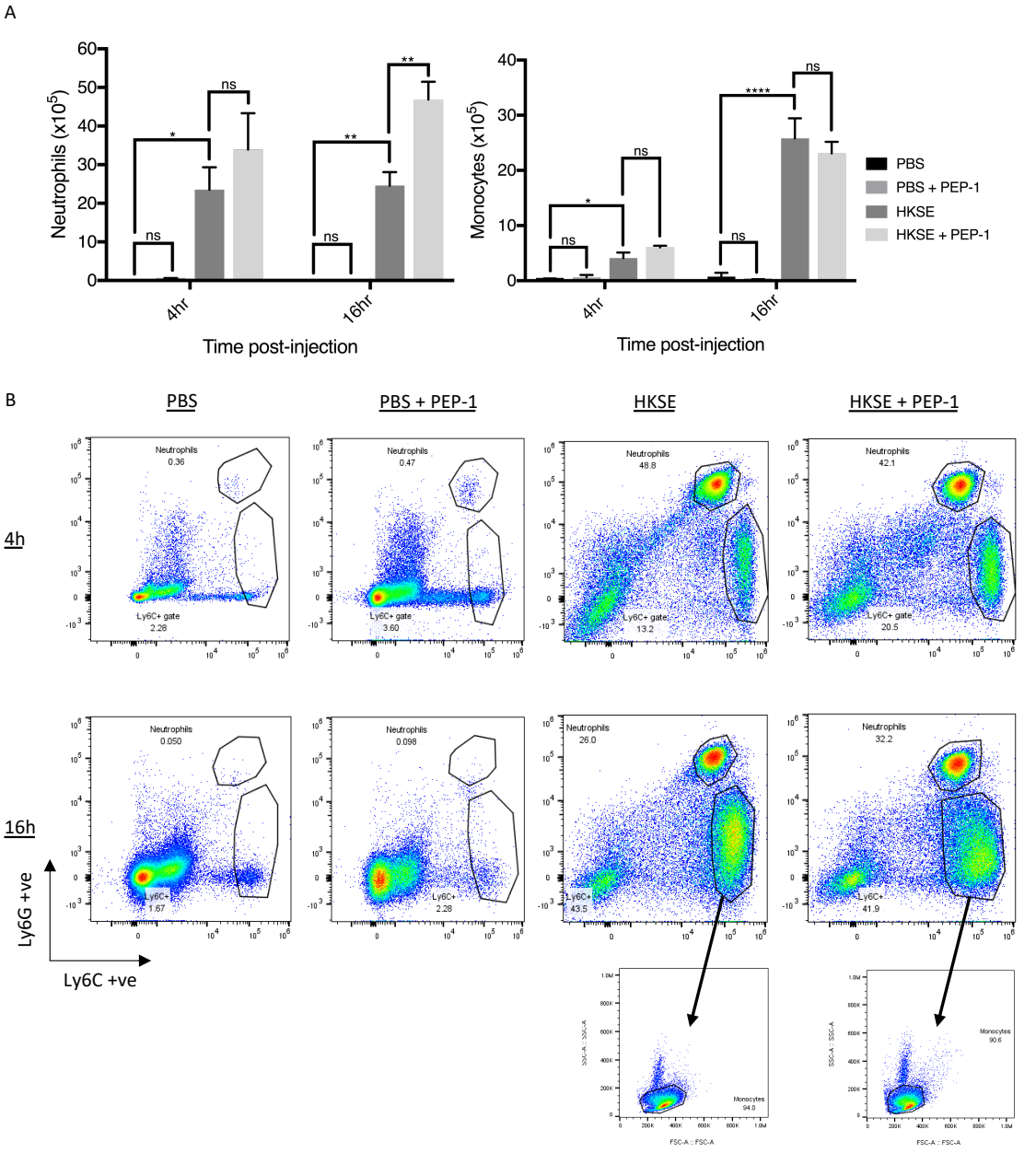

Figure 5.5 Binding of PEP-1 to HA leads to reproducible increased neutrophil recruitment following *S. epi* infection. Graphs showing absolute numbers of neutrophils ($Ly6C^+Ly6G^+$) and monocytes ($Ly6C^+Ly6G^{Low}$) from mice inoculated with PBS, HKSE alone or HKSE + PEP-1 **(A)**. Mice were innoculated with HKSE (5 x 10^8 cfu/mouse) in the presence/abscence of PEP-1 (500 µg/mouse) and sacrificed at the indicated time points. Control mice were inoculated with equivocal volume sterile PBS. The peritoneal cavity was lavaged and leukocyte populations were determined by $Ly6C^+Ly6G^+$, $Ly6C^+Ly6G^{Low}$ staining patterns. Representative flow cytometric analysis showing the percentages of $Ly6C^+$ or $Ly6G^+$ peritoneal cells **(B)**. Data represents the mean ± SEM derived from one experiment with 28 x 7-8-week old C57BL/6 mice (n=2 per control group and n=5 per treatment group). Data was analysed by two-way ANOVA followed by Tukeys post hoc analysis with $p<0.05$ considered as statistically significant (ns = $p>0.05$, * = $p\leq0.05$, ** = $p\leq0.01$, *** = $p\leq0.001$, **** = $p\leq0.0001$).

Effect of HA Blockade on Cytokine Profile 4 Hours after Peritoneal Infection

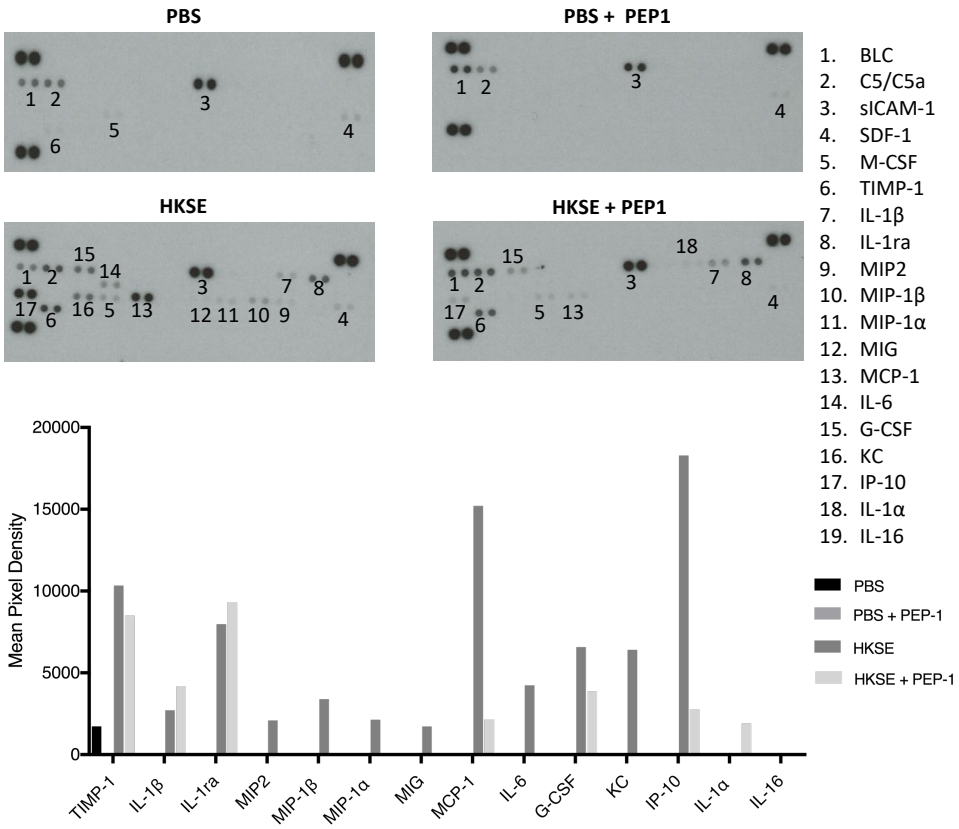

Figure 5.6 Binding of PEP-1 to HA alters cytokine production following *S.epi* infection. Cytokine profiles of peritoneal lavages from mice innoculated with PBS, PBS + PEP-1, HKSE or HKSE + PEP-1 after 4 hours and graphs showing mean pixel intensity of each cytokine. Mice were inoculated with HKSE (5 x 10^8 cfu/mouse) in the presence/absence of PEP-1 (500 µg/mouse), prepared and inoculated using the optimised protocol and sacrificed at 4 hours. Control mice were inoculated with equivocal volume sterile PBS or PBS + PEP-1. The peritoneal cavity was lavaged and cytokine profile determined by proteome profiler array. Graphs determined by pixel intensity analysis using ImageJ software. Data derived from one experiment with 7-8-week old C57BL/6 mice (n=1 per group).

Effect of HA Blockade on Cytokine Profile 16 Hours After Peritoneal Infection

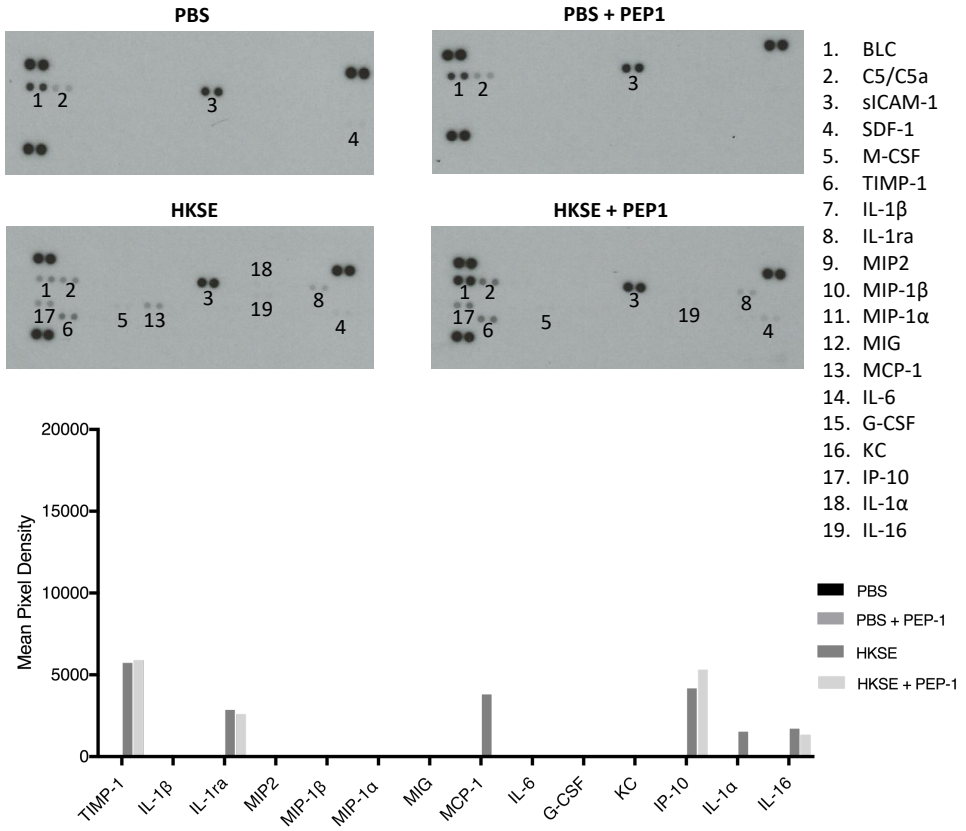

Figure 5.7 Binding of PEP-1 to HA alters cytokine production following *S.epi* infection. Cytokine profiles of peritoneal lavages from mice inoculated with PBS, PBS + PEP-1, HKSE or HKSE + PEP-1 after 16 hours and graphs showing mean pixel intensity of each cytokine. Mice were inoculated with HKSE (5 x 10^8 cfu/mouse) in the presence/absence of PEP-1 (500 µg/mouse), prepared and inoculated using the optimised protocol and sacrificed at 16 hours. Control mice were inoculated with equivocal volume sterile PBS or PBS + PEP-1. The peritoneal cavity was lavaged and cytokine profile determined by proteome profiler array. Graphs determined by pixel intensity analysis using ImageJ software. Data derived from one experiment with 7-8-week old C57BL/6 mice (n=1 per group).

Effect of HA Blockade on HA Generation During Peritoneal Infection

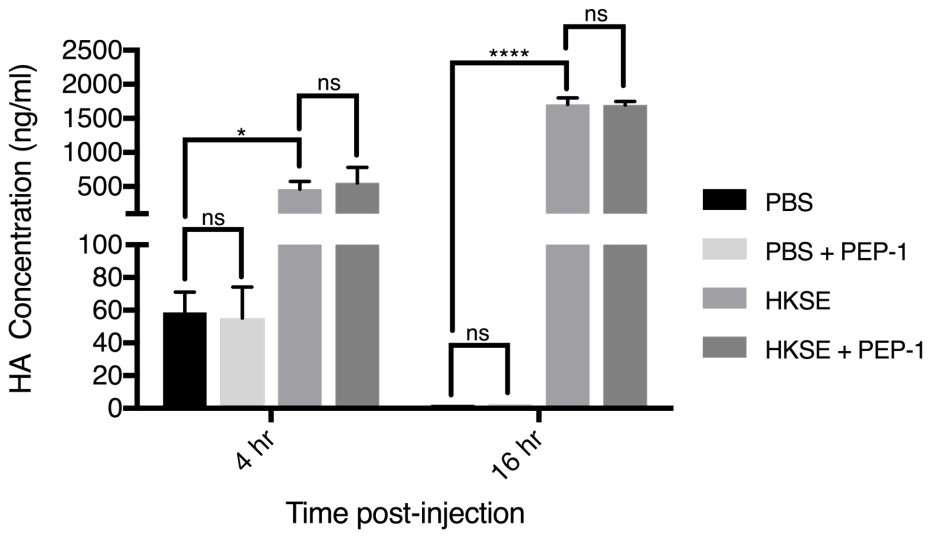

Figure 5.8 Binding of PEP-1 to HA doesn't affect total HA concentration following *S.epi* infection. Quantification of HA in cell-free peritoneal lavages from mice inoculated with PBS, PBS + PEP-1, HKSE or HKSE + PEP-1. Mice were inoculated with HKSE (5 x 10^8 cfu/mouse) in the presence/absence of PEP-1 (500 µg/mouse) and sacrificed at the indicated time points. Control mice were inoculated with equivocal volume sterile PBS. The peritoneal cavity was lavaged and HA concentration determined by HA ELISA. Data represents the mean ± SEM derived from one experiment with 28 x 7-8-week old C57BL/6 mice (n=2 per control group and n=5 per treatment group). Data was analysed by two-way ANOVA followed by Tukeys post hoc analysis with $p<0.05$ considered as statistically significant (ns = $p>0.05$, * = $p\leq0.05$, ** = $p\leq0.01$, *** = $p\leq0.001$, **** = $p\leq0.0001$).

Effect of HA Blockade on HA-Associated Gene Expression During Peritoneal Infection

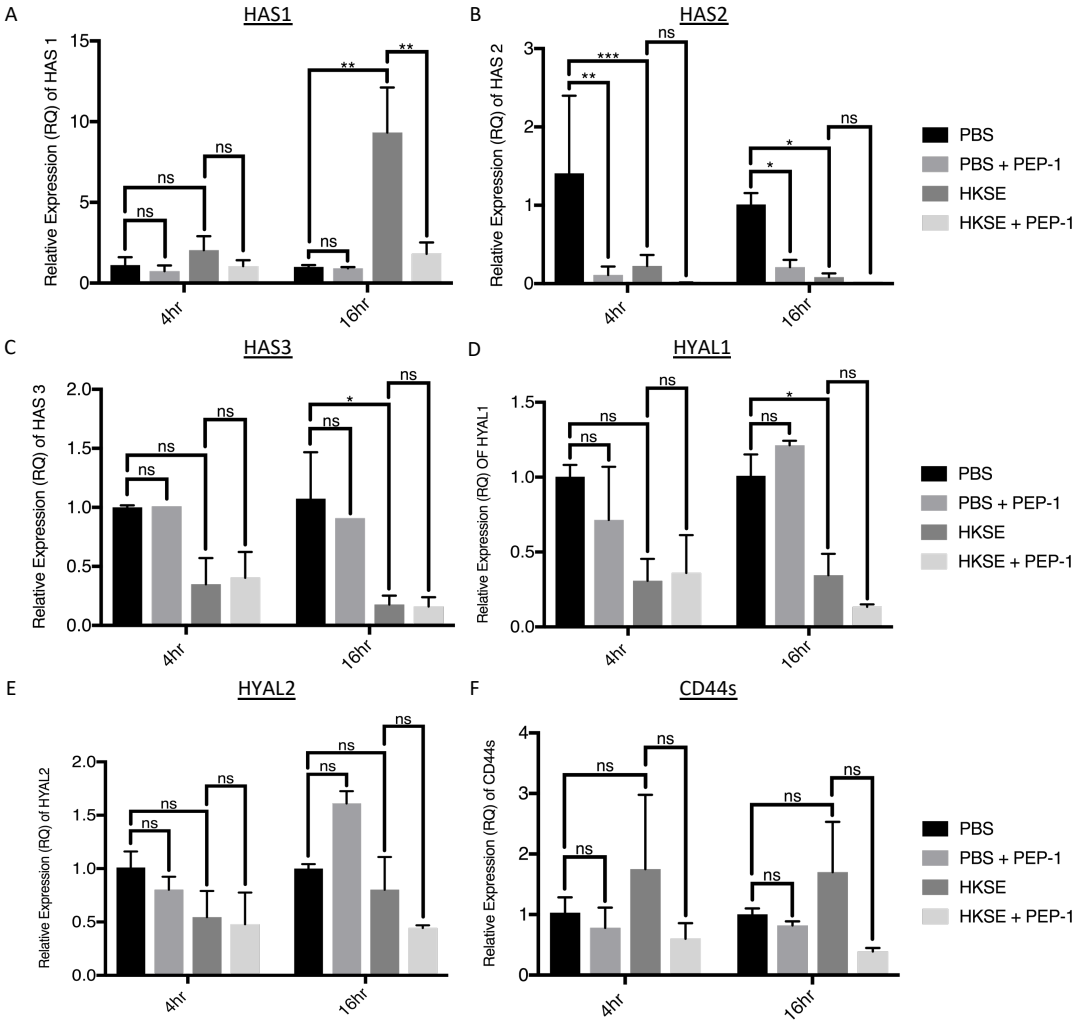

Figure 5.9 Binding of PEP-1 to HA attenuates HAS1 expression following *S.epi* infection. mRNA expression of HA synthase enzymes; HAS1, HAS2 and HAS3 **(A-C)** Hyaluronidase enzymes; HYAL1 and HYAL2 **(D-E)** and HA receptor protein CD44s (standard isoform)**(F)** from peritoneal membranes of mice inoculated with PBS, PBS + PEP-1, HKSE or HKSE + PEP-1. Mice were inoculated with HKSE (5 x 10^8 cfu/mouse) in the presence/absence of PEP-1 (500 µg/mouse), prepared and inoculated using the optimised protocol and sacrificed at the indicated time points. Control mice were inoculated with equivocal volume sterile PBS or PBS + PEP-1. The peritoneal membranes were removed and mRNA was extracted as described in 2.13. mRNA expression of all markers analysed by RT-qPCR and normalised to YWHAZ mRNA expression. Data represents the mean ± SEM derived from one experiment with 28 x 7-8-week old C57BL/6 mice (n=2 per control group and n=5 per treatment group). Data was analysed by two-way ANOVA followed by Tukeys post hoc analysis with $p<0.05$ considered as statistically significant (ns = $p>0.05$, * = $p\leq0.05$, ** = $p\leq0.01$, *** = $p\leq0.001$, **** = $p\leq0.0001$).

Analysis of PEP-1 Cytotoxicity in Mesothelial Cells

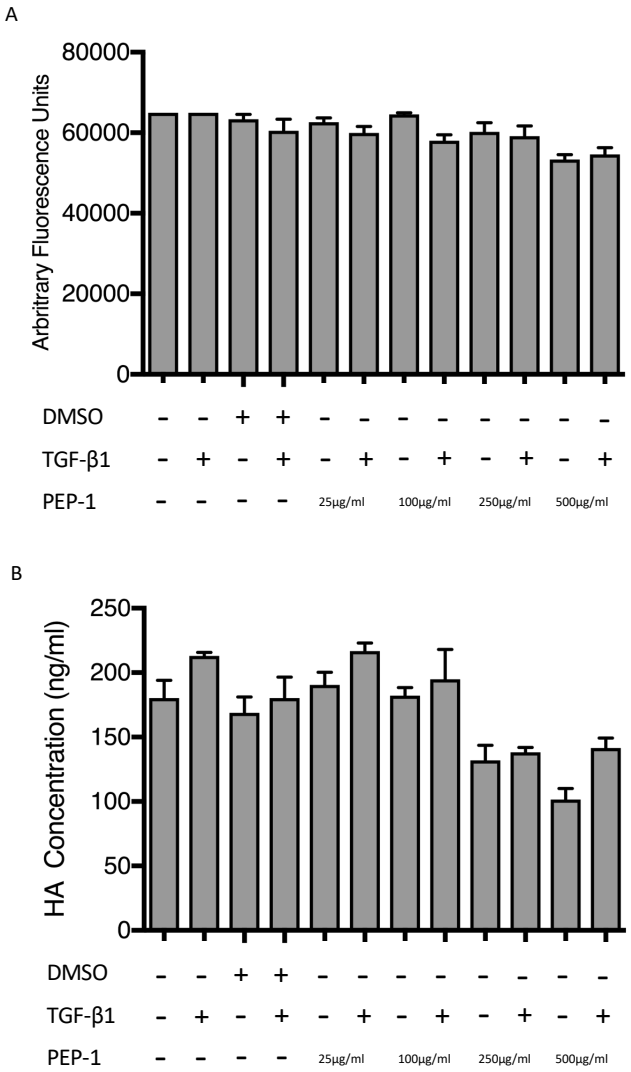

Figure 5.10 Analysis of PEP-1 cytotoxicity in human peritoneal mesothelial cells. (A) Confluent monolayers of omentum derived mesothelial cells treated with 0.1% DMSO, TGF-β1 10 ng/ml, 25, 100, 250 or 500 µg/ml for 16 hours. Cell viability was performed as described in section 2.7. **(B)** Quantification of HA by ELISA in confluent monolayers of omentum derived mesothelial cells treated with 0.1% DMSO, TGF-β1 10 ng/ml, 25, 100, 250 or 500 µg/ml for 16 hours. Data represented as mean ± SEM derived from triplicate single donor experiments.

Effect of PEP-1-Mediated HA Blockade on HA-Associated Gene Expression During TGF-β1-Driven MMT

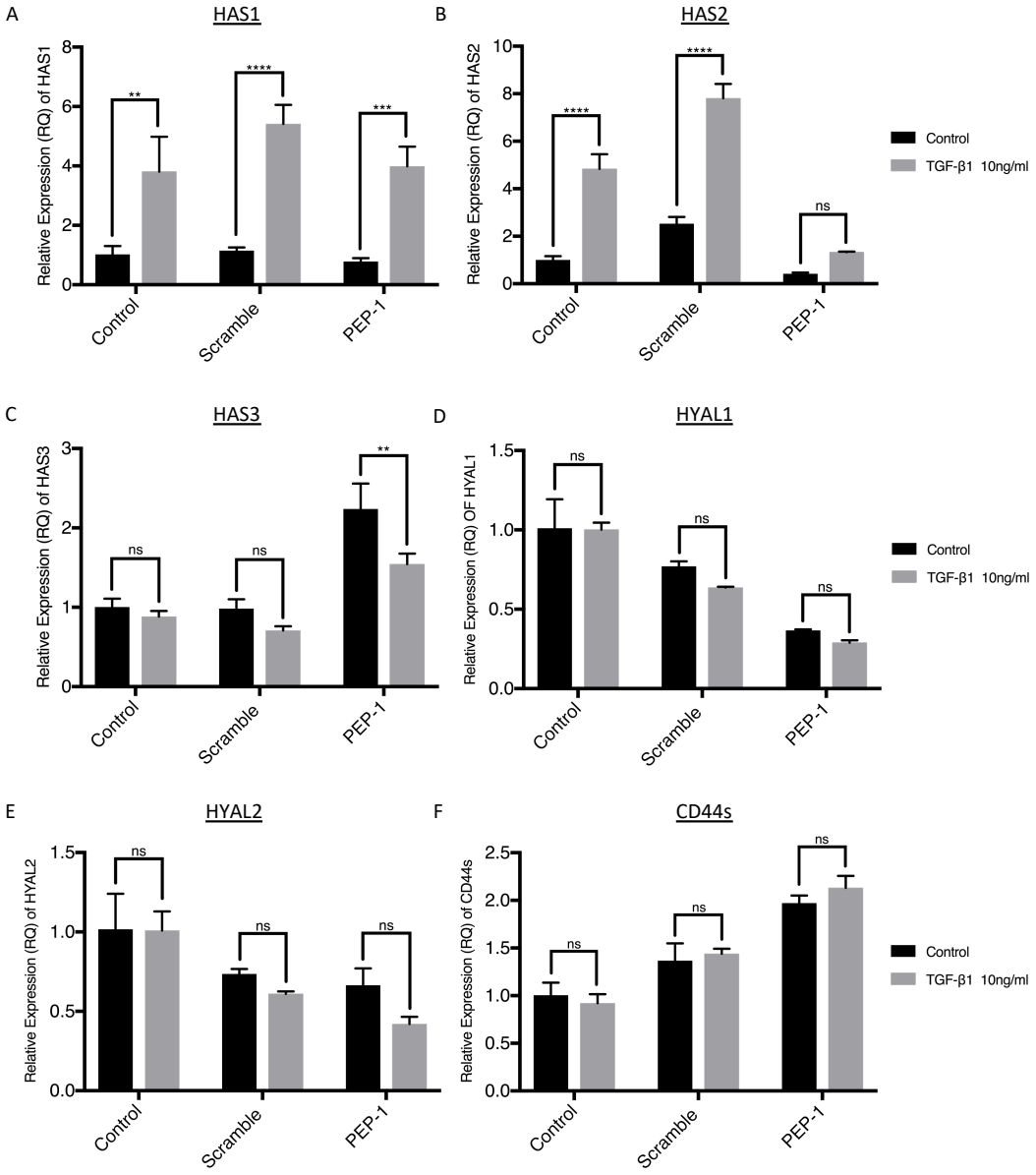

Figure 5.11 Binding of PEP-1 to HA attenuates HAS2 expression in human peritoneal mesothelial cells stimulated with TGF-β1. Confluent monolayers of omentum derived mesothelial cells treated with 250 µg/ml PEP-1 and 10ng/ml TGF-β1 for 16 hours. Expression of HA synthase enzymes: HAS1, HAS2, HAS3 **(A-C)** Hyaluronidase enzymes: HYAL1 and HYAL 2 (**D-E)** and HA receptor protein: CD44s (standard isoform) **(F).** mRNA expression analysed by RT-qPCR and normalised to GAPDH mRNA expression. Data represents the mean ± S.E.M of 2 triplicate experiments from single donor. Data was analysed by two-way ANOVA followed by Tukeys post hoc analysis with $p<0.05$ considered as statistically significant (ns = $p>0.05$, * = $p\leq0.05$, ** = $p\leq0.01$, *** = $p\leq0.001$, **** = $p\leq0.0001$).

5.3 Discussion

Responses to peritoneal injury and infection share many features with other models of wound healing, as a well-coordinated host response is required to limit the extent of tissue damage [173]. Mesothelial cells are an integral part of the innate response in the peritoneum, and along with resident macrophages and fibroblasts, work together to recruit other inflammatory cells including mononuclear phagocytes, lymphocytes and neutrophils during an inflammatory episode [114]. This inflammatory response is characterised by enhanced vascular permeability, an initial influx of neutrophils followed by their clearance and replacement by a more sustained population of mononuclear cells. In this chapter, intraperitoneal administration of HKSE resulted in increased neutrophil levels in the peritoneum, which was associated with increased production of various cytokines and chemokines, namely macrophage inflammatory proteins (MIPs), keratinocyte chemoattractant (KC), IL-6, macrophage chemoattractant protein-1 (MCP-1) and IFN induced protein-10 (IP-10). By 16 hours, the neutrophil population was joined/replaced by a monocyte population, and this was associated with a decrease in cytokine and chemokine levels back to basal levels, indicative of a system attempting to resolve inflammation. The principles of resolution of inflammation include the limitation or cessation of neutrophil infiltration, the counter-regulation of cytokines and chemokines, the induction of neutrophil apoptosis and phagocytosis by transformed or activated macrophages and the return of non-apoptotic cells to the vasculature or lymphatics [440].

A hallmark of tissue injury and repair is the turnover of ECM components, and the increased deposition of HA into the ECM after tissue injury and inflammation is well described [269].

The peritoneum is not different in this respect as numerous studies have indicated that exposure to PD fluid continuously, or episodes of PD peritonitis are associated with significantly increased levels of HA [341, 375]. In this chapter, we re-confirmed that HA levels are detectable in patients on PD and these levels were increased in response to peritoneal infection. We have demonstrated in previous chapters that the HA generated by mesothelial cells, which accounts for most of the local HA generated in the peritoneum, is not associated with MMT and the development or prevention of fibrosis of the peritoneal membrane. Thus, we proposed that HA generated by mesothelial cells was involved in the mediation and/or modulation of inflammation in the peritoneum.

In this chapter, induction of inflammation by HKSE led to early and sustained increases in HA levels in the peritoneum of mice. One of the most important factors that governs HA function during inflammation is the size of the HA polymer, as HA with different molecular weights can bind to different receptors and induce different signaling pathways. Evidence that HA can have opposing actions depending on its size is seen in normal tissues; when HA exists as a HMW polymer it has anti-inflammatory, anti-angiogenic and immunosuppressive functions; in inflammatory settings, HA is significantly more polydisperse and HA polymers exist with overlapping lengths and functions [269]. During inflammation, LMW-HA has been shown to be pro-inflammatory, pro-angiogenic and has been shown to augment immune responses [269]. Short HA fragments, that is LMW-HA with an average molecular mass of <500 kDa, are particularly pro-inflammatory and are produced as a result of increased hyaluronidase activity and/or by reactive oxygen species (ROS), followed by increased HAS activity. After injury or inflammation, HA fragments can induce expression of pro-inflammatory genes, such as MIP,

KC, MCP-1 and IP-10 as well as various cytokines including IL-1β, IL-6, IL-8, IL-10 and TNF-α [281, 286, 441-452]. Whilst we did not specifically look at the molecular weight of HA in response to HKSE, levels of HA were significantly increased, presumably including an increased concentration of LMW-HA and HA fragments that induced the expression of the various pro-inflammatory cytokines. The expression levels of HAS1 were also significantly increased 16 hours after HKSE infection, associated with a significant decrease in HAS2 and HAS3 expression. Similar findings were also seen when assessing the effect of PEP-1 on hPMCs, with increased HAS1 expression and decreased HAS2 and HAS3 expression.

This chapter explored the role of HA in regulating peritoneal inflammation after *S. epidermidis* infection by using a HA binding peptide; PEP-1 to block the effects of HA. PEP-1 is a 12mer peptide sequence (GAHWQFNALTVR) with two areas for HA binding (W, Q, F and L, T, V) that was first identified by Mummert *et al* using phage display techniques [298]. Whilst the exact mechanism of PEP-1 binding to HA is still unknown, the two HA binding areas of PEP-1 are hydrophobic in nature and don't resemble the known HA-binding sequences of various hyaladherins, described in section 1.3.4. Thus, it has been inferred that PEP-1 may be binding to HA along "hydrophobic" patches [453]. Despite this unknown mechanism, numerous *in-vitro* and *in-vivo* studies have demonstrated that PEP-1 is highly effective at blocking HA function [272, 278, 279, 298, 437-439, 453, 454].

In this chapter, intraperitoneal administration of HKSE and PEP-1 had no effect on overall HA generation when compared to HKSE alone but led to a significant attenuation of HAS1

expression at 16 hours. This finding supports the notion that HAS1 is the main contributor to the generation of HA in the mouse peritoneum in response to inflammation and supports the previous findings in chapter 3 showing that HA synthesized by mesothelial cells is predominantly through HAS1 expression. Furthermore, these experiments demonstrate that HA is generated exclusively by HAS1 in response to peritoneal infection or inflammation as HAS2 and HAS3 were significantly downregulated early during an inflammatory response and we didn't see a compensatory increase with PEP-1 attenuation of HAS1. As previously mentioned, HA can have distinct and sometimes opposing functions depending on its manner of synthesis, size location and interaction with receptors. A recent report by Chan *et al* [390] found that *HAS1*$^{-/-}$ mice developed chronic joint inflammation following acute injury related to dysregulated inflammatory and apoptotic pathways and dysfunctional ECM remodeling. Siiskonen *et al* [455] demonstrated that stimulation of HAS1-overexpressing human breast cancer cells with IL-1β, TNF-α or TGF-β rapidly developed HA pericellular coats *in-vitro.* It is therefore possible that IL-1β, along with the other cytokines, is inducing HAS1 transcription preferentially in the mouse peritoneum in response to HKSE infection to generate HA. It is important to consider that these cytokines could be abrogating HAS2 transcription and HAS1 is increased in a compensatory mechanism. However, we demonstrated that HAS2 expression was already downregulated at 4 hours and it is therefore unlikely that increased cytokine production in the peritoneum could influence HAS2 transcription within this time.

Blockade of HA with PEP-1 also led to a significant increase in peritoneal neutrophils after 16 hours, above that of HKSE alone, without the corresponding increase in monocyte that one would expect. This was an interesting and unexpected finding and whilst it is unclear why

HKSE + PEP-1 resulted in increased levels of neutrophils in these experiments, there are several possible explanations. One explanation could be related to resident macrophages that initiate inflammation and activate mesothelial cells in response to infection or tissue injury. Resident macrophages in the peritoneum can activate mesothelial cells with inflammatory cytokines such as IL-1β, TNF-α and IFN-γ. IL-1β, IL-1α and IL-ra either remained unchanged or were increased in the presence of PEP-1, thus, it is possible that macrophage governed neutrophil influx was unimpeded by PEP-1. Furthermore, IL-1β has also been demonstrated to delay constitutive neutrophil apoptosis, which could explain their delayed clearance [456-460]. It is also unclear why a corresponding increase in monocyte populations were not seen, and in some earlier experiments, levels were actually attenuated in response to PEP-1. These findings could be related to the effect of PEP-1 on mesothelial cells. We and others have shown that mesothelial cells generate most of the HA in the peritoneum. It is therefore not unreasonable to assume that PEP-1 is predominantly having an effect on mesothelial cells in these experiments. There was a decrease in the production of important cytokines and chemokines known to drive leukocyte recruitment with PEP-1 administration, namely MCP-1, IL-6, KC, IL-10 and the various MIPs. As previously discussed, activation of mesothelial cells, either directly by tissue injury or through macrophage-induced cytokine stimulation, induces the production of various cytokines such as MCP-1, RANTES, IL-8 and various adhesion molecules [35, 52, 56, 434, 435]. The net effect of these cytokines is to further recruit leukocytes and facilitate leukocyte adherence and migration across the mesothelium [56]. It is therefore possible that PEP-1 binding to HA generated by mesothelial cells prevents their activation and subsequent cytokine production, thereby attenuating further leukocyte recruitment. This could also explain, the increased neutrophil levels as the attenuated

monocyte recruitment could affect their ability to phagocytose and clear the neutrophils that have already accumulated.

Another possible explanation could be that PEP-1 binding to HA was not instantaneous, thus HA fragments generated as a result of HKSE were able to initiate an inflammatory response. It is unlikely that PEP-1 itself was having an additional inflammatory effect given that i.p administration of PEP-1 and PBS had no effect on neutrophil and monocyte levels. It is also possible that the dose of PEP-1 was too low and did not saturate the large quantities of HA generated in response to infection. However, the concentrations of PEP-1 used in these experiments were similar to others [272, 278, 279, 298, 437].

In summary the data from this chapter shows that HA modulates immune cells and inflammatory cytokines in the peritoneum. Blocking HA in the peritoneum with PEP1 during infection leads to a delayed resolution of inflammation, characterized by increased and persistent neutrophil infiltration, dysregulated monocyte recruitment and decreased cytokine and chemokine release. HA can form pericellular coats around cells, and can interact with cell-surface receptors to prevent immune cell recognition and block phagocytosis by macrophages [269]. Following injury to the peritoneum, HA generated by mesothelial cells is mediated by HAS1 expression providing cellular cues to regulate inflammation and repair of the peritoneal membrane.

Chapter 6

General Discussion

PD causes characteristic changes in the peritoneal membrane over time. As a result of the constant exposure to bioincompatible PD solutions and recurrent episodes of peritonitis, the peritoneal membrane undergoes progressive fibrosis, angiogenesis and hyalinizing vasculopathy [42, 43, 102]. These changes eventually culminate in increased small-solute transport and loss of ultrafiltration leading to failure of PD as a means of renal replacement therapy [29, 42, 101]. It has been clear for some time that the pro-fibrotic cytokine TGF-β1 is a master molecule in the development of peritoneal membrane fibrosis, and its overexpression has been correlated with worse PD outcomes [100, 114, 379, 380].

Mesothelial cells arguably undergo the greatest structural and functional alterations during PD and TGF-β1 -driven MMT is a key mechanism through which TGF-β1 promotes peritoneal membrane fibrosis. A reliable and reproducible method to study HPMCs *in vitro* has been utilised by our group for 20 years to study the effects of PD, which has been adopted by other researchers in this field. Despite its widespread use, it is important to acknowledge some inconsistencies and shortcomings from this work relating to the use of primary cultures of mesothelial cells that could be improved upon in future studies. Primary cultures of mesothelial cells are isolated directly from tissues of healthy volunteers undergoing a donor nephrectomy. These tissues are then digested using a well-established protocol used in our laboratory and elsewhere to harvest mesothelial cells. However, cross-contamination with other cell types is possible. In this instance, introducing a purification step by determining the expression of standard mesothelial markers: ICAM-1, Cytokeratin and E-Cadherin and using flow cytometry to discriminate levels of fibroblast contamination would improve the quality and purity of peritoneal mesothelial cells to reduce inter-experimental variations in results.

This process could be embedded in the existing protocols within our laboratory and elsewhere. Primary cultures also have a finite lifespan and are studied in the absence of their local environment that often includes interactions with other cell types, which may be critical to the hypothesis being tested and may explain further inconsistencies in results. The use of TGF-β1 and BMP-7 stimulation to induce MMT also led to further inconsistencies in the data presented, leading to differences in the expression levels of MMT markers and HA-matrix proteins from different omentum donors. Again, these could be improved by the addition of additional purification steps when harvesting mesothelial cells for culture.

Mesothelial cells have been demonstrated to generate HA in response to TGF-β1 in numerous animal and *in vitro* studies but the role of this HA generated in driving peritoneal membrane fibrosis through MMT has never been studied. HA is known to play an important role in regulating other TGF-β1-driven cellular processes [125, 126, 182-184, 190, 236, 237, 253, 332, 348, 362, 363]. It is enriched in many types of human cancers and there is considerable experimental evidence implicating HA as a mediator of TGF-β1-driven type III EMT and thereby facilitating tumour progression [166, 364-372]. Moreover, TGF-β1 found within cancer exosomes can cause differentiation of fibroblasts to myofibroblasts associated with an increase in HA pericellular coat generation through upregulated HAS2 expression [166, 373]. HA has also been shown to mediate TGF-β1-driven type II EMT in proximal tubular epithelial cells in kidney fibrosis [333]. Numerous studies on mesothelial cells during PD have indicated that these cells demonstrate alterations in HA generation during PD [341, 343, 346, 374, 375]. HA levels in peritoneal fluid are persistently elevated during PD. HA levels are increased further during episodes of peritoneal infection (PD peritonitis) and with increasing patient

time on PD [335]. The aim of this work was to characterise the HA matrix profile and associated profile of HA-binding proteins in the mesothelium during peritoneal infection, inflammation and fibrosis. Previous studies have shown that PD therapy increases HA synthesis by mesothelial cells, which is associated with increased cell migration, proliferation and phenotypic changes [365]. Yung et al previously demonstrated that mesothelial cells develop a migratory phenotype following disruption of the mesothelial monolayer associated with induction of HA synthesis [55]. The work outlined in this thesis indicates that the majority of HA generated by mesothelial cells following TGF-β1 stimulation is secreted extracellularly. Some of this, forms HA pericellular coats associated with the cell. Largely, however, the HA generated is released into the extracellular space and into the peritoneal effluent.

In solid organ fibrosis in vivo studies in tissues as well as in vitro studies in fibroblasts and epithelial cells indicate that HAS2 is the prominent HAS isoform that is expressed under basal conditions. Furthermore, in these tissues/cells, HAS2 is preferentially induced following disease and/or myofibroblast differentiation. HAS1 expression is generally low-level and only demonstrates slight (if any) induction following injury/stimulation. In contrast to other solid organ fibroses, removal of HA pericellular coats or interference in HA/HAS synthesis does not appear to prevent the ability of mesothelial cells to undergo MMT following TGF-β1 stimulation. Rather the increased HA levels appeared to be a consequence rather than a cause of TGF-β1-driven MMT. The data in this study shows that HAS1 expression in the mesothelium is significantly higher than in other tissues we have studied. Furthermore, HAS1 expression is significantly induced following injury/stimulation with TGF-β1. HAS2 is also expressed in the mesothelium and also demonstrates increased expression following TGF-β1-driven MMT, but

the expression levels are lower compared to other tissues we have studied. The data also demonstrates that TGF-β1-driven MMT is associated with attenuated HAS3 and HYAL1 mRNA expression and cellular re-distribution of CD44. Of note, removal of pericellular HA and overall inhibition of HA synthesis led to significant upregulation of HAS1 expression whilst HAS2 was attenuated. This again indicates that elevated HAS1 levels may be the main driver of mesothelial cell generated HA in the peritoneum. Removal of pericellular HA and general inhibition of HA synthesis led to significant upregulation of HAS1 expression but not HAS2, indicating that HAS1 may be the main contributor to the development and maintenance of HA pericellular coats in mesothelial cells as opposed to HAS2. Future work looking at the role of HAS1 in mesothelial cells, using knockout of HAS1 or GFP-labelling of HAS1 to elucidate its function in mesothelial cells is an interesting prospect. Other additional experiments would also be required to corroborate the findings of this thesis in future. During this thesis, most of the data generated from experiments focussed on mRNA levels to confirm MMT and HA matrix protein levels, with supplementary immunohistochemistry and ELISA to support these findings. However, more detailed qualitative work to assess the protein levels to corroborate these mRNA changes are necessary. Specifically, assessing the effect of HAS/CD44 knockdown or efficacy of 4-MU inhibition by confocal and light microscopy staining for HA/CD44 would be a focus of immediate work to assess their effects on HA biosynthesis. Also, demonstrating that the optimised concentration of 4-MU used for inhibition of HA synthesis actually has a direct effect on HA biosynthesis will be important. Use of HA ELISA assays to assess HA levels following 4-MU inhibition, alongside confocal microscopy staining for HA could address these shortcomings.

In contrast to solid organ fibrosis, the work in this thesis also suggests that HA generated by mesothelial cells is not involved in the prevention of TGF-β1-driven MMT. It is widely recognised that the way in which HA is assembled, its interaction with a wide variety of HA-binding proteins and its manner of organisation within the pericellular matrix, are crucial in determining its subsequent biological actions [138, 218]. Work from our lab and elsewhere have elucidated that TGF-β1-driven HA and BMP-7-driven HA mediate opposing actions on myofibroblast phenotype. Whilst TGF-β1 promotes HAS2-driven HA pericellular coat formation, BMP-7 has been shown to promote internalisation of HA for breakdown thereby preventing TGF-β1-mediated fibroblast-to-myofibroblast differentiation. The findings in this thesis also indicate that BMP-7 stimulation does not lead to HA internalisation nor removal of HA pericellular coat, and again, does not appear to mediate prevention/reversal of myofibroblast differentiation. This is different to previous studies from our group in solid organ fibrosis that demonstrate that BMP-7 driven internalisation of pericellular HA mediates myofibroblast prevention/reversal. In fibroblasts and epithelial cells, HAS1 is poorly expressed and only shows little (if any) induction following TGF-β1 stimulation, whilst HAS2 expression predominates. It is possible that HAS1-derived HA seen in the peritoneum is distinct to HAS2-derived HA that is observed in solid organ fibrosis and propose that it is the difference in expression of HAS isoenzyme expression that could explains why HA does not mediate TGF-β1-driven MMT in the peritoneum.

HAS1 has been shown to be upregulated in cancer cells with malignant properties [178, 461-463] and has been demonstrated to have different substrate requirements, subcellular localisation and HA coat structure to other HAS isoforms [156, 455, 462, 464, 465]. Recent

reports support our hypothesis that HAS1 isoenzyme-specific HA has distinct functions. Recent reports from Chan et al [390] and Siiskonen et al [178] suggest that HAS1 has a crucial role in inflammation, displaying both pro- and anti-inflammatory properties depending on the length of HA generated. HA normally exists as a HMW polymer, and plays an important role in the interplay between cells and other components of the ECM in the maintenance of normal physiological processes. Disruption of ECM homeostasis, for example during inflammation and tumorigenesis, leads to fragmentation of HMW-HA into LMW-HA and HA fragments that mediate pro-inflammatory responses. In a model of collagen-induced arthritis [278, 279, 437], IL-1β stimulation of murine chondrocytes induced a significant increase in HA fragments and LMW-HA that activated HA signalling pathways to promote inflammatory cell recruitment. Initial reports in this field indicated that HAS1 and HAS2 synthesize HMW-HA, whereas HAS3 predominantly produced LMW-HA. Despite their tendencies to synthesize similar molecular weight HA, HAS1 and HAS2 produce distinctly different HA matrices. HAS2 generates large HA pericellular matrices, whereas HAS1 pericellular matrices a smaller and less well defined. This may be relevant in inflammatory contexts, as numerous inflammatory cytokines and glycaemic stress have been shown to induce formation of HAS1-dependent pericellular coats [455].

The final part of this thesis alludes to a potential role for HA generated by mesothelial cells, in regulating the peritoneal immune response following acute bacterial infection. Our in vivo findings in the mouse-model give the same impression as with our in vitro findings in mesothelial cells identifying HAS1 as the HA Synthase isoform that predominates in the peritoneum. Blocking HA in the peritoneum using the PEP-1 antibody appears to change the

pattern of leukocytes and attenuates the inflammatory cytokine response, in particular attenuating MIP2, MIP-1α, MIP-1β, MIG, MCP-1, IL-6, and KC levels. A potential role for HA in the peritoneum could therefore be to contribute to the maintenance of HA glycocalyces/pericellular coats and modulate the acute inflammatory response when challenged by invading pathogens or tissue injury (Figure 6.1).

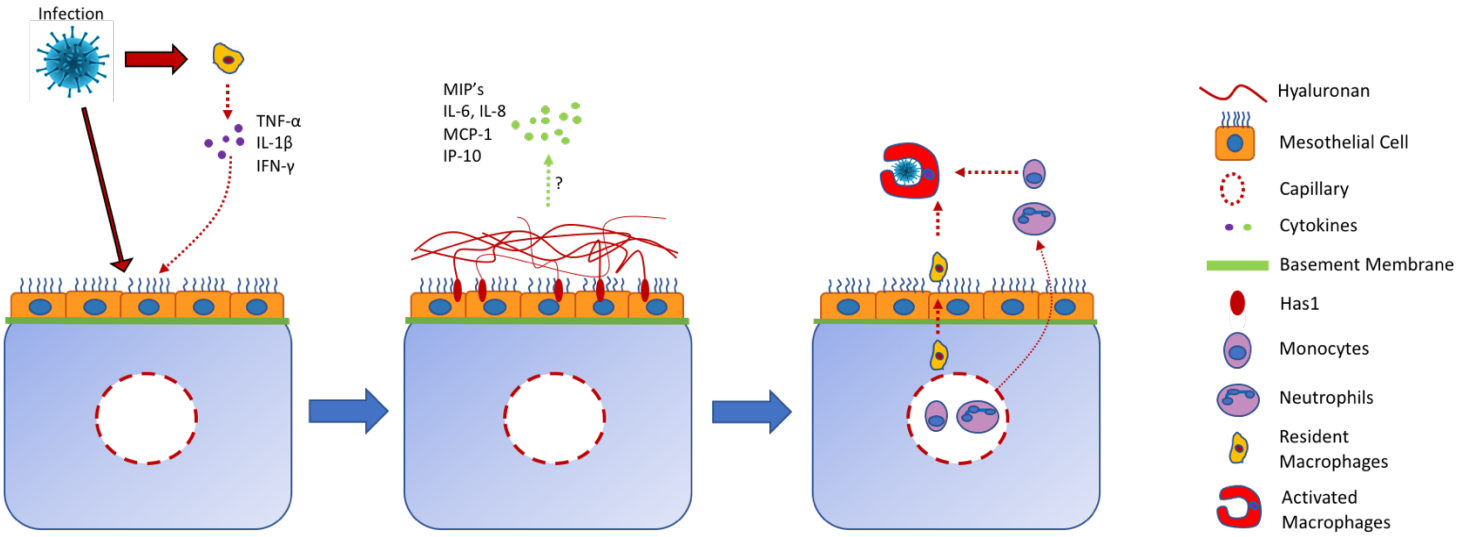

Figure 6.1 Potential role for mesothelial Generated HA during PD Peritonitis. Mesothelial cells are the first line of defence against bacterial peritonitis alongside resident macrophages in the peritoneum. Resident macrophages recognise and induce and inflammatory response by secreting inflammatory mediators such as TNF-α, IL-1β and IFN-γ, which in turn stimulate mesothelial cells to produce cytokines and chemokines such as MIP's, IL-6, IL-8, MCP-1 and IP-10. This appears to be mediated by HAS1 generated HA but a yet to be determined mechanism. The main effect of these is to elicit the recruitment of leukocytes that are normally restricted to the blood vessels to the site of injury and facilitate leukocyte adherence and directed transmigration across the mesothelium in order to resolve the inflammatory episode.

However, there remain a number of uncertainties relating to the mechanism underlying the involvement of HA during pro-inflammatory responses in mesothelial cells that need to be elucidated. In particular, the specific mechanisms how mesothelial HA promotes leukocyte recruitment in response to peritoneal infection remains uncertain and needs further

investigation. In these experiments, we did not assess whether PEP-1 blocked HA binding prior to use *in vivo*. Future work would need to confirm its effects on HA:CD44 binding prior to further use. However, it may be more prudent to utilise HAS1$^{-/-}$ mice or TLR2/4$^{-/-}$ mice and repeating the HKSE model to unpick the interesting effects of HA during infection and acute inflammation. New techniques such as next generation sequencing could then be used to identify relevant HA signalling pathways in the peritoneum. Further work is also necessary to investigate the effect of HA in bacterial clearance. This is important in order to understand how blocking HA affects during PD might impact upon the hosts response to infections.

To conclude, the work outlined in this thesis identifies differences in the role of HA in mesothelial cells when compared to other solid organ fibroses. In mesothelial cells, HA appears to be generated differently, which seems to be driving mostly extracellular HA, not a HA pericellular coat, which may have a different biological function in the peritoneum. This thesis has created a basis for future research to continue to understand the role of HA in peritoneal inflammation and elucidate the physiological role of HAS1 isoenzymes that could highlight possible therapeutic targets for PD in the future.

Chapter 7

Appendix

HAS1 Expression in TGF-β1 Stimulated Mesothelial Cells Over 24/48h

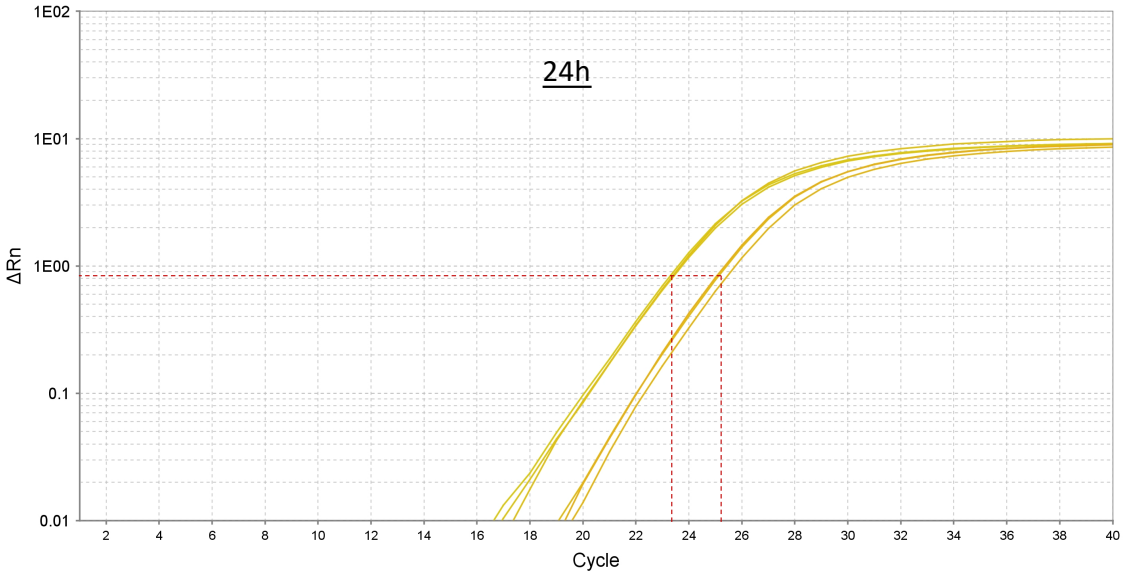

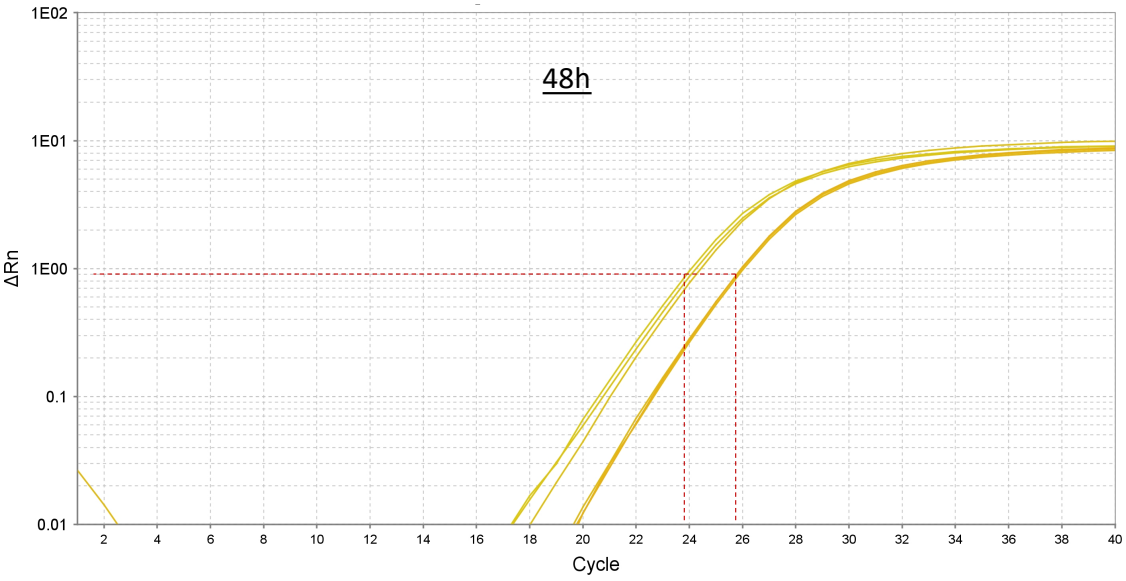

Figure 1 HAS1 expression in TGF-β1 stimulated mesothelial cells at 24/48h. QPCR amplification plots showing expression of HAS1 at 24 and 48 hours**.** Data shown above representative of 3 different donor experiments.

HAS2 Expression in TGF-β1 Stimulated Mesothelial Cells Over 24/48h

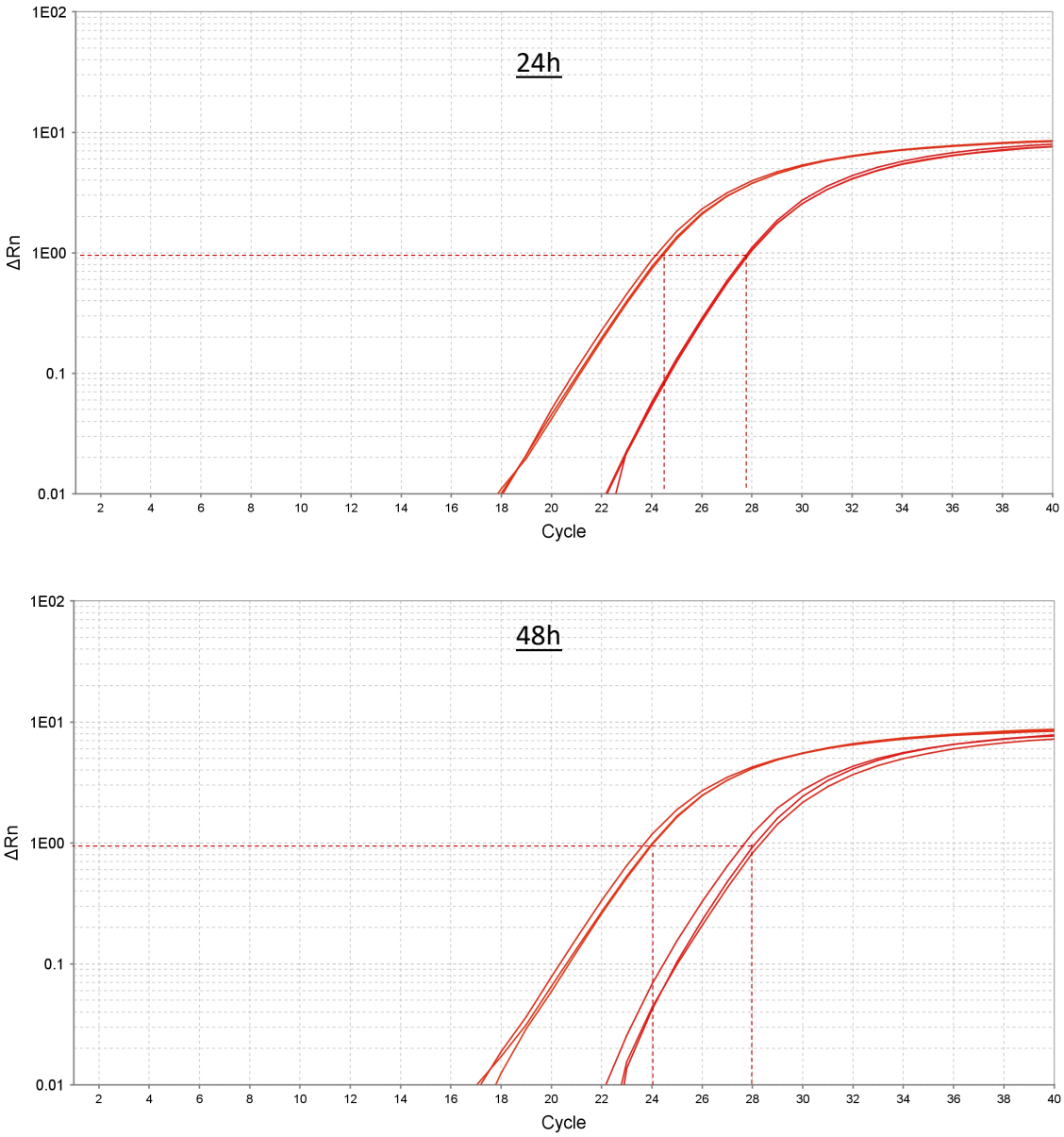

Figure 2 HAS2 expression in TGF-β1 stimulated mesothelial cells at 24/48h. QPCR amplification plots showing expression of HAS2 at 24 and 48 hours**.** Data shown above representative of 3 different donor experiments.

Chapter 8

References

1. WHO, *The global burden of disease: 2004 update*. 2008.
2. Nugent, R.A., et al., *The burden of chronic kidney disease on developing nations: a 21st century challenge in global health.* Nephron Clin Pract, 2011. **118**(3): p. c269-77.
3. Alebiosu, C.O. and O.E. Ayodele, *The global burden of chronic kidney disease and the way forward.* Ethn Dis, 2005. **15**(3): p. 418-23.
4. Ebert, N., et al., *Prevalence of reduced kidney function and albuminuria in older adults: the Berlin Initiative Study.* Nephrol Dial Transplant, 2017. **32**(6): p. 997-1005.
5. De Nicola, L., et al., *Prevalence and cardiovascular risk profile of chronic kidney disease in Italy: results of the 2008-12 National Health Examination Survey.* Nephrol Dial Transplant, 2015. **30**(5): p. 806-14.
6. Diabetes, G.B.D.E.M.R., C.K.D. Collaborators, and A.H. Mokdad, *Diabetes mellitus and chronic kidney disease in the Eastern Mediterranean Region: findings from the Global Burden of Disease 2015 study.* Int J Public Health, 2017.
7. Bruck, K., et al., *CKD Prevalence Varies across the European General Population.* J Am Soc Nephrol, 2016. **27**(7): p. 2135-47.
8. Stanifer, J.W., et al., *The epidemiology of chronic kidney disease in sub-Saharan Africa: a systematic review and meta-analysis.* Lancet Glob Health, 2014. **2**(3): p. e174-81.
9. Coresh, J., et al., *Prevalence of chronic kidney disease in the United States.* JAMA, 2007. **298**(17): p. 2038-47.
10. Outcomes, K.D.I.G., *KDIGO 2012 Clinical Practice Guideline for the Evaluation and Management of Chronic Kidney Disease.* Kidney International Supplements, 2013. **3**: p. 136-150.
11. Byrne C, C.F., Castledine C, Dawnay A, Ford D, Fraser S, Lambie M, Maxwell H, Steenkamp R, Wilkie M, Williams AJ, *UK Renal Registry: 19th Annual Report of the Renal Association.* Nephron, 2017. **137**.
12. Kerr, M., et al., *Estimating the financial cost of chronic kidney disease to the NHS in England.* Nephrol Dial Transplant, 2012. **27 Suppl 3**: p. iii73-80.
13. Abecassis, M., et al., *Kidney transplantation as primary therapy for end-stage renal disease: a National Kidney Foundation/Kidney Disease Outcomes Quality Initiative (NKF/KDOQITM) conference.* Clin J Am Soc Nephrol, 2008. **3**(2): p. 471-80.
14. Garcia, G.G., P.N. Harden, and J.R. Chapman, *The global role of kidney transplantation.* Kidney Int, 2012. **81**(5): p. 425-7.
15. Winterbottom, A., et al., *Choosing dialysis modality: decision making in a chronic illness context.* Health Expect, 2014. **17**(5): p. 710-23.
16. Vonesh, E.F., et al., *Mortality studies comparing peritoneal dialysis and hemodialysis: what do they tell us?* Kidney Int Suppl, 2006(103): p. S3-11.
17. Chanouzas, D., et al., *What influences patient choice of treatment modality at the pre-dialysis stage?* Nephrol Dial Transplant, 2012. **27**(4): p. 1542-7.
18. Stack, A.G., *Determinants of modality selection among incident US dialysis patients: results from a national study.* J Am Soc Nephrol, 2002. **13**(5): p. 1279-87.
19. Korevaar, J.C., et al., *Effect of starting with hemodialysis compared with peritoneal dialysis in patients new on dialysis treatment: a randomized controlled trial.* Kidney Int, 2003. **64**(6): p. 2222-8.
20. Termorshuizen, F., et al., *Hemodialysis and peritoneal dialysis: comparison of adjusted mortality rates according to the duration of dialysis: analysis of The Netherlands Cooperative Study on the Adequacy of Dialysis 2.* J Am Soc Nephrol, 2003. **14**(11): p. 2851-60.

21. McDonald, S.P., et al., *Relationship between dialysis modality and mortality.* J Am Soc Nephrol, 2009. **20**(1): p. 155-63.
22. Couchoud, C., et al., *Associations between comorbidities, treatment choice and outcome in the elderly with end-stage renal disease.* Nephrol Dial Transplant, 2007. **22**(11): p. 3246-54.
23. Noordzij, M. and K.J. Jager, *Survival comparisons between haemodialysis and peritoneal dialysis.* Nephrol Dial Transplant, 2012. **27**(9): p. 3385-7.
24. Sinnakirouchenan, R. and J.L. Holley, *Peritoneal dialysis versus hemodialysis: risks, benefits, and access issues.* Adv Chronic Kidney Dis, 2011. **18**(6): p. 428-32.
25. Davies, S.J., et al., *What really happens to people on long-term peritoneal dialysis?* Kidney Int, 1998. **54**(6): p. 2207-17.
26. Brimble, K.S., et al., *Meta-analysis: peritoneal membrane transport, mortality, and technique failure in peritoneal dialysis.* J Am Soc Nephrol, 2006. **17**(9): p. 2591-8.
27. Pajek, J., et al., *Outcomes of peritoneal dialysis patients and switching to hemodialysis: a competing risks analysis.* Perit Dial Int, 2014. **34**(3): p. 289-98.
28. Perl, J., et al., *The Peritoneal Dialysis Outcomes and Practice Patterns Study (PDOPPS): Unifying Efforts to Inform Practice and Improve Global Outcomes in Peritoneal Dialysis.* Perit Dial Int, 2016. **36**(3): p. 297-307.
29. Devuyst, O., P.J. Margetts, and N. Topley, *The pathophysiology of the peritoneal membrane.* J Am Soc Nephrol, 2010. **21**(7): p. 1077-85.
30. Yung, S. and T.M. Chan, *Preventing peritoneal fibrosis--insights from the laboratory.* Perit Dial Int, 2003. **23 Suppl 2**: p. S37-41.
31. de Lima, S.M., et al., *Inflammation, neoangiogenesis and fibrosis in peritoneal dialysis.* Clin Chim Acta, 2013. **421**: p. 46-50.
32. Blackburn, S.C. and M.P. Stanton, *Anatomy and physiology of the peritoneum.* Semin Pediatr Surg, 2014. **23**(6): p. 326-30.
33. Capobianco, A., et al., *The peritoneum: healing, immunity, and diseases.* J Pathol, 2017. **243**(2): p. 137-147.
34. do Amaral, R., et al., *The Peritoneum: Health, Disease, and Perspectives regarding Tissue Engineering and Cell Therapies.* Cells Tissues Organs, 2017. **204**(5-6): p. 211-217.
35. Mutsaers, S.E., et al., *Mesothelial cells in tissue repair and fibrosis.* Front Pharmacol, 2015. **6**: p. 113.
36. Yung, S., F.K. Li, and T.M. Chan, *Peritoneal mesothelial cell culture and biology.* Perit Dial Int, 2006. **26**(2): p. 162-73.
37. van Baal, J.O., et al., *The histophysiology and pathophysiology of the peritoneum.* Tissue Cell, 2017. **49**(1): p. 95-105.
38. Lachaud, C.C., et al., *Use of Mesothelial Cells and Biological Matrices for Tissue Engineering of Simple Epithelium Surrogates.* Frontiers in bioengineering and biotechnology, 2015. **3**.
39. Nagy, J.A., *Peritoneal membrane morphology and function.* Kidney Int Suppl, 1996. **56**: p. S2-11.
40. Paulsson, M., *Basement membrane proteins: structure, assembly, and cellular interactions.* Crit Rev Biochem Mol Biol, 1992. **27**(1-2): p. 93-127.
41. Zweers, M.M., et al., *Ultrastructure of basement membranes of peritoneal capillaries in a chronic peritoneal infusion model in the rat.* Nephrol Dial Transplant, 2001. **16**(3): p. 651-4.

42. Williams, J.D., et al., *Morphologic changes in the peritoneal membrane of patients with renal disease.* J Am Soc Nephrol, 2002. **13**(2): p. 470-9.
43. Yung, S. and T.M. Chan, *Pathophysiological changes to the peritoneal membrane during PD-related peritonitis: the role of mesothelial cells.* Mediators Inflamm, 2012. **2012**: p. 484167.
44. Mutsaers, S.E., *The mesothelial cell.* International Journal of Biochemistry & Cell Biology, 2004. **36**(1): p. 9-16.
45. Mutsaers, S.E. and S. Wilkosz, *Structure and function of mesothelial cells*, in *Peritoneal Carcinomatosis*. 2007, Springer. p. 1-19.
46. Mutsaers, S.E., *Mesothelial cells: their structure, function and role in serosal repair.* Respirology, 2002. **7**(3): p. 171-91.
47. Yung, S. and T.M. Chan, *Pathophysiology of the peritoneal membrane during peritoneal dialysis: the role of hyaluronan.* J Biomed Biotechnol, 2011. **2011**: p. 180594.
48. van Roy, F. and G. Berx, *The cell-cell adhesion molecule E-cadherin.* Cell Mol Life Sci, 2008. **65**(23): p. 3756-88.
49. Margetts, P.J., et al., *Transient overexpression of TGF-{beta}1 induces epithelial mesenchymal transition in the rodent peritoneum.* J Am Soc Nephrol, 2005. **16**(2): p. 425-36.
50. Strippoli, R., et al., *Epithelial-to-mesenchymal transition of peritoneal mesothelial cells is regulated by an ERK/NF-kappaB/Snail1 pathway.* Dis Model Mech, 2008. **1**(4-5): p. 264-74.
51. Ferrandez-Izquierdo, A., et al., *Immunocytochemical typification of mesothelial cells in effusions: in vivo and in vitro models.* Diagn Cytopathol, 1994. **10**(3): p. 256-62.
52. Jonjic, N., et al., *Expression of adhesion molecules and chemotactic cytokines in cultured human mesothelial cells.* J Exp Med, 1992. **176**(4): p. 1165-74.
53. Martin, J., et al., *Production and regulation of matrix metalloproteinases and their inhibitors by human peritoneal mesothelial cells.* Perit Dial Int, 2000. **20**(5): p. 524-33.
54. Yung, S. and T.M. Chan, *The Role of Hyaluronan and CD44 in the Pathogenesis of Lupus Nephritis.* Autoimmune Dis, 2012. **2012**: p. 207190.
55. Yung, S. and M. Davies, *Response of the human peritoneal mesothelial cell to injury: an in vitro model of peritoneal wound healing.* Kidney Int, 1998. **54**(6): p. 2160-9.
56. Liberek, T., et al., *Adherence of neutrophils to human peritoneal mesothelial cells: role of intercellular adhesion molecule-1.* J Am Soc Nephrol, 1996. **7**(2): p. 208-17.
57. Robson, R.L., et al., *Differential regulation of chemokine production in human peritoneal mesothelial cells: IFN-gamma controls neutrophil migration across the mesothelium in vitro and in vivo.* J Immunol, 2001. **167**(2): p. 1028-38.
58. Jones, S.A., *Directing transition from innate to acquired immunity: defining a role for IL-6.* J Immunol, 2005. **175**(6): p. 3463-8.
59. Topley, N., et al., *Activation of inflammation and leukocyte recruitment into the peritoneal cavity.* Kidney Int Suppl, 1996. **56**: p. S17-21.
60. Shaw, T.J., et al., *Human Peritoneal Mesothelial Cells Display Phagocytic and Antigen-Presenting Functions to Contribute to Intraperitoneal Immunity.* Int J Gynecol Cancer, 2016. **26**(5): p. 833-8.
61. Valle, M.T., et al., *Antigen-presenting function of human peritoneum mesothelial cells.* Clin Exp Immunol, 1995. **101**(1): p. 172-6.

62. Hausmann, M.J., et al., *Accessory role of human peritoneal mesothelial cells in antigen presentation and T-cell growth.* Kidney Int, 2000. **57**(2): p. 476-86.
63. Mackman, N., *The role of tissue factor and factor VIIa in hemostasis.* Anesth Analg, 2009. **108**(5): p. 1447-52.
64. Holmdahl, L., *The role of fibrinolysis in adhesion formation.* Eur J Surg Suppl, 1997(577): p. 24-31.
65. Catar, R., et al., *IL-6 Trans-Signaling Links Inflammation with Angiogenesis in the Peritoneal Membrane.* J Am Soc Nephrol, 2016.
66. Cho, Y., C.M. Hawley, and D.W. Johnson, *Clinical causes of inflammation in peritoneal dialysis patients.* Int J Nephrol, 2014. **2014**: p. 909373.
67. Li, P.K., J.K. Ng, and C.W. McIntyre, *Inflammation and Peritoneal Dialysis.* Semin Nephrol, 2017. **37**(1): p. 54-65.
68. Wang, A.Y., et al., *Is a single time point C-reactive protein predictive of outcome in peritoneal dialysis patients?* J Am Soc Nephrol, 2003. **14**(7): p. 1871-9.
69. Pecoits-Filho, R., et al., *Associations between circulating inflammatory markers and residual renal function in CRF patients.* Am J Kidney Dis, 2003. **41**(6): p. 1212-8.
70. Su, H., C.T. Lei, and C. Zhang, *Interleukin-6 Signaling Pathway and Its Role in Kidney Disease: An Update.* Front Immunol, 2017. **8**: p. 405.
71. Wanner, C., et al., *Inflammation and cardiovascular risk in dialysis patients.* Kidney Int Suppl, 2002(80): p. 99-102.
72. Chung, S.H., et al., *Association between residual renal function, inflammation and patient survival in new peritoneal dialysis patients.* Nephrol Dial Transplant, 2003. **18**(3): p. 590-7.
73. Lambie, M., et al., *Independent effects of systemic and peritoneal inflammation on peritoneal dialysis survival.* J Am Soc Nephrol, 2013. **24**(12): p. 2071-80.
74. Cho, Y., et al., *Baseline serum interleukin-6 predicts cardiovascular events in incident peritoneal dialysis patients.* Perit Dial Int, 2015. **35**(1): p. 35-42.
75. Lee, B.T., et al., *Association of C-reactive protein, tumor necrosis factor-alpha, and interleukin-6 with chronic kidney disease.* BMC Nephrol, 2015. **16**: p. 77.
76. Descamps-Latscha, B., et al., *Balance between IL-1 beta, TNF-alpha, and their specific inhibitors in chronic renal failure and maintenance dialysis. Relationships with activation markers of T cells, B cells, and monocytes.* J Immunol, 1995. **154**(2): p. 882-92.
77. Dai, L., et al., *End-Stage Renal Disease, Inflammation and Cardiovascular Outcomes.* Contrib Nephrol, 2017. **191**: p. 32-43.
78. Yao, Q., et al., *Chronic systemic inflammation in dialysis patients: an update on causes and consequences.* ASAIO J, 2004. **50**(6): p. lii-lvii.
79. Shlipak, M.G., et al., *Elevations of inflammatory and procoagulant biomarkers in elderly persons with renal insufficiency.* Circulation, 2003. **107**(1): p. 87-92.
80. Baroni, G., et al., *Inflammation and the peritoneal membrane: causes and impact on structure and function during peritoneal dialysis.* Mediators Inflamm, 2012. **2012**: p. 912595.
81. Demirci, M.S., et al., *Relations between malnutrition-inflammation-atherosclerosis and volume status. The usefulness of bioimpedance analysis in peritoneal dialysis patients.* Nephrol Dial Transplant, 2011. **26**(5): p. 1708-16.
82. Li, P.K. and Y.L. Cheng, *Therapeutic options for preservation of residual renal function in patients on peritoneal dialysis.* Perit Dial Int, 2007. **27 Suppl 2**: p. S158-63.

83. Nongnuch, A., et al., *Strategies for preserving residual renal function in peritoneal dialysis patients.* Clin Kidney J, 2015. **8**(2): p. 202-11.
84. Kjaergaard, K.D., et al., *Preserving residual renal function in dialysis patients: an update on evidence to assist clinical decision making.* NDT Plus, 2011. **4**(4): p. 225-30.
85. Marron, B., et al., *Benefits of preserving residual renal function in peritoneal dialysis.* Kidney Int Suppl, 2008(108): p. S42-51.
86. Chan, T.M. and S. Yung, *Studying the effects of new peritoneal dialysis solutions on the peritoneum.* Perit Dial Int, 2007. **27 Suppl 2**: p. S87-93.
87. Yung, S., et al., *Impact of a low-glucose peritoneal dialysis regimen on fibrosis and inflammation biomarkers.* Perit Dial Int, 2015. **35**(2): p. 147-58.
88. Witowski, J., et al., *Prolonged exposure to glucose degradation products impairs viability and function of human peritoneal mesothelial cells.* J Am Soc Nephrol, 2001. **12**(11): p. 2434-41.
89. Rippe, B., et al., *Long-term clinical effects of a peritoneal dialysis fluid with less glucose degradation products.* Kidney Int, 2001. **59**(1): p. 348-57.
90. Rippe, B., A. Wieslander, and B. Musi, *Long-term results with low glucose degradation product content in peritoneal dialysis fluids.* Contrib Nephrol, 2003(140): p. 47-55.
91. Linden, T., et al., *Glucose degradation products in peritoneal dialysis fluids may have both local and systemic effects: a study of residual fluid and mesothelial cells.* Perit Dial Int, 2001. **21**(6): p. 607-10.
92. Wieslander, A., et al., *Biological significance of reducing glucose degradation products in peritoneal dialysis fluids.* Perit Dial Int, 2000. **20 Suppl 5**: p. S23-7.
93. McIntyre, C.W., *Update on peritoneal dialysis solutions.* Kidney Int, 2007. **71**(6): p. 486-90.
94. Garcia-Lopez, E., B. Lindholm, and S. Davies, *An update on peritoneal dialysis solutions.* Nat Rev Nephrol, 2012. **8**(4): p. 224-33.
95. Li, P.K., et al., *ISPD Peritonitis Recommendations: 2016 Update on Prevention and Treatment.* Perit Dial Int, 2016. **36**(5): p. 481-508.
96. Davenport, A., *Peritonitis remains the major clinical complication of peritoneal dialysis: the London, UK, peritonitis audit 2002-2003.* Perit Dial Int, 2009. **29**(3): p. 297-302.
97. Brown, M.C., et al., *Peritoneal dialysis-associated peritonitis rates and outcomes in a national cohort are not improving in the post-millennium (2000-2007).* Perit Dial Int, 2011. **31**(6): p. 639-50.
98. Kavanagh, D., G.J. Prescott, and R.A. Mactier, *Peritoneal dialysis-associated peritonitis in Scotland (1999-2002).* Nephrol Dial Transplant, 2004. **19**(10): p. 2584-91.
99. Cho, Y. and D.G. Struijk, *Peritoneal Dialysis-Related Peritonitis: Atypical and Resistant Organisms.* Semin Nephrol, 2017. **37**(1): p. 66-76.
100. Lai, K.N., et al., *Changes of cytokine profiles during peritonitis in patients on continuous ambulatory peritoneal dialysis.* Am J Kidney Dis, 2000. **35**(4): p. 644-52.
101. Margetts, P.J. and D.N. Churchill, *Acquired ultrafiltration dysfunction in peritoneal dialysis patients.* J Am Soc Nephrol, 2002. **13**(11): p. 2787-94.
102. Williams, J.D., et al., *The natural course of peritoneal membrane biology during peritoneal dialysis.* Kidney Int Suppl, 2003(88): p. S43-9.
103. Bajo, M.A., et al., *Low-GDP peritoneal dialysis fluid ('balance') has less impact in vitro and ex vivo on epithelial-to-mesenchymal transition (EMT) of mesothelial cells than a standard fluid.* Nephrol Dial Transplant, 2011. **26**(1): p. 282-91.

104. Vlahu, C.A., et al., *Damage of the endothelial glycocalyx in dialysis patients.* J Am Soc Nephrol, 2012. **23**(11): p. 1900-8.
105. Retana, C., et al., *Retinoic acid improves morphology of cultured peritoneal mesothelial cells from patients undergoing dialysis.* PLoS One, 2013. **8**(11): p. e79678.
106. Lopez-Cabrera, M., et al., *Ex vivo analysis of dialysis effluent-derived mesothelial cells as an approach to unveiling the mechanism of peritoneal membrane failure.* Perit Dial Int, 2006. **26**(1): p. 26-34.
107. Topley, N. and J.D. Williams, *Effect of peritoneal dialysis on cytokine production by peritoneal cells.* Blood Purif, 1996. **14**(2): p. 188-97.
108. Topley, N., R.K. Mackenzie, and J.D. Williams, *Macrophages and mesothelial cells in bacterial peritonitis.* Immunobiology, 1996. **195**(4-5): p. 563-73.
109. Kalluri, R. and R.A. Weinberg, *The basics of epithelial-mesenchymal transition.* J Clin Invest, 2009. **119**(6): p. 1420-8.
110. Yáñez-Mó, M., et al., *Peritoneal dialysis and epithelial-to-mesenchymal transition of mesothelial cells.* New England Journal of Medicine, 2003. **348**(5): p. 403-413.
111. Aroeira, L.S., et al., *Epithelial to mesenchymal transition and peritoneal membrane failure in peritoneal dialysis patients: pathologic significance and potential therapeutic interventions.* J Am Soc Nephrol, 2007. **18**(7): p. 2004-13.
112. Lamouille, S., J. Xu, and R. Derynck, *Molecular mechanisms of epithelial-mesenchymal transition.* Nature Reviews Molecular Cell Biology, 2014. **15**(3): p. 178-96.
113. Witowski, J., K. Książek, and A. Jörres, *New insights into the biology of peritoneal mesothelial cells: the roles of epithelial-to-mesenchymal transition and cellular senescence.* Nephron Experimental Nephrology, 2008. **108**(4): p. e69-e73.
114. Lopez-Cabrera, M., *Mesenchymal Conversion of Mesothelial Cells Is a Key Event in the Pathophysiology of the Peritoneum during Peritoneal Dialysis.* Adv Med, 2014. **2014**: p. 473134.
115. Duffield, J.S. and B.D. Humphreys, *Origin of new cells in the adult kidney: results from genetic labeling techniques.* Kidney international, 2011. **79**(5): p. 494-501.
116. Humphreys, B.D., et al., *Fate tracing reveals the pericyte and not epithelial origin of myofibroblasts in kidney fibrosis.* Am J Pathol, 2010. **176**(1): p. 85-97.
117. Yang, A.H., J.Y. Chen, and J.K. Lin, *Myofibroblastic conversion of mesothelial cells.* Kidney Int, 2003. **63**(4): p. 1530-9.
118. Hinz, B., et al., *The myofibroblast: one function, multiple origins.* Am J Pathol, 2007. **170**(6): p. 1807-16.
119. Strippoli, R., et al., *Molecular Mechanisms Underlying Peritoneal EMT and Fibrosis.* Stem Cells Int, 2016. **2016**: p. 3543678.
120. Loureiro, J., et al., *Blocking TGF-beta1 protects the peritoneal membrane from dialysate-induced damage.* J Am Soc Nephrol, 2011. **22**(9): p. 1682-95.
121. Strippoli, R., et al., *Caveolin-1 deficiency induces a MEK-ERK1/2-Snail-1-dependent epithelial-mesenchymal transition and fibrosis during peritoneal dialysis.* EMBO Mol Med, 2015. **7**(1): p. 102-23.
122. Vargha, R., et al., *Effects of epithelial-to-mesenchymal transition on acute stress response in human peritoneal mesothelial cells.* Nephrol Dial Transplant, 2008. **23**(11): p. 3494-500.
123. Margetts, P.J., et al., *Gene transfer of transforming growth factor-beta to the rat peritoneum: Effects on membrane function.* Journal of the American Society of Nephrology, 2001. **12**(10): p. 2029-2039.

124. Meran, S. and R. Steadman, *Fibroblasts and myofibroblasts in renal fibrosis.* Int J Exp Pathol, 2011. **92**(3): p. 158-67.
125. Webber, J., et al., *Hyaluronan orchestrates transforming growth factor-beta1-dependent maintenance of myofibroblast phenotype.* J Biol Chem, 2009. **284**(14): p. 9083-92.
126. Webber, J., et al., *Modulation of TGFbeta1-dependent myofibroblast differentiation by hyaluronan.* Am J Pathol, 2009. **175**(1): p. 148-60.
127. Meng, X.M., A.C.K. Chung, and H.Y. Lan, *Role of the TGF-beta/BMP-7/Smad pathways in renal diseases.* Clinical Science, 2013. **124**(3-4): p. 243-254.
128. Wang, S.N., J. Lapage, and R. Hirschberg, *Loss of tubular bone morphogenetic protein-7 in diabetic nephropathy.* J Am Soc Nephrol, 2001. **12**(11): p. 2392-9.
129. Wang, S., et al., *Bone morphogenic protein-7 (BMP-7), a novel therapy for diabetic nephropathy.* Kidney Int, 2003. **63**(6): p. 2037-49.
130. Wang, Z., et al., *Protective effect of BMP-7 against aristolochic acid-induced renal tubular epithelial cell injury.* Toxicol Lett, 2010. **198**(3): p. 348-57.
131. Vukicevic, S., et al., *Osteogenic protein-1 (bone morphogenetic protein-7) reduces severity of injury after ischemic acute renal failure in rat.* J Clin Invest, 1998. **102**(1): p. 202-14.
132. Sugimoto, H., et al., *Renal fibrosis and glomerulosclerosis in a new mouse model of diabetic nephropathy and its regression by bone morphogenic protein-7 and advanced glycation end product inhibitors.* Diabetes, 2007. **56**(7): p. 1825-33.
133. Zeisberg, M., et al., *BMP-7 counteracts TGF-beta1-induced epithelial-to-mesenchymal transition and reverses chronic renal injury.* Nat Med, 2003. **9**(7): p. 964-8.
134. Hruska, K.A., et al., *Osteogenic protein-1 prevents renal fibrogenesis associated with ureteral obstruction.* Am J Physiol Renal Physiol, 2000. **279**(1): p. F130-43.
135. Morrissey, J., et al., *Bone morphogenetic protein-7 improves renal fibrosis and accelerates the return of renal function.* J Am Soc Nephrol, 2002. **13 Suppl 1**: p. S14-21.
136. Zeisberg, M., et al., *Bone morphogenic protein-7 inhibits progression of chronic renal fibrosis associated with two genetic mouse models.* Am J Physiol Renal Physiol, 2003. **285**(6): p. F1060-7.
137. Yang, T., et al., *Bone morphogenetic protein 7 suppresses the progression of hepatic fibrosis and regulates the expression of gremlin and transforming growth factor beta1.* Mol Med Rep, 2012. **6**(1): p. 246-52.
138. Midgley, A.C., et al., *Hyaluronan Regulates Bone Morphogenetic Protein-7-dependent Prevention and Reversal of Myofibroblast Phenotype.* Journal of Biological Chemistry, 2015. **290**(18): p. 11218-11234.
139. Laurent, T.C., U.B. Laurent, and J.R. Fraser, *The structure and function of hyaluronan: An overview.* Immunol Cell Biol, 1996. **74**(2): p. A1-7.
140. Meyer, K.P., J.W., *The polysaccharide of the vitreous humour.* Journal of Biological Chemistry 1934. **107**(3): p. 629-634.
141. Hascall, V. and J.D. Esko, *Hyaluronan*, in *Essentials of Glycobiology*, rd, et al., Editors. 2015: Cold Spring Harbor (NY). p. 197-206.
142. Fraser, J.R., T.C. Laurent, and U.B. Laurent, *Hyaluronan: its nature, distribution, functions and turnover.* J Intern Med, 1997. **242**(1): p. 27-33.
143. Cyphert, J.M., C.S. Trempus, and S. Garantziotis, *Size Matters: Molecular Weight Specificity of Hyaluronan Effects in Cell Biology.* Int J Cell Biol, 2015. **2015**: p. 563818.

144. Toole, B.P., *Hyaluronan is not just a goo!* J Clin Invest, 2000. **106**(3): p. 335-6.
145. Cowman, M.K. and S. Matsuoka, *Experimental approaches to hyaluronan structure.* Carbohydr Res, 2005. **340**(5): p. 791-809.
146. Blundell, C.D., P.L. Deangelis, and A. Almond, *Hyaluronan: the absence of amide-carboxylate hydrogen bonds and the chain conformation in aqueous solution are incompatible with stable secondary and tertiary structure models.* Biochem J, 2006. **396**(3): p. 487-98.
147. Evanko, S.P., et al., *Hyaluronan-dependent pericellular matrix.* Adv Drug Deliv Rev, 2007. **59**(13): p. 1351-65.
148. Itano, N. and K. Kimata, *Mammalian hyaluronan synthases.* IUBMB Life, 2002. **54**(4): p. 195-9.
149. Vigetti, D., et al., *Hyaluronan: biosynthesis and signaling.* Biochim Biophys Acta, 2014. **1840**(8): p. 2452-9.
150. Lindahl, U., et al., *Proteoglycans and Sulfated Glycosaminoglycans*, in *Essentials of Glycobiology*, rd, et al., Editors. 2015: Cold Spring Harbor (NY). p. 207-221.
151. DeAngelis, P.L., J. Papaconstantinou, and P.H. Weigel, *Molecular cloning, identification, and sequence of the hyaluronan synthase gene from group A Streptococcus pyogenes.* J Biol Chem, 1993. **268**(26): p. 19181-4.
152. DeAngelis, P.L., J. Papaconstantinou, and P.H. Weigel, *Isolation of a Streptococcus pyogenes gene locus that directs hyaluronan biosynthesis in acapsular mutants and in heterologous bacteria.* J Biol Chem, 1993. **268**(20): p. 14568-71.
153. Crater, D.L., B.A. Dougherty, and I. van de Rijn, *Molecular characterization of hasC from an operon required for hyaluronic acid synthesis in group A streptococci. Demonstration of UDP-glucose pyrophosphorylase activity.* J Biol Chem, 1995. **270**(48): p. 28676-80.
154. Dougherty, B.A. and I. van de Rijn, *Molecular characterization of hasB from an operon required for hyaluronic acid synthesis in group A streptococci. Demonstration of UDP-glucose dehydrogenase activity.* J Biol Chem, 1993. **268**(10): p. 7118-24.
155. Itano, N. and K. Kimata, *Expression cloning and molecular characterization of HAS protein, a eukaryotic hyaluronan synthase.* J Biol Chem, 1996. **271**(17): p. 9875-8.
156. Itano, N., et al., *Three isoforms of mammalian hyaluronan synthases have distinct enzymatic properties.* J Biol Chem, 1999. **274**(35): p. 25085-92.
157. Spicer, A.P., et al., *Chromosomal localization of the human and mouse hyaluronan synthase genes.* Genomics, 1997. **41**(3): p. 493-7.
158. Itano, N. and K. Kimata, *Molecular cloning of human hyaluronan synthase.* Biochem Biophys Res Commun, 1996. **222**(3): p. 816-20.
159. Monslow, J., et al., *The human hyaluronan synthase genes: genomic structures, proximal promoters and polymorphic microsatellite markers.* Int J Biochem Cell Biol, 2003. **35**(8): p. 1272-83.
160. Monslow, J., et al., *Identification and analysis of the promoter region of the human hyaluronan synthase 2 gene.* Journal of Biological Chemistry, 2004. **279**(20): p. 20576-20581.
161. Michael, D.R., et al., *The human hyaluronan synthase 2 (HAS2) gene and its natural antisense RNA exhibit coordinated expression in the renal proximal tubular epithelial cell.* J Biol Chem, 2011. **286**(22): p. 19523-32.
162. Wang, S., et al., *Identification and analysis of the promoter region of the human HAS3 gene.* Biochem Biophys Res Commun, 2015. **460**(4): p. 1008-14.

163. Bowen, T., et al., *Regulation of Synthesis and Roles of Hyaluronan in Peritoneal Dialysis.* Biomed Res Int, 2015. **2015**: p. 427038.
164. Camenisch, T.D., et al., *Disruption of hyaluronan synthase-2 abrogates normal cardiac morphogenesis and hyaluronan-mediated transformation of epithelium to mesenchyme.* J Clin Invest, 2000. **106**(3): p. 349-60.
165. Spicer, A.P. and J.A. McDonald, *Characterization and molecular evolution of a vertebrate hyaluronan synthase gene family.* J Biol Chem, 1998. **273**(4): p. 1923-32.
166. Karousou, E., et al., *Roles and targeting of the HAS/hyaluronan/CD44 molecular system in cancer.* Matrix Biol, 2016.
167. Heldermon, C., P.L. DeAngelis, and P.H. Weigel, *Topological organization of the hyaluronan synthase from Streptococcus pyogenes.* J Biol Chem, 2001. **276**(3): p. 2037-46.
168. Jiang, D., J. Liang, and P.W. Noble, *Hyaluronan as an immune regulator in human diseases.* Physiological Reviews, 2011. **91**(1): p. 221-64.
169. Mack, J.A., et al., *Enhanced inflammation and accelerated wound closure following tetraphorbol ester application or full-thickness wounding in mice lacking hyaluronan synthases Has1 and Has3.* J Invest Dermatol, 2012. **132**(1): p. 198-207.
170. Bai, K.J., et al., *The role of hyaluronan synthase 3 in ventilator-induced lung injury.* Am J Respir Crit Care Med, 2005. **172**(1): p. 92-8.
171. Kobayashi, N., et al., *Hyaluronan deficiency in tumor stroma impairs macrophage trafficking and tumor neovascularization.* Cancer Res, 2010. **70**(18): p. 7073-83.
172. Tammi, R.H., et al., *Transcriptional and post-translational regulation of hyaluronan synthesis.* FEBS J, 2011. **278**(9): p. 1419-28.
173. Jiang, D., J. Liang, and P.W. Noble, *Hyaluronan in tissue injury and repair.* Annu Rev Cell Dev Biol, 2007. **23**: p. 435-61.
174. Weigel, P.H., *Hyaluronan Synthase: The Mechanism of Initiation at the Reducing End and a Pendulum Model for Polysaccharide Translocation to the Cell Exterior.* Int J Cell Biol, 2015. **2015**: p. 367579.
175. Rilla, K., et al., *Plasma membrane residence of hyaluronan synthase is coupled to its enzymatic activity.* J Biol Chem, 2005. **280**(36): p. 31890-7.
176. Mullegger, J., et al., *'Piggy-back' transport of Xenopus hyaluronan synthase (XHAS1) via the secretory pathway to the plasma membrane.* Biol Chem, 2003. **384**(1): p. 175-82.
177. Bart, G., et al., *Fluorescence resonance energy transfer (FRET) and proximity ligation assays reveal functionally relevant homo- and heteromeric complexes among hyaluronan synthases HAS1, HAS2, and HAS3.* J Biol Chem, 2015. **290**(18): p. 11479-90.
178. Siiskonen, H., et al., *Hyaluronan synthase 1: a mysterious enzyme with unexpected functions.* Front Immunol, 2015. **6**: p. 43.
179. Knudson, W., et al., *The pericellular hyaluronan of articular chondrocytes.* Matrix Biol, 2018.
180. Pienimaki, J.P., et al., *Epidermal growth factor activates hyaluronan synthase 2 in epidermal keratinocytes and increases pericellular and intracellular hyaluronan.* J Biol Chem, 2001. **276**(23): p. 20428-35.
181. Selbi, W., et al., *Overexpression of hyaluronan synthase 2 alters hyaluronan distribution and function in proximal tubular epithelial cells.* J Am Soc Nephrol, 2006. **17**(6): p. 1553-67.

182. Meran, S., et al., *Hyaluronan facilitates transforming growth factor-beta1-dependent proliferation via CD44 and epidermal growth factor receptor interaction.* J Biol Chem, 2011. **286**(20): p. 17618-30.
183. Meran, S., et al., *Involvement of hyaluronan in regulation of fibroblast phenotype.* J Biol Chem, 2007. **282**(35): p. 25687-97.
184. Simpson, R.M., et al., *Age-related changes in pericellular hyaluronan organization leads to impaired dermal fibroblast to myofibroblast differentiation.* Am J Pathol, 2009. **175**(5): p. 1915-28.
185. Vigetti, D., et al., *Modulation of hyaluronan synthase activity in cellular membrane fractions.* J Biol Chem, 2009. **284**(44): p. 30684-94.
186. Kultti, A., et al., *4-Methylumbelliferone inhibits hyaluronan synthesis by depletion of cellular UDP-glucuronic acid and downregulation of hyaluronan synthase 2 and 3.* Exp Cell Res, 2009. **315**(11): p. 1914-23.
187. Jacobson, A., et al., *Expression of human hyaluronan synthases in response to external stimuli.* Biochem J, 2000. **348 Pt 1**: p. 29-35.
188. Heldin, P., et al., *Characterization of the molecular mechanism involved in the activation of hyaluronan synthetase by platelet-derived growth factor in human mesothelial cells.* Biochem J, 1992. **283 (Pt 1)**: p. 165-70.
189. Wilkinson, T.S., et al., *Pro- and anti-inflammatory factors cooperate to control hyaluronan synthesis in lung fibroblasts.* Am J Respir Cell Mol Biol, 2004. **31**(1): p. 92-9.
190. Simpson, R.M., et al., *Aging fibroblasts resist phenotypic maturation because of impaired hyaluronan-dependent CD44/epidermal growth factor receptor signaling.* Am J Pathol, 2010. **176**(3): p. 1215-28.
191. Ghatak, S., et al., *TGF beta-1 regulates CD44v6 expression and activity through ERK-induced EGR1 in pulmonary fibrogenic fibroblasts.* J Biol Chem, 2017.
192. Sugiyama, Y., et al., *Putative hyaluronan synthase mRNA are expressed in mouse skin and TGF-beta upregulates their expression in cultured human skin cells.* J Invest Dermatol, 1998. **110**(2): p. 116-21.
193. Sayo, T., et al., *Hyaluronan synthase 3 regulates hyaluronan synthesis in cultured human keratinocytes.* J Invest Dermatol, 2002. **118**(1): p. 43-8.
194. Chen, L., et al., *Identification and analysis of the human hyaluronan synthase 1 gene promoter reveals Smad3- and Sp3-mediated transcriptional induction.* Matrix Biol, 2012. **31**(7-8): p. 373-9.
195. Stuhlmeier, K.M. and C. Pollaschek, *Differential effect of transforming growth factor beta (TGF-beta) on the genes encoding hyaluronan synthases and utilization of the p38 MAPK pathway in TGF-beta-induced hyaluronan synthase 1 activation.* J Biol Chem, 2004. **279**(10): p. 8753-60.
196. Oguchi, T. and N. Ishiguro, *Differential stimulation of three forms of hyaluronan synthase by TGF-beta, IL-1beta, and TNF-alpha.* Connect Tissue Res, 2004. **45**(4-5): p. 197-205.
197. Suzuki, K., et al., *Expression of hyaluronan synthase in intraocular proliferative diseases: regulation of expression in human vascular endothelial cells by transforming growth factor-beta.* Jpn J Ophthalmol, 2003. **47**(6): p. 557-64.
198. Chow, G., J. Tauler, and J.L. Mulshine, *Cytokines and growth factors stimulate hyaluronan production: role of hyaluronan in epithelial to mesenchymal-like transition in non-small cell lung cancer.* J Biomed Biotechnol, 2010. **2010**: p. 485468.

199. Recklies, A.D., et al., *Differential regulation and expression of hyaluronan synthases in human articular chondrocytes, synovial cells and osteosarcoma cells.* Biochem J, 2001. **354**(Pt 1): p. 17-24.
200. Kaback, L.A. and T.J. Smith, *Expression of hyaluronan synthase messenger ribonucleic acids and their induction by interleukin-1beta in human orbital fibroblasts: potential insight into the molecular pathogenesis of thyroid-associated ophthalmopathy.* J Clin Endocrinol Metab, 1999. **84**(11): p. 4079-84.
201. van Zeijl, C.J., et al., *Effects of thyrotropin and thyrotropin-receptor-stimulating Graves' disease immunoglobulin G on cyclic adenosine monophosphate and hyaluronan production in nondifferentiated orbital fibroblasts of Graves' ophthalmopathy patients.* Thyroid, 2010. **20**(5): p. 535-44.
202. Yamada, Y., et al., *Differential regulation by IL-1beta and EGF of expression of three different hyaluronan synthases in oral mucosal epithelial cells and fibroblasts and dermal fibroblasts: quantitative analysis using real-time RT-PCR.* J Invest Dermatol, 2004. **122**(3): p. 631-9.
203. Li, L., et al., *Growth factor regulation of hyaluronan synthesis and degradation in human dermal fibroblasts: importance of hyaluronan for the mitogenic response of PDGF-BB.* Biochem J, 2007. **404**(2): p. 327-36.
204. Evanko, S.P., et al., *Platelet-derived growth factor stimulates the formation of versican-hyaluronan aggregates and pericellular matrix expansion in arterial smooth muscle cells.* Arch Biochem Biophys, 2001. **394**(1): p. 29-38.
205. Freudenberger, T., et al., *Estradiol inhibits hyaluronic acid synthase 1 expression in human vascular smooth muscle cells.* Basic Res Cardiol, 2011. **106**(6): p. 1099-109.
206. Kuroda, K., et al., *Up-regulation of putative hyaluronan synthase mRNA by basic fibroblast growth factor and insulin-like growth factor-1 in human skin fibroblasts.* J Dermatol Sci, 2001. **26**(2): p. 156-60.
207. Midgley, A.C. and T. Bowen, *Analysis of human hyaluronan synthase gene transcriptional regulation and downstream hyaluronan cell surface receptor mobility in myofibroblast differentiation.* Methods Mol Biol, 2015. **1229**: p. 605-18.
208. Udabage, L., et al., *Antisense-mediated suppression of hyaluronan synthase 2 inhibits the tumorigenesis and progression of breast cancer.* Cancer Res, 2005. **65**(14): p. 6139-50.
209. Chao, H. and A.P. Spicer, *Natural antisense mRNAs to hyaluronan synthase 2 inhibit hyaluronan biosynthesis and cell proliferation.* J Biol Chem, 2005. **280**(30): p. 27513-22.
210. El-Safory, N.S., A.E. Fazary, and C.K. Lee, *Hyaluronidases, a group of glycosidases: Current and future perspectives.* Carbohydrate Polymers, 2010. **81**(2): p. 165-181.
211. Csoka, A.B., G.I. Frost, and R. Stern, *The six hyaluronidase-like genes in the human and mouse genomes.* Matrix Biol, 2001. **20**(8): p. 499-508.
212. Csoka, A.B., S.W. Scherer, and R. Stern, *Expression analysis of six paralogous human hyaluronidase genes clustered on chromosomes 3p21 and 7q31.* Genomics, 1999. **60**(3): p. 356-61.
213. Frost, G.I., et al., *Purification, cloning, and expression of human plasma hyaluronidase.* Biochem Biophys Res Commun, 1997. **236**(1): p. 10-5.
214. Colombaro, V., et al., *Hyaluronidase 1 and hyaluronidase 2 are required for renal hyaluronan turnover.* Acta Histochem, 2015. **117**(1): p. 83-91.

215. Chowdhury, B., et al., *Murine hyaluronidase 2 deficiency results in extracellular hyaluronan accumulation and severe cardiopulmonary dysfunction.* J Biol Chem, 2013. **288**(1): p. 520-8.
216. Muggenthaler, M.M., et al., *Mutations in HYAL2, Encoding Hyaluronidase 2, Cause a Syndrome of Orofacial Clefting and Cor Triatriatum Sinister in Humans and Mice.* PLoS Genet, 2017. **13**(1): p. e1006470.
217. Stern, R. and M.J. Jedrzejas, *Hyaluronidases: their genomics, structures, and mechanisms of action.* Chem Rev, 2006. **106**(3): p. 818-39.
218. Midgley, A.C., et al., *Nuclear hyaluronidase 2 drives alternative splicing of CD44 pre-mRNA to determine profibrotic or antifibrotic cell phenotype.* Sci Signal, 2017. **10**(506).
219. Lepperdinger, G., B. Strobl, and G. Kreil, *HYAL2, a human gene expressed in many cells, encodes a lysosomal hyaluronidase with a novel type of specificity.* J Biol Chem, 1998. **273**(35): p. 22466-70.
220. Bourguignon, L.Y., et al., *CD44 interaction with Na+-H+ exchanger (NHE1) creates acidic microenvironments leading to hyaluronidase-2 and cathepsin B activation and breast tumor cell invasion.* J Biol Chem, 2004. **279**(26): p. 26991-7007.
221. Erickson, M. and R. Stern, *Chain gangs: new aspects of hyaluronan metabolism.* Biochem Res Int, 2012. **2012**: p. 893947.
222. Hemming, R., et al., *Mouse Hyal3 encodes a 45- to 56-kDa glycoprotein whose overexpression increases hyaluronidase 1 activity in cultured cells.* Glycobiology, 2008. **18**(4): p. 280-9.
223. Atmuri, V., et al., *Hyaluronidase 3 (HYAL3) knockout mice do not display evidence of hyaluronan accumulation.* Matrix Biol, 2008. **27**(8): p. 653-60.
224. Hsu, L.J., et al., *Transforming growth factor beta1 signaling via interaction with cell surface Hyal-2 and recruitment of WWOX/WOX1.* J Biol Chem, 2009. **284**(23): p. 16049-59.
225. Day, A.J. and G.D. Prestwich, *Hyaluronan-binding proteins: tying up the giant.* J Biol Chem, 2002. **277**(7): p. 4585-8.
226. Kohda, D., et al., *Solution structure of the link module: a hyaluronan-binding domain involved in extracellular matrix stability and cell migration.* Cell, 1996. **86**(5): p. 767-75.
227. Noble, P.W., *Hyaluronan and its catabolic products in tissue injury and repair.* Matrix Biol, 2002. **21**(1): p. 25-9.
228. Skandalis, S.S., et al., *Proteomic identification of CD44 interacting proteins.* IUBMB Life, 2010. **62**(11): p. 833-40.
229. Xu, H., et al., *The role of CD44 in epithelial-mesenchymal transition and cancer development.* Onco Targets Ther, 2015. **8**: p. 3783-92.
230. Barshishat, M., et al., *TNFalpha and IL-8 regulate the expression and function of CD44 variant proteins in human colon carcinoma cells.* Clin Exp Metastasis, 2002. **19**(4): p. 327-37.
231. Andhare, R.A., et al., *Hyaluronan promotes the chondrocyte response to BMP-7.* Osteoarthritis Cartilage, 2009. **17**(7): p. 906-16.
232. Chow, G., et al., *Increased expression of CD44 in bovine articular chondrocytes by catabolic cellular mediators.* J Biol Chem, 1995. **270**(46): p. 27734-41.
233. Nishida, Y., et al., *Osteogenic protein 1 stimulates cells-associated matrix assembly by normal human articular chondrocytes: up-regulation of hyaluronan synthase, CD44, and aggrecan.* Arthritis Rheum, 2000. **43**(1): p. 206-14.

234. Ono, Y., et al., *Chondrogenic capacity and alterations in hyaluronan synthesis of cultured human osteoarthritic chondrocytes.* Biochem Biophys Res Commun, 2013. **435**(4): p. 733-9.
235. Osada, A., et al., *Up-regulation of CD44 expression by tumor necrosis factor-alpha is neutralized by interleukin-10 in Langerhans cells.* J Invest Dermatol, 1995. **105**(1): p. 124-7.
236. Meran, S., et al., *Interleukin-1beta induces hyaluronan and CD44-dependent cell protrusions that facilitate fibroblast-monocyte binding.* Am J Pathol, 2013. **182**(6): p. 2223-40.
237. Ito, T., et al., *Hyaluronan regulates transforming growth factor-beta1 receptor compartmentalization.* J Biol Chem, 2004. **279**(24): p. 25326-32.
238. Bourguignon, L.Y., et al., *Hyaluronan promotes signaling interaction between CD44 and the transforming growth factor beta receptor I in metastatic breast tumor cells.* J Biol Chem, 2002. **277**(42): p. 39703-12.
239. Orian-Rousseau, V., *CD44 Acts as a Signaling Platform Controlling Tumor Progression and Metastasis.* Front Immunol, 2015. **6**: p. 154.
240. Misra, S., et al., *Interactions between Hyaluronan and Its Receptors (CD44, RHAMM) Regulate the Activities of Inflammation and Cancer.* Front Immunol, 2015. **6**: p. 201.
241. Lesley, J., R. Hyman, and P.W. Kincade, *CD44 and its interaction with extracellular matrix.* Adv Immunol, 1993. **54**: p. 271-335.
242. Danielson, B.T., C.B. Knudson, and W. Knudson, *Extracellular processing of the cartilage proteoglycan aggregate and its effect on CD44-mediated internalization of hyaluronan.* J Biol Chem, 2015. **290**(15): p. 9555-70.
243. Knudson, C.B., *Hyaluronan receptor-directed assembly of chondrocyte pericellular matrix.* J Cell Biol, 1993. **120**(3): p. 825-34.
244. Knudson, W., et al., *CD44-anchored hyaluronan-rich pericellular matrices: an ultrastructural and biochemical analysis.* Exp Cell Res, 1996. **228**(2): p. 216-28.
245. Wight, T.N., I. Kang, and M.J. Merrilees, *Versican and the control of inflammation.* Matrix Biol, 2014. **35**: p. 152-61.
246. Martin, J., et al., *Tumor Necrosis Factor-stimulated Gene 6 (TSG-6)-mediated Interactions with the Inter-alpha-inhibitor Heavy Chain 5 Facilitate Tumor Growth Factor beta1 (TGFbeta1)-dependent Fibroblast to Myofibroblast Differentiation.* J Biol Chem, 2016. **291**(26): p. 13789-801.
247. Yang, B., L. Zhang, and E.A. Turley, *Identification of two hyaluronan-binding domains in the hyaluronan receptor RHAMM.* J Biol Chem, 1993. **268**(12): p. 8617-23.
248. Turley, E.A., et al., *Ras-transformed cells express both CD44 and RHAMM hyaluronan receptors: only RHAMM is essential for hyaluronan-promoted locomotion.* Exp Cell Res, 1993. **207**(2): p. 277-82.
249. Maxwell, C.A., J. McCarthy, and E. Turley, *Cell-surface and mitotic-spindle RHAMM: moonlighting or dual oncogenic functions?* J Cell Sci, 2008. **121**(Pt 7): p. 925-32.
250. Turley, E.A., P.W. Noble, and L.Y. Bourguignon, *Signaling properties of hyaluronan receptors.* J Biol Chem, 2002. **277**(7): p. 4589-92.
251. Tolg, C., et al., *RHAMM promotes interphase microtubule instability and mitotic spindle integrity through MEK1/ERK1/2 activity.* J Biol Chem, 2010. **285**(34): p. 26461-74.
252. Tammi, M.I., A.J. Day, and E.A. Turley, *Hyaluronan and homeostasis: a balancing act.* J Biol Chem, 2002. **277**(7): p. 4581-4.

253. Meran, S., et al., *Hyaluronan facilitates transforming growth factor-beta1-mediated fibroblast proliferation.* J Biol Chem, 2008. **283**(10): p. 6530-45.
254. Kawasaki, T. and T. Kawai, *Toll-like receptor signaling pathways.* Front Immunol, 2014. **5**: p. 461.
255. Bjermer, L., et al., *Hyaluronic acid in bronchoalveolar lavage fluid in patients with sarcoidosis: relationship to lavage mast cells.* Thorax, 1987. **42**(12): p. 933-8.
256. Colombel, J.F., et al., *Hyaluronic acid and type III procollagen peptide in jejunal perfusion fluid as markers of connective tissue turnover.* Gastroenterology, 1989. **96**(1): p. 68-73.
257. Dahl, L.B., et al., *Concentration and molecular weight of sodium hyaluronate in synovial fluid from patients with rheumatoid arthritis and other arthropathies.* Ann Rheum Dis, 1985. **44**(12): p. 817-22.
258. Engstrom-Laurent, A. and R. Hallgren, *Circulating hyaluronate in rheumatoid arthritis: relationship to inflammatory activity and the effect of corticosteroid therapy.* Ann Rheum Dis, 1985. **44**(2): p. 83-8.
259. Engstrom-Laurent, A., et al., *Raised serum hyaluronate levels in scleroderma: an effect of growth factor induced activation of connective tissue cells?* Ann Rheum Dis, 1985. **44**(9): p. 614-20.
260. Engstrom-Laurent, A. and R. Hallgren, *Circulating hyaluronic acid levels vary with physical activity in healthy subjects and in rheumatoid arthritis patients. Relationship to synovitis mass and morning stiffness.* Arthritis Rheum, 1987. **30**(12): p. 1333-8.
261. Hallgren, R., et al., *Hyaluronate in bronchoalveolar lavage fluid: a new marker in sarcoidosis reflecting pulmonary disease.* Br Med J (Clin Res Ed), 1985. **290**(6484): p. 1778-81.
262. Hallgren, R., A. Engstrom-Laurent, and U. Nisbeth, *Circulating hyaluronate. A potential marker of altered metabolism of the connective tissue in uremia.* Nephron, 1987. **46**(2): p. 150-4.
263. Lundin, A., et al., *Circulating hyaluronate in psoriasis.* Br J Dermatol, 1985. **112**(6): p. 663-71.
264. Wells, A., et al., *Increased hyaluronan in acutely rejecting human kidney grafts.* Transplantation, 1993. **55**(6): p. 1346-9.
265. Wells, A., et al., *Role of hyaluronan in chronic and acutely rejecting kidneys.* Transplant Proc, 1993. **25**(2): p. 2048-9.
266. Sanchez-Rodriguez, A., et al., *Correlation of high levels of hyaluronan and cytokines (IL-1beta, IL-6, and TGF-beta) in ascitic fluid of cirrhotic patients.* Dig Dis Sci, 2000. **45**(11): p. 2229-32.
267. Goldberg, R.L., et al., *Elevated plasma levels of hyaluronate in patients with osteoarthritis and rheumatoid arthritis.* Arthritis Rheum, 1991. **34**(7): p. 799-807.
268. Jouzeau, J.Y., et al., *Clinical significance of hyaluronan in rheumatic diseases: comment on the articles by Goldberg et al and Woessner.* Arthritis Rheum, 1992. **35**(10): p. 1253-4.
269. Petrey, A.C. and C.A. de la Motte, *Hyaluronan, a crucial regulator of inflammation.* Front Immunol, 2014. **5**: p. 101.
270. Kobayashi, I. and M. Ziff, *Electron microscopic studies of lymphoid cells in the rheumatoid synovial membrane.* Arthritis Rheum, 1973. **16**(4): p. 471-86.
271. Ishikawa, H. and M. Ziff, *Electron microscopic observations of immunoreactive cells in the rheumatoid synovial membrane.* Arthritis Rheum, 1976. **19**(1): p. 1-14.

272. Jiang, D., et al., *Regulation of lung injury and repair by Toll-like receptors and hyaluronan.* Nat Med, 2005. **11**(11): p. 1173-9.
273. Nakamura, K., et al., *High, but not low, molecular weight hyaluronan prevents T-cell-mediated liver injury by reducing proinflammatory cytokines in mice.* J Gastroenterol, 2004. **39**(4): p. 346-54.
274. Teder, P., et al., *Resolution of lung inflammation by CD44.* Science, 2002. **296**(5565): p. 155-8.
275. Termeer, C., et al., *Oligosaccharides of Hyaluronan activate dendritic cells via toll-like receptor 4.* J Exp Med, 2002. **195**(1): p. 99-111.
276. Fieber, C., et al., *Hyaluronan-oligosaccharide-induced transcription of metalloproteases.* J Cell Sci, 2004. **117**(Pt 2): p. 359-67.
277. Khaldoyanidi, S., et al., *Hyaluronate-enhanced hematopoiesis: two different receptors trigger the release of interleukin-1beta and interleukin-6 from bone marrow macrophages.* Blood, 1999. **94**(3): p. 940-9.
278. Campo, G.M., et al., *Inhibition of small HA fragment activity and stimulation of A2A adenosine receptor pathway limit apoptosis and reduce cartilage damage in experimental arthritis.* Histochem Cell Biol, 2015. **143**(5): p. 531-43.
279. Campo, G.M., et al., *Adenosine A2A receptor activation and hyaluronan fragment inhibition reduce inflammation in mouse articular chondrocytes stimulated with interleukin-1beta.* FEBS J, 2012. **279**(12): p. 2120-33.
280. Avenoso, A., et al., *Hyaluronan in experimental injured/inflamed cartilage: In vivo studies.* Life Sci, 2018. **193**: p. 132-140.
281. Scheibner, K.A., et al., *Hyaluronan fragments act as an endogenous danger signal by engaging TLR2.* J Immunol, 2006. **177**(2): p. 1272-81.
282. Iijima, J., K. Konno, and N. Itano, *Inflammatory alterations of the extracellular matrix in the tumor microenvironment.* Cancers (Basel), 2011. **3**(3): p. 3189-205.
283. Anders, H.J. and L. Schaefer, *Beyond tissue injury-damage-associated molecular patterns, toll-like receptors, and inflammasomes also drive regeneration and fibrosis.* J Am Soc Nephrol, 2014. **25**(7): p. 1387-400.
284. Colmont, C.S., et al., *Human peritoneal mesothelial cells respond to bacterial ligands through a specific subset of Toll-like receptors.* Nephrol Dial Transplant, 2011. **26**(12): p. 4079-90.
285. Raby, A.C., et al., *Toll-Like Receptors 2 and 4 Are Potential Therapeutic Targets in Peritoneal Dialysis-Associated Fibrosis.* J Am Soc Nephrol, 2017. **28**(2): p. 461-478.
286. Taylor, K.R., et al., *Hyaluronan fragments stimulate endothelial recognition of injury through TLR4.* J Biol Chem, 2004. **279**(17): p. 17079-84.
287. Fielding, C.A., et al., *Interleukin-6 signaling drives fibrosis in unresolved inflammation.* Immunity, 2014. **40**(1): p. 40-50.
288. de la Motte, C.A., et al., *Mononuclear leukocytes bind to specific hyaluronan structures on colon mucosal smooth muscle cells treated with polyinosinic acid:polycytidylic acid: inter-alpha-trypsin inhibitor is crucial to structure and function.* Am J Pathol, 2003. **163**(1): p. 121-33.
289. Selbi, W., et al., *Characterization of hyaluronan cable structure and function in renal proximal tubular epithelial cells.* Kidney Int, 2006. **70**(7): p. 1287-95.
290. Mahadevan, P., et al., *Increased hyaluronan production in the glomeruli from diabetic rats: a link between glucose-induced prostaglandin production and reduced sulphated proteoglycan.* Diabetologia, 1995. **38**(3): p. 298-305.

291. Young, B.A., et al., *Cellular events in the evolution of experimental diabetic nephropathy.* Kidney Int, 1995. **47**(3): p. 935-44.
292. Sadowitz, B., et al., *The role of hyaluronic acid in atherosclerosis and intimal hyperplasia.* J Surg Res, 2012. **173**(2): p. e63-72.
293. Day, A.J. and C.A. de la Motte, *Hyaluronan cross-linking: a protective mechanism in inflammation?* Trends Immunol, 2005. **26**(12): p. 637-43.
294. Hascall, V.C., et al., *Intracellular hyaluronan: a new frontier for inflammation?* Biochim Biophys Acta, 2004. **1673**(1-2): p. 3-12.
295. Majors, A.K., et al., *Endoplasmic reticulum stress induces hyaluronan deposition and leukocyte adhesion.* J Biol Chem, 2003. **278**(47): p. 47223-31.
296. Selbi, W., et al., *BMP-7 modulates hyaluronan-mediated proximal tubular cell-monocyte interaction.* J Am Soc Nephrol, 2004. **15**(5): p. 1199-211.
297. McDonald, B. and P. Kubes, *Interactions between CD44 and Hyaluronan in Leukocyte Trafficking.* Front Immunol, 2015. **6**: p. 68.
298. Mummert, M.E., et al., *Development of a peptide inhibitor of hyaluronan-mediated leukocyte trafficking.* J Exp Med, 2000. **192**(6): p. 769-79.
299. DeGrendele, H.C., et al., *CD44 and its ligand hyaluronate mediate rolling under physiologic flow: a novel lymphocyte-endothelial cell primary adhesion pathway.* J Exp Med, 1996. **183**(3): p. 1119-30.
300. Hoogewerf, A.J., et al., *Glycosaminoglycans mediate cell surface oligomerization of chemokines.* Biochemistry, 1997. **36**(44): p. 13570-8.
301. Kuschert, G.S., et al., *Glycosaminoglycans interact selectively with chemokines and modulate receptor binding and cellular responses.* Biochemistry, 1999. **38**(39): p. 12959-68.
302. Tanaka, Y., D.H. Adams, and S. Shaw, *Proteoglycans on endothelial cells present adhesion-inducing cytokines to leukocytes.* Immunol Today, 1993. **14**(3): p. 111-5.
303. Butler, L.M., G.E. Rainger, and G.B. Nash, *A role for the endothelial glycosaminoglycan hyaluronan in neutrophil recruitment by endothelial cells cultured for prolonged periods.* Exp Cell Res, 2009. **315**(19): p. 3433-41.
304. Noble, P.W. and D. Jiang, *Matrix regulation of lung injury, inflammation, and repair: the role of innate immunity.* Proc Am Thorac Soc, 2006. **3**(5): p. 401-4.
305. Garantziotis, S., et al., *The role of hyaluronan in the pathobiology and treatment of respiratory disease.* Am J Physiol Lung Cell Mol Physiol, 2016. **310**(9): p. L785-95.
306. Excellence, N.I.f.H.a.C., *Idiopathic pulmonary fibrosis in adults: diagnosis and management.* NICE Guideline [CG163], 2013.
307. Inokoshi, Y., et al., *Clinical significance of serum hyaluronan in chronic fibrotic interstitial pneumonia.* Respirology, 2013. **18**(8): p. 1236-43.
308. Papakonstantinou, E., et al., *Increased hyaluronic acid content in idiopathic pulmonary arterial hypertension.* Eur Respir J, 2008. **32**(6): p. 1504-12.
309. de la Motte, C.A., *Hyaluronan in intestinal homeostasis and inflammation: implications for fibrosis.* Am J Physiol Gastrointest Liver Physiol, 2011. **301**(6): p. G945-9.
310. Gudowska, M., B. Cylwik, and L. Chrostek, *The role of serum hyaluronic acid determination in the diagnosis of liver fibrosis.* Acta Biochim Pol, 2017. **64**(3): p. 451-457.
311. Gudowska, M., et al., *Hyaluronic acid concentration in liver diseases.* Clin Exp Med, 2016. **16**(4): p. 523-528.

312. Sano, N., K. Kitazawa, and T. Sugisaki, *Localization and roles of CD44, hyaluronic acid and osteopontin in IgA nephropathy.* Nephron, 2001. **89**(4): p. 416-21.
313. Yung, S., D.Y. Yap, and T.M. Chan, *Recent advances in the understanding of renal inflammation and fibrosis in lupus nephritis.* F1000Res, 2017. **6**: p. 874.
314. Jun, Z., et al., *CD44 and hyaluronan expression in the development of experimental crescentic glomerulonephritis.* Clin Exp Immunol, 1997. **108**(1): p. 69-77.
315. Colombaro, V., et al., *Inhibition of hyaluronan is protective against renal ischaemia-reperfusion injury.* Nephrol Dial Transplant, 2013. **28**(10): p. 2484-93.
316. Decleves, A.E., et al., *Dynamics of hyaluronan, CD44, and inflammatory cells in the rat kidney after ischemia/reperfusion injury.* Int J Mol Med, 2006. **18**(1): p. 83-94.
317. Decleves, A.E., et al., *Synthesis and fragmentation of hyaluronan in renal ischaemia.* Nephrol Dial Transplant, 2012. **27**(10): p. 3771-81.
318. Lewis, A., et al., *Diabetic nephropathy, inflammation, hyaluronan and interstitial fibrosis.* Histol Histopathol, 2008. **23**(6): p. 731-9.
319. Albeiroti, S., A. Soroosh, and C.A. de la Motte, *Hyaluronan's Role in Fibrosis: A Pathogenic Factor or a Passive Player?* Biomed Res Int, 2015. **2015**: p. 790203.
320. Li, Y., et al., *Hyaluronan synthase 2 regulates fibroblast senescence in pulmonary fibrosis.* Matrix Biol, 2016. **55**: p. 35-48.
321. Savani, R.C., et al., *A role for hyaluronan in macrophage accumulation and collagen deposition after bleomycin-induced lung injury.* Am J Respir Cell Mol Biol, 2000. **23**(4): p. 475-84.
322. Li, Y., et al., *Severe lung fibrosis requires an invasive fibroblast phenotype regulated by hyaluronan and CD44.* J Exp Med, 2011. **208**(7): p. 1459-71.
323. Cantor, J.O., et al., *Aerosolized hyaluronan limits airspace enlargement in a mouse model of cigarette smoke-induced pulmonary emphysema.* Exp Lung Res, 2005. **31**(4): p. 417-30.
324. Watsky, M.A., et al., *New insights into the mechanism of fibroblast to myofibroblast transformation and associated pathologies.* Int Rev Cell Mol Biol, 2010. **282**: p. 165-92.
325. Border, W.A. and N.A. Noble, *Transforming growth factor beta in tissue fibrosis.* N Engl J Med, 1994. **331**(19): p. 1286-92.
326. Border, W.A. and N.A. Noble, *Fibrosis linked to TGF-beta in yet another disease.* J Clin Invest, 1995. **96**(2): p. 655-6.
327. Border, W.A. and N.A. Noble, *TGF-beta in kidney fibrosis: a target for gene therapy.* Kidney Int, 1997. **51**(5): p. 1388-96.
328. al-Khateeb, T., et al., *An investigation of preferential fibroblast wound repopulation using a novel in vitro wound model.* J Periodontol, 1997. **68**(11): p. 1063-9.
329. Bochaton-Piallat, M.L., G. Gabbiani, and B. Hinz, *The myofibroblast in wound healing and fibrosis: answered and unanswered questions.* F1000Res, 2016. **5**.
330. Otranto, M., et al., *The role of the myofibroblast in tumor stroma remodeling.* Cell Adh Migr, 2012. **6**(3): p. 203-19.
331. Carthy, J.M., *TGFbeta signaling and the control of myofibroblast differentiation: Implications for chronic inflammatory disorders.* J Cell Physiol, 2018. **233**(1): p. 98-106.
332. Midgley, A.C., et al., *Transforming growth factor-beta1 (TGF-beta1)-stimulated fibroblast to myofibroblast differentiation is mediated by hyaluronan (HA)-facilitated epidermal growth factor receptor (EGFR) and CD44 co-localization in lipid rafts.* J Biol Chem, 2013. **288**(21): p. 14824-38.

333. Bommaya, G., et al., *Tumour necrosis factor-stimulated gene (TSG)-6 controls epithelial-mesenchymal transition of proximal tubular epithelial cells.* Int J Biochem Cell Biol, 2011. **43**(12): p. 1739-46.
334. Peterson, R.S., et al., *CD44 modulates Smad1 activation in the BMP-7 signaling pathway.* J Cell Biol, 2004. **166**(7): p. 1081-91.
335. Breborowicz, A., et al., *Intraperitoneal hyaluronan administration in conscious rats: absorption, metabolism, and effects on peritoneal fluid dynamics.* Perit Dial Int, 2001. **21**(2): p. 130-5.
336. Yamagata, K., C. Tomida, and A. Koyama, *Intraperitoneal hyaluronan production in stable continuous ambulatory peritoneal dialysis patients.* Perit Dial Int, 1999. **19**(2): p. 131-7.
337. Williams, J.D., et al., *The Euro-Balance Trial: the effect of a new biocompatible peritoneal dialysis fluid (balance) on the peritoneal membrane.* Kidney Int, 2004. **66**(1): p. 408-18.
338. Johnson, D.W., et al., *The effects of biocompatible compared with standard peritoneal dialysis solutions on peritonitis microbiology, treatment, and outcomes: the balANZ trial.* Perit Dial Int, 2012. **32**(5): p. 497-506.
339. Polubinska, A., et al., *Dialysis solution containing hyaluronan: effect on peritoneal permeability and inflammation in rats.* Kidney Int, 2000. **57**(3): p. 1182-9.
340. Rosengren, B.I., et al., *Isolation of interstitial fluid and demonstration of local proinflammatory cytokine production and increased absorptive gradient in chronic peritoneal dialysis.* Am J Physiol Renal Physiol, 2013. **304**(2): p. F198-206.
341. Yung, S., et al., *The source and possible significance of hyaluronan in the peritoneal cavity.* Kidney international, 1994. **46**(2): p. 527-533.
342. Yung, S., G.A. Coles, and M. Davies, *IL-1 beta, a major stimulator of hyaluronan synthesis in vitro of human peritoneal mesothelial cells: relevance to peritonitis in CAPD.* Kidney Int, 1996. **50**(4): p. 1337-43.
343. Breborowicz, A., et al., *Synthesis of hyaluronic acid by human peritoneal mesothelial cells: effect of cytokines and dialysate.* Perit Dial Int, 1996. **16**(4): p. 374-8.
344. Breborowicz, A., M. Breborowicz, and D.G. Oreopoulos, *Glucose-induced changes in the phenotype of human peritoneal mesothelial cells: effect of L-2-oxothiazolidine carboxylic acid.* Am J Nephrol, 2003. **23**(6): p. 471-6.
345. Stylianou, E., et al., *Isolation, culture and characterization of human peritoneal mesothelial cells.* Kidney Int, 1990. **37**(6): p. 1563-1570.
346. Yung, S., G.J. Thomas, and M. Davies, *Induction of hyaluronan metabolism after mechanical injury of human peritoneal mesothelial cells in vitro.* Kidney international, 2000. **58**(5): p. 1953-1962.
347. Horiuchi, T., et al., *Image analysis of remesothelialization following chemical wounding of cultured human peritoneal mesothelial cells: the role of hyaluronan synthesis.* Kidney Int, 2003. **64**(6): p. 2280-90.
348. Ito, T., et al., *Hyaluronan attenuates transforming growth factor-beta1-mediated signaling in renal proximal tubular epithelial cells.* Am J Pathol, 2004. **164**(6): p. 1979-88.
349. Lee, H.B. and H. Ha, *Mechanisms of epithelial-mesenchymal transition of peritoneal mesothelial cells during peritoneal dialysis.* J Korean Med Sci, 2007. **22**(6): p. 943-5.

350. Motazed, R., et al., *BMP-7 and proximal tubule epithelial cells: activation of multiple signaling pathways reveals a novel anti-fibrotic mechanism.* Pharm Res, 2008. **25**(10): p. 2440-6.
351. Weiskirchen, R. and S.K. Meurer, *BMP-7 counteracting TGF-beta1 activities in organ fibrosis.* Front Biosci (Landmark Ed), 2013. **18**: p. 1407-34.
352. Pegorier, S., et al., *Bone morphogenetic protein (BMP)-4 and BMP-7 regulate differentially transforming growth factor (TGF)-beta1 in normal human lung fibroblasts (NHLF).* Respir Res, 2010. **11**: p. 85.
353. Yu, M.-A., et al., *HGF and BMP-7 ameliorate high glucose–induced epithelial-to-mesenchymal transition of peritoneal mesothelium.* Journal of the American Society of Nephrology, 2009. **20**(3): p. 567-581.
354. Loureiro, J., et al., *BMP-7 blocks mesenchymal conversion of mesothelial cells and prevents peritoneal damage induced by dialysis fluid exposure.* Nephrol Dial Transplant, 2010. **25**(4): p. 1098-108.
355. Vargha, R., et al., *Ex vivo reversal of in vivo transdifferentiation in mesothelial cells grown from peritoneal dialysate effluents.* Nephrol Dial Transplant, 2006. **21**(10): p. 2943-7.
356. Nakamura, T., et al., *Hyaluronic-acid-deficient extracellular matrix induced by addition of 4-methylumbelliferone to the medium of cultured human skin fibroblasts.* Biochem Biophys Res Commun, 1995. **208**(2): p. 470-5.
357. Rilla, K., et al., *The hyaluronan synthesis inhibitor 4-methylumbelliferone prevents keratinocyte activation and epidermal hyperproliferation induced by epidermal growth factor.* J Invest Dermatol, 2004. **123**(4): p. 708-14.
358. Rilla, K., et al., *Pericellular hyaluronan coat visualized in live cells with a fluorescent probe is scaffolded by plasma membrane protrusions.* J Histochem Cytochem, 2008. **56**(10): p. 901-10.
359. Kudo, D., et al., *Effect of a hyaluronan synthase suppressor, 4-methylumbelliferone, on B16F-10 melanoma cell adhesion and locomotion.* Biochem Biophys Res Commun, 2004. **321**(4): p. 783-7.
360. Nakazawa, H., et al., *4-methylumbelliferone, a hyaluronan synthase suppressor, enhances the anticancer activity of gemcitabine in human pancreatic cancer cells.* Cancer Chemother Pharmacol, 2006. **57**(2): p. 165-70.
361. Patel, P., et al., *Smad3-dependent and -independent pathways are involved in peritoneal membrane injury.* Kidney International, 2010. **77**(4): p. 319-328.
362. Ito, T., et al., *Hyaluronan and proximal tubular cell migration.* Kidney Int, 2004. **65**(3): p. 823-33.
363. Jones, S.G., T. Ito, and A.O. Phillips, *Regulation of proximal tubular epithelial cell CD44-mediated binding and internalisation of hyaluronan.* Int J Biochem Cell Biol, 2003. **35**(9): p. 1361-77.
364. Porsch, H., et al., *Efficient TGFbeta-induced epithelial-mesenchymal transition depends on hyaluronan synthase HAS2.* Oncogene, 2013. **32**(37): p. 4355-65.
365. Toole, B.P., et al., *Hyaluronan: a critical component of epithelial-mesenchymal and epithelial-carcinoma transitions.* Cells Tissues Organs, 2005. **179**(1-2): p. 66-72.
366. Moustakas, A. and P. Heldin, *TGFbeta and matrix-regulated epithelial to mesenchymal transition.* Biochim Biophys Acta, 2014. **1840**(8): p. 2621-34.

367. Bouris, P., et al., *Estrogen receptor alpha mediates epithelial to mesenchymal transition, expression of specific matrix effectors and functional properties of breast cancer cells.* Matrix Biol, 2015. **43**: p. 42-60.
368. Cieply, B., C. Koontz, and S.M. Frisch, *CD44S-hyaluronan interactions protect cells resulting from EMT against anoikis.* Matrix Biol, 2015. **48**: p. 55-65.
369. Itano, N. and K. Kimata, *Altered hyaluronan biosynthesis in cancer progression.* Semin Cancer Biol, 2008. **18**(4): p. 268-74.
370. Itano, N., L. Zhuo, and K. Kimata, *Impact of the hyaluronan-rich tumor microenvironment on cancer initiation and progression.* Cancer Sci, 2008. **99**(9): p. 1720-5.
371. Li, Y., et al., *Silencing of hyaluronan synthase 2 suppresses the malignant phenotype of invasive breast cancer cells.* Int J Cancer, 2007. **120**(12): p. 2557-67.
372. Sironen, R.K., et al., *Hyaluronan in human malignancies.* Exp Cell Res, 2011. **317**(4): p. 383-91.
373. Webber, J., et al., *Cancer exosomes trigger fibroblast to myofibroblast differentiation.* Cancer Res, 2010. **70**(23): p. 9621-30.
374. Breborowicz, A., et al., *Role of peritoneal mesothelial cells and fibroblasts in the synthesis of hyaluronan during peritoneal dialysis.* Perit Dial Int, 1998. **18**(4): p. 382-6.
375. Lai, K.N., et al., *Increased production of hyaluronan by peritoneal cells and its significance in patients on CAPD.* Am J Kidney Dis, 1999. **33**(2): p. 318-24.
376. Ha, H., M.R. Yu, and H.B. Lee, *High glucose-induced PKC activation mediates TGF-beta 1 and fibronectin synthesis by peritoneal mesothelial cells.* Kidney Int, 2001. **59**(2): p. 463-70.
377. Zweers, M.M., et al., *Growth factors VEGF and TGF-beta1 in peritoneal dialysis.* J Lab Clin Med, 1999. **134**(2): p. 124-32.
378. Stojimirovic, B., et al., *Levels of transforming growth factor beta1 during first six months of peritoneal dialysis.* Ren Fail, 2015. **37**(4): p. 640-5.
379. Gangji, A.S., K.S. Brimble, and P.J. Margetts, *Association between markers of inflammation, fibrosis and hypervolemia in peritoneal dialysis patients.* Blood Purif, 2009. **28**(4): p. 354-8.
380. Yao, Q., et al., *The role of the TGF/Smad signaling pathway in peritoneal fibrosis induced by peritoneal dialysis solutions.* Nephron Exp Nephrol, 2008. **109**(2): p. e71-8.
381. Zoltan-Jones, A., et al., *Elevated hyaluronan production induces mesenchymal and transformed properties in epithelial cells.* J Biol Chem, 2003. **278**(46): p. 45801-10.
382. Grass, G.D., et al., *CD147, CD44, and the epidermal growth factor receptor (EGFR) signaling pathway cooperate to regulate breast epithelial cell invasiveness.* J Biol Chem, 2013. **288**(36): p. 26089-104.
383. Heffler, M., et al., *FAK and HAS inhibition synergistically decrease colon cancer cell viability and affect expression of critical genes.* Anticancer Agents Med Chem, 2013. **13**(4): p. 584-94.
384. Hiraga, T., S. Ito, and H. Nakamura, *Cancer stem-like cell marker CD44 promotes bone metastases by enhancing tumorigenicity, cell motility, and hyaluronan production.* Cancer Res, 2013. **73**(13): p. 4112-22.
385. Misra, S., et al., *Hyaluronan-CD44 interactions as potential targets for cancer therapy.* FEBS J, 2011. **278**(9): p. 1429-43.
386. Voon, D.C., et al., *EMT-induced stemness and tumorigenicity are fueled by the EGFR/Ras pathway.* PLoS One, 2013. **8**(8): p. e70427.

387. Li, L., et al., *Transforming growth factor-beta1 induces EMT by the transactivation of epidermal growth factor signaling through HA/CD44 in lung and breast cancer cells.* International Journal of Molecular Medicine, 2015. **36**(1): p. 113-22.
388. Kakizaki, I., et al., *A novel mechanism for the inhibition of hyaluronan biosynthesis by 4-methylumbelliferone.* J Biol Chem, 2004. **279**(32): p. 33281-9.
389. Ishizuka, S., et al., *4-Methylumbelliferone Diminishes Catabolically Activated Articular Chondrocytes and Cartilage Explants via a Mechanism Independent of Hyaluronan Inhibition.* J Biol Chem, 2016. **291**(23): p. 12087-104.
390. Chan, D.D., et al., *Deficiency of hyaluronan synthase 1 (Has1) results in chronic joint inflammation and widespread intra-articular fibrosis in a murine model of knee joint cartilage damage.* Osteoarthritis Cartilage, 2015. **23**(11): p. 1879-89.
391. Assmann, V., et al., *The human hyaluronan receptor RHAMM is expressed as an intracellular protein in breast cancer cells.* J Cell Sci, 1998. **111 (Pt 12)**: p. 1685-94.
392. Assmann, V., et al., *The intracellular hyaluronan receptor RHAMM/IHABP interacts with microtubules and actin filaments.* J Cell Sci, 1999. **112 (Pt 22)**: p. 3943-54.
393. Clark, R.A., R. Alon, and T.A. Springer, *CD44 and hyaluronan-dependent rolling interactions of lymphocytes on tonsillar stroma.* J Cell Biol, 1996. **134**(4): p. 1075-87.
394. Wang, Q., et al., *CD44 deficiency leads to enhanced neutrophil migration and lung injury in Escherichia coli pneumonia in mice.* Am J Pathol, 2002. **161**(6): p. 2219-28.
395. Bourguignon, L.Y., D. Zhu, and H. Zhu, *CD44 isoform-cytoskeleton interaction in oncogenic signaling and tumor progression.* Front Biosci, 1998. **3**: p. d637-49.
396. Rampanelli, E., et al., *Opposite role of CD44-standard and CD44-variant-3 in tubular injury and development of renal fibrosis during chronic obstructive nephropathy.* Kidney Int, 2014. **86**(3): p. 558-69.
397. Misra, S., et al., *Delivery of CD44 shRNA/nanoparticles within cancer cells: perturbation of hyaluronan/CD44v6 interactions and reduction in adenoma growth in Apc Min/+ MICE.* J Biol Chem, 2009. **284**(18): p. 12432-46.
398. Guo, W. and P.S. Frenette, *Alternative CD44 splicing in intestinal stem cells and tumorigenesis.* Oncogene, 2014. **33**(5): p. 537-8.
399. Seiter, S., D.S. Schmidt, and M. Zoller, *The CD44 variant isoforms CD44v6 and CD44v7 are expressed by distinct leukocyte subpopulations and exert non-overlapping functional activities.* Int Immunol, 2000. **12**(1): p. 37-49.
400. Zoller, M., *CD44: physiological expression of distinct isoforms as evidence for organ-specific metastasis formation.* J Mol Med (Berl), 1995. **73**(9): p. 425-38.
401. Kasper, M., et al., *Distinct expression patterns of CD44 isoforms during human lung development and in pulmonary fibrosis.* Am J Respir Cell Mol Biol, 1995. **13**(6): p. 648-56.
402. Pei, D., et al., *Mesenchymal-epithelial transition in development and reprogramming.* Nat Cell Biol, 2019. **21**(1): p. 44-53.
403. Kalluri, R. and E.G. Neilson, *Epithelial-mesenchymal transition and its implications for fibrosis.* J Clin Invest, 2003. **112**(12): p. 1776-84.
404. Zeisberg, E.M., et al., *Endothelial-to-mesenchymal transition contributes to cardiac fibrosis.* Nat Med, 2007. **13**(8): p. 952-61.
405. Zeisberg, M., et al., *Fibroblasts derive from hepatocytes in liver fibrosis via epithelial to mesenchymal transition.* J Biol Chem, 2007. **282**(32): p. 23337-47.
406. Kalluri, R. and M. Zeisberg, *Exploring the connection between chronic renal fibrosis and bone morphogenic protein-7.* Histol Histopathol, 2003. **18**(1): p. 217-24.

407. Kinoshita, K., et al., *Adenovirus-mediated expression of BMP-7 suppresses the development of liver fibrosis in rats.* Gut, 2007. **56**(5): p. 706-14.
408. Myllarniemi, M., et al., *Gremlin-mediated decrease in bone morphogenetic protein signaling promotes pulmonary fibrosis.* Am J Respir Crit Care Med, 2008. **177**(3): p. 321-9.
409. Yang, G., et al., *Bone morphogenetic protein-7 inhibits silica-induced pulmonary fibrosis in rats.* Toxicol Lett, 2013. **220**(2): p. 103-8.
410. Buijs, J.T., et al., *Bone morphogenetic protein 7 in the development and treatment of bone metastases from breast cancer.* Cancer Res, 2007. **67**(18): p. 8742-51.
411. Zabkiewicz, C., et al., *Bone morphogenetic proteins, breast cancer, and bone metastases: striking the right balance.* Endocr Relat Cancer, 2017. **24**(10): p. R349-R366.
412. Derynck, R. and Y.E. Zhang, *Smad-dependent and Smad-independent pathways in TGF-beta family signalling.* Nature, 2003. **425**(6958): p. 577-84.
413. Hu, M.C., et al., *p38MAPK acts in the BMP7-dependent stimulatory pathway during epithelial cell morphogenesis and is regulated by Smad1.* J Biol Chem, 2004. **279**(13): p. 12051-9.
414. Leung, J.C., et al., *Regulation of CCN2/CTGF and related cytokines in cultured peritoneal cells under conditions simulating peritoneal dialysis.* Nephrol Dial Transplant, 2009. **24**(2): p. 458-69.
415. Zarrinkalam, K.H., et al., *Connective tissue growth factor and its regulation in the peritoneal cavity of peritoneal dialysis patients.* Kidney Int, 2003. **64**(1): p. 331-8.
416. Szeto, C.C., et al., *Differential effects of transforming growth factor-beta on the synthesis of connective tissue growth factor and vascular endothelial growth factor by peritoneal mesothelial cell.* Nephron Exp Nephrol, 2005. **99**(4): p. e95-e104.
417. Mizutani, M., et al., *Connective tissue growth factor (CTGF/CCN2) is increased in peritoneal dialysis patients with high peritoneal solute transport rate.* Am J Physiol Renal Physiol, 2010. **298**(3): p. F721-33.
418. Zeisberg, M., *Bone morphogenic protein-7 and the kidney: current concepts and open questions.* Nephrol Dial Transplant, 2006. **21**(3): p. 568-73.
419. Luo, N., et al., *CD44 and hyaluronan promote the bone morphogenetic protein 7 signaling response in murine chondrocytes.* Arthritis Rheumatol, 2014. **66**(6): p. 1547-58.
420. Wu, R.L., et al., *Hyaluronic acid-CD44 interactions promote BMP4/7-dependent Id1/3 expression in melanoma cells.* Sci Rep, 2018. **8**(1): p. 14913.
421. Steinhauer, H.B., B. Gunter, and P. Schollmeyer, *Stimulation of peritoneal synthesis of vasoactive prostaglandins during peritonitis in patients on continuous ambulatory peritoneal dialysis.* Eur J Clin Invest, 1985. **15**(1): p. 1-5.
422. Steinhauer, H.B. and P. Schollmeyer, *Prostaglandin-mediated loss of proteins during peritonitis in continuous ambulatory peritoneal dialysis.* Kidney Int, 1986. **29**(2): p. 584-90.
423. Moutabarrik, A., et al., *Interleukin-1 and its naturally occurring antagonist in peritoneal dialysis patients.* Clin Nephrol, 1995. **43**(4): p. 243-8.
424. Zemel, D., et al., *Appearance of tumor necrosis factor-alpha and soluble TNF-receptors I and II in peritoneal effluent of CAPD.* Kidney Int, 1994. **46**(5): p. 1422-30.

425. Zemel, D. and R.T. Krediet, *Cytokine patterns in the effluent of continuous ambulatory peritoneal dialysis: relationship to peritoneal permeability.* Blood Purif, 1996. **14**(2): p. 198-216.
426. Brauner, A., B. Hylander, and B. Wretlind, *Interleukin-6 and interleukin-8 in dialysate and serum from patients on continuous ambulatory peritoneal dialysis.* Am J Kidney Dis, 1993. **22**(3): p. 430-5.
427. Brauner, A., B. Hylander, and B. Wretlind, *Tumor necrosis factor-alpha, interleukin-1 beta, and interleukin-1 receptor antagonist in dialysate and serum from patients on continuous ambulatory peritoneal dialysis.* Am J Kidney Dis, 1996. **27**(3): p. 402-8.
428. Lu, Y., B. Hylander, and A. Brauner, *Interleukin-10, interferon gamma, interleukin-2, and soluble interleukin-2 receptor alpha detected during peritonitis in the dialysate and serum of patients on continuous ambulatory peritoneal dialysis.* Perit Dial Int, 1996. **16**(6): p. 607-12.
429. Witowski, J., et al., *Superinduction of IL-6 synthesis in human peritoneal mesothelial cells is related to the induction and stabilization of IL-6 mRNA.* Kidney Int, 1996. **50**(4): p. 1212-23.
430. Topley, N., *The cytokine network controlling peritoneal inflammation.* Perit Dial Int, 1995. **15**(7 Suppl): p. S35-9; discussion S39-40.
431. Topley, N. and J.D. Williams, *Role of the peritoneal membrane in the control of inflammation in the peritoneal cavity.* Kidney Int Suppl, 1994. **48**: p. S71-8.
432. Lambie, M.R., et al., *Peritoneal inflammation precedes encapsulating peritoneal sclerosis: results from the GLOBAL Fluid Study.* Nephrol Dial Transplant, 2016. **31**(3): p. 480-6.
433. Jantz, M.A. and V.B. Antony, *Pathophysiology of the pleura.* Respiration, 2008. **75**(2): p. 121-33.
434. Cannistra, S.A., et al., *Vascular cell adhesion molecule-1 expressed by peritoneal mesothelium partly mediates the binding of activated human T lymphocytes.* Exp Hematol, 1994. **22**(10): p. 996-1002.
435. van Grevenstein, W.M., et al., *Inflammatory cytokines stimulate the adhesion of colon carcinoma cells to mesothelial monolayers.* Dig Dis Sci, 2007. **52**(10): p. 2775-83.
436. Haslinger, B., et al., *Hyaluronan fragments induce the synthesis of MCP-1 and IL-8 in cultured human peritoneal mesothelial cells.* Cell Tissue Res, 2001. **305**(1): p. 79-86.
437. Campo, G.M., et al., *Combined treatment with hyaluronan inhibitor Pep-1 and a selective adenosine A2 receptor agonist reduces inflammation in experimental arthritis.* Innate Immun, 2013. **19**(5): p. 462-78.
438. Lee, J.C., et al., *Modulation of the local neutrophil response by a novel hyaluronic acid-binding peptide reduces bacterial burden during staphylococcal wound infection.* Infect Immun, 2010. **78**(10): p. 4176-86.
439. Zaleski, K.J., et al., *Hyaluronic acid binding peptides prevent experimental staphylococcal wound infection.* Antimicrob Agents Chemother, 2006. **50**(11): p. 3856-60.
440. Headland, S.E. and L.V. Norling, *The resolution of inflammation: Principles and challenges.* Semin Immunol, 2015. **27**(3): p. 149-60.
441. Hodge-Dufour, J., et al., *Induction of IL-12 and chemokines by hyaluronan requires adhesion-dependent priming of resident but not elicited macrophages.* J Immunol, 1997. **159**(5): p. 2492-500.

442. Horton, M.R., et al., *Hyaluronan fragments synergize with interferon-gamma to induce the C-X-C chemokines mig and interferon-inducible protein-10 in mouse macrophages.* J Biol Chem, 1998. **273**(52): p. 35088-94.
443. McKee, C.M., et al., *Hyaluronan (HA) fragments induce chemokine gene expression in alveolar macrophages. The role of HA size and CD44.* J Clin Invest, 1996. **98**(10): p. 2403-13.
444. McKee, C.M., et al., *Hyaluronan fragments induce nitric-oxide synthase in murine macrophages through a nuclear factor kappaB-dependent mechanism.* J Biol Chem, 1997. **272**(12): p. 8013-8.
445. Boodoo, S., et al., *Differential regulation of hyaluronan-induced IL-8 and IP-10 in airway epithelial cells.* Am J Physiol Lung Cell Mol Physiol, 2006. **291**(3): p. L479-86.
446. Boyce, D.E., et al., *Hyaluronic acid induces tumour necrosis factor-alpha production by human macrophages in vitro.* Br J Plast Surg, 1997. **50**(5): p. 362-8.
447. de la Motte, C., et al., *Platelet-derived hyaluronidase 2 cleaves hyaluronan into fragments that trigger monocyte-mediated production of proinflammatory cytokines.* Am J Pathol, 2009. **174**(6): p. 2254-64.
448. Jobe, K.L., et al., *Interleukin-12 release from macrophages by hyaluronan, chondroitin sulfate A and chondroitin sulfate C oligosaccharides.* Immunol Lett, 2003. **89**(2-3): p. 99-109.
449. Noble, P.W., et al., *Hyaluronate activation of CD44 induces insulin-like growth factor-1 expression by a tumor necrosis factor-alpha-dependent mechanism in murine macrophages.* J Clin Invest, 1993. **91**(6): p. 2368-77.
450. Stern, R., A.A. Asari, and K.N. Sugahara, *Hyaluronan fragments: an information-rich system.* Eur J Cell Biol, 2006. **85**(8): p. 699-715.
451. Yamasaki, K., et al., *NLRP3/cryopyrin is necessary for interleukin-1beta (IL-1beta) release in response to hyaluronan, an endogenous trigger of inflammation in response to injury.* J Biol Chem, 2009. **284**(19): p. 12762-71.
452. Shimada, M., et al., *Hyaluronan fragments generated by sperm-secreted hyaluronidase stimulate cytokine/chemokine production via the TLR2 and TLR4 pathway in cumulus cells of ovulated COCs, which may enhance fertilization.* Development, 2008. **135**(11): p. 2001-11.
453. Mummert, M.E., *Immunologic roles of hyaluronan.* Immunol Res, 2005. **31**(3): p. 189-206.
454. Guan, H., P.S. Nagarkatti, and M. Nagarkatti, *Blockade of hyaluronan inhibits IL-2-induced vascular leak syndrome and maintains effectiveness of IL-2 treatment for metastatic melanoma.* J Immunol, 2007. **179**(6): p. 3715-23.
455. Siiskonen, H., et al., *Hyaluronan synthase 1 (HAS1) produces a cytokine-and glucose-inducible, CD44-dependent cell surface coat.* Exp Cell Res, 2014. **320**(1): p. 153-63.
456. Colotta, F., et al., *Modulation of granulocyte survival and programmed cell death by cytokines and bacterial products.* Blood, 1992. **80**(8): p. 2012-20.
457. Bossu, P., et al., *Balance between autocrine interleukin-1beta and caspases defines life versus death of polymorphonuclear cells.* Eur Cytokine Netw, 2001. **12**(1): p. 177-86.
458. Grutkoski, P.S., et al., *IL-1beta stimulation induces paracrine regulation of PMN function and apoptosis.* Shock, 1999. **12**(5): p. 373-81.
459. Watson, R.W., et al., *The IL-1 beta-converting enzyme (caspase-1) inhibits apoptosis of inflammatory neutrophils through activation of IL-1 beta.* J Immunol, 1998. **161**(2): p. 957-62.

460. Prince, L.R., et al., *The role of interleukin-1beta in direct and toll-like receptor 4-mediated neutrophil activation and survival.* Am J Pathol, 2004. **165**(5): p. 1819-26.
461. Hognas, G., et al., *Cytokinesis failure due to derailed integrin traffic induces aneuploidy and oncogenic transformation in vitro and in vivo.* Oncogene, 2012. **31**(31): p. 3597-606.
462. Adamia, S., et al., *Aberrant posttranscriptional processing of hyaluronan synthase 1 in malignant transformation and tumor progression.* Adv Cancer Res, 2014. **123**: p. 67-94.
463. Auvinen, P., et al., *Hyaluronan synthases (HAS1-3) in stromal and malignant cells correlate with breast cancer grade and predict patient survival.* Breast Cancer Res Treat, 2014. **143**(2): p. 277-86.
464. Rilla, K., et al., *Hyaluronan synthase 1 (HAS1) requires higher cellular UDP-GlcNAc concentration than HAS2 and HAS3.* J Biol Chem, 2013. **288**(8): p. 5973-83.
465. Torronen, K., et al., *Tissue distribution and subcellular localization of hyaluronan synthase isoenzymes.* Histochem Cell Biol, 2014. **141**(1): p. 17-31.